Technische Universität München

Fakultät für Medizin

Antioxidant-based preventive therapy and detection of early biomarkers in serum for non-alcoholic steatohepatitis (NASH)-induced hepatocellular carcinoma (HCC)

Valentina Leone

Vollständiger Abdruck der von der Fakultät für Medizin der Technischen Universität München zur Erlangung des akademischen Grades eines

Doktors der Naturwissenschaften (Dr. rer. nat.)

genehmigten Dissertation.

Vorsitzender: Prof. Dr. Percy A. Knolle

Prüfer der Dissertation: 1. Prof. Dr. Radu Roland Rad

2. Prof. Dr. Dirk Haller

Die Dissertation wurde am 11.12.2019 bei der Technische Universität München eingereicht und durch die Fakultät für Medizin am 16.06.2020 angenommen.

Table of Contents

Summary

Alterations in our life-style such as high caloric intake combined with a sedentary life style have highly augmented the number of obese people in developed countries over the last decades, and it is expected to increase further in the near future. Non-alcoholic fatty liver disease (NAFLD) represents the most common liver morbidity, characterized by excessive fat accumulation (steatosis). Approximately 30% of patients with NAFLD develop non-alcoholic steatohepatitis (NASH) which in addition to steatosis also involves chronic inflammation, hepatocellular damage and fibrosis. NASH constitutes a major risk factor for hepatocellular carcinoma (HCC), which is the most common primary liver malignancy and the third most common cause worldwide of cancer-related death. To date, the exact mechanism underlying NASH and NASH-induced HCC is still unknown.

A prolonged high caloric diet intake leads to oxidative stress due to increased levels of reactive oxygen species (ROS) produced mainly by endogenous aberrant mitochondria, endoplasmic reticulum (ER) and peroxisomes. ROS negatively affect lipids and proteins, thus generating lipid peroxidation and protein carbonylation (protein adducts by ROS or by lipid peroxidation products). These oxidative stress by-products deregulate the hepatic fatty acids homeostasis and induce ER stress. Lipid peroxidation in particular is considered a relevant source of mutagens triggered by ROS.

Beyond lipids and proteins modification, oxidative stress modifies also DNA, generating DNA adducts. Furthermore, it favors the activation of the immune response and increases proliferation, eventually resulting in tumorigenesis. This is relevant not only in livers of NASH-affected patients, but also in HCC cases.

To study the role of ROS in NASH and in NASH-induced HCC mouse models, I tested the effects of two different antioxidant compounds, one synthetic and one natural, termed respectively butylated hydroxyanisole (BHA) and astaxanthin (AXT) in mouse models of NASH. The aim was to assess whether

therapeutic treatment with antioxidants would ameliorate NASH and reduce cancer incidence.

To test this hypothesis, I prophylactically fed C57Bl/6J mice on a choline-deficient, high-fat diet (CDHFD), which induces NASH, in combination with BHA or AXT. The BHA+CDHFD group did not develop obesity or NASH, in contrast to the AXT+CDHFD mice which became obese but had ameliorated NASH and significantly reduced inflammation and proliferation.

To investigate the effect of antioxidants on HCC development, CDHFD feeding regimen was exchanged with BHA+CDHFD or AXT+CDHFD after 6 months, time point in which NASH is already established. The BHA+CDHFD diet-switch group showed a cancer incidence of 10%, while for the AXT+CDHFD diet-switch group the incidence was 11.5%. The control group fed only a CDHFD displayed a 34% HCC incidence.

In order to evaluate the role of ROS in the transition from NAFLD to NASH, we switched the diet at early NASH stage. This group was on CDHFD for 3 months and then kept on AXT+CDHFD for 9 months. These mice developed no tumors and exhibited reduced NAFLD Activity Score.

To determine whether there is a point of no return for liver tumor development over the course of NASH, I performed two additional experiments where CDHFD was switched to normal diet at late NASH stages (at 6 and 9 months). Since the tumor incidence was not different between the two groups, I concluded that the crucial changes which eventually lead to cancer probably happen before the 6-month time point of CDHFD feeding regimen.

I also performed a search for early serological biomarkers of NASH-induced HCC risk. This analysis revealed a potential candidate involved in glycolysis, which is one key metabolic pathway involved in energy consumption by neoplastic cells.

In addition, within the frame of my PhD studies, I established a protocol for RNA extraction from mass-spectrometry imaging (MSI)-processed human intrahepatic cholangiocarcinoma (iCCA) samples. The samples were used for the preparation of RNA sequencing libraries, with the final aim to characterize

intra-tumor heterogeneity in iCCA defined by the spatial distribution of metabolites' expression.

Overall, these data indicate that oxidative stress is indeed an important driver of tumorigenesis that should be considered in NASH therapeutic practice in order to reduce cancer risk. In addition, changing lifestyle before the establishment of full-blown NASH may be required to substantially reduce the risk of developing liver cancer.

Zusammenfassung

Veränderungen in unserem Lebensstil, wie z.B. eine hohe Kalorienzufuhr in Kombination mit einem bewegungsarmen Lebensstil, haben die Zahl der fettleibigen Menschen in entwickelten Ländern in den letzten Jahrzehnten stark erhöht, und es wird erwartet, dass sie in naher Zukunft weiter zunehmen wird. Die nichtalkoholische Fettlebererkrankung (NAFLD) stellt die häufigste Lebererkrankung dar, und ist durch eine übermäßige Fettansammlung (Steatose) gekennzeichnet. Etwa 30% der Patienten mit NAFLD entwickeln eine nichtalkoholische Steatohepatitis (NASH), die neben der Steatose auch chronische Entzündungen, hepatozelluläre Schäden und Fibrose mit sich bringt. NASH stellt einen wichtigen Risikofaktor für das hepatozelluläre Karzinom (HCC) dar, die häufigste primäre Lebermalignität und die weltweit dritthäufigste Ursache für krebsbedingten Tod. Bis heute ist der genaue Mechanismus, der NASH und NASH-induziertem HCC zugrunde liegt, noch unbekannt.

Eine verlängerte Zufuhr von hochkalorischer Nahrung führt zu oxidativem Stress aufgrund erhöhter Mengen an reaktiven Sauerstoffspezies (ROS), die hauptsächlich durch endogene, aberrante Mitochondrien, endoplasmatisches Retikulum (ER) und Peroxisomen produziert werden. ROS beeinflusst Lipide und Proteine negativ und erzeugt Lipidperoxidation und Proteincarbonylierung (Proteinaddukte durch Lipidperoxidationsprodukte). Diese aus oxidativem Stress stammenden Nebenprodukte regulieren die Homöostase der Leberfettsäuren und induzieren ER-Stress. Insbesondere die

Lipidperoxidation gilt als eine relevante Quelle für Mutagene, die durch ROS ausgelöst werden.

Neben der Modifikation von Lipiden und Proteinen verändert oxidativer Stress auch die DNA und erzeugt DNA-Addukte. Darüber hinaus begünstigt es die Aktivierung der Immunantwort und erhöht die Proliferation, was zu einer Tumorgenese führt. Dies ist nicht nur bei Lebern von NASH-behafteten Patienten relevant, sondern auch bei HCC-Fällen.

Um die Rolle von ROS in NASH und in NASH-induzierten HCC-Mausmodellen zu untersuchen, habe Ich die Effekte von zwei verschiedenen antioxidativen Verbindungen, einer synthetischen (butyliertes Hydroxyanisol (BHA)) und einer natürlichen (Astaxanthin (AXT)) in Mausmodellen von NASH getestet. Unser Ziel war es, zu beurteilen, ob eine therapeutische Behandlung mit Antioxidantien das Krankheitsbild von NASH verbessern und die Krebsinzidenz reduzieren würde.

Um diese Hypothese zu testen, behandelten wir C57Bl/6J-Mäuse welche mit einer cholinarmen, fettreichen Ernährung (CDHFD) gefüttert wurden, die NASH induziert, prophylaktisch mit BHA oder AXT. Die BHA+CDHFD-Gruppe entwickelte weder Fettleibigkeit noch NASH, im Gegensatz zu den AXT+CDHFD-Mäusen, welche fettleibig wurden, aber abgemilderte NASH und deutlich reduzierte Entzündung und Proliferation zeigten.

Um die Wirkung von Antioxidantien auf die HCC-Entwicklung zu untersuchen, wurde das Ernährungsregime von CDHFD nach 6 Monaten mit BHA+CDHFD oder AXT+CDHFD ausgetauscht, ein Zeitpunkt, an dem NASH bereits etabliert ist. Die BHA+CDHFD-Diät-Switchgruppe zeigte eine Krebsinzidenz von 10%, während die AXT+CDHFD-Diät-Switchgruppe eine Inzidenz von 11,5% aufwies. Die Kontrollgruppe, die nur mit einer CDHFD versorgt wurde, zeigte eine 34%ige HCC-Inzidenz.

Um die Rolle von ROS beim Übergang von NAFLD zu NASH zu bewerten, stellte Ich die Ernährung in einem frühen NASH-Stadium um. Diese Gruppe war 3 Monate lang auf CDHFD und blieb dann 9 Monate lang auf

AXT+CDHFD. Diese Mäuse zeigten keine Tumore und reduzierten den NAFLD Activity Score.

Um festzustellen, ob es einen Umkehrgrenzpunkt gibt, an dem die Entwicklung eines Lebertumors im Laufe von NASH nicht mehr aufzuhalten ist, führten wir zwei zusätzliche Experimente durch, bei denen CDHFD-Mäuse in späten NASH-Stadien (nach 6 und 9 Monaten) auf normale Chow-Diät umgestellt wurden. Da die Tumorinzidenz zwischen den beiden Gruppen nicht unterschiedlich war, kommen wir zu dem Schluss, dass die entscheidenden Veränderungen, die schließlich zu Krebs führen, wahrscheinlich vor dem 6-Monats Zeitpunkt des CDHFD-Fütterungsprogramms stattfinden.

Ich habe auch eine Suche nach frühen serologischen Biomarkern für das NASH-induzierte HCC-Risiko durchgeführt. Diese Thesis zeigt einen potenziellen Kandidaten, der an der Glykolyse beteiligt ist, einem Stoffwechselweg, der bekanntermaßen am Energieverbrauch neoplastischer Zellen beteiligt ist.

Darüber hinaus habe ich im Rahmen meines Dissertationsprojektes ein Protokoll für die RNA-Extraktion aus Massen-Spektrometrie (MSI)-verarbeiteten humanen intrahepatischen Cholangiokarzinom (iCCA)-Proben erstellt. Die Proben wurden für die Vorbereitung von RNA-Sequencing libraries verwendet, mit dem Ziel, die intratumorale Heterogenität in iCCA zu charakterisieren, definiert durch die räumliche Verteilung der Metabolitenexpression.

Insgesamt deuten unsere Daten darauf hin, dass oxidativer Stress in der Tat ein wichtiger Treiber der Tumorgenese ist, der in der therapeutischen Praxis von NASH berücksichtigt werden sollte, um das Krebsrisiko zu reduzieren. Darüber hinaus kann eine Änderung des Lebensstils vor der Etablierung von NASH erforderlich sein, um das Risiko der Entstehung von Leberkrebs erheblich zu reduzieren.

1 Introduction

1.1 The liver

1.1.1 Liver physiology and cell composition

The liver, technically classified as a gland, is the largest solid organ in the human body. It is located in the upper right-hand quadrant of the abdominal cavity and it exerts several different functions, such as bile production necessary for digestion, metabolism of lipids, proteins and carbohydrates, vitamin and mineral storage (e.g. vitamins A, D, E, K, and B12; minerals as iron in the form of ferritin and copper), detoxification, blood volume regulation, and regulating immune responses. The hepatic cellular structure can be divided into liver parenchymal cells composed of hepatocytes, accounting for 60-80% of the liver total number of cells, and the non-parenchymal cells comprising the liver sinusoidal endothelial cells (LSECs), resident macrophages called Kupffer cells (KCs) and hepatic stellate cells (HSCs) (Crispe, 2009). The liver is the only organ capable of regeneration: after partial hepatectomy, it regenerates due to the capability of the hepatocytes to pass from a quiescent state to compensatory hyperplasia. In the case of acute liver failure, the process is driven by the differentiation of progenitor cells (Fausto et al., 2006).

1.1.2 The immune functions of the liver

Antigens produced by different sources (e.g. diet, drugs, viruses, bacteria) are metabolized in the liver, and the immunological response towards them is strictly regulated. In fact, liver homeostasis is necessary to prevent tissue damage in response to external stimuli. The LSECs are the gatekeepers of liver homeostasis. They comprise 50% of the non-parenchymal cells and form the fenestrated capillaries of the liver. This vascular system allows the blood

flow to slow down in order to increase the chances of recognition of antigens from arterial (hepatic artery) and venous blood (portal vein) (Jenne and Kubes, 2013). The LSECs have an important role in antigen presentation. LSECs, by binding CD8^{+} T cells via the major histocompatibility complex I (MHC-I), generate tolerogenic CD8^{+} T cells that are incapable of producing effector cytokines. In addition, they regulate immune homeostasis by blocking the activation of CD8^{+} T cells from the dendritic cells (DCs) through downregulation of DC costimulatory molecules such as CD80/86 and interleukin-2 (IL-2) (Schildberg et al., 2008). Adjacent to the LSECs are the resident liver macrophages, the KCs, which are directly exposed to the blood flow. They make up approximately 35% of the non-parenchymal cells. The KCs are able to capture bacteria and become activated through scavenger receptors, Toll-like receptors (TLRs), complement and antibody receptors (Jenne and Kubes, 2013). These cells are so important for the function of phagocytosis of pathogens, that their absence causes bacteremia and host death (Helmy et al., 2006). KCs participate, together with the natural killer cells (NKs) and natural killer T cells (NKTs), in the innate immune response. Through the pattern recognition receptors (PRRs), they recognize pathogen-derived molecules (pathogen-associated molecular pattern (PAMPs), such as lipopolysaccharide (LPS)), and during the sterile inflammatory response, they recognize molecules such as denatured proteins, or released DNA after necrosis (damage-associated molecular pattern (DAMPS)). KCs and NKs participate in the activation of pro-inflammatory or anti-inflammatory responses via cytokine release and antigen presentation (via major histocompatibility complex I and II; MHCI and MHCII) to adaptive immune cells. The major pro-inflammatory cytokines released by KCs are tumor necrosis factor-alpha (TNF-α) and interleukin-6 (IL-6). During acute liver injury the KCs recruit myeloid cells to the site of inflammation, and they further produce pro-inflammatory cytokines. Neutrophils also participate in this response, which after infiltration in the liver generate ROS to promote hepatocyte death (Weston et al., 2019). The resolution of the inflammation is exerted by release from KCs of anti-inflammatory cytokines (e.g. interleukin-10 (IL-10)) and by the clearance of neutrophils through restorative macrophages (Triantafyllou et al., 2018).

1.2 Non-Alcoholic Steatohepatitis (NASH)

1.2.2 NASH epidemiology and risk factors

Over the last decades, unhealthy lifestyles, characterized by high caloric intake and physical inactivity, have led to a dramatic increase of obesity (BMI ≥30 kg/m^2) and related diseases (W.H.O., 2017), particularly in Western countries such as the USA and Europe (Blüher, 2019). Consequently, a link between obesity and increased cancer incidence has been observed (Polednak, 2008). A constant regimen of high caloric food induces a state of chronic inflammation in different organs, in particular in the adipose tissues, the gut, and the liver. One of the most frequent chronic liver diseases worldwide is non-alcoholic fatty liver disease (NAFLD), affecting 25% of the population (Younossi and Henry, 2016; Younossi et al., 2019) **(fig.1)**.
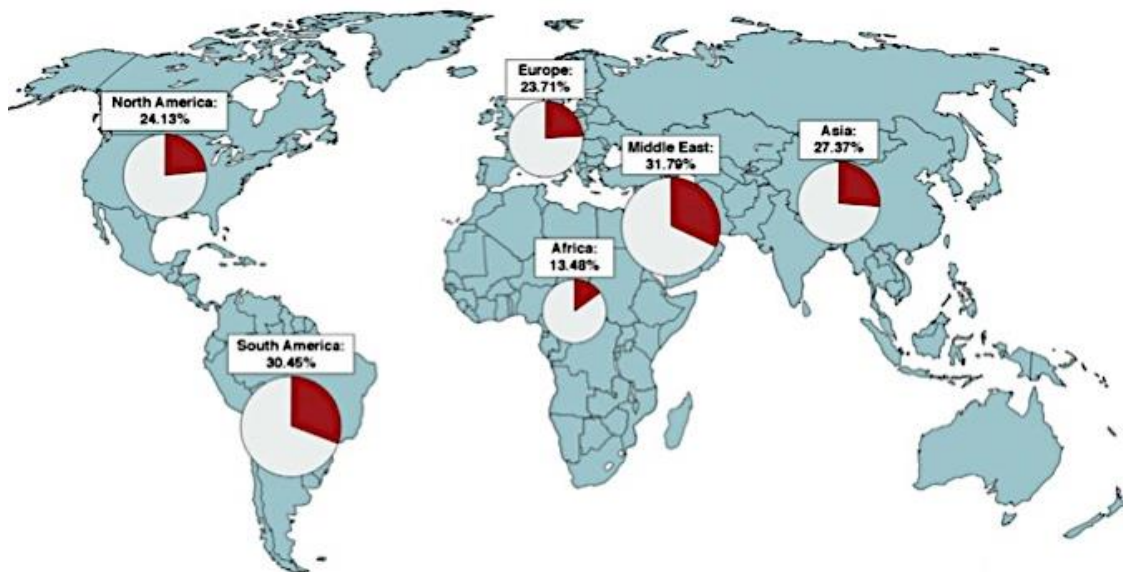
Figure 1. Global NAFLD prevalence (from Younossi and Henry, 2016).

NAFLD risk factors include obesity, type 2 diabetes mellitus (T2DM), metabolic syndrome (abdominal obesity, hypertriglyceridemia, hyperlipidemia, high blood pressure) and genetic polymorphisms (e.g. *PNPLA3* and *TM6SF2*) (Younossi et al., 2018). NAFLD is marked by fatty acid accumulation (steatosis), low-grade to high-grade inflammation, and can display hepatocellular injury ((EASL) et al., 2016). Globally, the NAFLD prevalence

has been estimated to be 25.24% (fig.1) and is foreseen to increase in the next decade, especially in industrialized countries (Estes et al., 2018a; Estes et al., 2018b; Younossi et al., 2018). Non-alcoholic steatohepatitis (NASH) manifests when the liver is severely inflamed, having reached a state of chronic inflammation resulting in high liver damage. A percentage of around 30% of NAFLD-affected patients develop NASH (Musso et al., 2010), which is 3-5% of the entire population (Povsic et al., 2019). Of those NASH patients, 15-25% can end up with cirrhosis, which is thought to increase the risk of liver failure and cancer (Bugianesi et al., 2002; Hossain et al., 2016).

1.2.3 NASH pathogenesis

The molecular pathogenesis of NASH was initially described by the two-hit hypothesis, with the first hit defined by fatty acid accumulation in the liver (steatosis), whereas the second hit marked by oxidative stress, endoplasmic reticulum (ER) stress, inflammation, and hepatocytes cell death (Buzzetti et al., 2016; Day and Saksena, 2002). A new consensus instead supports a multi-parallel hits hypothesis **(fig.2)**, where dyslipidemia, oxidative and ER stress, mitochondrial dysfunction, altered immune response and dysbiosis (imbalanced gut microbiota) contribute concurrently to the development of NASH (Takaki et al., 2013; Tilg and Moschen, 2010).
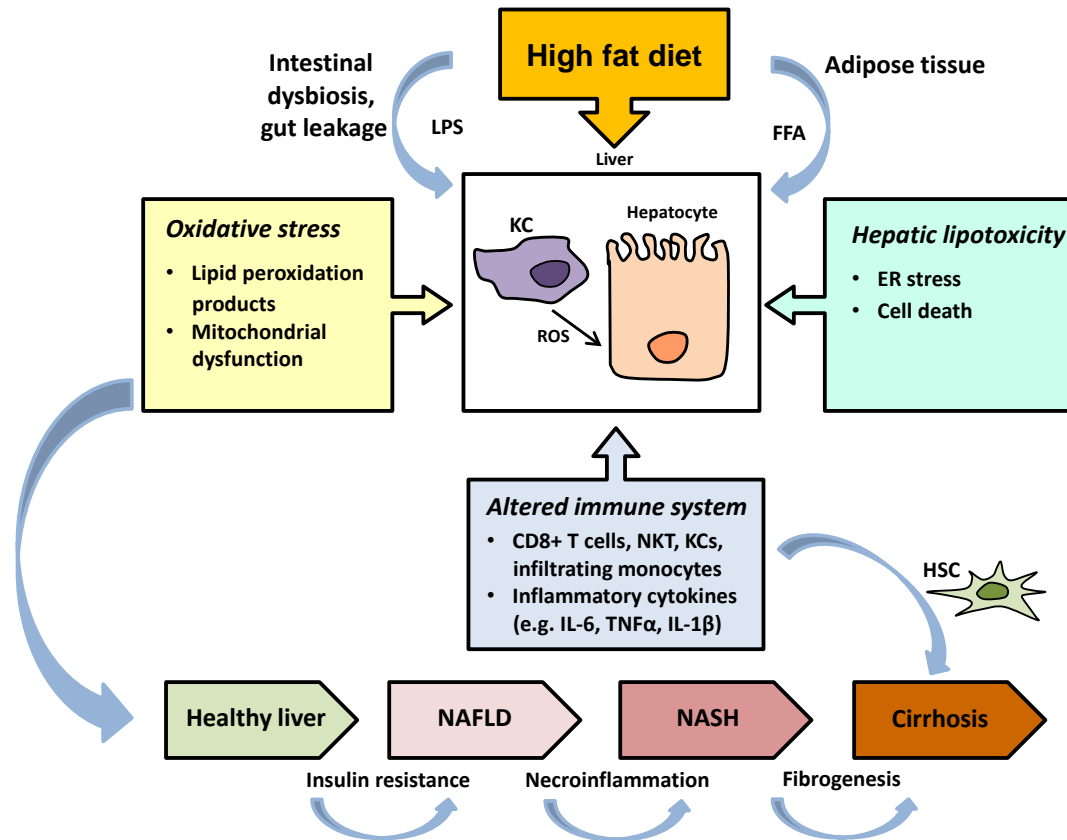
Figure 2. The "multiple hits theory" of NAFLD and NASH pathogenesis. The "multiple hits theory" for the development of NAFLD and NASH is based on the hypothesis that different insults act together to drive the disease. A high-fat diet, combined with a sedentary lifestyle, contributes to establishing intestinal gut leakage and subsequent release of lipopolysaccharide (LPS). LPS targets hepatocytes and Kupffer cells (KCs) inducing a pro-inflammatory response. Free fatty acids (FFA) coming from dietary intake, adipose tissue lipolysis, or from *de novo* hepatocytes lipogenesis, lead to hepatic lipotoxicity. Lipotoxicity is characterized by hepatocytes ER stress and cell death forms (e.g. apoptosis, necroptosis). Oxidative stress (OxS), caused by continuous hepatic lipid overload, results from the initial mitochondrial radical oxygen species (ROS) overproduction and from impaired antioxidant machinery. Furthermore, OxS is involved in the generation of lipid peroxidation products, which contributes to DNA damage and protein modifications. Simultaneously to these processes, also the immune system contributes to liver damage by establishing a chronic inflammatory status, typical of NASH. The unresolved inflammation results in activation of the hepatic stellate cells (HSCs) responsible for the development of liver fibrosis.

1.2.3.1 Lipotoxicity: ER stress and apoptosis

In the transition from NAFLD to NASH, a continuous intake of a diet rich in fat content leads to lipotoxicity (Lee et al., 1994), which causes dysfunction of organelles, inflammation and subsequent cell death (e.g. apoptosis, necrosis and necroptosis) (Neuschwander-Tetri, 2010). The intrahepatic fatty acid overload may derive from dietary lipids (15%), free fatty acids resulting from lipolysis of adipose tissue (60-80%), impaired lipid catabolism (reduced mitochondrial fatty acid oxidation and their export through the very low-density lipoprotein (VLDL) particles), up-regulation of fatty acid uptake and *de novo* lipogenesis (5%) (Marchesini et al., 2016). The constant lipid overload deregulates fatty acid metabolism and subsequently affects ER and mitochondrial functions (Kawano and Cohen, 2013). The endoplasmic reticulum (ER) regulates calcium homeostasis, protein metabolism, lipid biosynthesis, and biogenesis of lipid droplets.

During NAFLD pathogenesis, in order to cope with excess fatty acid intake, free fatty acids are converted into triglycerides (TGs) that accumulate in the subdomain of the ER. Subsequently, the accumulated TGs are released from the ER through single membrane budding (Akazawa and Nakao, 2018). Animal models and human studies have shown that lipid droplets formation and accumulation is not the cause of hepatocyte injury (Neuschwander-Tetri, 2010). The harmful fatty acids contributing to lipotoxicity are rather free fatty acids, also called non-esterified fatty acids (NEFAs). They are released from lipolysis of adipocyte TGs or from lysosomal breakdown of vesicles containing lipoprotein remnants or they can be generated through *de novo* lipogenesis (Gentile et al., 2011). In particular, saturated fatty acids (SFAs) are reported to be involved in hepatic injury since they are poorly internalized by the conversion of triglycerides in lipid droplets, and their structure affects the fluidity of cellular membranes.

One SFA known to be involved in NAFLD and NASH pathogenesis is palmitic acid, a saturated long fatty acid (Miura et al., 2013; Ogawa et al., 2018). A high-fat diet leads to the depletion of calcium stores (Wires et al., 2017),

accumulation of NEFAs and/or misfolded or unfolded proteins in the ER lumen, resulting in ER stress and activation of the unfolded protein response (UPR) (Basseri and Austin, 2012). The UPR signaling pathway, in addition to its role in activating chaperones and protein degradation enzymes, is also involved in hepatic lipid accumulation via PKR-like ER kinase (PERK) and inositol-requiring enzyme 1 (IRE-1α): PERK induces sterol regulatory element binding protein 1 (SREBP1) and IRE-1α activates X-box binding protein 1 (XBP-1). The activation of these regulatory proteins leads to the expression of lipogenic genes that favor the development of steatosis and lipid droplet formation (Basseri and Austin, 2012; Sharma et al., 2018). Phosphorylation of IRE-1α can promote the activation of kinases involved in stress and inflammatory responses, such as p38 mitogen-activated kinase (MAPK14), extracellular-regulated kinase (ERK), and c-Jun-NH$_2$-terminal kinase (JNK). Activated PERK can also drive inflammation via phosphorylation of the eukaryotic translation initiation factor 2A (eIF2a) which also leads to the regulation of the nuclear factor kappa-light-chain-enhancer of activated B cells (NF-κB) pathway (Gentile et al., 2011).

Lipotoxicity, in addition to ER stress, is also characterized by apoptosis (Cao et al., 2012). In NASH, NEFA-induced apoptotic hepatocyte cell death is termed lipo-apoptosis and interconnects ER stress and apoptosis. Under sustained ER stress, phosphorylated IRE-1α forms a pro-apoptotic complex that, together with the apoptosis signal-regulating kinase 1 (ASK1), eventually phosphorylates and activates the Jun-N-terminal kinase (JNK) pathway (Hapala et al., 2011). It has been shown that hepatic lipotoxicity is mediated by JNK signaling, and in particular, by the JNK2 isoform (Malhi et al., 2006).

In NAFLD and NASH, hepatocyte apoptosis is executed by the extrinsic and the intrinsic pathways (Kanda et al., 2018; Syn et al., 2009). The extrinsic pathway is mediated by ligation of TNF-α, FasL, or TNF-α-related apoptosis-inducing ligand (TRAIL) to death receptors that activate caspase 8 and eventually caspase 3 (Hirsova and Gores, 2015). The intrinsic pathway becomes activated by mitochondrial dysfunction driven by ER stress-activated JNK, C/EBP homologous protein (CHOP) and calcium release. The resulting increased membrane permeability and cytochrome c release, eventually

activates caspase 3, thus converging with the extrinsic pathway for the execution of apoptosis. The intrinsic pathway can be also be induced by the release of proteolytic enzyme cathepsin B in the cytosol from disrupted lysosomes (Alkhouri et al., 2011). Histopathological evaluation with liver biopsy stained with hematoxylin-eosin allows to determine apoptotic hepatocytes by the typical ballooning feature (Caldwell et al., 2010). In NAFLD patients, the detection of NASH serum biomarkers, such as cytokeratin-18 fragments and Bcl-2, precedes NASH detection via biopsy. These markers correlate with the degree of hepatocyte apoptosis (Arab et al., 2017; El Bassat et al., 2014; Feldstein et al., 2009; He et al., 2017).

Lipo-apoptosis (cell death induced by dyslipidemia) plays a pivotal role in chronic inflammation and fibrosis (Brenner et al., 2013). Hepatocytes that underwent lipo-apoptosis are phagocytized by KCs, which recruit circulating monocytes and neutrophils to the liver via the TLR4 pathway. Infiltrating monocytes are characterized by the expression of lymphocyte antigen 6 complex, locus C1 (Ly6C$^+$). The Ly6C^{high} positive cells are known to be profibrogenic by inducing, via cytokines, collagen formation from HSCs (Ogawa et al., 2018; Tacke and Zimmermann, 2014). In the hepatocytes, when apoptotic signaling is initiated but not completed, "sub-lethal" death signaling occurs, which also induces inflammation and fibrosis (Kakisaka et al., 2012; Machado et al., 2015).

Other lipotoxic lipids are lysophosphatidylcholine (LPC) (generated from phosphatidylcholine of cellular membranes), ceramides (synthesized from serine and palmitic acid or from hydrolysis of plasma membrane sphingomyelin) and eicosanoids (products of arachidonic acid´s metabolism). LPC and ceramide induce ER stress and apoptosis (Kakazu et al., 2016). The ER releases ceramide-enriched extracellular vesicles which induce KC activation and monocyte chemotaxis to the liver (Musso et al., 2018). In addition, ceramides can directly affect the mitochondrial electron transport chain (ETC) and can block the insulin pathway by inhibiting the phosphorylation and activation of AKT, resulting in insulin resistance (Musso et al., 2018). The eicosanoids (prostacyclins, thromboxane, leukotrienes, prostaglandins) are known to be lipid effectors of inflammation, produced

mainly by the oxidation of arachidonic acid, mediated by the cyclooxygenases (COX-1 and COX-2) (Musso et al., 2018) **(fig.3)**.
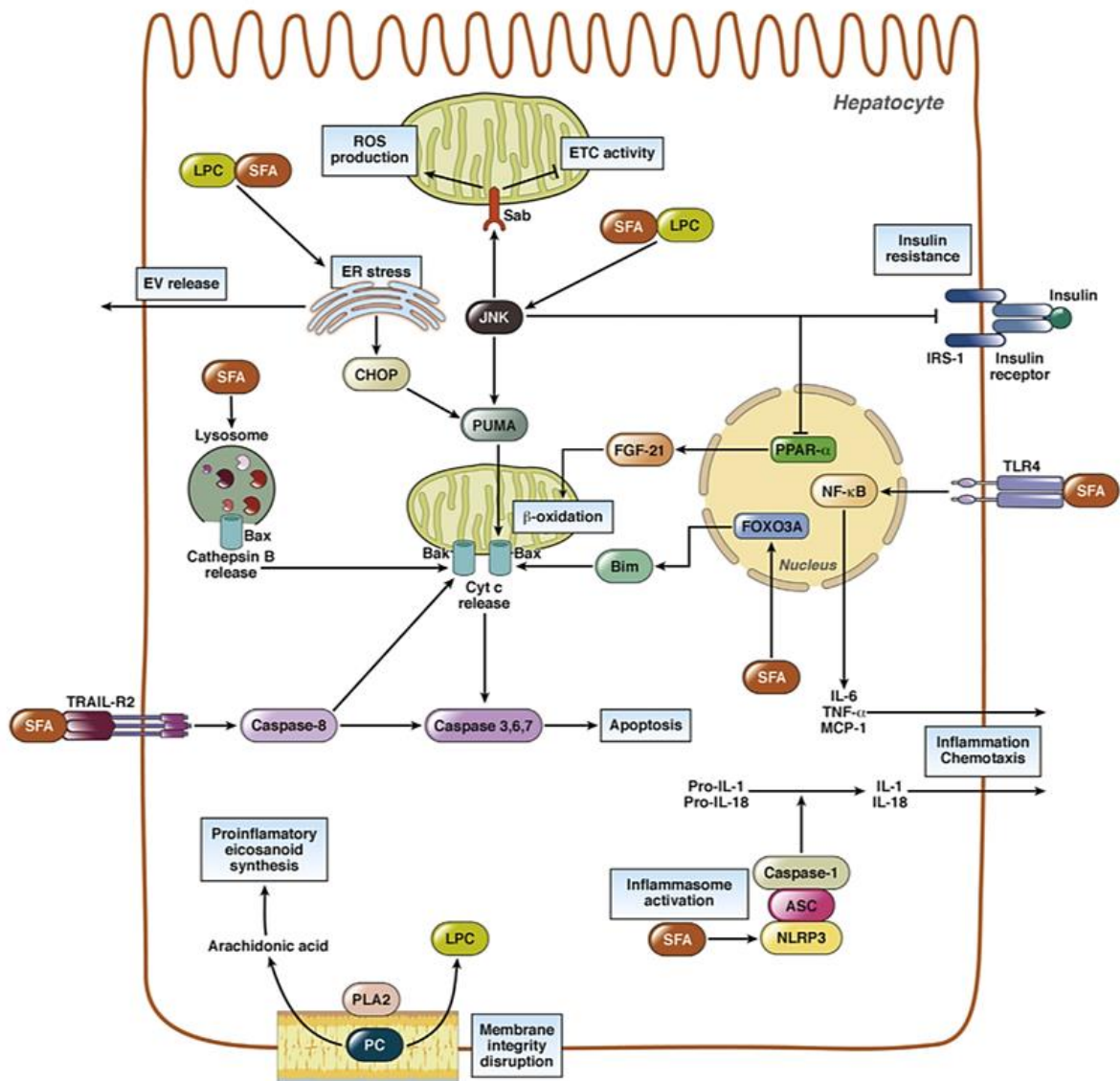
Figure 3. Mechanisms of lipotoxicity in hepatocytes during NAFLD and NASH progression (from Musso et al., 2018). Saturated fatty acids (SFAs) and lysophosphatidylcholine (LPC) can induce apoptosis executing the extrinsic (via death-receptors) and the intrinsic (via JNK and ER stress) pathways. JNK also leads to insulin resistance, ETC impaired activity and increased mitochondrial ROS production. Through binding with TLR4, SFAs can drive the activation of NF-κB signaling and following production of pro-inflammatory cytokines. Furthermore, SFAs can promote inflammasome activation. The activity of the phospholipase A2 (PLA2) produces arachidonic acid (precursor for the synthesis of the pro-inflammatory eicosanoids) and LPC, and at the same time has detrimental effects on membrane integrity.

1.2.3.2 Mitochondrial dysfunction and NASH

The mitochondrion is an essential organelle of eukaryotic cells, responsible for fat and energy homeostasis. Its ultrastructure comprises a double membrane, where the inner membrane contains the chemiosmotic apparatus for the production of energy in the form of adenosine triphosphate (ATP). The space enclosed in the inner membrane is called matrix and contains mitochondrial DNA, enzymes involved in the citric acid cycle (Krebs cycle), mitochondrial ribosomes and tRNA. In the mitochondrial matrix, the majority of the reactions of β-oxidation for the catabolism of fatty acids takes place, followed by peroxisomes, and in minor form, as ω-oxidation, by microsomal enzymes (Bellanti et al., 2017). When energy is needed (e.g. during fasting), complex lipids (TGs) are firstly catabolized by lipases that generate non-esterified fatty acids (NEFAs) by hydrolysis. The activation and the transport of NEFAs inside the mitochondria happen after their conversion into Acyl-CoA. Moreover, in the mitochondrial matrix Acyl-CoA undergoes a series of oxidative modifications in the frame of the β-oxidation process, which eventually generates Acetyl-CoA. From these reactions, the resulting products, such Acetyl-CoA and NADH/FADH$_2$, are fed into the Krebs cycle and the electron transport chain (ETC), respectively (Bellanti et al., 2017).

The process of producing ATP by phosphorylation of ADP is called oxidative phosphorylation: it occurs by a sequence of reduction and oxidation (redox) reactions that generate a transmembrane electric potential coupled with the transport of protons across the inner mitochondrial membrane. The system is composed of an orchestrated chain of enzymes called Complex I to Complex IV and F$_1$F$_0$-ATP synthase, which function as proton pumps, plus two intermediary substrates (coenzyme Q and cytochrome c). They are located at the inner mitochondrial membrane and are associated with electron donors (NADH and FADH$_2$). During the ETC steps, a small percentage of electrons does not react with protons and instead directly reacts with oxygen at the phase of complex I and complex III, forming the radical oxygen species (ROS) superoxide anion radicals (O$_2^{\bullet-}$) (Mansouri et al., 2018; St-Pierre et al., 2002).

Enzymes such as NADPH oxidase (NOS), xanthine oxidase (XO), lipoxygenases (LOX), and cyclooxygenases (COX) can also produce superoxide anions (Curtin et al., 2002).

Secondary ROS can be produced via enzymatic activity, like superoxide dismutase (SOD). SOD reduces superoxide anion to hydrogen peroxide (H_2O_2), which can be transformed via the Fenton reaction into hydroxyl free radical ($HO^\bullet$). Nitric oxide (NO), an important intracellular signal transducer, is produced by inducible NO synthase (iNOS) in the cytosol of hepatocytes (or Kupffer cells or endothelial cells) under stimuli such as endotoxin and pro-inflammatory cytokines (Tirmenstein et al., 2000). NO can diffuse inside the mitochondria and react with superoxide, generating the free radical peroxynitrite ($ONOO^-$).

The mitochondrion has a refined system of ROS detoxification: superoxide anions are converted first into H_2O_2 by superoxide dismutase (SOD) followed by transformation into oxygen and water by the enzyme catalase (CAT). H_2O_2, as well as peroxynitrite, can also be safely removed by the action of thioredoxin associated with thioredoxin reductase (TXNRD1) and peroxiredoxin (PRDX), or by reduced glutathione with glutathione peroxidase (GPX) (Balaban et al., 2005). Enzymes that regenerate glutathione and thioredoxin require NADPH, which is used as a substrate for oxidation (Hayes and Dinkova-Kostova, 2014). Mitochondria can generate NADPH via catalytic reaction of the nicotinamide nucleotide transhydrogenase (NNT), isocitrate dehydrogenases 2 (IDH2) and malic enzyme 3 (ME3) (Dey et al., 2016). The enzyme NNT is particularly important for the provision of NADPH since it directly catalyzes the reduction of $NADP^+$ to NADPH coupled to inward proton translocation across the inner mitochondrial membrane (Nickel et al., 2015).

Mitochondrial dysfunction has been shown to be characteristic of NASH affected patients (Bellanti et al., 2017). During the development of NAFLD and subsequent NASH, mitochondria react to the excessive hepatic fatty acid accumulation by increasing β-oxidation. Subsequently, ETC respiration increases, and this favors the overall overproduction of ROS that affects the mitochondrion itself, especially the mitochondrial DNA, which is not protected

by histones and is therefore more prone to oxidative damage and mutations (Begriche et al., 2013). Mitochondrial DNA depletion due to mutations can lead to impairment of proteins involved in the respiratory chain. Moreover, mtDNA depletion triggers the expression of genes that synthesize serine, which feeds the one-carbon (1C) metabolism.

The 1C-metabolism, also called folate metabolism or the folate cycle, has a role in transferring one unit of carbon to 1C-dependent biosynthetic pathways, including nucleotide synthesis and methylation reactions, and for amino acid homeostasis (Bao et al., 2016). During organ development and in proliferative tissues, folate metabolism has an anabolic role in generating mainly purines and thymidine, and secondarily methionine, glycine, or serine. In the frame of increased DNA synthesis during hepatocytes proliferation and neoplastic transformation, the 1C metabolism is upregulated as well (Ducker and Rabinowitz, 2017). The collapsing mitochondrial system at some point manifests electron leakage due to alterations in the ETC complexes and membrane potential ($\Delta\psi m$), which follows mitochondrial permeability transition (MPT) pore opening. The latter results in reduced production of ATP, and promotes ER stress via the UPR (Simões et al., 2018).

There is a strong interconnection between ER stress and mitochondrial dysfunction. The ER requires ATP for protein folding while decreased ATP exacerbates ER stress, since the system continues to accumulate unfolded proteins in the ER lumen. Mitochondria are also highly influenced by ER stress leading to the activation of the intrinsic pathway of mitochondria-mediated apoptosis through JNK regulation and excessive calcium transport to the mitochondria (Ashraf and Sheikh, 2015). JNK, in particular, plays a central role in cell death: its activation can be a product of ER stress and UPR, mediated by IRE-1α and ASK1. JNK can also be activated by SFAs, such as palmitic acid, which promotes lipo-apoptosis. This is driven by palmitic acid, and studies have shown that phosphorylated JNK directly interacts with the outer mitochondrial protein SH3-domain binding protein 5 (SH3BP5/SAB). Subsequently, phosphorylated Sab inactivates the Proto-oncogene tyrosine-protein kinase c-Src, a protein required for a proper ETC function (Win et al., 2015).

The resulting impaired electron transport leads to overproduction of ROS, like superoxide and hydrogen peroxide, which sustain JNK activation (Win et al., 2018). Continuous positive regulation of JNK generates activation of caspase 8 and subsequent BH3 interacting domain death agonist (BID) cleavage and activation of BCL2 associated X protein (BAX) and BCL2-like 11 (BIM). These steps promote outer membrane polarization and cytochrome c release, which executes apoptosis via caspases (Win et al., 2018). The permeability transition pores for cytochrome c release can also be formed due to calcium release from SFA-induced ER stress. This impacts mitochondrial membranes and deregulates ETC (Masarone et al., 2018).

Another direct source of ROS, the mitochondrial cytochrome P450 2E1 (CYP2E1), has been reported in *in vivo* NASH models and in NASH patients (Masarone et al., 2018). CYP2E1 exerts a role in PUFAs metabolism, generating ω-hydroxylated fatty acids from linoleic acid and arachidonic acid. The subsequent metabolism of ω-hydroxylated fatty acids produces dicarboxylic acids, which are known to be toxic at high concentrations (Aubert et al., 2011).

Other factors that drive mitochondrial dysfunction during NAFLD/NASH are GSH depletion and the impairment of the antioxidant defense. In particular, the deregulated genes are mainly catalase (CAT), superoxide dismutase (SOD), and glutathione superoxide transferases (GSTA/GSTM), thus allowing ROS accumulation and mitochondria injury (Simões et al., 2018). In the transition from steatosis to steatohepatitis, free cholesterol, but not FFAs, accumulates in mitochondria resulting firstly in sensitization to TNF-α and Fas, and then in mitochondrial GSH depletion (Marí et al., 2006).

1.2.3.3 Oxidative stress and NASH

Per definition, oxidative stress (OxS) is the unbalanced overproduction of ROS in which the redox homeostasis is lost. During this process, ROS modify

proteins, lipids, and DNA, and the antioxidant and DNA repair mechanisms fail to fix the damage. Under normal physiological conditions, ROS are the by-products of mitochondrial energy metabolism, peroxisomes, ER protein folding and fat metabolism of cytochrome P450. As an exogenous source, ROS act in response to immune stimuli of inflammatory cytokines and against bacterial infection (Zhang et al., 2016). Since the early phase of NAFLD development, until cancer development, ROS interact with many pathways: 1) NF-κB signaling pathway (targeting IκBα and NIK); 2) MAPKs signaling pathway (targeting ERK, JNK, p38); 3) KEAP-NRF2-ARE signaling pathway (dissociating NRF2/KEAP, thus activating NRF2); 4) PI3K-AKT signaling pathway (activating PI3K and inactivating PTEN promoting its degradation); 5) ROS and Ca^{2+} regulation (ROS produced by Ca^{2+} targeting mitochondria for increasing respiration and ROS influences Ca^{2+} channels); 6) ROS and mitochondria potential transition pore opening and apoptosis induction; 7) ROS and blockage of ubiquitination/proteasome, with subsequent mitochondrial dysfunction (Zhang et al., 2016). Apart from mitochondria, ER and peroxisomes produce basal levels of ROS during physiological functions (i.e. protein folding in the ER and β-oxidation in peroxisomes) and higher levels during pathological conditions (Fransen et al., 2012; Yoboue et al., 2018). During oxidative stress ROS attack lipids, proteins, and DNA (Bartsch and Nair, 2006).

Under physiological conditions, fatty acid intermediates function as second messengers for many processes, such as inflammation, survival, proliferation, migration, adhesion, metabolism and stress response (Ayala et al., 2014). But in the context of a prolonged oxidative stress, lipid peroxidation leads to cytotoxic products, starting from the metabolism of ω-3 PUFAs (e.g. docosahexaenoic acid and eicosapentaenoic acid) and ω-6 PUFAS (e.g. arachidonic acid and α-linoleic acid). Lipids, including PUFAs, glycolipids, and cholesterol, are particularly targeted on the site of their carbon-carbon double bonds by hydroxyl radical ($HO^{\bullet}$) and hydroperoxyl radical ($HO_2^{\bullet}$). The $HO_2^{\bullet}$ is formed by the Fenton reaction, where free iron (Fe^{2+}) reacts with H_2O_2, becoming ferric iron (Fe^{3+}). The hydroperoxyl radical ($HO_2^{\bullet}$) is an intermediate between superoxide anion and hydrogen peroxide and is particularly reactive

in initiating the oxidation chain of PUFAs. The lipid peroxidation process consists of three steps: initiation, propagation and termination. In the first step, the radical species abstracts the allylic hydrogen generating the carbon-centered lipid radical (L$^\bullet$). During the propagation step the lipid radical (L$^\bullet$) is transformed interacting with oxygen to lipid peroxyl radical (LOO$^\bullet$), which subsequently extracts hydrogen from another lipid to create a new lipid radical (L$^\bullet$) plus a lipid hydroperoxide (LOOH). Antioxidants in the terminal phase can donate hydrogen to the LOO$^\bullet$ species and form a corresponding antioxidant radical that becomes non-radical reacting with another LOO$^\bullet$.

In NASH and in other chronic liver diseases, the impaired antioxidant response to lipid peroxidation leads to the alternative molecule to the LOOH, termed endoperoxide. Endoperoxide can break down, giving rise to malondialdehyde (MDA) (Ayala et al., 2014). Other major products of lipid peroxidation are 4-hydroxynonenal (4-HNE) and F_2-isoprostane (Linhart et al., 2015; Morrow et al., 1995; Piłacik et al., 2002). These compounds are renowned markers of lipid peroxidation in oxidative stress conditions. MDA and 4-HNE are very reactive towards DNA and induce its modification (Tuma, 2002). In addition, they are involved in processes such as ER stress, senescence, apoptosis and compensatory proliferation (Ayala et al., 2014). Protein carbonylation is an irreversible post-translational modification of protein amino acids carried out by hydroxyl radicals ("primary protein carbonylation") or by aldehydes previously generated by lipid peroxidation such as MDA and 4-HNE ("secondary") (Fedorova et al., 2014). Recently it was found that ROS-induced protein carbonylation can also result in change of amino acids, as it occurs in the reaction Arginine/Proline oxidation → glutamyl semialdehyde oxidation → Glutamic acid, leading not necessarily to loss of function (Suzuki, 2019). The process of lipid peroxidation can also be mediated enzymatically via lipoxygenase (LOX), cyclooxygenase (COX), xanthine oxidase (XO) and cytochrome P-450 (CYP), in the presence of molecular oxygen. In both cases, lipid peroxidation is facilitated by Fe2$^+$ ions (Halliwell and Gutteridge, 1984). For example, XO produces superoxide ions, leading to the generation of singlet oxygen, which undergoes subsequent

reactions with unsaturated fatty acids to form fatty acid hydroperoxides (Pedersen and Aust, 1973).

Several pre-clinical and clinical studies have demonstrated the importance of the microsomal CYP2E1 in exacerbating oxidative stress and in the development of NAFLD and NASH (Leung and Nieto 2013). CYP2E1 plays a role in phase-I detoxification, generating free radicals (Kathirvel et al., 2010). In NAFLD and NASH, CYP2E1 exerts an adaptive response to impaired β-oxidation from peroxisomes and mitochondria, mediating ω-hydroxylation of fatty acids for the compensation of lipid overload. Patients with NASH also display up-regulated levels of the enzyme (Sumida et al., 2013). CYP2E1 KO mice are protected from high-fat diet-induced insulin resistance but are not protected from lipid peroxidation, since compensatory mechanisms increased expression levels of cytochrome 450 CYP4a. In mice overexpressing CYP2E1, insulin resistance, oxidative stress and steatosis were increased (Kathirvel et al., 2010). CYP2E1 is also involved in the oxidation of low-density lipoprotein (LDL), forming oxidized-LDL, responsible for initiation and sustenance of the pro-inflammatory environment in atherosclerosis (Aviram et al., 1999).

Hepatic damage and steatosis can also be induced by hepatotoxic chemical carbon tetrachloride (CCl_4) (Dai et al., 2014; Van Herck et al., 2017). NAFLD models on methionine-choline deficient diet (MCD) in combination with CCl_4, displayed steatosis, mitochondrial dysfunction (ATP depleted), ER stress, senescence (up-regulated p21), fibrosis (up-regulated transforming growth factor beta (TGF-β)), increased p53, lipid peroxidation products, all resulting in defective tissue repair and liver injury (Donthamsetty 2007; Lee 2011; Pan 2007). CCl_4 metabolism by cytochrome P450 in the liver microsome produces reactive intermediates, including trichloromethyl radical ($CCl_3\bullet$) and its derivative, trichloromethylperoxy radical ($CCl_3OO\bullet$) (Dai et al., 2014). CCl_4 reacts with oxygen to form $CCl_3OO\bullet$ and to initiate lipid peroxidation. In addition, it binds covalently to lipids and proteins, leading to hepatocyte damage (Boll et al., 2001). Moreover, lipid peroxidation products, such as F_2-isoprostane, stimulate collagen formation from the HSCs and subsequent

fibrosis (Comporti et al., 2005). The levels of F_2-isoprostane correlated with NAFLD severity and fibrosis in patients (Konishi et al., 2006). Antioxidants such as carotenoids (e.g. Vitamin E, Astaxanthin) and polyphenol catechins (e.g. green tea extract) can inhibit lipid peroxidation and prevent CCl_4-induced hepatic injury (Boll et al., 2001; Elgawish et al., 2015; Kang et al., 2001; Pickett-Blakely et al., 2018).

Another consequence of oxidative stress is the execution of the programmed form of necrosis, termed necroptosis (mediated by TNF-α) (Gautheron et al., 2015; Shindo et al., 2013), and a novel form of cell death mediated by iron, indicated as ferroptosis (Feng 2018; Yang 2016): these forms of cell death further contribute to hepatic injury. In NASH, the accumulation of iron favors Fenton chemistry and the initiation and propagation of lipid peroxidation (Feng et al., 2018; Yang et al., 2016).

1.2.3.4 Chronic inflammation in NASH

Chronic inflammation is a result of the unresolved tissue damage due to the deregulation of the immune system. From a molecular point of view, it is mediated via extrinsic pathways (induced by PAMPs/DAMPs and TLR activation) and by intrinsic pathways (induced by DNA damage, viral DNA integration, oxidative stress) (Yu et al., 2018). Both extrinsic and intrinsic pathways lead to the activation of NF-κB signaling and signal transducer and activator of transcription 3 (STAT3) transcription factors, which stimulate the production of pro-inflammatory chemokines and cytokines, prostaglandins and ROS (Yu et al., 2018). In many cases, a NASH-affected liver shows fibrosis, various forms of cell death (such as apoptosis and necroptosis) and compensatory proliferation of hepatocytes (Akazawa and Nakao, 2018; Boege et al., 2017; Luedde et al., 2014).

NASH is considered a risk factor for developing liver cancers such as hepatocellular carcinoma (HCC) and intrahepatic cholangiocarcinoma (iCCA) (De Lorenzo, 2019; Seydel et al., 2016). Major immune cell contributors to

chronic inflammation in NASH are the KCs (MHCII[+], F4/80[+]) that get activated due to stimulation by PAMPS (e.g. LPS) and DAMPS (apoptotic hepatocytes, lipids) (Miura et al., 2013; Tacke, 2017). KCs mainly get activated through recognition of LPS or other bacterial antigens by TLRs (e.g. TRL4, TRL2, TRL9) and by lipids through scavenger receptors (e.g.CD36). TLR activation leads to the production of pro-inflammatory chemokines and cytokines (e.g. CXCL1, CXCL2, IL-1α and monocyte chemoattractant protein-1 (MCP-1) that recruits neutrophils and circulating monocytes to the liver. Chronic inflammation is established due to the sustained survival of neutrophils by KC-produced growth factors like granulocyte-macrophage colony-stimulating factor (GM-CSF), granulocyte colony-stimulating factor (G-CSF) and TNF-α (Prame Kumar et al., 2018).

Moreover, neutrophils produce IL-6, which induces naive T helper cells to differentiate into Th17 cells. Th17 amplifies the pro-inflammatory signals with interleukin-17 (Gomes et al., 2016). High levels of IL-17 are also found in NASH patients (Rau et al., 2016). During early events in NASH development, KCs induce hepatic steatosis and liver injury by secretion of interleukin 1α (IL-1α), IL-6 and TNF-α, which promotes fatty acid uptake, reduces lipid export, suppresses β-oxidation, and promotes hepatic apoptosis (Tacke, 2017; Tosello-Trampont et al., 2012). Fundamental for the transition from NAFL to NASH is the production of ROS by KCs and of pro-inflammatory cytokines such as TNF-α, IL-6 and the chemokine CCL2, which recruits circulating Ly6C^{+} monocytes. These infiltrative Ly6C^{+} monocytes, commonly deriving from bone marrow progenitor cells (called bone-marrow monocyte-derived macrophages-MoMFs), differentiate into pro-inflammatory macrophages: they are able to activate HSCs which transdifferentiate in collagen-producing myofibroblasts (secreting TGF-β1 and PDGF) and at the same time they recruit NK cells to the liver (Tacke, 2017).

Recently it was found that MoMFs, under conditions of hepatic injury or due to massive KC depletion, can replenish the liver macrophage population by differentiating into KCs (Guillot and Tacke, 2019). Pharmacological inhibition of CCL2 or genetic deletion of CCR2/CCL2 could ameliorate liver fibrosis in

pre-clinical models and in patients with NASH (Friedman et al., 2018; Krenkel et al., 2018). We have recently shown that KCs are involved in the initiation as well as in the late stages of NASH through hyaluronan-CD44 interaction with platelets (Malehmir et al., 2019). The platelets also contribute to the recruitment of neutrophils to the liver (Rossaint et al., 2018). KCs can take up oxidized low-density lipoproteins (oxLDL) and oxidized lipids derived from apoptotic hepatocytes (e.g. oxidized phosphatidylcholine, oxPC) via the class B-scavenger receptor CD36 (Ikura et al., 2005). CD36 upregulation is linked to NF-κB-mediated inflammatory responses which follows pro-inflammatory cytokines release (IL-1β, IL-6 and IL-8) and T cell proliferation (Chávez-Sánchez et al., 2014). The regulation of CD36 is transcriptionally regulated by pregnane X receptor (PXR), peroxisome proliferation-activated receptor gamma (PPRγ) and by liver X receptor (LXR) (He et al., 2011).

Scavenger receptors for oxLDL are also expressed by hepatocytes (CD36), HSCs (CD36 and lectin-like oxLDL receptor 1(LOX-1)) and LSECs (Houben et al., 2017). The detrimental effects of oxLDL uptake rely on KC inflammasome activation and on impaired autophagy. In the hepatocytes, CD36 activation leads to inflammasome activation plus apoptosis. In HSCs the activation of scavenger receptors results in the synthesis of extracellular matrix and fibrosis, whereas in LSECs, activation of NF-κB signaling, endothelial injury and defenestration occurs (Houben et al., 2017).

Apart from macrophages, other immune cells are involved in chronic inflammation of NASH pathogenesis, such as T cells, NKT, NK cells and neutrophils. CD8^{+} T and NKT cells (Wolf et al., 2014) have been shown to play a role in exacerbating NASH in mouse models where depletion of these cells ameliorates fibrosis and reduces the activation of KCs and infiltrating macrophages. In particular, CD8^{+} T cells are increased in livers of NASH-affected patients (Bhattacharjee et al., 2017).

1.2.4 Therapies against NASH

Current therapies and clinical trials for NASH **(table 1)** aim to target metabolic dysfunction, oxidative stress, inflammation, apoptosis and fibrosis. The main goal of NASH therapies is to ameliorate dyslipidemia, reduce inflammation and apoptosis, but most of all they aim to reverse or prevent liver fibrosis/cirrhosis. The presence of advanced fibrosis constitutes not only a predictor of liver-related mortality in NAFLD/NASH patients but also a relevant risk factor for developing HCC (Chalasani et al., 2018; White et al., 2012). A novel, accurate, non-invasive method was recently developed to distinguish advanced- from early-stage fibrosis: it measures the liver stiffness through vibration-controlled transient elastography (VCTE) (Siddiqui et al., 2019).

The most recommended and adopted therapy for biopsy-proven NASH patients so far is the combination of pioglitazone and vitamin E, but the long-term efficacy or safety still need to be evaluated (Sumida and Yoneda, 2018; Chalasani et al., 2018). Statins and PPARα/δ agonists have been proven to ameliorate steatosis by increasing fatty acid β-oxidation and reversing insulin resistance, although they cannot improve hepatic injury, which phenotypically by ballooning of hepatocytes (Ratziu et al., 2010). The phase-II trial of the inhibitor of the vascular adhesion protein-1 (VAP-1) (BI 1467335) has been proven to have anti-inflammatory and antifibrotic effects in NASH patients by reducing oxidative stress (Weston et al., 2015). Based on the promising effects of these antioxidant therapies, preclinical studies are directed now towards a novel treatment using a synthetic recombinant form of the antioxidant enzyme mitochondrial manganese (Mn) SOD (MnSOD-2), which can reach the mitochondrial matrix and can effectively scavenge intra- and extracellular superoxide ions. Preclinical tests in CCl_4-treated mice have already shown reduced cirrhosis and portal hypertension in the liver (Borrelli et al., 2018).

Drug class	Compound	Target	Ref.
Anti-lipopolysaccharide antibody	IMM124E	LPS	NCT02316717
Antioxidants	Vitamin E, cysteamine	oxidative stress	Sanyal et al., 2010; Schwimmer et al., 2016
Apoptosis signal regulating kinase 1/mitogen-activated protein kinase-5 inhibitors	Selosertib/GS-4997	ASK1/MAP3K5 (oxidative stress)	Loomba et al., 2018
Caspase inhibitors	Emricasan/ IDN-6556, GS-9450/LB84451	caspases	Barreyro et al., 2015; Shiffman et al., 2019; Ratziu et al., 2012
CC-chemokine receptor 2/5 inhibitor	Cenicriviroc	CCR2/CCR5	Friedman et al., 2018
Dipeptidyl peptidase-4 inhibitor	Sitagliptin, Evogliptin	DDP-4	Cui et al., 2016
Farnesoid X receptor agonists	Obeticolic acid	Farnesoid X receptor	Hegade et al., 2016
Glucagon-like peptide-1 analogue	Liraglutide	GLP-1 mimic	Armstrong et al., 2016
Mechanistic target of rapamycin protein inhibitors	MSDC-0602K	mTOR	NCT02784444
Peroxisome proliferator-activator receptor agonists	Rosiglitazone, Pioglitazone	PPARα/δ	Ratziu et al., 2016
Semicarbazide-sensitive amine oxidase/vascular adhesion protein-1 inhibitors	PXS4728A	SSAO/VAP1	NCT03166735
Statins	Rosuvastatin, Atorvastatin,	HMG-CoA reductase	Kargiotis et al., 2015
Toll-like receptor 4 antagonists	Nalmafene/JKB-121	TLR4	NCT02442687

Table 1. NASH therapies and clinical trials (source: ClinicalTrials.gov).

1.3 Hepatocellular carcinoma (HCC)

1.3.2 HCC epidemiology and risk factors

Hepatocellular carcinoma is the most prevalent primary liver cancer and the fourth leading cause of cancer-related death worldwide (Yang et al., 2019). The highest HCC incidence rates are observed in Asia and Africa, followed by Central Europe (O´Rourke et al., 2018) **(fig.4)**.
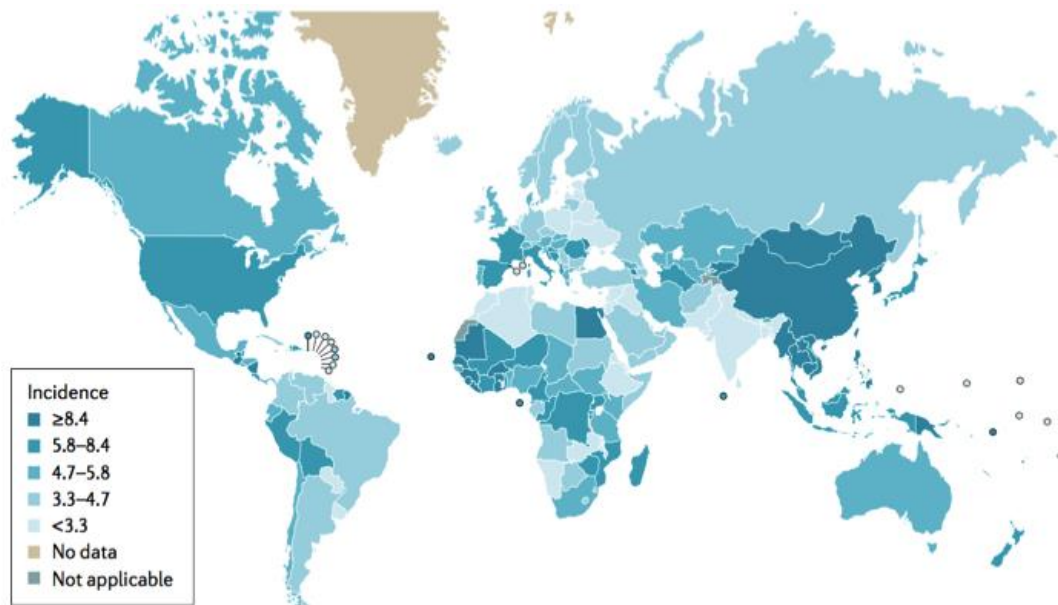
Figure 4. Worldwide incidence of primary liver cancer. Indicated are the incidences per 100,000 person-years. HCC accounts for 80–90% of primary liver cancer (adapted from Yang et al., 2019).

The predominance of specific risk factors depends on the geographical area. In Asia and Africa, hepatitis B virus (HBV) infection and exposure to the hepatotoxic chemical aflatoxin B1 are common risk factors (McGlynn and London, 2011). In industrialized countries, the highest risk factors are hepatitis C virus (HCV) infection, alcohol consumption (leading to alcoholic liver disease, ALD), obesity (Larsson and Wolk, 2007) and related diseases like metabolic syndrome, diabetes, NAFLD and NASH (Afshin et al., 2017). Other risks factors include hereditary metabolic diseases, such as genetic hemochromatosis (defect in iron metabolism with associated hepatic iron overload), Wilson`s diseases (defect in copper metabolism with associated copper deposition in the liver), α1-antitrypsin deficiency (accumulation of mutated α1-antitrypsin in hepatocytes). Finally, the presence of autoimmune diseases such as autoimmune hepatitis (AIH) and primary biliary cholangitis (PBC) is also a risk factor for HCC (Trivedi and Cullen, 2011).

HCC generally occurs on the background of long-lasting chronic disease, characterized by a dysregulated immune system and fibrosis, which eventually might progress to cirrhosis (Fattovich et al., 2004). Although cirrhosis is present in the 70-80% of HCC cases, it is not a necessary

precondition to getting cancer. There are conditions without cirrhosis associated with HCC, such as metabolic pathologies (NAFLD, hemochromatosis, α1-antitrypsin deficiency, Type 1 glycogen storage disease, Type 1 hypercitrullinemia), chemical substances intoxication like aflatoxin B1, some congenital conditions (Alagille syndrome), sex hormones (anabolic steroids) or for vascular pathologies (e.g. Budd Chiari) (O´Rourke et al., 2018). This suggests that it is rather the duration and severity of the chronic inflammation and the unresolved hepatocyte damage with subsequent genetic instability that ultimately determines the risk for HCC development (Boege et al., 2017).

1.3.3 NASH-induced HCC

Non-resolving inflammation characterizes the development and progression of HCC. NASH, being a chronic inflammatory disease, is now one of the major risk factors for HCC development, together with HCV-induced hepatitis and alcoholic steatohepatitis (ASH) (Singal and El-Serag, 2015) **(fig.5)**. Three major driver pathways have been identified in NASH-induced HCC: metabolic, immunological (activated by lipid peroxidation, dysbiosis and cell death) and genetic and epigenetic pathways (PNPLA3 and TM6SF2 genetic variations) (Kutlu et al., 2018).
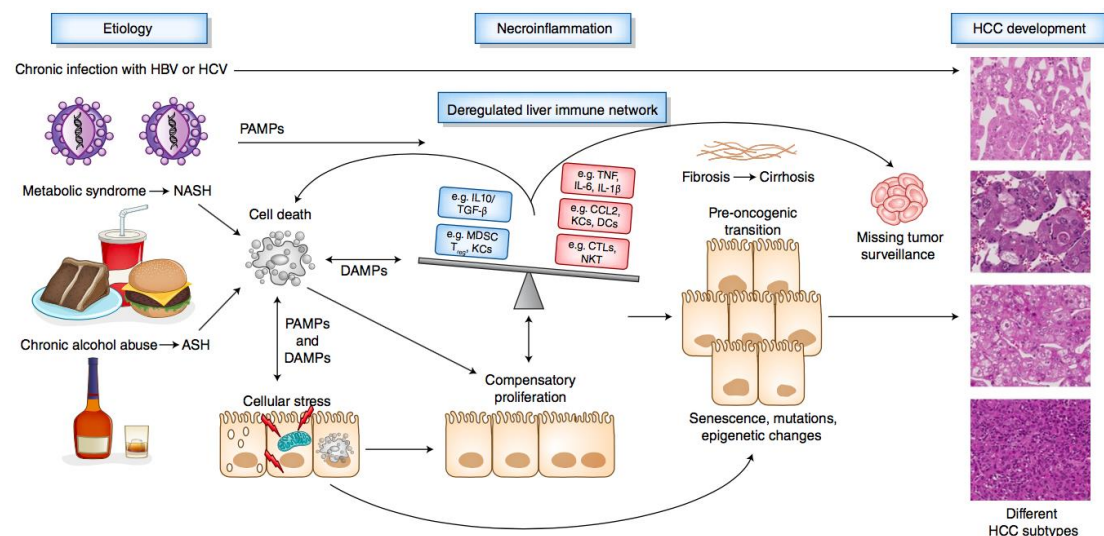
Figure 5. Non-resolving inflammation and HCC progression (from Ringelhan et al., 2018). Different etiologies (viral hepatitis, ASH and NASH) induce chronic liver disease, characterized by cell-death and inflammation (necroinflammation), compensatory proliferation and fibrosis, with subsequent neoplastic transformation and HCC formation. HCC development is also favored from a missing tumor surveillance.

The metabolic pathways contributing to the transition from NASH to HCC derive from the aberrant lipid metabolism that subsequently leads to hepatic lipotoxicity, insulin resistance, ER stress and oxidative stress (Hirsova and Gores, 2015). Insulin resistance is induced by lipotoxicity (Unger and Zhou, 2001), which impairs β cell function and increases the expression of insulin or of insulin-like growth factor-1 receptor (IGF1R) in hepatocytes. This initiates a signaling cascade that eventually activates PIK3K and MAPK pathways, via mTOR and Wnt/ß-catenin, respectively. This favors HCC development through increased proliferation and inhibition of apoptosis (Chettouh et al., 2015).

ER stress has been shown to be a major contributor to chronic liver damage and subsequent HCC, both in HCV transgenic mice and in a NASH model with upregulated folding and secretion capacity (urokinase plasminogen activator (uPA) from the liver-specific major urinary protein (MUP) promoter). In MuPA mice fed a high-fat diet, ER stress was established, together with the accumulation of the autophagy adaptor protein p62 (Nakagawa et al., 2014). The protein p62, encoded by *SQSTM1* gene, mediates the transport of polyubiquitinated proteins and organelles for autophagosomal-lysosomal degradation. In NASH, autophagy is impaired, allowing the accumulation of undegraded p62 (Tanaka et al., 2016).

Furthermore, p62 is a major component of Mallory-Denk bodies (MDB), together with intracellular hyaline bodies and cytokeratin 8 and 18. The presence of MDB is considered a hallmark of chronic liver disease and is associated with HCC predisposition (Zatloukal et al., 2007). P62-containing aggregates have been found in 50% of HCC specimens (Denk et al., 2006). A study investigating HCC *in vivo* has showed that the liver-specific p62 ablation could prevent HCC development (Umemura et al., 2016). Moreover, a genetic association between p62 and NASH-induced HCC has been identified (Pelusi

et al., 2019). Studies have proposed that p62 acts via NF-κB signaling or oxidative stress (Mathew et al., 2009). ER stress and oxidative stress are also intimately connected for the activation of immune pathways, through the execution of apoptosis following stimulation of IKKβ-(inhibitor of kappa light polypeptide gene enhancer in B-cells, kinase beta) dependent NF-κB signaling that results in hepatocyte survival and inflammatory response, thus promoting carcinogenesis (Pikarsky et al., 2004).

Furthermore, extracellular FFAs themselves can trigger IKKβ, engaging TRL4 on hepatocytes (Jia et al., 2014). ROS and products of oxidative stress, such as peroxidized lipids, increase the release of pro-inflammatory cytokines like TNF-α and IL-6 (Park et al., 2010). IL-6 has been reported to activate STAT3 (signal transducer and activator of transcription 3), a key transcription factor for T-cells independent NASH-HCC transition (Grohmann et al., 2018), for the transformation of tumor progenitor cells to HCC (He et al., 2013) and for HCC progression and metastasis (Li et al., 2006).

During NASH pathogenesis, the innate immune system, including KCs, is stimulated via TLRs by molecules released from gut microbiota. This includes PAMPS (such as LPS, peptidoglycans, unmethylated GpG motifs) (Miura et al., 2016) and DAMPS (apoptotic/necroptotic hepatocytes mediators as HMGB1, heat shock proteins, ATP) (Krysko et al., 2012; Kutlu et al., 2018). HCC development is also favored by gut microbial metabolites that activate the hepatic senescence secretome (Yoshimoto et al., 2013).

Liver fibrosis is regarded as risk factor for developing HCC (Llovet et al., 2016). The majority of HCC cases present on a background of cirrhosis (El-Serag and Rudolph, 2007). The development of fibrosis occurs when hepatocytes are repeatedly injured, thus leading to increased ROS and lipid peroxide production and secretion of pro-inflammatory and pro-fibrotic cytokines (e.g.TNF-α), platelet growth factor (PDGF), transforming growth factor β 1 (TGF-β1)) (Sircana et al., 2019). Quiescent HSCs get activated by cytokine stimulus by hepatocytes and by KCs, which respond by secreting collagen. In addition, TGF-β1 plays a crucial role in cancer progression since it promotes apoptosis resistance and cell proliferation in early stages of

hepatocarcinogenesis. TGF-β1 has been proposed as serological early detection marker for HCC (He and Liu, 2016). Moreover, high levels of TGF-β1 were associated with decreased survival in unresectable HCC cases (Chen et al., 2019).

The exact role of the adaptive immune system in the development of NASH-induced HCC still remains to be fully elucidated. Studies indicate the involvement of NKT and CD8$^+$ T cells in NASH pathogenesis and subsequent HCC via LTβR and canonical NF-κB signaling (Haas et al., 2019; Wolf et al., 2014). In addition, human liver sections from patients with NASH showed increased CD8$^+$ T-cells (Bhattacharjee et al., 2017). Another study has shown CD4$^+$ T cells are protective for HCC development: conceptually CD4$^+$ T cells, under PUFAs treatment, undergo mitochondrial-derived ROS accumulation which results in their depletion (Ma et al., 2016).

Important cells of the innate immune system promoting and sustaining HCC are the tumor-associated macrophages (TAMs), mainly derived from circulating monocytes (Capece et al., 2013). They are recruited to the liver by chemokine (C-C motif) ligand 2 (CCL2), macrophage colony-stimulating factor (M-CSF), VEGF and TGF-β1, and they primarily polarized towards the M2 phenotype, a macrophage subtype responsible for tissue remodeling and tumor progression. TAMs produce pro-inflammatory cytokines and growth factors that sustain tumor growth, such as IL-6 and TGF-β1. During the stage of invasion and metastasis, TAMs produce the cytokines TNF-α, osteopontin (OPN), metalloproteases (MMPs), and IL-6 (Capece et al., 2013). At early stages of hepatocarcinogenesis, IL-6 is mainly produced by KCs or macrophages (Maeda et al., 2005), upon stimulation of TLR-4 (by LPS), TNF-α, or IL-1 (Kishimoto, 2010). The binding of IL-6 to the IL-6 receptor (IL-6R) (or to the soluble receptor (sIL-6R)) leads to formation of a complex with the associated receptor glycoprotein 130 (gp130), that subsequently triggers intracellular signaling pathways such as MAPK, PI3K and STAT1/STAT3 pathway (Schaper et al., 2015). IL-6 is involved in acute phase response and infection defense, hepatic metabolism and regeneration, but a prolonged activation of IL-6 signaling eventually leads to the formation of HCC.

Many studies have demonstrated that DEN or CCl_4 treatment after metabolic activation of CYP2E1 generate metabolites that promote DNA adducts and stimulate secretion of IL-6 by KCs. Injured hepatocytes, stimulated by IL-6, undergo a process of compensatory proliferation and accumulate DNA mutations over time (Maeda et al., 2005). This process favors the transformation of hepatocytes in pre-neoplastic lesions, also called foci of altered hepatocytes (FAH). It was shown that pre-neoplastic lesions contain HCC progenitor cells (HcPCs), which have acquired an autocrine IL-6 secretion to sustain their expansion for HCC development in a pro-inflammatory environment (He et al., 2013). In the transition from NASH to HCC, the amount of Ly6C$^+$ macrophages also increase, augmenting the levels of IL-6 and TNF-α in response to LPS via TLR4 (Miura et al., 2016). Similarly, in NAFLD-associated HCC human specimens, mRNA expression levels of TLR4 in macrophages are increased (Nguyen et al., 2018). Moreover, high serum levels of IL-6 are correlated to HCC predisposition and are present in 40% of HCC cases (Soresi et al., 2006).

Genetics can also be an important predisposing factor to develop NASH and HCC. It has been reported in several human NASH and HCC studies the presence of variants of the genes *PNPLA2, TM6SF2, APOB* and *TERT* (Taliento et al., 2019). In NAFLD/NASH patients exists an association between fibrosis and a variant for *TM6SF2* (Liu et al., 2014). A polymorphism of *TM6SF2* gene (rs58542926) is associated with HCC occurrence in alcohol-related cirrhosis (Yang et al., 2018). The *PNPLA3* variant is instead linked to more severe NAFLD (Sookoian and Pirola, 2011). Those two variants are also linked to HCC development, in the context or not, of NASH and ALD. It has been identified that the *PNPLA3* variant can lead to HCC in non-fibrotic livers, thus suggesting a direct role of PNPLA3 in carcinogenesis (Yang et al., 2019).

1.3.4 Oxidative stress and HCC

Ninety percent of HCC cases are a result of chronic inflammatory diseases (Fu and Chung, 2018), whereas 10% are attributable to genetic diseases such as hereditary hemochromatosis (HH) (Ye et al., 2016) and α-1 anti-trypsin

deficiency (Topic et al., 2012). Chronic inflammatory liver diseases are characterized by the generation of oxidative stress that leads to sustained activation of the immune system and DNA damage, mediated by ROS themselves and resulting products like peroxidized lipids and modified proteins. It has been demonstrated that not only in NASH (Font-Burgada et al., 2016), but also in the context of HCC, oxidative stress plays a crucial role (Cardin et al., 2014). Liver cancer patients displayed much higher levels of oxidative damage in respect to controls and to chronic inflammatory diseases **(table 2)**.

DNA adducts	Tissue 8-OHdG (IHC): 8.605 staining intensity compared to 4.845 in nonalcoholic steatohepatitis controls (p = 0.003)
	Tissue 8-OHdG (HPLC): 52 fmol/µg DNA compared to 129 fmol/µg in adjacent normal tissues (p = 0.003)
Lipid peroxidation products	Plasma MDA (TBARS): 1.01 ± 0.28 µmol/L compared to 0.97 ± 0.88 µmol/L in corresponding post-resection samples (p < 0.05)
	Tissue MDA (TBARS): 0.46 ± 0.50 µmol/g protein compared to 0.85 ± 0.42 µmol/g in adjacent normal tissues (p < 0.05)
	Tissue MDA (TBARS): 0.49 nmol/mg protein compared to 0.71 nmol/mg in adjacent normal tissues (p = 0.001)
	Plasma MDA (HPLC): 3.26 ± 0.46 nmol/mL (stage I/II) and 5.83 ± 0.68 nmol/mL (stage III/IV) compared to 1.10 ± 0.23 in controls (p < 0.05)
	Plasma oxidized-LDL (ELISA): 37.64 ± 8.00 U/L compared to 33.72 ± 8.71 U/L in corresponding post-resection samples (p < 0.05)
	Urine 8-iso-PGF2α (LC-MS): 0.92 pmol/mg creatinine compared to 0.8 pmol/mg in controls (p < 0.001)
Protein carbonylation (PC) products	Plasma PC content (DNPH): 0.3 nmol/mg protein compared to 0.2 nmol/mg in controls (p = 0.0083)

Table 2. Direct and indirect clinical oxidative stress markers for liver cancer patients (modified from Katerji et al., 2019).

Oxidative stress also plays a role in the pathogenesis of genetic diseases that cause HCC (Houglum et al., 1997; Marcus et al., 2012). For example, in HH, the liver undergoes iron accumulation that increases ROS production and OxS through the iron-dependent Fenton reaction (Ko et al., 2007). There is also an increased primary liver cancer risk associated with high levels of serum ferritin and ferrous ions in the general population, as evaluated by meta-analysis (Tran et al., 2019). High levels of 4-HNE and MDA were found in a mouse model of chronic iron feeding (Moroishi et al., 2011). Furthermore, the endogenous antioxidant system was impaired, displaying depleted, reduced glutathione and decreased activity of SOD (Houglum et al., 1990). Muto and collaborators (2019) used an engineered mouse model was used with ablated iron-sensing ubiquitin ligase FBXL5 in combination with chemical or viral carcinogen treatments to show a link between iron overload and HCC. Iron homeostasis promoted OxS, followed by lipid peroxidation of cellular membranes and DNA damage, eventually leading to HCC (Muto et al., 2019).

Lipid peroxidation results in HNE adducts that can cause mutations in p53, which are reported to be prevalent in approximately 50% of HCC cases (Hu et al., 2002). The iron overload and mutations in p53 were also found in non-tumorous tissues (Hussain et al., 2000). HNE mainly forms HNE-dG adducts which lead to unrepaired single-strand breaks and increases liver cancer incidence (Huang et al., 2010; Winczura et al., 2014). Evidence of lipid peroxidation linked to carcinogenesis is found in propano DNA adducts (γ-OHPdG), which are mutagenic and promote DEN-induced HCC (Fu et al., 2018) and NASH-induced HCC (Coia et al., 2018b). Furthermore, γ-OHPdG adducts are frequently detected in human HCC specimens and are prognostic biomarkers predicting survival and HCC recurrence (Coia et al., 2018a; Fu et al., 2018). ROS can directly lead to the formation of pro-mutagenic DNA adducts. 8-oxo-7,8-dihydro-2′-deoxyguanosine (8-oxo-dG) is a common DNA mutation that is used as marker for OxS and as a putative predictor of carcinogenesis. 8-oxo-dG adducts are more prevalent in NASH-induced HCC patients compared to patients with NASH only (Tanaka et al., 2013).

The serum quantification of reactive oxygen metabolites, such as hydrogen peroxide, can be indicative of the risk of HCC recurrence after surgical resection or after treatment with radiofrequency ablation (RFA) (Suzuki et al., 2013). DNA modifications by ROS play a significant role in the transformation from normal to malignant cells. During chronic inflammation, oxidative stress leads to the activation of the NF-κB pathway, iNOS, and cyclooxygenase-2 that produces further ROS/RNS which, in addition to modifying DNA bases, can lead to DNA single-strand breakage, as is the case for peroxynitrite anion (ONOO⁻), produced by the combination of NO with oxygen species, that highly reacts with DNA (Bartsch and Nair, 2006). ROS/RNS can also induce point mutations, aberrant DNA cross-linking, and mutations in proto-oncogenes and tumor-suppressor genes, all favoring neoplastic transformation (Hussain et al., 2003).

Mitochondria are one of the first targets of OxS due to the proximity of ROS derived from oxidative phosphorylation. Mitochondrial DNA (mtDNA), protein and membrane lipids (e.g. cardiolipin) are affected by ROS modification, thus leading to cell death. Tetralinoleicardiolipin (L_4CL), the major form of

cardiolipin, contains four linoleic acid chains that are easily oxidized during oxidative stress (Zhong et al., 2017). The oxidation of L_4CL produces 4-HNE that attaches to mtDNA and also forms adducts with mitochondrial proteins, of which the majority belong to the ETC, which eventually results in depleted ATP and apoptosis (Zhong et al., 2017). The lipid hydroperoxide of L_4CL, which remains on the membrane, favors the permeabilization and mobilization of cytochrome c through BAX and BID that induce apoptosis (Hauck and Bernlohr, 2016).

Cell death induces a subsequent compensatory proliferation of hepatocytes (Kamata et al., 2005). In particular, OxS promotes hepatic injury, cell death and inflammation via the activation of pathways like mitogen-activated protein (MAP) kinase/AP-1, NF-kB and hypoxia-inducible transcription factor 1 alpha (HIF-1α) (Klauning et al., 2010). Additionally, nitrosative stress (overproduction of reactive nitrogen species for upregulation of the enzyme iNOS) is known to be involved in cancer promotion by activation of AP-1, which regulates proliferation (Reuter et al., 2010). Recently, it was shown that the hepatic oxidative environment causes an oxidation and inactivation of T cell tyrosine phosphatase (TCTPT), thereby increasing STAT1 and STAT3 signalling, subsequently leading to the development of NASH and fibrosis or HCC (Grohmann et al., 2018). The link between OxS and inflammation is exemplified by OxS-driven activation of NF-κB and the JNK/IKK/p38 MAPK signalling pathways (Li et al., 2016). Just recently, p38 MAPK was identified as an essential factor for cell cycle progression and liver cancer development (Tomás-Loba et al., 2019).

Although it is evident that OxS plays an important role in chronic inflammation and cancer, further studies are required to determine whether antioxidant therapies might be effective for HCC management (Takaki and Yamamoto, 2015). Several mouse models of NASH-induced HCC have been studied in order to unravel the mechanisms behind this transition (Anstee et al., 2019). A mouse models fed a long-term (12 months) choline-deficient high fat diet, following the choline deficiency as reported in NASH patients (Corbin and Zeisel, 2012), could recapitulate the human NASH-induced HCC (Wolf et al., 2014). Another model for diet-induced HCC instead combined CCl_4-treated

liver in combination with Western Diet (fat plus sucrose) and cholesterol (Tsuschida et al., 2018), which could establish 100% cases HCC in 5 months. A further model established in mice ER stress (MUP-uPA mice, overexpressing urokinase plasminogen activator (uPA) specifically in hepatocytes) in combination with high-fat diet, showing hallmarks of NASH and displayed NASH-induced HCC with an incidence of 50% at 10 months of diet (Nakagawa et al., 2014). Some other models employed carcinogenic as diethylnitrosamine (DEN) or overexpressed oncogenes (e.g. Proto-Oncogene C-Myc, Unconventional Prefoldin RPB5 Interactor (URI)) in combination with high fat diet to have faster and more aggressive tumors. Overall, all these models displayed oxidative stress, chronic inflammation and fibrosis (Anstee et al., 2019).

1.3.5 HCC therapies

First-line treatment for early diagnosed and localized HCC is surgical resection and liver transplantation. The vast majority of HCC cases unfortunately are diagnosed in advanced stages, when liver is already compromised, including NASH-associated HCC. This severe condition does not allow high dosages of chemotherapy or ionizing radiation treatment. Therefore, the only possible therapeutic treatment is carried out with the pan-kinase (VEGFR-2/3, PDGFR, and Raf) inhibitor Sorafenib, for which indication is limited due to its hepatotoxicity. In addition, this treatment does not have an impact on the 5-year survival rate, which is less than 8% for the very advanced stage (stage-4) (Altekruse et al., 2012). In NASH-affected patients, HCC represents the leading cause of cancer-related death (47%), which is typically diagnosed at advanced stages and which is associated with 5-year overall survival rate of 44.8% (Povsic et al., 2019).

In clinical trials, combined therapies with sorafenib have been shown to be associated with improved prognosis, as for the concomitant treatment with sorafenib and transcatheter chemoembolization (TACE) (Kudo, 2019), or sorafenib with zoledronic acid and clodronate-encapsulated liposomes, which

deplete macrophages (Zhang et al., 2010). Other therapies aim to target TGF-β and EGFR/VEGFR signaling in order to limit tumor growth and extravasation (Fransvea et al., 2010). A comprehensive molecular and immunological characterization has identified three major HCC subtypes: 1) proliferative and stem cell-like tumors displaying chromosomal instability; 2) tumors with β-catenin (CTNNB1/Wnt signaling) mutations with associated immune suppression; 3) metabolic disease-related tumors, further divided into immunogenic and non-immunogenic subclasses. This classification is particularly meaningful, because it does not depend on the origin of the tumor (primary or metastatic) defined by genomic and epigenomic distinction, but it is based on overall phenotypic similarities. Furthermore, this classification has the potential to be useful in the stratification of patients for immunotherapy (Shimada et al., 2019).

In another study it was shown that the steatohepatitis-induced HCC subtype displays frequent activation of IL-6/JAK/STAT3 (Calderaro et al., 2017). A comprehensive characterization based on integrative analysis allowed the identification of a p53 target gene expression signature correlated with poor survival. Furthermore, this study correlated with impaired survival also other frequently mutated genes which can be targetable such as MDM4, MET, VEGFA, MCL1, IDH1, TERT, impacting WNT signaling as well. This study moreover suggested that APOB may be one of the responsible genes involved in metabolic reprogramming from normal hepatocytes to malignant HCC cells (wheeler@bcm.edu and Network, 2017).

In current clinical studies the efficacy of immunotherapy in HCC treatment is investigated (Kudo, 2019). The three main classes of immune-therapy based approaches include checkpoint inhibitors (anti-PLD1, anti-CTLA4); adoptive cell transfer (chimeric antigen receptor (CAR) T cells, cytokine-induced killer (CIK) or NTK cells) and vaccination for the stimulation of peptide-specific cytotoxic T lymphocytes activity (CTLs) (Nobouka et al., 2013).

1.4 Endogenous defense and antioxidant compounds against oxidative stress

1.4.2 Nuclear erythroid 2-related factor 2 (NRF2) mediated antioxidant response

Nuclear erythroid 2-related factor 2 (NRF2) is the key regulator of ROS sensing and cytoprotection that mediates the activation of the antioxidant response when the levels of ROS exceed thus becoming toxic to the cell. Bad nutritional habits, alcohol consumption and exposure to hepatotoxic chemicals (e.g. Aflatoxin) lead to oxidative stress in the body that induces the release of the transcription factor NRF2 from its associated protein Kelch-like ECH associated protein 1 (KEAP1). Under basal conditions, KEAP1 facilitates the ubiquitination and proteasomal breakdown of NRF2, while in response to oxidative stress NRF2 dissociates from KEAP1, enabling NRF2 to translocate to the nucleus. In the nucleus NRF2 binds ARE sequences, allowing the transcriptional expression of proteins belonging to the categories of detoxification, antioxidant enzymes, NADPH regeneration and lipid metabolism (Hayes and Dinkova-Kostova, 2014).

In NASH, the major detoxification enzymes involved are NAD(P)H:quinone oxidoreductase (NQO1) and the family of glutathione-S-transferases (GST) (Itoh et al., 1997). In particular NQO1 contributes to cytoprotection against OxS by directly scavenging superoxides by the induction of endogenous antioxidant enzymes (e.g. SOD and CAT) and by the reduction of ubiquinone and vitamin E quinone to their antioxidant forms (Ross and Siegel, 2017). NRF2 also influences lipid metabolism by regulating the expression of lipases (lipase member H (LIPH), phospholipase A2 (PLA2G7), patatin-like phospholipase domain containing 2 (PNPLA2)) and of enzymes involved in β-oxidation (acetyl-CoA thioesterase (ACOT), acetyl-CoA oxidase (ACOX), carboxylesterase (CES), stearoyl-CoA desaturase-2 (SCD2)) (Hayes and Dinkova-Kostova 2014) **(fig.6)**.
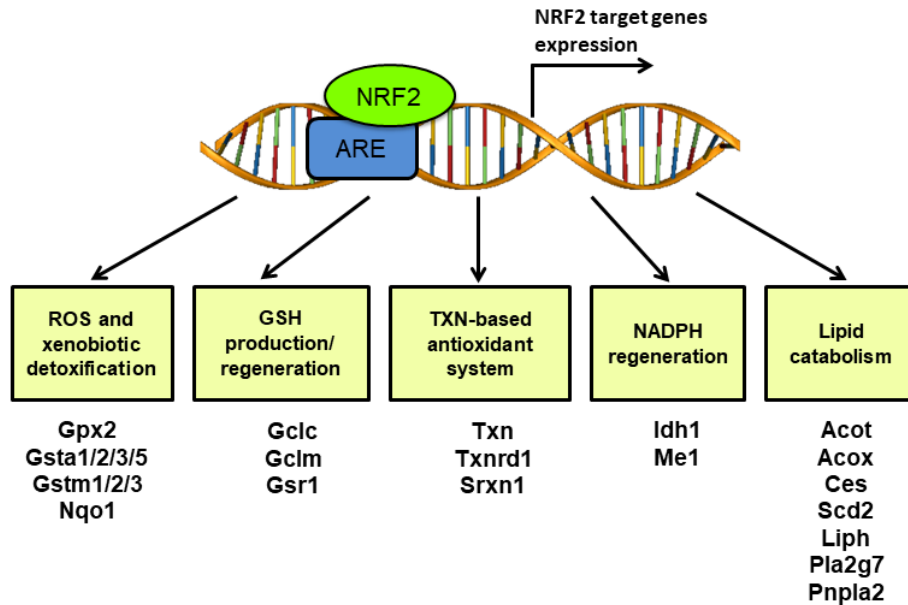
Figure 6. NRF2 and the expression of antioxidant genes. NRF2 translocates to the nucleus binding ARE for the expression of genes involved in xenobiotics detoxification, activity of antioxidant enzymes, NAPH regeneration and lipid catabolism. The latter category includes genes expressing lipases and enzymes involved in β-oxidation.

NRF2 can counteract hepatic fat accumulation by inhibiting lipogenesis, mediated by the repression of the lipogenic transcription factor liver X receptor-α (LXRα) (Kay et al., 2011). Moreover, NRF2 has shown preventive effects in inflammation via NF-κB down-regulation (Wakabayashi et al., 2010) in addition to fibrosis by inhibiting TGF-β signaling in HSCs (Oh et al., 2012; Shimozono et al., 2013). Surprisingly in NASH the expression and activation of NRF2 has been showed to be downregulated (Gupte et al., 2013).

1.4.3 Antioxidants

The function of antioxidant compounds relies on the inhibition of free radical (ROS or NOS) generation and propagation via three main mechanisms: 1) quenching peroxide anions, thereby preventing formation of peroxides, 2) scavenging species that initiate peroxidation (i.e. ROS/NOS), and 3) chelating metal ions (e.g. $Fe2^+$) thus preventing reactive species generation or breakage of lipid peroxides (Brewer, 2011). Antioxidants donate hydrogen to

the free radicals formed during oxidation becoming radicals themselves. Aromatic or phenolic rings of the antioxidants delocalize and so stabilize by resonance the electrons transferred from the free radicals (Lü et al., 2010).

1.4.3.1 Butylated hydroxyanisole (BHA)

Butylated hydroxyanisole (BHA) is a synthetic antioxidant agent belonging to the phenol family. It is widely used for the preservation of food, pharmaceutical products and petrochemicals (Chen and Shaw, 1974). For human consumption BHA is generally recognized as safe by the U.S. FDA (USFDA, 1984, US Food and Drug Administration Food and Drugs. US Codefed. Regul., Title 21, Part 182.3169(1984), p. 380), considering that the amount should not exceed the 0.02% wet weight (w/w) of the total fat or oil content of the food. As an animal food additive, the maximum concentration allowed is 150 mg/kg of feed (EFSA, 2018). Although considered a safe compound, experiments adopting high dosages of BHA have shown metabolic toxicity mainly driven by augmented ROS production (De Oliveira-Pateis et al., 2018).

In vivo studies have shown that BHA in association with carcinogens can enhance tumor development (Fukushima et al., 1987). The compound is commercialized as a mixture of 2 isomers, where the form 3-*tert*-butyl-4-hydroxyanisol (3-BHA) is widely used respect to the other form 2-*tert*-butyl-4-hydroxyanisol (2-BHA). The phenolic ring confers to the BHA an effective ROS scavenger activity and the capacity to enter in the mitochondria, an organelle known to be the highest source of ROS.

BHA is known to be protective against oxidative stress and carcinogenesis (Hirose et al., 1999). It is known to regulate the expression of the ROS sensor NRF2, thus leading to the upregulated expression of target genes such as NQO1 and GST, involved in the detoxification of toxic compounds as well as ROS (Itoh et al., 1997). The induction of NRF2 activation is believed to be due

to the oxidized form of BHA, the tert-butyl-1,4-benzoquinone (Hayes et al., 2000; Wang et al., 2010).

It has been shown that BHA can interfere with the synthesis of prostaglandin and reduce inflammation (Levine, 1983), In combination with its analogue, 2,6-di-tert-butyl-4- methylphenol (BHT), BHA strongly reduces inflammation by blocking COX-2 activity and TNF-α production upon LPS challenge (Murakami et al., 2015). In a study performed on rats receiving an oil-based fat diet at 50 mg/(kg.day), BHA abolished or majorly decrease fatty acid liver infiltration (Abu-el-zahab et al., 1993). When combined with a renal and hepatotoxic carcinogenic agent called ferric nitrilotriacetate, BHA diminished liver damage, lipid peroxidation, hydrogen peroxide production and increased antioxidant enzymes (Ansar and Iqbal, 2015). Similar effects were shown in a study using the lipophilic hepatotoxin CCl_4, in which BHA could block lipid peroxidation, reflected by reduced MDA levels. In addition, the activity of anti-oxidant genes (SOD, CAT, GPX and glutathione) was restored (Dassarma et al., 2018). Fatty acids, in particular saturated fatty acids, are also able to induce liver injury. BHA can reduce hepatic fatty acid accumulation, counteract diet-induced mitochondrial dysfunction and impede apoptotic cell death via JNK inhibition even more efficiently than the pan-caspase anti-apoptotic inhibitor zVAD (Win et al., 2015).

1.4.3.2 Astaxanthin (AXT)

Astaxanthin (3,3′-dihydroxy-β, β-carotene-4,4′dione) (AXT) is a xanthophyll carotenoid, mainly found in the microalgae *Haematococcus pluvialis (H.pluvialis)*. Its structure confers powerful anti-oxidant properties, thanks to the two terminal rings of cyclohexene with two oxo-groups joined by a long polyene chain of thirteen double bonds **(fig.7)**.
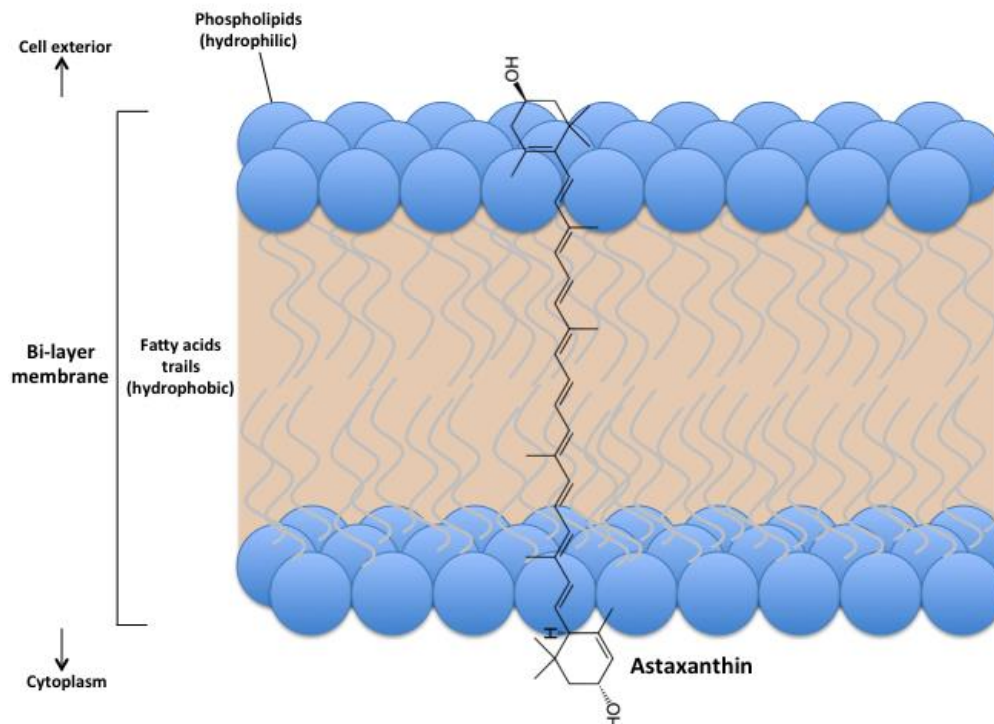
Figure 7. Astaxanthin membrane localization. The chemical structure of AXT allows the compound to intercalate between the phospholipidic by-layer of the cell membrane. This confers advantages respect to other antioxidants, since the ROS-scavenging activity is exerted both externally and internally to the cell.

AXT scavenges singlet oxygen a hundred times more effectively than vitamin E and five times more than β-carotene (Nishida 2007). This is due to the structure that gives polarity to the molecule that interpolates between the two phospholipidic cellular membranes. The free radicals are quenched either in the cell membrane due to the polyene chain, either at the surface and intracellularly due to the terminal rings (Goto et al., 2001; Yuan et al., 2011). The extract of *Haematococcus pluvialis* was approved by the Food and Drug Administration (FDA) as a safe food supplementation (EFSA, 2014; Spiller and Dewell, 2003).

AXT is a liposoluble compound and the degree of its absorption depends on the amount of ingested dietary lipids. As dietary fats, AXT is assimilated with lipoproteins and can be secreted into the circulation. Liver is the organ that predominantly accumulates the compound (Showalter et al., 2004). Clinical reports have demonstrated the efficacy of AXT in promoting redox balance (Park et al., 2010), which ameliorates the inflammatory status in obesity (Choi

et al., 2011a; Choi et al., 2011b) and cardiovascular diseases (Visioli and Artaria, 2017; Yoshida et al., 2010). Beneficial effects have also been shown for skin aging (Kim and Kim, 2018).

In numerous murine models for hepatocellular damage driven by chemicals (e.g. carbon tetrachloride, CCl_4), ischemic reperfusion injury (Li et al., 2017) and dietary-induced NAFLD and NASH (Romestaing 2007; Ni 2015; Ni 2016), treatments with AXT ameliorated the pathological conditions, mainly indirectly influencing the levels of ROS. AXT has proven its efficacy also against nitrosative stress (Bi et al., 2017). Although its direct antioxidant effect in scavenging ROS is proven in cell lines (Kim and Kim, 2018; Nishino et al., 2016), in the liver AXT counteracts OxS by inhibiting the levels of lipid peroxidation (Kang et al., 2001; Karppi et al., 2007) and by increasing the activity of endogenous cellular antioxidant enzyme such as SOD and CAT (Kim and Kim, 2018). The lipophilic property of the molecule favors accumulation in the mitochondria (Takahashi et al., 2004), where it intercalates in the inner mitochondrial membrane and helps maintain energy metabolism via increased activity of SOD and CAT (Wan et al., 2019). In this way, AXT is able to repress the loss of mitochondrial membrane potential induced by overproduction of ROS, thus preventing the opening of the mitochondrial permeability transition pores and subsequent activation of pro-apoptotic caspases mediated by cytochrome C release (Baburina et al., 2019; Chen and Kotani, 2016; Kim and Kim, 2018). Furthermore, the restoration of the electron transport chain promotes the increase of fatty acid β-oxidation, ameliorating hepatic lipid accumulation (Ikeuchi et al., 2007; Wolf et al., 2010). The antioxidative effect of AXT can also be promoted by increased expression of Nrf2 and its antioxidant-related genes (Yang et al., 2014).

1.4.3.2.1 Effects of astaxanthin in NASH

AXT exerts its beneficial role on NASH acting not only on reducing oxidative stress and their harmful products, but also by affecting inflammation response. AXT can raise the endogenous activity levels of cellular antioxidant

enzymes (e.g. SOD and CAT) and induce up-regulation of NRF2, which in NASH models and NASH patients is usually down-regulated (Chen and Kotani, 2016). It counteracts steatosis by induction of proliferator-activated receptor (PPAR) alpha, thus promoting the catabolism of fatty acids via carbohydrate responsive element binding protein (CPT1) upregulation and by blocking PPAR gamma and protein kinase B (AKT) involved in hepatic lipogenesis (Jia 2016). Ni and colleagues have shown that, in addition to *de novo* lipogenesis, AXT also blocks insulin resistance and, most importantly, diminishes lipid peroxidation (Ni et al., 2015).

Lipid peroxidation is considered pivotal in NASH when taking into account oxidative stress and the risk of cancer development due to the toxic by-products of lipids. In a mouse NASH model, Astaxanthin prevented lipid peroxidation, which was shown by reduced levels of MDA (Ni et al., 2016; Karppi et al., 2007). Another important favorable effect of AXT is its effects on mitochondria, where it is able to prevent the loss of membrane mitochondrial potential. AXT maintains mitochondria in a reduced state and increases oxygen consumption, something known to be impaired in NASH, where the overproduction of ROS leads to the leakage of protons and to a chronic ATP depletion (Serviddio et al., 2008; Wolf et al., 2010). Moreover, AXT, by preventing the release from mitochondria to the cytosol of the cytochrome c, attenuates the pro-apoptotic signaling (Paradies et al., 2014). AXT also counteracts lipid peroxidation of the mitochondrial lipid membrane, cardiolipin (Mano et al., 2018). Cardiolipin is a specific inner mitochondrial membrane phospholipid, very susceptible to oxidative damage. Oxidized cardiolipin alters the inner membrane fluidity, subsequently leading to destabilization and loss of the ETC complex, eventually inducing MPT pore opening (Li et al., 2010).

Since oxidative stress and lipid peroxidation promote activation of inflammatory signaling, treatment with AXT in NASH-affected mice was shown to block hepatic NF-κB, IL-6, IL-1β and to restore the inflammatory environment by switching the activation from pro-inflammatory macrophages M1 towards the anti-inflammatory type M2 (Ni et al., 2015). In addition, AXT interferes with the activation of HSCs by down-regulation of transforming

growth factor beta (TGF-β) (Ni et al., 2015, Kim et al., 2017). In subjects with mild hyperlipidemia and BMI 23-25 kg/m^2, AXT decreased TGs and increased HDL-cholesterol and adiponectin (Yoshida et al., 2010).

Studies on obese patients treated with AXT for three weeks reported reduced levels of lipid peroxidation evaluated by malondialdehyde and isoprostane and augmented activity of superoxide dismutase (Choi et al., 2011a). AXT treatment for 12 weeks demonstrated, in addition, decreased LDL cholesterol levels and APOB protein translation (Choi et al., 2011b). Currently, a clinical trial is recruiting for the evaluation of AXT in overweight/obese and insulin-resistant subjects (NCT03310359).

1.4.3.2.2 Astaxanthin and anti-cancer effects

Preclinical studies have demonstrated that AXT exerts anti-tumor effects in different cancer models, including oral cancer, bladder cancer, leukemia, colon cancer, lung cancer, breast cancer and hepatocellular carcinoma (Zhang and Wang, 2015). A wide range of evidence supports the link between chronic inflammation and cancer development (Balkwill and Mantovani, 2001). Astaxanthin has been shown to be anti-inflammatory in the leukemia cells line U937 (Franceschelli et al., 2014) and in a mouse model of colitis-induced colon cancer (Yasui et al., 2011), by inhibiting ROS-induced activation of NF-κB and therefore the production of pro-inflammatory cytokines such as TNF-α, IL-6, IL-1β and the enzyme cyclooxygenase-2 (COX-2). In an *in vivo* model of oral cancer, it has been found that AXT diminishes cell proliferation, invasion and angiogenesis through inhibition of Janus Kinase 2 (JAK2)/signal transducer and activator of transcription 3 (STAT3) signaling. The treatment suppressed via STAT3 the levels of proliferating cell nuclear antigen (PCNA) and cyclin D1 (Kowshik et al., 2014). The same pathway was also affected in a rat hepatocellular carcinoma cell line, CBRH-7919, showing reduction in tumor cell growth after treatment with AXT (Song et al., 2012). In human colon cancer cells, AXT was able to inhibit cell proliferation via

PI3K/AKT/mTOR, inducing both cell death and downregulation of downstream mTOR signaling targets associated to proliferation (Palozza et al., 2009).

1.5 Cholangiocarcinoma (CCA) and intrahepatic CC (iCCA)

Cholangiocarcinoma (CCA) comprises a heterogeneous group of malignant neoplasms affecting any level of the biliary duct. The epithelial cells forming the bile duct are called cholangiocytes and they exert functions such as bile acid alkalinisation and fluidification, known to interact with many resident and non-resident cell types, including hepatocytes, hepatic stellate cells (HSCs), stem cells and inflammatory cells (Strazzabosco et al., 2000). The classification of CCA defines three subtypes according to their anatomic location: intrahepatic CC (iCCA), perihilar and extrahepatic CCA. ICCA can originate from two different stem cell niches: from the hepatic parenchyma with the canals of Herrings and from the large and extrahepatic bile ducts with the peribiliary glands. ICCA is known to display high molecular heterogeneity (Brandi et al., 2015; Putra et al., 2015; Sia et al., 2013; Walter et al., 2017). Therapy of iCCA is challenging which is reflected by its dismal prognosis of 5-years of 20-35 %, and in case of extravasation in distal extrahepatic structures the 5-years survival is only of 8-12% (Waisberg et al., 2018).

1.5.2 Etiology and molecular pathology of intrahepatic cholangiocarcinoma

After hepatocellular carcinoma, iCCA represents the second most common primary liver malignancy, with an incidence of 10% to 20% of all primary liver cancers (Shaib et al., 2005) **(fig.8)**. Over the last 40 years, the trend of epidemiology of iCCA has shown an important incidence increase worldwide, reaching a 165% increase in the United States (Dodson et al., 2013; Saha et al., 2016; Shaib et al., 2004). Half of deaths from primary liver cancers are due to iCCA (Bertuccio et al., 2013). The reason for this high mortality is

associated with the asymptomatic nature of the disease during its growth, which leads to diagnose the tumor already in an advanced stage, with metastasis for most of the cases. Nevertheless, for patients in which iCCA was resectable and without metastasis, the 5-years survival is only 20-35 % (Waisberg et al., 2018).
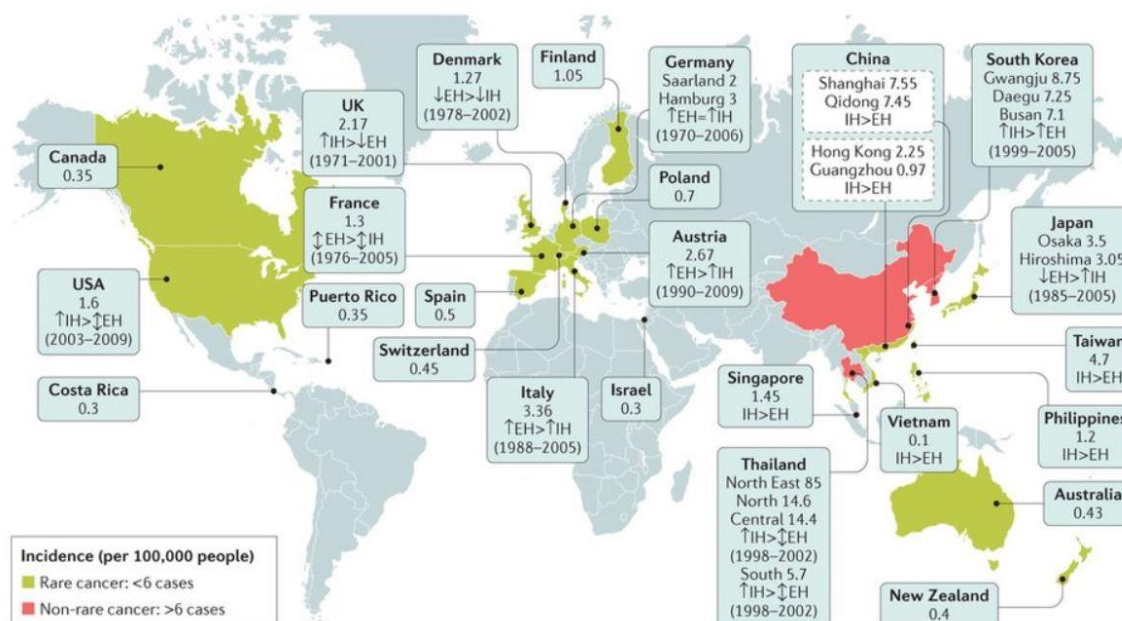
Figure 8. Etiology and molecular pathology of cholangiocarcinoma (CCA) (from Banales et al., 2016). Worldwide incidence indicating CC cases per 100,000. Data cover the period from 1971–2009. With arrows is indicated the trend on incidence among intrahepatic CC (IH) and extrahepatic (EH) and the trend of incidence over time (↑increasing trend; ↔ stable trend; ↓decreasing trend).

The major risk factor to develop iCCA, in the spectrum of bile duct diseases and conditions, is primary sclerosis cholangitis (PSC) (Welzel et al., 2007), followed by hepatolithiasis (Shaib et al.,2005) and primary biliary cirrhosis (Brito et al., 2015; Dodson et al., 2013). Another important risk factor for iCCA is represented by liver flukes, such as the *Clonorchis sinensis* and *Opisthorchis viverrini* infections, particularly present in East Asia (Sripa et al., 2007). Among other risk factors associated to iCCA are hepatitis B and C viral infections, smoking (Brito et al., 2015; Lipshutz et al., 2002; Ohta et al., 1984), alcoholic liver cirrhosis (Petrick et al., 2018a; Xiong et al., 2018b), obesity (Petrick et al., 2018b), diabetes (Petrick et al., 2018b) and metabolic

syndrome (Xiong et al., 2018a). As for HCC, non-alcoholic steatohepatitis (NASH) is considered a risk factor for iCCA (De Lorenzo, 2019). Under the spectrum of chronic liver diseases, non-specific liver cirrhosis represents as well a considerable risk factor (Palmer and Patel, 2012).

The pathogenesis of CCA mainly derives from chronic bile duct inflammation, in which cyclooxygenase-2 (COX-2) is upregulated by bile acids and oxidized forms of cholesterol (oxysterols) (Yoon et al., 2004). In human liver samples of patients affected by primary sclerosing cholangitis, a chronic bile duct inflammation and premalignant disease of the biliary tract *de novo* expression of iNOS and the presence of oxidative stress markers such as 3-nitrotyrosine and 8-oxo-dG was shown (Jaiswal et al., 2001). Yuan and collaborators demonstrated that KCs-derived TNF-α triggers cholangiocytes proliferation via JNK activation, ROS production and paracrine TNF-α, inducing oncogenic transformation (Yuan et al., 2017).

With the attempt to dissect iCCA heterogeneity, transcriptomic analysis, clinical histopathology and patients' outcome have identified two main biological classes: the inflammation class (38% of iCCA cases) and the proliferation class (62%). The inflammation class, as the name suggests, is characterized by the activation of inflammatory signaling pathways, STAT3 in conjunction with overexpression of inflammatory cytokines. The proliferation class instead involved the activation of oncogenic signaling pathways (e.g. RAS, MAP-kinases, HGF/MET), chromosomal aberrations (e.g. amplifications at 11q13.2 and deletions at 14q22.1), mutations in KRAS and BRAF (Sia et al., 2013). Epigenetic alterations (e.g. IDH1 and IDH2) and chromatin remodelling factors (ARID1A, PBRM1 and BAP1) are as well characteristic of iCCA (Jiao et al., 2013).

Regarding perihilar and extrahepatic CCA and iCCA therapies, tumor resection is usually considered the preferred venue of treatment. For inoperable tumor cases, locoregional therapy with transarterial chemoembolization can be applied (Poultsides et al., 2010). Genetic and transcriptomic analysis has revealed molecular targets which are currently used in therapy such as driver mutations (IDH1/2, EGFR, KRAS, ERBB-2,

Wnt, BAP1, c-Met) and fusion genes (FGFR2/4, ROS1, ALK) and angiogenesis-related overexpressed genes (VGFR, RET, KIT, BRAF, PDGFRB). Checkpoint inhibitors (PD-L1, PD-1, CTLA-4) based-therapies are currently under clinical trials evaluation (Shiao et al., 2018).

Aim of study

Oxidative stress has been demonstrated in several studies to be a crucial factor in driving diseases in the context of chronic inflammation, but is also important in aging and in cancer. So far, the focus has always been in evaluating the role of ROS in defined contexts, such as in models of chronic disease or in cancer studies. For this reason, we still lack a comprehensive overview about the role of oxidative stress from the establishment of chronic disease until cancer development. In this thesis, it was my focus to examine the role of oxidative stress in driving NASH and NASH-induced HCC. Adopting two different antioxidants (synthetic and naturally-derived) in combination with CDHFD, I aimed to assess whether it was possible to prevent or reduce oxidative stress, cell death, inflammation, liver fibrosis and tumor development. To discern between NASH and HCC prevention, I have established prophylactic treatment regimen for 6 months and therapeutic treatment regimen until 12 months. For the therapeutic treatments, two diet-switch time points for the diet at 3 months (initial stage of NASH) and at 6 months (late NASH stage), respectively, were selected.

In a second project, I wanted to investigate the existence of a point-of-no-return in carcinogenesis, and to identify serological biomarkers for the prediction of cancer development. For the first question it was firstly established NASH with CDHFD feeding regimen, afterward the diet was switched with normal diet at late NASH stages (at 6 months and at 9 months). The second question was addressed by performing serum proteomic analysis over time in NASH-affected mice, in which the mice developing tumors revealed potential biomarkers to be considered as predictors for HCC.

In the third project, the aim was to characterize the intra- and intertumoral heterogeneity of iCCA by sequential identification of heterogeneous regions within clinical human iCCA tumor samples by mass-spectrometry imaging (MALDI-MSI), followed by RNA-sequencing analysis. The workflow was completed until extraction of RNA from the identified, laser-microdissected tumor areas and successful generation of RNA-sequencing libraries.

2 Materials and methods

2.1 Mice and diets

Four weeks old male C57BL/6JOlaHsd (C57BL/6J) mice were purchased from Envigo. Mice were housed at the German Cancer Research Center (DKFZ), Heidelberg. Animal experiments were performed according to German Law (G267/15, approval no.55.2-1-54-2532-39-15).

Four weeks old male mice were fed a normal chow diet (ND), a 45% choline-deficient high-fat diet (CDHFD) (Research Diets cat.no. D05010402); 0.7% butylated hydroxyanisole w/w (BHA) supplemented CDHFD (Research Diets cat.no.D16041502); 0.026% w/w Astaxanthin (AXT) supplemented CDHFD (Research Diets; D17061306). BHA compound was purchased from Sigma-Aldrich (cat.no.B1253). Astaxanthin compound (Astaxanthin Oleoresin 5%) was purchased from AstALPHY™, Yunnan Alcom BiotechCO. Animals were euthanized using CO_2, as recommended by the german animal protection law. The endpoints were at 6-months and 12-months on diet. Immunohistochemistry (IHC), flow cytometry analysis, biochemical and molecular assays were performed from harvested serum and organs.

2.2 Measurements of serum parameters

Heart blood was harvested from mice after CO_2-euthanasia, and the serum was collected using a Z-Gel microtube (Sarstedt). Serum parameters such as alanine aminotransferase (ALT), total cholesterol and low-density lipoprotein cholesterol (LDLC3) were measured on a Cobas Reader in collaboration with the Institute for Clinical Chemistry and Pathobiochemistry, TUM, Munich.

2.3 Intraperitoneal glucose tolerance test

A 20% glucose solution (NaCl, 0.9%), 5µl/g body weight, was intraperitoneally (i.p.) injected in mice after overnight fasting.

The blood was gathered by puncturing the lateral tail vein, the measurement of the blood glucose was performed using *Accu-chek Performa* Glucometer and *Accu-check* stripes, before glucose injection and at 15, 30, 60, 90 and 120 minutes after glucose injection.

2.4 Calorimetric TSE analysis

Indirect calorimetry was performed on individually housed mice using *PhenoMaster* (TSE systems). For the first 3 days, mice were allowed to acclimate to the new environment. Afterward, metabolic parameters such as food and water intake, O_2 consumption, CO_2 production, respiratory exchange ratio (RER) and total activity were measured. The aforementioned parameters were evaluated for at least four consecutive days, with five measurement values every hour. To exclude the body weight effect on measured parameters, analysis of covariance (ANOVA) was carried out.

2.5 Isolation from liver and staining of lymphocytes and monocytes for flow cytometry

After mice euthanasia with CO_2, livers were dissected, minced with scissors and incubated for 35 minutes at 37°C with digestion buffer (Collagen IV (Sigma) 1:10 (60 U f.c.) and DNase I (Sigma) 1:100 (25 µg/ml f.c.) in RPMI 1640 medium). After the incubation, digested livers were first filtrated 100µm filter and then washed with RPMI 1640 medium with centrifugation of 7min, 300g at 4°C. Lymphocytes and monocytes were enriched with a two-steps Percoll gradient (20ml 25% Percoll/HBSS underlay with 20ml 50% Percoll/HBSS) followed by centrifugation for 15min, 1800 g at 4°C (acceleration:1; deceleration:0). The sample collection was carried out transferring in a new 50 ml falcon the ring of lymphocytes formed after the gradient. Then cells were washed with HBSS, centrifuged for 10min, 700g at 4°C, counted and transferred to a 15ml Falcon for a final washing step with FACS buffer (PBS supplemented with v/v 0.4% 0.5M EDTA pH= 8 and w/v 0.5% albumin fraction V (cat.no.90604-29-8). Isolated cells were first stained

for live/dead cell discrimination with ZombieDyeNIR, according to the manufacturer´s instructions. Subsequently, cells were washed with FACS buffer and stained with CD16/CD32 (FC-block), in order to prevent non-specific binding of IgG to the FcγIII and FcγII receptors prior to staining with antigen-specific primary antibodies. After washing with FACS buffer (1500 rpm, 5min, 4°C), cells were stained for 20min at 4°C with surface-specific primary antibodies as displayed on table 3 **(table 3)**. After another washing step as reported above, cells were fixed with eBioscience IC fixation (cat.no.00-8222-49), according to the manufacturer´s instructions. Cells were analyzed using BD FACSFortessa. Data were analyzed by Dr. Elena Kotsiliti using FlowJo.

Fluorochrome	Name	Clone	Company
Alexa700	CD4	RM4-5	Biolegend
Alexa700	CD45	30-F11	Biolegend
APC	CD11b	M1/70	Biolegend
APC	CD3	17A2	Biolegend
APC	CD44	IM7	Biolegend
FITC	CD19	6D5	Biolegend
FITC	CD45	I3/2.3	Biolegend
PE	CD69	H1.2F3	Biolegend
PE	F4/80	13M8	Biolegend
PE/Cy7	CD3	17A2	Biolegend
PE/Cy7	Ly6G	I/78	Biolegend
PE/Dazzle	CD11c	N418	Biolegend
PE/Dazzle	CD62L	MEL-14	Biolegend
PerCP/Cy5.5	CD8a	53-6.7	Biolegend
PerCP/Cy5.5	Ly6C	H14.4	Biolegend
	CD16/32	93	Biolegend

Table 3. Antibodies used for flow cytometry experiments, for the analysis of CD8^{+} T cells, macrophages and infiltrating monocytes.

2.6 Histology, immunohistochemistry and quantification

Harvested organs were fixed in 4% paraformaldehyde and paraffin-embedded at the Technical University of Munich (TUM) or at the Department of Chronic Inflammation and Cancer (DKFZ, Heidelberg). The resulting formalin-fixed paraffin-embedded (FFPE) blocks were cut in sections of 2µm. Sections were then baked 15 min at 70°C. For Hematoxylin/Eosin (H&E) or immunohistochemistry (IHC) staining **(table 4)**, slides were stained with Bond

MAX (Leica). For Sudan Red staining, cryosections (5µm) were cut and stained with Sudan Red (0.25% Sudan IV in ethanolic solution). Slides were scanned with SCN400 slide scanner (Leica) and analyzed using ImageJ. The technical staff (Anne Jacob, Danijela Heide and Jenny Hetzer) supported the blocks' sectioning, staining and scanning procedures.

Target	Dilution	Company
CD3	1:250	Zytomed
F4/80	1:120	Linaris
Gp73	1:100	Santa Cruz
Ki-67	1:200	Thermo Scientific
MHCII	1:500	Novus Biologicals

Table 4. Antibodies used for IHC.

2.7 Non-Alcoholic Fatty Liver Disease (NAFLD) activity score (NAS)

The NAS score was used for the grading of NAFLD-NASH, accordingly to Takahashi and Fokusato (Takahashi and Fokusato, 2014). The H&E stained liver sections were evaluated: the resulting score was calculated as the sum of the scores for steatosis (0-3), lobular inflammation (0-3), and ballooning (0-2), and ranges from 0 to 8 **(table5)**.

Item	Extent	Score
Steatosis	<5%	0
	5% - 33%	1
	>33%-66%	2
	>66%	3
Lobular inflammation	No foci	0
	<2 foci per 200x field	1
	2-4 foci per 200x field	2
	>4 foci per 200x field	3
Ballooning	None	0
	Few ballooning hepatocytes	1
	Many ballooning hepatocytes	2

Table 5. NAS scoring system.

2.8 DNA extraction and quantification

The extraction of DNA was performed from fresh frozen liver tissues using the QIAamp DNA Mini Kit (cat.no. 51304, Qiagen, Hilden Germany). Briefly, ≤25 mg of tissue was cut and put in a 1.5 ml microcentrifuge tube together with 180 µl of Buffer ATL and 20 µl of Proteinase K for incubation of 4 hours at 56°C. After incubation, 200 µl of Buffer AL were added to the lysed tissue and incubated at 70°C for 10 min. 200 µl of 100% ethanol were added before thorough mixing the solution. The solution was then placed in a QIAamp Mini spin column and centrifuged at 8000 rpm for 1 min. After discarding the flow-through from the collection tube, the column was washed two times: at 8000 rpm for 1 min, with 500 µl of Buffer AW1 followed by centrifugation of 500 µl of Buffer AW2 through the column. After discarding the flow-through, possible Buffer AW2 carryover was eliminated by centrifuging the column at full speed (14,000 rpm) for 3 min. DNA was eluted from the column using 50 µl of sterile water placing on the top of the column and incubating for 5 minutes at room temperature prior centrifugation at 8000 rpm for 1 min. The DNA concentration was determined using a NanoDrop 2000 photo spectrometer (instrument of Peqlab, Erlangen, Germany; software of Thermo Fisher Scientific, Waltham, USA).

2.9 Genomic copy number analysis by array CGH

To characterize genomic copy number alterations of tumors from 12-months CDHFD group and from the Astaxanthin diet-switch group (CDHFD 6-months→AXT+CDHFD 6-months), array comparative genomic hybridization (aCGH) was performed using high-resolution oligonucleotide-based G4126A SurePrint G3 Custom Mouse 8x60K CGH microarrays (cat.no. 4839A, Agilent Technologies, USA). 250 ng of tumor DNA and 250 ng of reference DNA (from healthy livers on chow diet mice) were labelled respectively with Cy3 and Cy5 fluorochromes, using the CGH labelling kit for oligo arrays (Enzo, USA). To remove unincorporated nucleotides were used Microcon YM-30

columns (Millipore, USA). Labeled DNA was subsequently hybridized on Mouse Genome CGH 8x60K microarrays for 40 hours. After washing steps according to the manufacturer´s protocol, the array slides were processed on a G2505C Sure Scan Microarray Scanner (Agilent Technologies, USA). The Agilent Technologies' Feature Extraction 10.7 software (Agilent Technologies, USA) was then adopted for data quality control and extraction. The raw data were subsequently imported into the R statistical platform (R Development Core Team. R: A language and environment for statistical computing. R Foundation for Statistical Computing, Vienna, Austria. ISBN 3-900051-07-0, URL: http://www.R-project.org/) in order to first subtract the median intensity signals of the background and then to generate log2 ratios. The Agilent feature extraction software was then applied to normalize median values and for quality filtering. Afterwards the log2 ratios were segmented, called and defined in copy number regions by the functions from the CGHcall (van de Wiel et al., 2007) and CGHregions (van de Wiel and van Wieringen, 2007) packages.

2.10 Protein extraction and quantification from liver murine samples

Liver fresh frozen tissues were homogenized using a GentleMACS dissociator (Miltenyi) and RIPA buffer (20 mM Tris-Cl (pH 7.4), 3 mM EDTA, 2% Triton X-100, 150 mM NaCl) with 1x cOmplete™ protease inhibitor (Roche) and 1x PhosSTOP™ phosphatase inhibitor (Roche), at a ratio of 100µl buffer per 10mg tissue sample. After homogenization, lysates were transferred into 1.5 ml tubes and centrifuged for 10 min at 4°C and 13,000 rpm in an Eppendorf tabletop centrifuge. Supernatants were then transferred to fresh 1.5 ml tubes and stored at -80°C until further used. Protein concentrations were determined using a Pierce BCA Protein Assay Kit (Thermo Fisher Scientific) according to the manufacturer's instructions. In brief, standard dilutions were prepared in RIPA buffer, covering a range from 25µg/ml to 2,000µg/ml protein. Samples were diluted 1:25 in RIPA buffer. The working reagent was prepared as described in the protocol. 25 µl of sample or standard solution

were incubated with 200µl of working reagent for 30 min at 37°C. Spectrophotometric measurements were obtained from a Tecan Infinite200 pro (Tecan Group Ltd.) at 560nm. Concentrations were determined by linear regression of standard curve absorption using Microsoft Excel.

2.11 Abundant protein depletion and quantification from serum samples

The depletion of abundant proteins (albumin and IgG) was carried out using the Proteome Purify™ 2 - Mouse Serum Protein Immunodepletion Resin (cat.no. MIDR002-040, R&D systems/Biotechne). Ten µL of serum was placed on a 1.5 ml tube, followed by 1 ml of suspended resin. The mix was placed in a rotary shaker and mixed for 45 minutes. After the incubation time, the suspension was filtered in two Spin-X Filter Units by 2000 g centrifugation for 2 minutes. The resulting filtrates were combined (for each sample) in a new 1.5 ml tube and was added 5 volumes of cold (-20°C) 100% acetone for an overnight precipitation at -20 °C. The next day samples were centrifuged at 15,000 g for 30 minutes at 4 °C. The supernatant was discarded and was added an equal volume of cold 50% acetone and centrifuged at 15,000 g for 30 minutes at 4°C. This step was repeated, subsequently the pellet was allowed to air dry for 30 minutes at room temperature. The dried pellet was dissolved in 15-25ul (depending from the pellet size) of urea/thiourea buffer (6M Urea / 2M Thiourea in 10mM of HEPES (pH 8.0)). Protein quantification was performed with Qubit Protein assay (cat.no. Q33211, Invitrogen) according the manufacturer's instructions.

2.12 Quantitative protein analysis by mass spectrometry for murine samples

MS measurement and raw data processing were performed in collaboration with the core facility of Genomics and Proteomics Core Facility (GPCF), Protein Analysis Unit - W120. Briefly, 1 or 10 µg of sample was loaded on SDS-gel and let to run for a short distance of 0.5 cm. After Coomassie

staining, the total sample was cut out unfractionated and used for subsequent Trypsin digestion according to a protocol modified from the original of Shevchenko et al. (Shevchenko et al., 2006) digestion performed on the DigestPro MSi robotic system (INTAVIS Bioanalytical Instruments AG). Digested samples were then loaded on a cartridge trap column, packed with Acclaim PepMap300 C18, 5µm, 300Å wide pore (Thermo Fisher Scientific) and separated in a 180 min gradient from 3% to 40% ACN on a nanoEase MZ Peptide analytical column (300Å, 1.7 µm, 75 µm x 200 mm, Waters) plus an UltiMate 3000 UHPLC system. The analysis of eluting peptides was performed by an online coupled Q-Exactive-HF-X mass spectrometer (Thermo Fisher Scientific) running in a data-dependent acquisition mode consisting of one full scan, followed by up to 12 MSMS scans of eluting peptides. MaxQuant was adopted for data analysis (version 1.6.0.16) (Tyanova et al., 2016) using an organism-specific database extracted from Uniprot.org under default settings. FDR cutoffs were 0.01 for both peptide and protein level identification. Quantification was done using a label-free quantification approach based on the MaxLFQ algorithm (Cox et al., 2014). A minimum of two quantified peptides per protein was required for protein quantification. Filtering, imputation of missing values and statistical analysis were performed using Perseus software package (version 1.6.2.5) (Tyanova and Cox, 2018).

2.13 ICC human sample preparation for Mass Spectrometry Imaging (MSI)

Human intrahepatic cholangiocarcinoma tissue sections of 3 µm were mounted on a Matrix-Assisted Laser Desorption/Ionization (MALDI)-compatible target carrier (cat.no. 8237001, Bruker) composed of the electrically conductive indium tin oxide (ITO)-coated glass slides. After deparaffinization, samples were coated with a 9-aminoacridine-based matrix allowing the absorption and transferring of the laser energy to the samples for their subsequent desorption and ionization. Samples were analyzed with

quantitative measurement for metabolites (Ly et al., 2016). The Mass Spectrometry Imaging (MSI) was performed in negative mode at 50 µm spatial resolution and a range of *m/z* 50-1000 using a rapifleX MALDI-ToF/ToF (Bruker Daltonik GmbH, Germany). Red phosphorus was used for external calibration. Consecutive sections were stained with H&E and scanned using a Mirax Desk slide scanner (Carl Zeiss AG, Germany). Tumor areas, defined as regions-of-interest (ROIs), were annotated digitally (Pannoramic Viewer, 3DHISTECH Ltd., Hungary) by the pathologist Prof.Dr.Terracciano (University-Hospital of Basel). The subsequent data analysis was performed by the import of the annotations together with the MSI data into SCiLS Lab 2019b (Bruker Daltonics GmbH, Germany). Tumor-associated spectra were first normalized to their total ion current and subsequently clustered by *k-means* with five classes (Dewez et al., 2019). The resulting segmented regions were then imported into Matlab R2017b for image processing. Then the boundaries of the segmented regions were determined and exported as *XML* file compatible with the laser microdissection system. The identified boundaries were then burned within the tissue section by the laser of a Leica LMD 7000 system (Leica Microsystems, Wetzlar, Germany).

2.14 Manual microdissection

The isolation of single clusters from the samples was performed using an inverted microscope (HAL 100, Zeiss, Germany) and a scalpel. The burned boundaries helped the tissue detachment with the scalpel. The small areas from the same cluster per each sample were pooled in a 1.5 µl tube.

2.15 **RNA extraction**

For the RNA extraction of isolated clusters of each sample, a combination of two protocols from the RNeasy FFPE kit (cat.no.73504, Qiagen, Germany) and from RNeasy Micro kit (cat.no.74004, Qiagen, Germany) was applied. This adjustment was carried out in order to achieve better yield from low amounts and low quality of RNA. The optimization of the procedure was obtained with the support of the scientist Lisa Kreutzer, with additional technical assistance provided by Laura Dajka. Briefly, 150 µl of Buffer PKD together with 10 µl of Proteinase K was added to the tube containing the collected tissue from microdissected clusters. Samples were digested in a shaking thermomixer at 55°C overnight. The day after, samples were vortexed and heated up at 80°C for 15 min in a heating block. To adjust binding conditions 320 µl RBC buffer were added. The resulting lysates were then mixed thoroughly and transferred to a gDNA Eliminator spin column placed in a 2 ml collection tube. The spin columns were centrifuged for 30 sec at ≥8000 x g (≥10,000 rpm). Then the columns were discarded while keeping the flow-through. Subsequently 560 µl of 100% ethanol were added twice to the flow-through and mixed well by pipetting. The mixtures were transferred to a RNeasy MinElute spin column and centrifuged for 15 sec at ≥8000 x g (≥10,000 rpm). The flow-through was discarded and the column membranes were washed twice with 500 µl RPE buffer centrifuging for 15 sec at ≥8000 x g (≥10,000 rpm) and the flow-through was discarded. In order to completely dry the membrane for the elimination of ethanol residuals that interfere with downstream reactions, the columns were placed on a new collection tube of 2 ml and centrifuged at full speed for 5 minutes. Afterward the RNeasy MinElute spin columns were placed in a new 1.5 ml collection tube and for the RNA elution, 15-30 µl of RNase-free water were added directly to the spin column membranes. Centrifugation for 1 min at full speed allowed the elution of the RNA. The quality and the integrity of the RNA were checked using the Bioanalyzer 2100 Systems (Agilent Technologies, Inc., USA) together with Agilent RNA 6000 Pico Kit (cat.no.5067-1513, Agilent Technologies, Inc., USA) provided measurements for RNA quality, and further calculation of

percentage from fragments >200 nucleotides (DV_{200}) was assessed to determine the RNA integrity.

2.16 Library preparation for RNA sequencing (RNAseq)

The libraries were prepared with 30 ng of total RNA using QuantSeq 3′ mRNA-Seq Library Prep Kit FWD for Illumina (SKU: 015.96, Lexogen GmbH, Austria) with single-indexing, according to the manufacturer's instruction for low-quality RNA. To determine the optimal cycle number for the library amplification the PCR Add-on Kit from Illumina (SKU: 020.96, Lexogen GmbH, Austria) was used. The individual libraries were eventually amplified with 24 PCR cycles.

MALDI MSI analysis and laser microdissection were conducted in collaboration with Prof. Benjamin Balluff (M4I Division of Imaging Mass Spectrometry, Maastricht University, The Netherlands). Sample preparation, with manual microdissection, RNA extraction and library preparation, was performed with the support of Lisa Kreutzer, Theresa Heider, Steffen Heuer and Laura Dajka, from the Research Unit Radiation Cytogenetics at Helmholtz Zentrum München.

2.17 Statistical analysis

All data are presented as the mean ±SEM. GraphPad Prism software version 8.01 (GraphPad Software) was used for graphical visualization and for the statistical analysis. Data were analyzed by unpaired, parametric t-test. For comparing multiple groups, data were analyzed by one-way ANOVA with Turkey's multiple comparison test. Statistical significance for HCC incidence was calculated using Fisher's exact test. Statistical significance is indicated as follows: $p < 0.05$, $p < 0.01$, $p < 0.001$ and $p < 0.0001$.

3 Results

3.1 Prophylactic supplementation of CDHFD with the synthetic antioxidant compound BHA prevents NASH and liver damage

In our study on the role of oxidative stress in NASH and NASH-induced HCC, we wanted to evaluate the effects of two potent antioxidants, different in nature. BHA, a synthetic antioxidant widely used to prevent food oxidation, was added to CDHFD. Mice were fed a BHA+CDHFD for 6 months, starting at 4-weeks age. The body weight of the CDHFD group increased over time, in contrast to the BHA+CDHFD fed mice that maintained a body weight similar to the normal diet (ND) group **(fig. 9A)**. Upon glucose challenge performed by intraperitoneal glucose tolerance test (IPGTT), BHA+CDHFD mice did not show impaired glucose response **(fig. 9B)**. The antioxidant-treated mice showed no liver damage, as indicated by ALT values **(fig. 9C)**. Cholesterol was also reduced in BHA+CDHFD mice compared to CDHFD fed mice **(fig. 9D)**. The CDHFD group upon H&E staining of liver sections displayed lipid accumulation, ballooning hepatocytes and immune cells infiltration, all NASH hallmarks which were not observed in BHA+CDHFD-treated mice **(fig. 9E)**. Accordingly, the NAS score **(fig. 9F)** indicated that BHA protected from NASH and prevented hepatic lipid accumulation, as shown also by Sudan red staining **(fig. 9G, H)**.
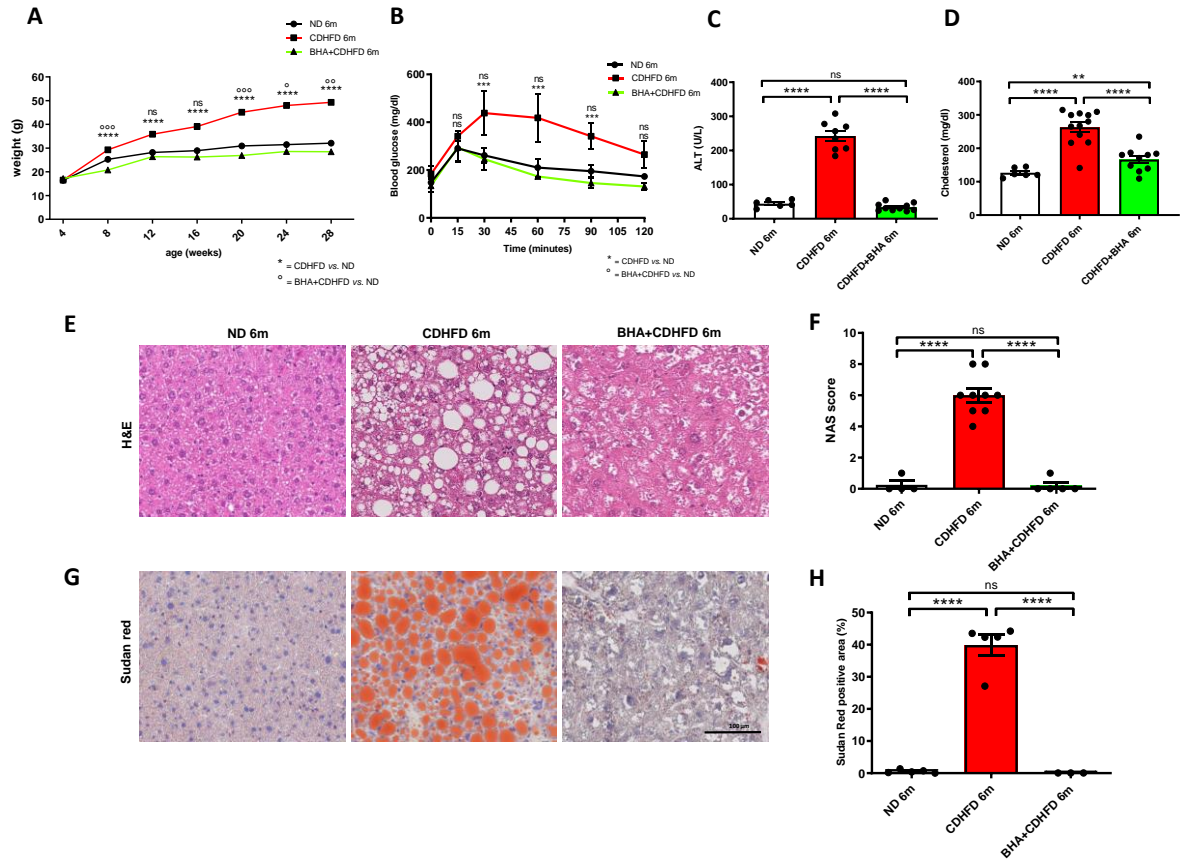
Figure 9. Prophylactic BHA protects from NASH and liver damage

A) Monthly weight measurements in male C57Bl/6 J Ola Hsd ND, CDHFD and prophylactic BHA+CDHFD mice (n=25). **B)** Glucose tolerance test achieved with 6-month-old male mice on ND, CDHFD or prophylactic BHA+CDHFD group (n=4 each). **C)** Quantification of serum alanine transaminase (ALT) and of free cholesterol **(D)** in male 6-month-old male mice on ND, CDHFD or prophylactic BHA+CDHFD group (n ≥ 6 each). **E)** H&E representative pictures demonstrating NASH presence or absence for ND, CDHFD or prophylactic BHA+CDHFD livers. **F)** NAFLD Activity Score (NAS) evaluated for the three groups (n ≥ 4 each). **G)** Sudan red staining indicating hepatic fat accumulation in ND, CDHFD or prophylactic BHA+CDHFD group. **H)** Quantification of total Sudan red positive area for the three groups (n ≥ 3 each). The scale bar indicates 100 μm. All data were analyzed using two-tailed Student's t test or with one-way ANOVA with Turkey's multiple comparison test and are shown as mean ± s.e.m, with statistical significance displayed for p-values <0.05.

3.2 Prophylactic BHA treatment reduces fibrosis and immune response activation, but not proliferation

In order to check for the presence of perisinusoidal fibrosis, liver tissues were stained with Sirius red. The prophylactic BHA treatment in CDHFD mice could prevent fibrosis normally present in CDHFD livers **(fig. 10A)**. Ki67 staining showed no significant difference in hepatic proliferation between BHA+CDHFD fed mice and CDHFD fed mice **(fig. 10B).** Similarly, CD3 IHC showed that the number of $CD3^+$ cells did not significantly differ from the CDHFD group **(fig. 10C).** Instead, the $CD8^+$ T cell population was reduced in BHA+CDHFD mice, as seen by flow cytometric analysis **(fig. 10F).** By IHC, it was observed that $MHCII^+$ cells and $F4/80^+$ cells were significantly reduced, compared to CDHFD **(fig. 10D, E).** Accordingly, flow cytometry analysis revealed a strong reduction of KCs ($CD11b^+$, $F4/80^+$) and of infiltrating monocytes ($CD11b^+$, $F4/80^-$, $Ly6C^+$) **(fig.10 G, H).**
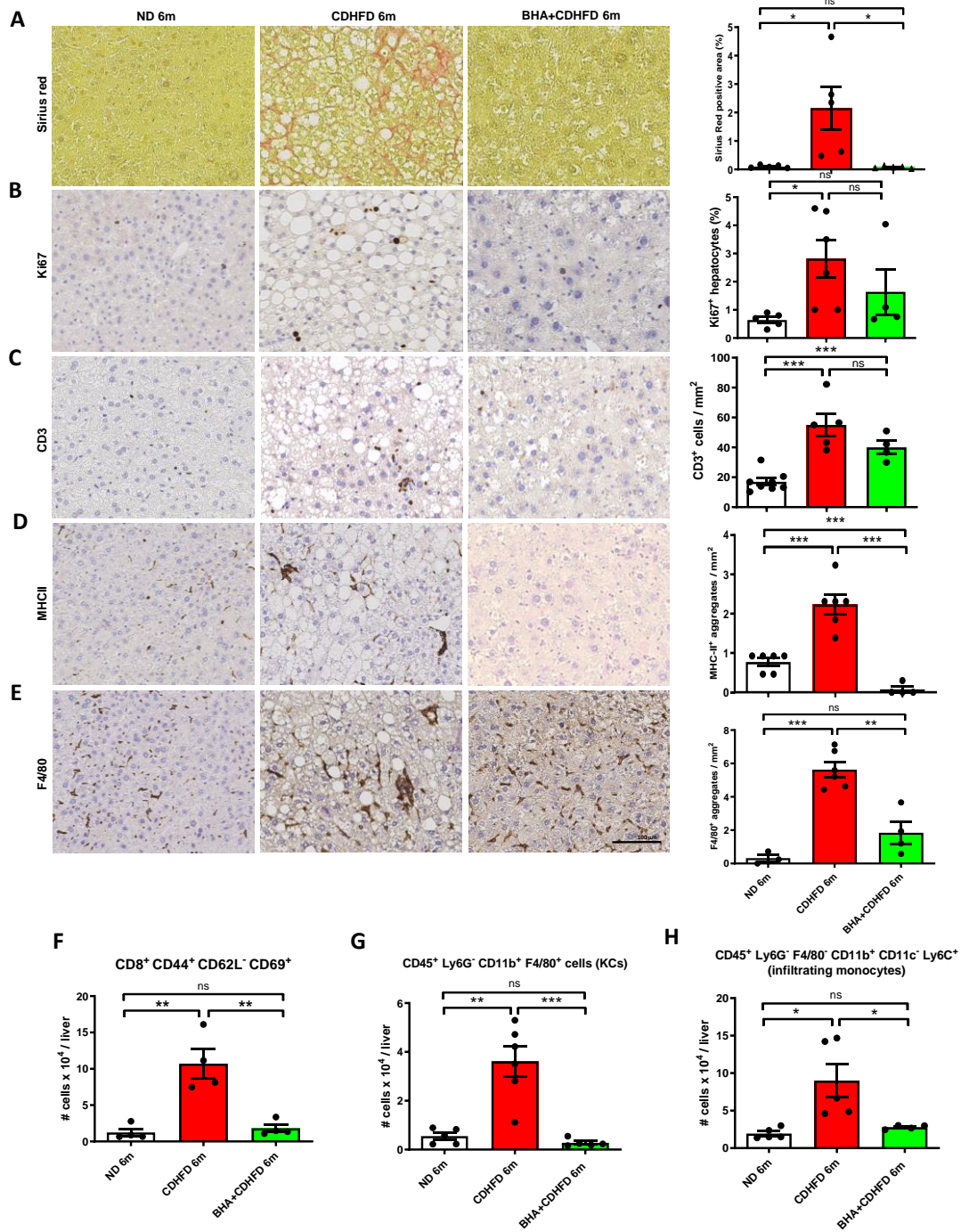
Figure 10. Prophylactic BHA prevents fibrosis and immune response activation

A) Representative Sirius red staining showing perisinusoidal fibrosis, with quantifications to the right for the ND, CDHFD and prophylactic BHA+CDHFD groups (n=5). **B)** Representative immunohistological staining for Ki67$^+$ hepatocytes with respective quantification in percentages of the right side for the three groups (n ≥ 4), **D)** Histological representative pictures for CD3$^+$ T cells (n ≥ 4), plus quantification per mm^2 on the right side, for the three groups (n ≥ 4). **D)** The myeloid compartment evaluated by IHC staining for MHCII$^+$ and **(E)** F4/80$^+$ cells with respective quantification per mm^2 on the right side (MHCII: n ≥ 4), (F4/80: n ≥ 3). Quantifications of flow cytometric analyses for liver activated CD8$^+$ T cells **(F)**, Kupffer cells **(G)** and infiltrating myeloid cells **(H)** from ND, CDHFD or prophylactic BHA+CDHFD group

(n ≥ 4). The scale bar represents 100μm. All data were analyzed using two-tailed Student's t test and are shown as mean ± s.e.m, with statistical significance displayed for p-values <0.05.

3.3 Prophylactic supplementation of CDHFD with the natural antioxidant compound astaxanthin partially prevents NASH and reduces liver damage

Then we applied a second antioxidant compound, this time of natural origin, coming from the microalga *Haematococcus pluvialis.* As in the previous treatment, the compound has been added to the CDHFD, and the resulting diet was given to the mice for 6 months. This supplementation did not prevent weight gain but significantly reduced the weight in the last two months compared to CDHFD **(fig. 11A).** Although prophylactic AXT+CDHFD mice were obese, in 50% of the cases livers did not show NASH, whereas the other half showed moderate NAFLD activity score **(fig. 11F).** AXT could also diminish, compared to CDHFD fed mice, hepatic lipid accumulation **(fig.11 E, G, H).** Furthermore, AXT+CDHFD fed mice did not show any impaired glucose response towards glucose injection **(fig. 11B).** Serum analysis revealed that AXT supplementation significantly reduced ALT values compared to CDHFD **(fig. 11C).** Serum cholesterol remained the same as CDHFD mice **(fig. 11D).**
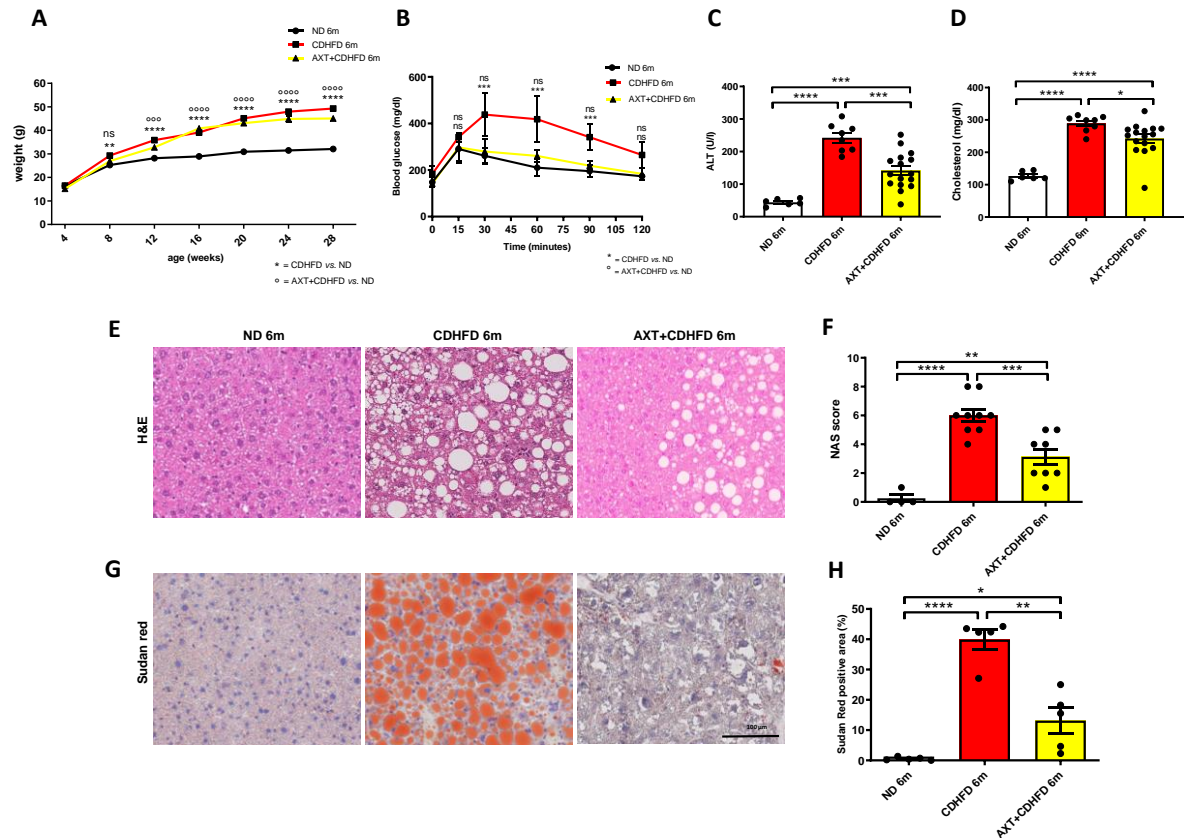
Figure 11. Prophylactic AXT induces obesity but ameliorates NASH and liver damage

A) Monthly weight measurements in male C57Bl/6 J Ola Hsd ND, CDHFD and prophylactic AXT+CDHFD mice (n=25). **B)** Glucose tolerance test achieved with 6-month-old male mice on ND, CDHFD or prophylactic AXT+CDHFD group (n=4 each). **C)** Quantification of serum alanine transaminase (ALT) and of free cholesterol **(D)** in male 6-month-old male mice on ND, CDHFD or prophylactic AXT+CDHFD group (n ≥ 6 each). **E)** H&E representative pictures demonstrating NASH presence or absence for ND, CDHFD or prophylactic AXT+CDHFD livers. **F)** NAFLD Activity Score (NAS) evaluated for the three groups (n ≥ 4 each). **G)** Sudan red staining indicating hepatic fat accumulation in ND, CDHFD or prophylactic AXT+CDHFD group. **H)** Quantification of total Sudan red positive area for the three groups (n ≥ 3 each). The scale bar indicates 100 μm. All data were analyzed using two-tailed Student's t test or with one-way ANOVA with Turkey's multiple comparison test and are shown as mean ± s.e.m, with statistical significance displayed for p-values <0.05.

3.4 Prophylactic treatment with astaxanthin diet supplementation decreases fibrosis, inflammation and hepatic proliferation

Notably, although not affecting systemic weight gain, prophylactic AXT+CDHFD mice did not show fibrosis, in contrast to CDHFD fed mice **(fig. 12A).** AXT supplementation inhibited hepatocyte proliferation, as shown by

ki67 IHC **(fig. 12B).** In the AXT+CDHFD group, absolute numbers of CD3$^+$ **(fig. 12C)** and activated CD8$^+$ T cells **(fig. 12F)** were significantly reduced when compared to CDHFD, as it was shown by flow cytometry. KCs were reduced in number in the AXT+CDHFD group when compared to the CDHFD, as demonstrated by histology via anti-MHCII and anti-F4/80 staining **(fig. 12 D, E)** and with flow cytometry analysis **(fig. 12G)**. Furthermore, the infiltrating monocytes were also reduced compared to NASH-affected mice **(fig. 12H)**.
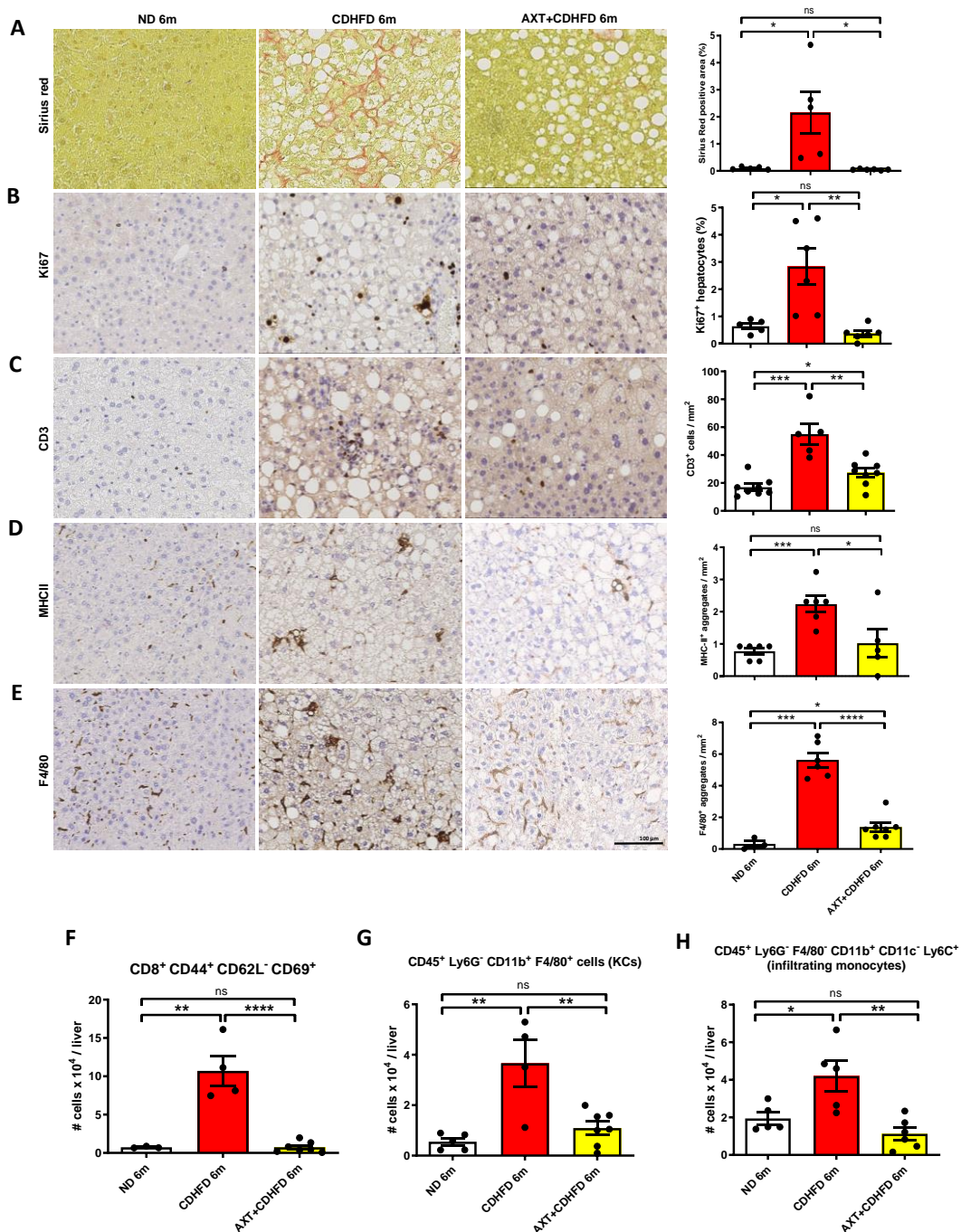
Figure 12. Prophylactic AXT prevents fibrosis and immune response activation

A) Representative Sirius red staining showing perisinusoidal fibrosis, with quantifications to the right for the ND, CDHFD and prophylactic AXT+CDHFD groups (n ≥ 5). **B)** Representative immunohistological staining for Ki67^{+} hepatocytes with respective quantification in percentages of the right side for the three groups (n ≥ 4), **C)** Histological representative pictures for CD3^{+} T cells (n ≥ 5), plus quantification per mm^2 on the right side, for the three groups (n ≥ 4). **D)** The myeloid compartment evaluated by IHC staining for MHCII[+] and **(E)** F4/80^{+} cells with respective quantification per mm^2 on the right side (MHCII: n ≥ 5), (F4/80: n ≥ 3). Quantifications of flow cytometric analyses for liver activated CD8^{+} T cells **(F)**, Kupffer cells **(G)** and infiltrating myeloid cells **(H)** from ND, CDHFD or prophylactic AXT+CDHFD group (n ≥ 4). The scale bar represents 100μm. All data were analyzed using two-tailed Student's t test and are shown as mean ± s.e.m, with statistical significance displayed for p-values <0.05.

3.5 Liver proteomic analyses of prophylactic antioxidant treatments

Proteomic analysis of liver mass-spectrometry data revealed that 6-months CDHFD fed mice upregulate proteins involved in typical pathways characteristic of NASH (fig.13A). The enrichment performed with STRING (*string-db.org*) in combination with literature correlation, allowed us to identify five major clusters in which the pathways were grouped **(fig. 13A)**. Cluster-I contains lipid metabolism-related pathways including: *de novo* lipogenesis, lipid elongation and ceramide synthesis **(fig. 13B)**. Cluster-II includes pathways related to lipotoxicity such as apoptosis and ER stress, the latter including the unfolded protein response (UPR) and the ER-associated degradation (ERAD) pathways **(fig. 13C)**. Cluster-III includes pathways related to oxidative stress, like lipid peroxidation and peroxidized lipid transport, antioxidant response and DNA damage response **(fig. 13D)**. Cluster-IV pathways are involved in inflammation and fibrosis, which include: inflammatory cascade (eicosanoids), NF-κB signaling, macrophages activation and fibrosis **(fig. 13E)**. Cluster-V combines pathways involved in neoplastic transformation, among them proliferation and glycolysis, and tumor-associated proteins. Notably, prophylactic antioxidant treatments with either BHA or AXT supplementation could prevent the upregulation of the aforementioned pathways, with the exception of few candidates for the BHA+CDHFD group. The prophylactic BHA+CDHFD group strongly downregulated the lipogenic protein Acetyl-CoA carboxylase 2

(ACACB/ACC2) **(fig. 13B)**. In addition, BHA led to the upregulation of target genes of NRF2, especially high for carbonyl reductase 3 (CBR3) and NAD(P)H dehydrogenase [quinone] 1 (NQO1) **(fig. 13D)**.

A
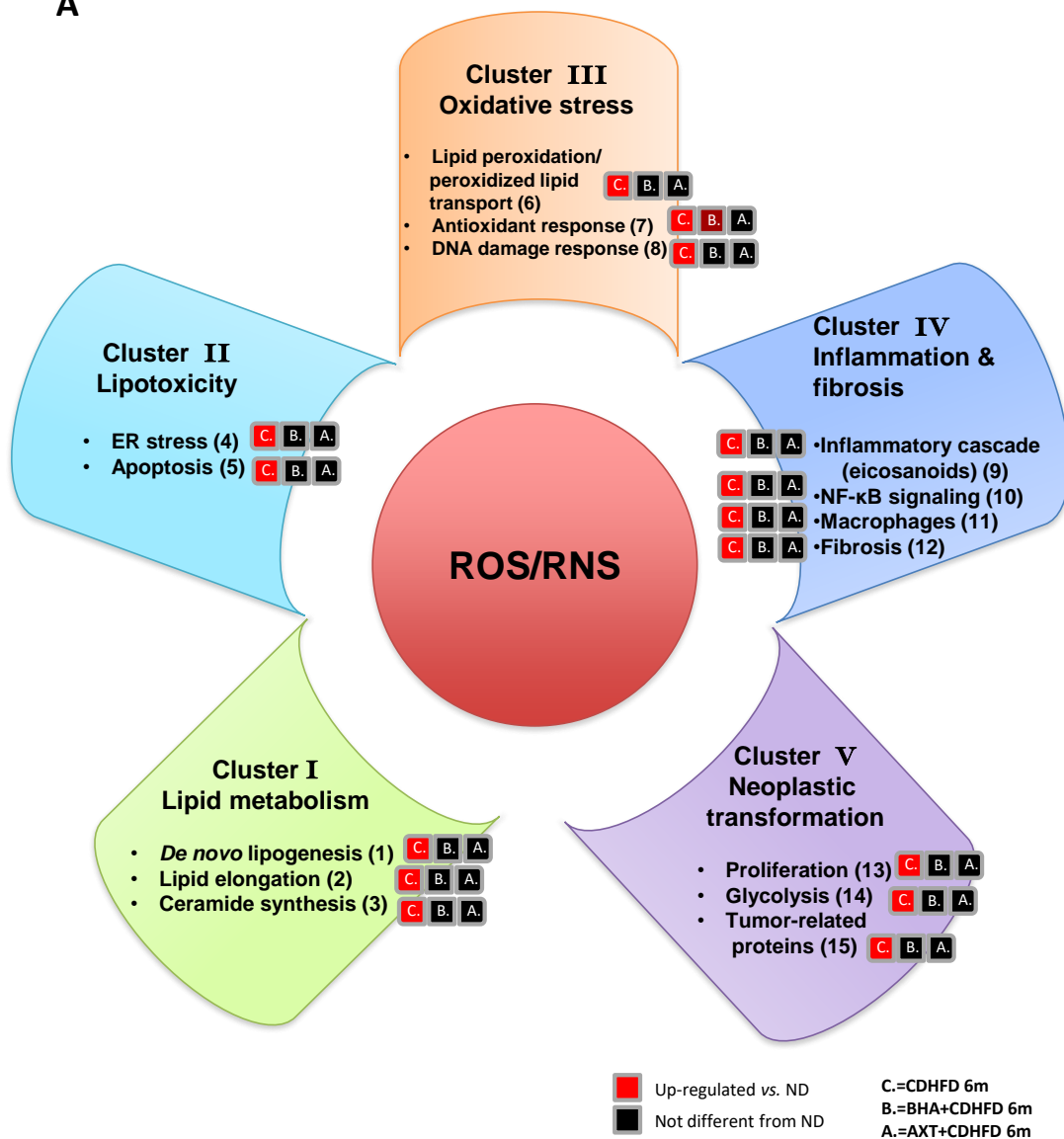
B

Cluster Ⅰ
Lipid metabolism

1) *De novo* lipogenesis
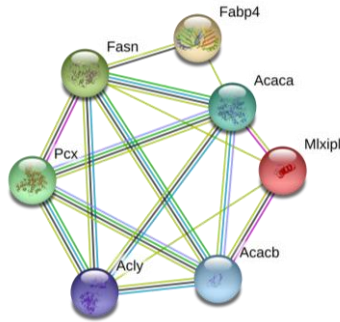
2) Lipid elongation
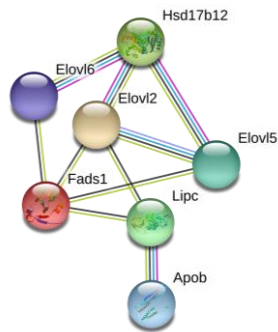
3) Ceramide synthesis
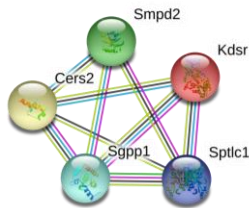
	CDHFD 6m	BHA+CDHFD 6m	AXT+CDHFD
ACACA	1.67 *	-0.81	-0.02
ACACB	1.25 *	-2.13 *	-0.45
ACLY	1.32 *	-0.76	-0.17
ChREBP	2.50 *	-0.24	0.75
FABP4	2.33 *	0.03	0.40
FASN	1.81 *	-0.65	0.29
PCX	1.60 *	-0.04	0.55
ELOVL2	2.52 *	0.31	1.06
ELOVL5	1.91 *	-0.34	0.98
ELOVL6	2.17 *	0.69	2.61
FADS1	0.85 *	-0.04	0.69
HSD17B12	1.22 *	0.07	0.25
LIPC	0.78 *	-0.15	-0.02
CERS2	1.18 *	0.30	0.29
KDSR	1.94 *	0.46	-0.22
SGPP1	1.41 *	0.12	0.38
SMPD2	1.11 *	0.17	0.38
SPTLC1	3.00 *	1.11	0.38

Log$_2$FC
- 3   + 3

Known Interactions		Predicted Interactions		Others	
	from curated databases		*gene neighborhood*		*textmining*
	experimentally determined		*gene fusions*		*co-expression*
			gene co-occurrence		*protein homology*

string-db.org

75

Cluster II
Lipotoxicity

4) ER stress associates pathways: Unfolded protein response (UPR) and ER-associated degradation (ERAD)

	CDHFD 6m	BHA+CDHFD 6m	AXT+CDHFD 6m
CAPN1	1.57*	0.60	0.20
CAPN2	1.86*	0.38	0.33
EIF2A	0.54*	-0.46	-0.05
ERLEC1	1.45*	0.28	-1.37
ERO1L	1.33*	0.28	-0.09
ERO1LB	1.17*	0.68	-0.87
HSPA5	1.09*	-0.08	-0.15
PSME1	0.62*	0.04	-0.77
PSME2	2.20*	0.73	0.02
PSME3	1.06*	0.24	-0.40
PSME4	1.09*	0.66	0.09
SEL1L	1.62*	0.65	0.19
SYVN1	3.02*	0.98	0.90

5) Apoptosis

	CDHFD 6m	BHA+CDHFD 6m	AXT+CDHFD 6m
AIFM1	0.69*	-0.17	0.11
BCL2L13	1.60*	0.06	0.19
BID	1.11*	0.35	-0.25
CASP1	1.10*	0.01	-0.52
CASP6	1.44*	0.40	-0.08
CASP7	1.22*	-0.98	0.70
CASP8	1.13*	-0.21	-0.21
CCAR1	2.35*	-0.39	0.65
CCAR2	1.31*	-0.59	-0.24
CYC1	1.05*	0.08	-0.24
CYCS	0.93*	0.14	0.25
DAPK2	1.49*	-0.06	-0.96
FADD	4.48*	0.75	1.66
STK4	0.97*	-0.26	0.13
STK24	1.18*	0.09	-0.01
STK38	1.31*	0.38	-0.29
SUMO-2/3	2.49*	1.82	0.71
TRADD	2.19*	0.59	1.11
UBA2	1.98*	0.31	0.39

Log$_2$FC
- 4.5   + 4.5

D

6) Lipid peroxidation/ peroxidazed lipid transport

	CDHFD 6m	BHA+CDHFD 6m	AXT+CDHFD 6m
AOX1	1.58*	1.42	0.09
AOX3	1.32*	-0.67	0.10
APOB	1.30*	0.55	0.61
APOE	1.56*	-0.09	0.26
CYP2E1	1.03*	0.23	0.34
LDLR	2.05*	0.02	0.56
OSBP	1.33*	0.41	-0.39
OSBPL1A	1.73*	0.57	-0.21
OSBPL3	2.82*	2.26*	1.19
OSBPL9	1.69*	0.14	-0.21
POR	1.15*	0.42	-0.21
VAPA	1.77*	0.61	0.84
XDH	1.75*	0.55*	0.57

7) Antioxidant response
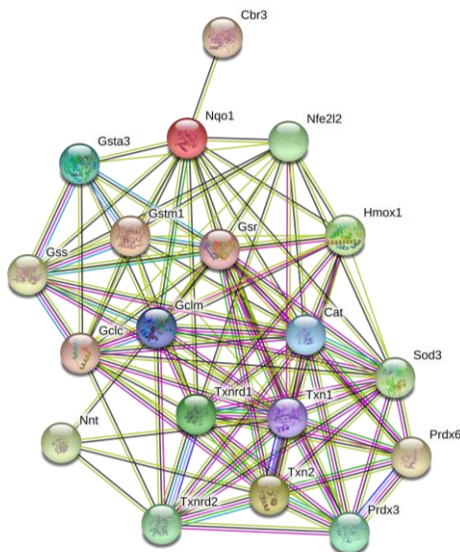
	CDHFD 6m	BHA+CDHFD 6m	AXT+CDHFD 6m
CAT	1.28*	0.54	0.03
CBR3	1.90*	8.39*	0.28
GCLC	1.29*	1.44*	0.10
GCLM	0.81*	1.03*	-0.43
GSR	1.22*	0.96*	-0.22
GSS	1.60*	1.27*	0.25
GSTA3	0.81*	0.22	-0.22
GSTM1	1.17*	2.18*	-0.15
HMOX1	1.67*	0.57	0.20
NNT	-6.57*	0.42	0.36
NQO1	2.35*	4.38*	-0.15
NRF2	-1.34*	0.21	-0.31
PRDX3	1.13*	-0.004	-0.06
PRDX6	0.92*	0.04	-0.20
SOD3	1.99*	-0.16	0.38
TXN	0.77*	0.49	0.21
TXN2	1.48*	0.28	-0.14
TXNRD1	1.40*	1.32*	0.14
TXNRD2	2.04*	-0.37	0.42

8) DNA damage response
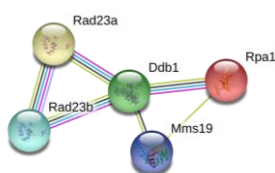
	CDHFD 6m	BHA+CDHFD 6m	AXT+CDHFD 6m
DDB1	1.23*	0.22	-0.004
MMS19	2.35*	0.19	0.86
RAD23A	2.49*	NaN	NaN
RAD23B	1.75*	0.16	0.15
RPA1	2.59*	0.78	-0.03

Log_2FC - 8.5   + 8.5

E Cluster IV
Inflammation and fibrosis

9) Inflammatory cascade (eicosanoids)
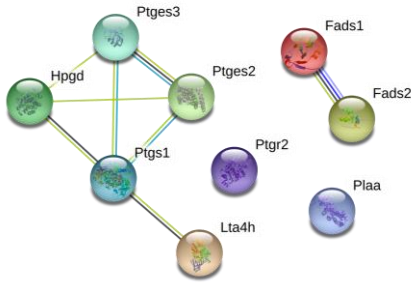
10) NF-κB signaling
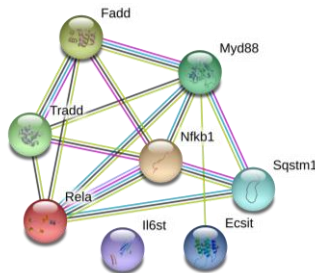
11) Macrophages
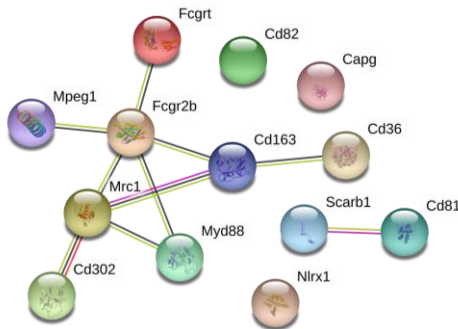
12) Fibrosis
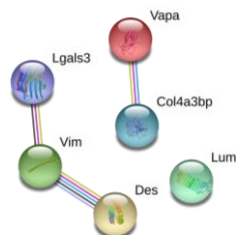
	CDHFD 6m	BHA+CDHFD 6m	AXT+CDHFD 6m
FADS1	0.85 *	-0.04	0.69
FADS2	1.19 *	0.08	0.73
HPGD	1.46 *	1.89	0.28
LTA4H	1.11 *	0.16	-0.29
PLAA	1.36 *	0.24	0.13
PTGES2	1.12 *	-0.76 *	-0.22
PTGES3	1.32 *	0.28	0.11
PTGR2	1.53 *	0.41	0.16
PTGS1	1.66 *	0.36 *	-0.27
ECSIT	1.53 *	0.39	0.54
FADD	4.48 *	0.75	1.66
IL6ST	2.00 *	-0.52	-0.11
MYD88	4.18 *	NaN	2.45
NFKB1	1.49 *	0.67	0.06
RELA	1.90 *	0.76	-0.04
SQSTM1	1.73 *	1.25	0.37
TRADD	2.19 *	0.59	1.11
CAPG	2.58 *	0.84	0.09
CD163	2.80 *	1.26	1.77
CD302	1.29 *	-0.25	0.05
CD36	2.67 *	1.31 *	0.82
CD81	1.65 *	0.71	0.12
CD82	1.66 *	0.64	-0.45
FCGR2/2B	1.28 *	-0.005	-0.02
FCGRT	1.19 *	-0.09	-0.39
MPEG1	1.59 *	-1.12	0.03
MRC1/CD206	1.50 *	0.46	-0.08
MYD88	4.18 *	NaN	2.45
NLRX1	1.22 *	0.42	0.46
SCARB1	1.72 *	0.15	0.13
COL4A3BP	1.49 *	0.29	0.40
Desmin	3.65 *	-0.37	0.59
LGALS3	3.15 *	0.75	1.12
Lumican	2.12 *	0.63	0.60
VIM	2.61 *	0.22	0.06
VAPA	1.77 *	0.61	0.84

Log₂FC -4.5 +4.5

F

Cluster V
Neoplastic transformation

13) Proliferation
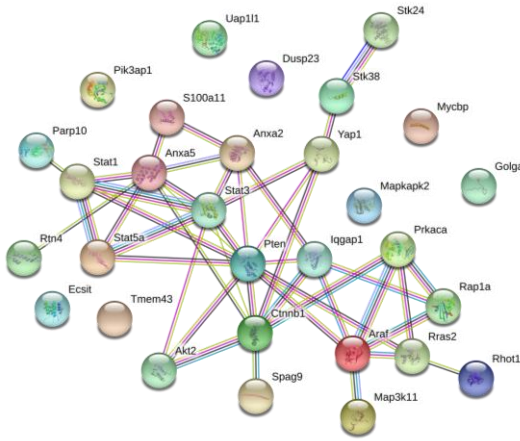
	CDHFD 6m	BHA+CDHFD 6m	AXT+CDHFD 6m		CDHFD 6m	BHA+CDHFD 6m	AXT+CDHFD 6m
AKT2	1.64*	-1.27	-0.94	RAC-1/3	1.98*	-0.24	0.01
ANXA2	2.32*	0.31	0.59	RAP1A	1.91*	1.11	0.33
ANXA5	1.68*	0.07	0.20	RHOT1	1.10*	0.34	0.40
ARAF	1.14*	0.24	0.28	RRAS2	2.74*	-0.07	-0.03
CTNNB1	1.60*	0.09	0.28	RTN4	1.61*	1.02*	0.60
ECSIT	1.53*	0.39	0.54	S100A11	4.39*	1.59	2.42
GOLGA2	1.78*	1.71	2.28	SPAG9	1.59*	0.46	-0.07
IQGAP1	1.19*	0.57	0.13	STAT1	1.76*	-0.04	0.53
MAPK1/ERK2	0.94*	0.14	-0.03	STAT3	1.41*	0.18	0.08
MAPK14/p38	1.26*	0.20	-0.28	STAT5A	3.37*	0.22	1.53
MAPK3/ERK1	1.54*	0.11	-0.06	STK24	1.18*	0.09	-0.01
MAPK9/JNK2	1.13*	0.46	-0.34	STK38	1.31*	0.38	-0.29
MAPKAPK2	1.70*	-0.50	0.70	TMEM43	1.78*	0.75	0.08
MYCBP	0.60*	0.07	-0.36	UAP1L1	1.74*	0.59	0.45
PARP10	2.46*	0.62	0.07	YAP1	2.22*	0.63	0.99
PIK3AP1	1.29*	0.23	0.09				
PRKACA	1.70*	0.09	-0.11				
PRKC-A/B	2.28*	1.30*	0.99				
PTEN	1.55*	-0.51	-0.26				

14) Glycolysis
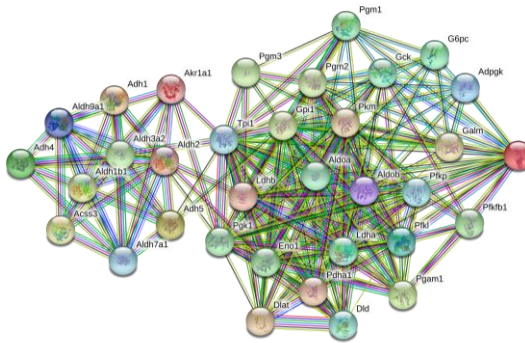
	CDHFD 6m	BHA+CDHFD 6m	AXT+CDHFD 6m		CDHFD 6m	BHA+CDHFD 6m	AXT+CDHFD 6m
ACSS3	1.68*	0.02	0.46	GCK	1.63*	-0.29	0.25
ADH1	0.77*	0.23	-0.07	GPI	1.70*	0.34	-0.07
ADH4	1.22*	0.59	0.29	HK2	3.07*	1.05	0.91
ADH5	1.32*	0.25	0.13	LDHA	1.83*	0.19	0.39
ADPGK	1.32*	0.19	-0.22	LDHB	1.83*	0.75	-0.28
AKR1A1	1.30*	0.51	0.02	PDHA1	1.48*	-0.06	-0.07
ALDH1B1	2.15*	-0.15	0.56	PFKFB1	1.28*	0.01	0.00
ALDH2	0.96*	-0.15	-0.11	PFKL	1.54*	0.17	0.05
ALDH3A2	1.68*	0.24	0.28	PFKP	1.67*	-0.52	-0.24
ALDH7A1	1.27*	0.07	-0.14	PFKP	1.67*	-0.52	-0.24
ALDH9A1	1.32*	-0.01	0.08	PGAM1	1.11*	0.13	0.04
ALDOA	1.15*	0.60	-0.20	PGK1	1.12*	0.14	0.07
ALDOB	1.36*	0.03	0.17	PGM1	1.30*	0.24	-0.11
DLAT	1.27*	-0.08	-0.01	PGM2	2.00*	0.57	0.08
DLD	1.23*	-0.32	-0.09	PGM3	2.31*	0.77	0.92
ENO1	1.46*	0.17	0.24	PKM	1.48*	0.79	0.01
G6PC	2.44*	0.33	0.58	TPI1	1.07*	0.13	-0.21
GALM	1.50*	0.45	-0.02				

15) Tumor-related proteins
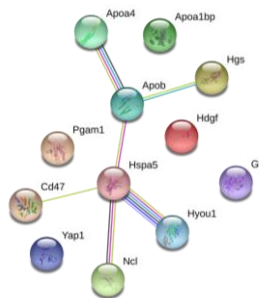
	CDHFD 6m	BHA+CDHFD 6m	AXT+CDHFD 6m		CDHFD 6m	BHA+CDHFD 6m	AXT+CDHFD 6m
APOA1BP	1.25*	0.23	-0.18	HGS	2.97*	0.56	1.22
APOA4	2.70*	2.46	2.72	HSPA5	1.09*	-0.08	-0.15
APOB	1.30	0.55	0.61	HYOU1	1.18	0.34	-0.17
CD47	1.60*	0.37	0.33	NCL	0.69*	0.01	-0.11
GLUL	2.22*	0.33	1.09	PGAM1	1.11*	0.13	0.04
HDGF	1.75*	0.27	-0.13	YAP1	2.22*	0.63	0.99

Log$_2$FC - 4.5 ←→ + 4.5

Figure 13. Proteomic analysis of pathways affected by prophylactic BHA and AXT treatment

A) Graphical summary representative upregulated proteins in most relevant NASH inducing pathways, grouped in five clusters. The enrichment for upregulated proteins in NASH-affected mice was based on KEGG and literature correlation. **B)** Cluster-I grouping lipid metabolism related pathways, with STRING-network illustrations and corresponding heatmaps, displaying fold change (FC) differences of C57Bl/6 J Ola Hsd 6-month-old male mice CDHFD, prophylactic BHA+CDHFD and prophylactic AXT+CDHFD, compared against ND (n ≥ 6 each). Lipid metabolism related pathways include: 1) *de novo* lipogenesis, 2) lipid elongation, 3) ceramide synthesis. **C)** Cluster-II grouping lipotoxicity related pathways, with STRING-network illustrations and corresponding heatmaps. Lipotoxicity related pathways include: 4) ER stress associated pathways (Unfolded protein response (UPR) and ER-associated degradation (ERAD)) and 5) apoptosis. **D)** Cluster-III grouping oxidative stress related pathways, with STRING-network illustrations and corresponding heatmaps. Oxidative stress related pathways include: 6) lipid peroxidation/peroxidized lipid transport, 7) antioxidant response, 8) DNA damage response. **E)** Cluster-IV grouping inflammation and fibrosis related pathways, with STRING-network illustrations and corresponding heatmaps. Inflammation and fibrosis related pathways include: 9) inflammatory cascade (eicosanoids), 10) NF-κB signalling, 11) macrophages, 12) fibrosis**. F)** Cluster-V grouping neoplastic transformation related pathways, with STRING-network illustrations and corresponding heatmaps. Neoplastic transformation related pathways include: 13) proliferation, 14) glycolysis, 15) tumor-associated proteins. Significance displayed on top-right of each logarithmic 2 (Log2) FC value on the heatmaps, indicates false discovery rate (FDR) < 0.01 between experimental groups (CDHFD, BHA+CDHFD or AXT+CDHFD) and ND fed mice ND (n ≥ 6 each). STRING-network (string-db.org) legend displaying known/predicted or other (textmining, co-expression, protein homology) interactions.

3.6 Therapeutic BHA treatment at late NASH stage reverts NASH phenotype and liver damage

In order to evaluate the role of antioxidants in tumor prevention or incidence reduction, we firstly established NASH phenotype by feeding mice with CDHFD for a period of 6 months, and then we changed the diet to BHA+CDHFD or AXT+CDHFD.

The therapeutic treatment with BHA supplementation led to a strong weight reduction compared to the CDHFD group, which was maintained over time until the end point of 12-months **(fig. 14A)**. The weight reduction most likely is not due to a reduced food intake, as evaluated in a short-term feeding experiment. More specifically, it was observed that mice switched to BHA reduced their food consumption to 78% (first week) and 34% (third week), with respect to the beginning of the feeding experiment. By the fourth week, the BHA-switched group reached the initial food consumption **(fig. 14I)**, indicating that the mice had adjusted to the new diet. The food intake per mouse and the metabolic parameters where assessed by the TSE Systems Indirect gas calorimetry. The respiratory exchange ratio, which shows the volume of carbon dioxide (CO_2) produced to the volume of oxygen (O_2) used (VCO_2/VO_2), although decreased after diet switch, remained the same in the prophylactic BHA+CDHFD mice. The food intake did not differ between the CDHFD group and the prophylactic BHA+CDHFD group **(fig. 14J, K)**.

Regarding 6-months switched BHA+CDHFD therapeutic group, serological measurement for ALT values showed a strong reduction in liver damage **(fig. 14C)**. Serological cholesterol displayed as well a significant reduction in the diet-switch group compared to the CDHFD 12-months **(fig. 14D)**. H&E and Sudan red staining revealed a reduction in steatosis and an absence of hepatic lipid accumulation **(fig. 14E, F, G, H)**. The therapeutic BHA+CDHFD treated mice did not demonstrate glucose impairment upon G.T.T., revealing a very similar profile to the ND control mice **(fig. 14B)**.
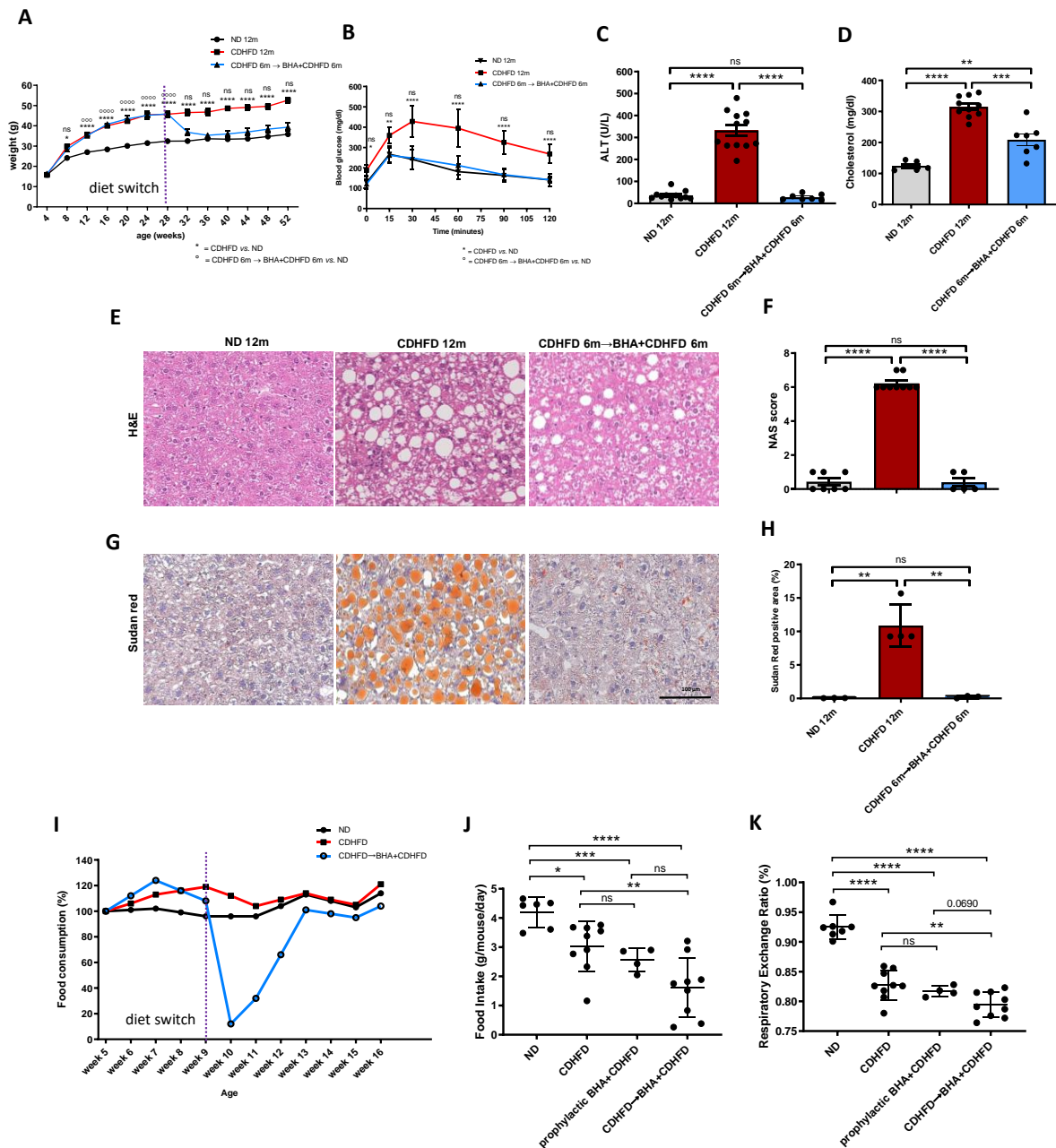
Figure 14. Therapeutic BHA treatment at late NASH stage rescues NASH phenotype and liver damage

A) Monthly weight measurements in male C57Bl/6 J Ola Hsd ND, CDHFD and therapeutic BHA+CDHFD mice (n=25). **B)** Glucose tolerance test achieved with 12-month-old male mice on ND, CDHFD or therapeutic BHA+CDHFD group (n=4 each). **C)** Quantification of serum alanine transaminase (ALT) and of free cholesterol **(D)** in male 12-month-old male mice on ND, CDHFD or therapeutic BHA+CDHFD group (n ≥ 5 each). **E)** H&E representative pictures demonstrating absence or presence of NASH of ND, CDHFD or therapeutic BHA+CDHFD livers. **F)** NAFLD Activity Score (NAS) evaluated for the three groups (n ≥ 7 each). **G)** Sudan red staining indicating hepatic fat accumulation in ND, CDHFD or therapeutic BHA+CDHFD group. **H)** Quantification of total Sudan red positive area for the three groups (n ≥ 3 each). **I)** Food consumption measurements in percentages for short term BHA+CDHFD diet-switch with ND and CDHFD control groups; each dot illustrates food consumption for

a cage containing 4 mice. **J)** Metabolic measurements performed in TSE unit, displaying food intake in grams per mouse/day in ND, CDHFD or therapeutic BHA+CDHFD group (n ≥ 4 each). **K)** Metabolic measurements performed in TSE unit, displaying respiratory exchange ratio, which shows the volume of carbon dioxide (CO_2) produced to the volume of oxygen (O_2) used (VCO_2/VO_2) in ND, CDHFD or therapeutic BHA+CDHFD group (n ≥ 4 each). The scale bar indicates 100 μm. All data were analyzed using two-tailed Student's t test or with one-way ANOVA with Turkey's multiple comparison test and are shown as mean ± s.e.m, with statistical significance displayed for p-values <0.05.

3.7 Therapeutic BHA treatment decreases fibrosis and inflammation but not hepatic proliferation

Therapeutic treatment with BHA+CDHFD for 6-months was able to fully reduce fibrosis, as shown by Sirius red staining **(fig. 15A)**. The number of proliferating hepatocytes in the therapeutic BHA treated group displayed a decreasing trend when compared to the CDHFD group **(fig. 15B)**. The numbers of CD3$^+$ cells as well as activated CD8$^+$ T cells were not different in the therapeutic group in comparison with ND mice **(fig.15C, F)**.

The same was observed for the myeloid compartment, where MHCII$^+$ and F4/80$^+$ cells did not show any difference in numbers in the BHA therapeutic group versus the ND group **(fig. 15D, E)**. The same profiles, in terms of total cell numbers, were also demonstrated with flow cytometry analysis for KCs and infiltrating monocytes **(fig. 15G, H)**. The tumor incidence in the therapeutic BHA+CDHFD group was significantly reduced, with 10% incidence versus 34% in the CDHFD 12-month group **(fig. 15I)**.
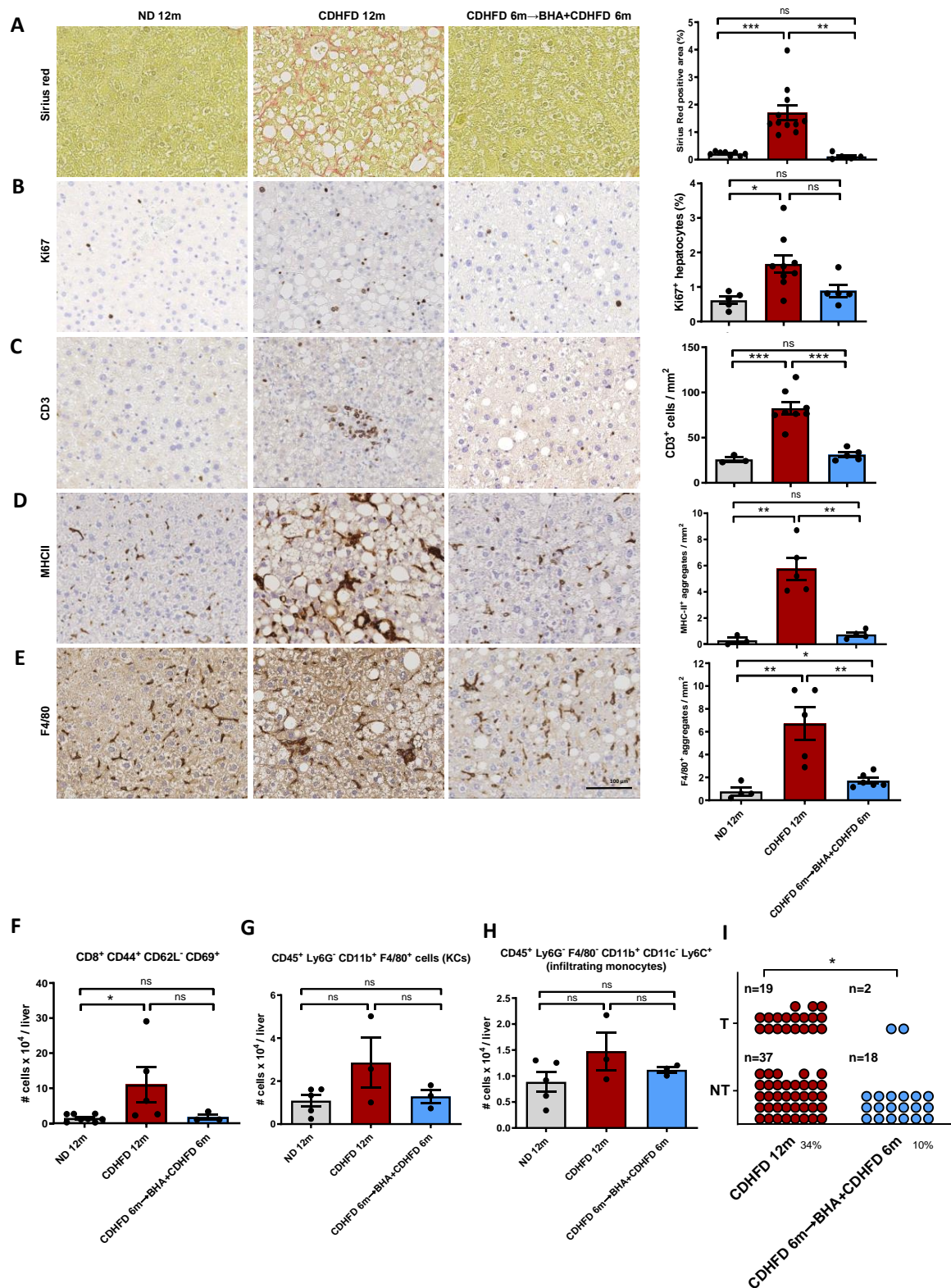
Figure 15. Therapeutic BHA abrogates fibrosis, immune response activation and reduces tumor incidence

A) Representative Sirius red staining showing perisinusoidal fibrosis, with quantifications to the right for the ND, CDHFD or therapeutic BHA+CDHFD group (n ≥ 5). **B)** Representative immunohistological

staining for Ki67$^+$ hepatocytes with respective quantification in percentages of the right side for the three groups (n ≥ 3), **D)** Histological representative pictures for CD3$^+$ T cells (n ≥ 3), plus quantification per mm^2 on the right side, for the three groups (n ≥ 4). **D)** The myeloid compartment was evaluated by IHC staining for MHCII$^+$ and **(E)** F4/80$^+$ cells with respective quantification per mm^2 on the right side (MHCII: n ≥ 3), (F4/80: n ≥ 4). Quantifications of flow cytometric analyses for liver activated CD8$^+$ T cells **(F)**, Kupffer cells **(G)** and infiltrating myeloid cells **(H)** from ND, CDHFD or therapeutic BHA+CDHFD group (n ≥ 4). **I)** Tumor incidence of 12-months CDHFD fed mice and therapeutic BHA+CDHFD. The scale bar represents 100μm. All data were analyzed using two-tailed Student's t test and are shown as mean ± s.e.m, with statistical significance displayed for p-values <0.05. For tumor incidence comparisons was used the Exact-Fisher test, significant values showed for p-value < 0.05.

3.8 Therapeutic astaxanthin supplementation at late NASH stage ameliorates NASH phenotype but has no effects on liver damage

We then tested AXT+CDHFD in a therapeutic approach starting with mice already on CDHFD for 6 months (late NASH stage), up until 12 months on diet. The mice became obese and continued to gain weight after diet switch, even slightly more than CDHFD only **(fig. 16A)**. The AXT+CDHFD therapeutic group did not show a reduction in serum ALT and cholesterol levels **(fig. 16C, D).** Although AXT did not prevent hepatic lipid accumulation, as shown by H&E and Sudan red **(fig. 16E, G)**, the treated mice displayed a significant decrease in NAFLD activity score compared to the CDHFD 12-months group **(fig. 16F)**. Of note, the lipid accumulation in the AXT-therapeutic treated livers actually increased **(fig. 16H)**, most likely because the compound´s vehicle made of oleoresin increased the overall diet kilocalories by 5%. Despite the fact that AXT could not reverse obesity, liver damage and cholesterol levels, thus exhibiting some features of metabolic syndrome, upon glucose challenge, the therapeutic AXT+CDHFD treated mice did not show insulin resistance **(fig. 16B)**.
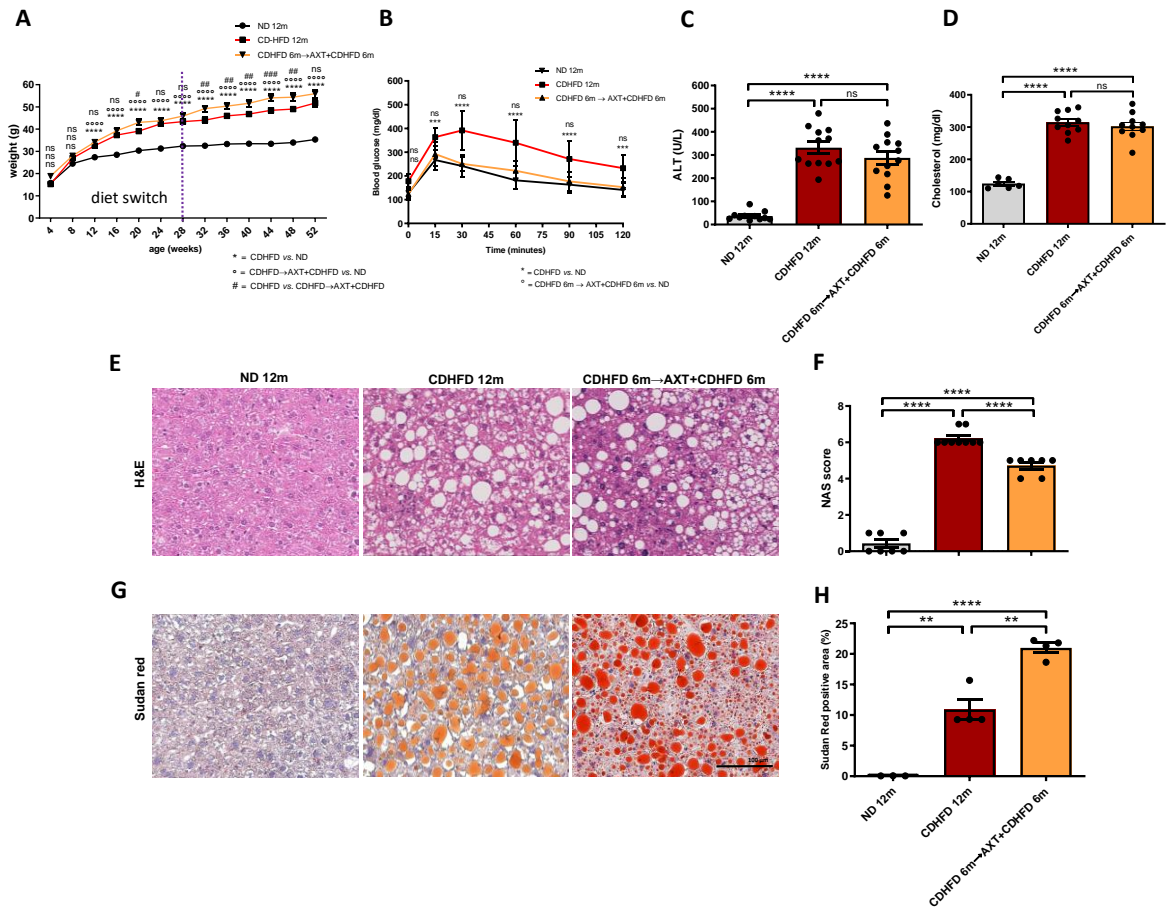
Figure 16. Therapeutic AXT at late NASH stage does not rescue from NASH and liver damage

A) Monthly weight measurements in male C57Bl/6 J Ola Hsd ND, CDHFD and therapeutic AXT+CDHFD mice (n=25) for late stage NASH. **B)** Glucose tolerance test achieved with 12-month-old male mice on ND, CDHFD or therapeutic AXT+CDHFD group (n=4 each). **C)** Quantification of serum alanine transaminase (ALT) and of free cholesterol **(D)** in male 12-month-old male mice on ND, CDHFD or therapeutic AXT+CDHFD group (n ≥ 5 each). **E)** H&E representative pictures demonstrating absence or presence of NASH of ND, CDHFD or therapeutic AXT+CDHFD livers. **F)** NAFLD Activity Score (NAS) evaluated for the three groups (n ≥ 7 each). **G)** Sudan red staining indicating hepatic fat accumulation in ND, CDHFD or therapeutic AXT+CDHFD group. **H)** Quantification of total Sudan red positive area for the three groups (n ≥ 3 each). Scale bar indicates 100 μm. All data were analyzed using two-tailed Student's t test or with one-way ANOVA with Turkey's multiple comparison test and are shown as mean ± s.e.m, with statistical significance displayed for p-values <0.05.

3.9 Therapeutic astaxanthin treatment decreased fibrosis, inflammation and hepatic proliferation

Therapeutic AXT+CDHFD treatment at late-stage NASH was able to reverse fibrosis, as shown by Sirius red staining in liver sections **(fig. 17A)** and most surprisingly, significantly reduced hepatocyte proliferation, as shown by ki67 IHC **(fig. 17B)**. IHC showed a reduction of CD3$^+$ **(fig. 17C)** and MHC$^+$ cells **(fig. 17D)** for the therapeutic group versus CDHFD fed mice 12-months. F4/80$^+$ IHC showed a trend of decrease in the therapeutic group compared to the CDHFD mice **(fig. 17E)**. Flow cytometry analysis revealed no activated CD8$^+$ T cells **(fig. 17F)**, and no increase of KCs **(fig. 17G)** and infiltrating monocytes **(fig. 17H)**, similar to ND group.
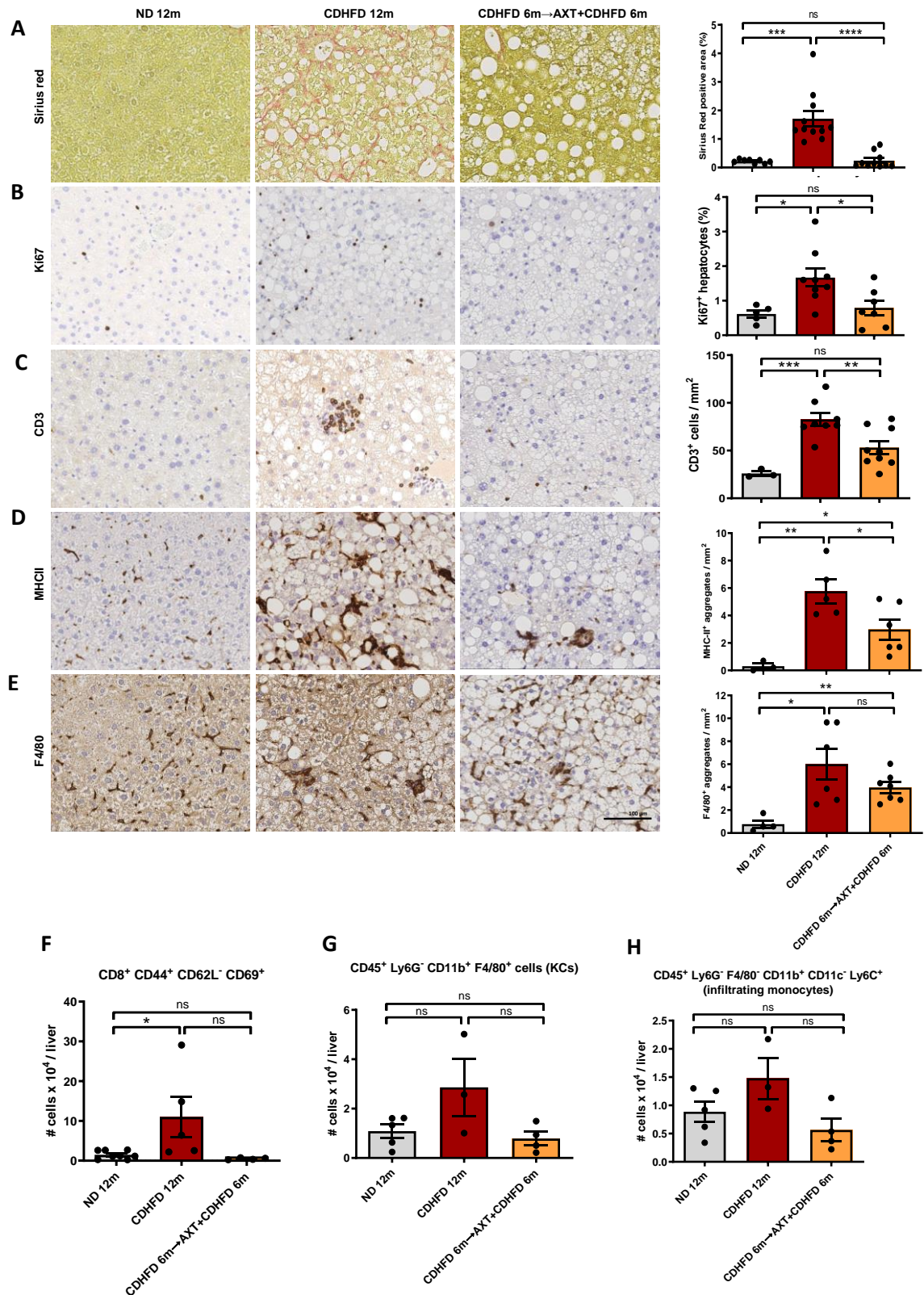
Figure 17. Therapeutic AXT at late NASH stage reduces fibrosis, infiltration of CD3+ cells, KCs cells and hepatocytes proliferation

A) Representative Sirius red staining showing perisinusoidal fibrosis, with quantifications to the right for the ND, CDHFD or therapeutic AXT+CDHFD group (n ≥ 5) for late NASH stage. **B)** Representative

immunohistological staining for Ki67^{+} hepatocytes with respective quantification in percentages of the right side for the three groups (n ≥ 3), **D)** Histological representative pictures for CD3^{+} T cells (n ≥ 3), plus quantification per mm^2 on the right side, for the three groups (n ≥ 4). **D)** The myeloid compartment was evaluated by IHC staining for MHCII[+] and **(E)** F4/80^{+} cells with respective quantification per mm^2 on the right side (MHCII: n ≥ 3), (F4/80: n ≥ 4). Quantifications of flow cytometric analyses for liver activated CD8^{+} T cells **(F)**, Kupffer cells **(G)** and infiltrating myeloid cells **(H)** from ND, CDHFD or therapeutic BHA+CDHFD group (n ≥ 4). The scale bar represents 100μm. All data were analyzed using two-tailed Student's t test and are shown as mean ± s.e.m, with statistical significance displayed for p-values <0.05.

3.10 Therapeutic astaxanthin treatment at late stage reduces tumor incidence and hepatocytes'proliferation in tumor nodules

An overall tumor characterization was performed in tumor samples from C57Bl/6J kept on CDHFD for 12-months or on AXT switched-diet, by measurement of tumor nodules size, by H&E staining and by IHC using the HCC tumor marker Golgi protein 73 (GP73). Hepatocyte proliferation was assessed by IHC with anti-Ki67 antibody and quantified by using five different and independent areas randomly selected within the nodules. The tumor incidence of therapeutic AXT treated mice was significantly reduced compared to untreated CDHFD mice **(fig. 18D)**. Although the average size of the nodules did not show any significant difference among the aforementioned two groups **(fig.18E)**, the H&E staining revealed a difference in terms of lipid accumulation, a feature that the tumors of CDHFD 12-month group had lost. Furthermore, the GP73 staining showed reduced accumulation of GP73 protein in the cytoplasm of hepatocytes in the AXT+CDHFD group **(fig. 18B)**. Interestingly, hepatocytes' proliferation in the nodules of AXT+CDHFD was significantly reduced compared to the CDHFD group **(fig. 18F)**. Genomic copy number alterations were characterized using array comparative genomic hybridization: no differences with regard to the frequencies of copy number alterations between the AXT and CDHFD (CTR) groups were identified **(fig. 18G, H).**
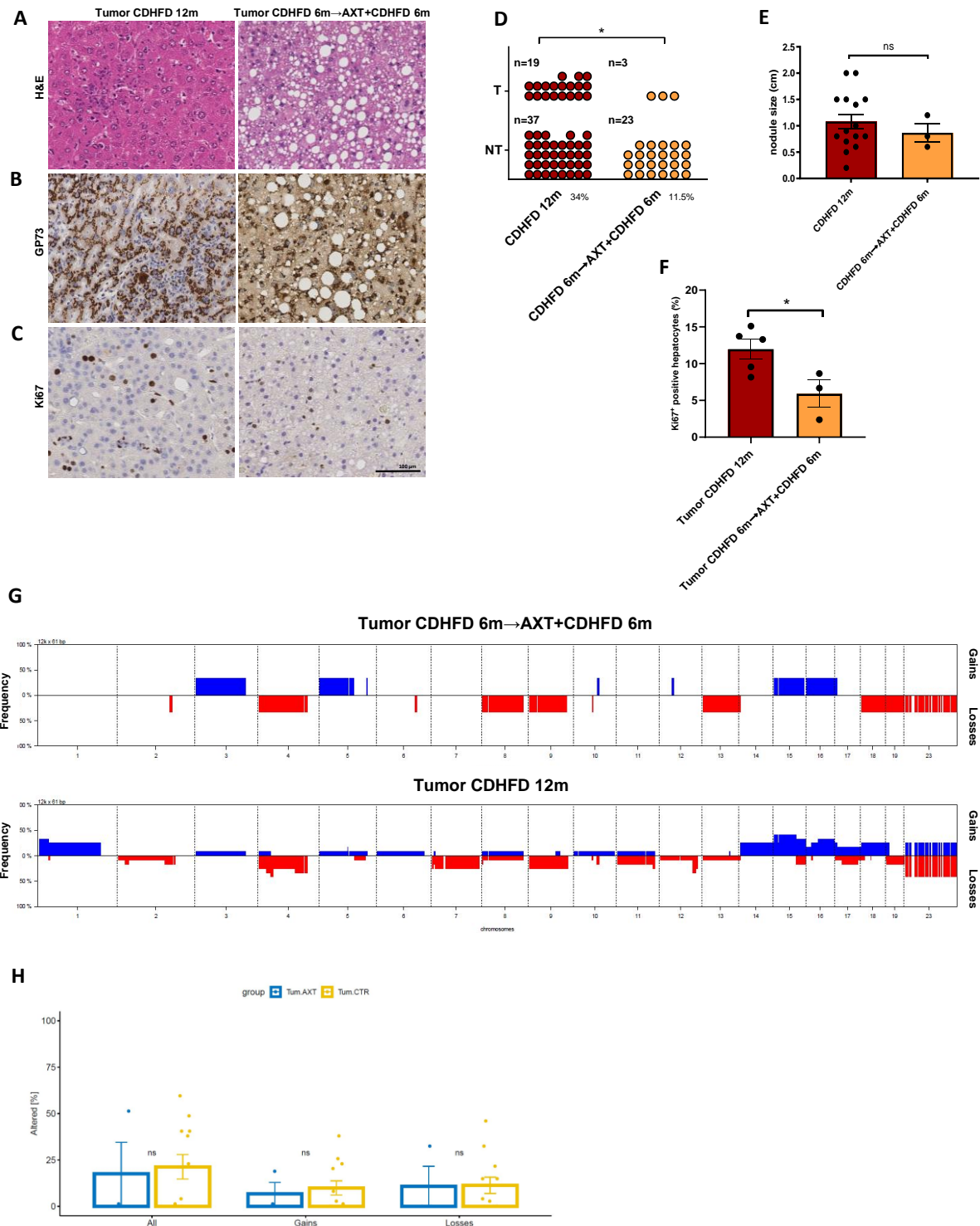
Figure 18. Therapeutic Astaxanthin treatment at late stage reduces hepaticytes' proliferation in tumor nodules

A) Representative H&E staining from tumor samples of CDHFD 12-months group and for late NASH stage therapeutic AXT+CDHFD (CDHFD 6-months→AXT+CDHFD 6-months) group. **B)** Immunohistochemical staining for tumor marker GP73. **C)** Ki67^{+} representative immunohistochemical staining for proliferative hepatocytes for 12-months CDHFD and therapeutic AXT-treated mice. **D)** Graphical summary of individuals (in symbols) under 12-months CDHFD or under therapeutic

AXT+CDHFD without tumor (NT) and with tumor (T) (n ≥ 23 each). **E)** Measurements of size of tumor nodules (n ≥ 3). **F)** Quantification of Ki67^{+} hepatocytes in nodules of the two groups (n ≥ 3). **G)** Frequency plots from aCGH analysis: in upper row is shown the frequency for chromosomal aberrations of therapeutic CDHFD 6m→AXT+CDHFD 6m tumor nodules (n=2); in the lower row is displayed the frequency plot for CDHFD 12-months tumor nodules (n=7). The scale bar indicates 100 μm. All data were analyzed using two-tailed Student's t test and are shown as mean ± s.e.m, with statistical significance displayed for p-values <0.05.

3.11 Liver proteomic analysis of putative candidates driving cancer in NASH-affected mice

Using differentially expressed data from liver proteomic analysis, I have developed an approach to identify common proteins from late NASH (6-months), very advanced NASH (12-months) and tumor CDHFD-induced (12-months), all versus ND group age-matched. The 6-months CDHFD fed mice showed in total 2385 upregulated proteins when compared to 6-months ND fed mice. Among them, 84 proteins were held in common with the prophylactic 6-months BHA+CDHFD mice, and 9 proteins in common with the prophylactic 6-months AXT+CDHFD group. Four proteins intersected among the three groups **(fig. 19A)**. The 12-months CDHFD fed mice groups, with or without tumors, displayed 233 and 173 upregulated proteins, respectively **(fig. 19B)**. They shared 74 proteins, which intersected with 2385 proteins of the 6-month CDHFD group: the 41 proteins held in common were considered putative cancer-driving proteins due to upregulated expression pattern over time until tumor establishment **(fig. 19C)**. Among these shared candidates, proteins involved in cell metabolism, such as glycolysis, lipid metabolism, mitochondrial DNA damage response and mitochondrial tetrahydrofolate synthesis were identified. In addition, proteins associated with proliferation, inflammation and fibrosis were detected. One candidate for antioxidant response, glutathione synthetase, was found among the common proteins.
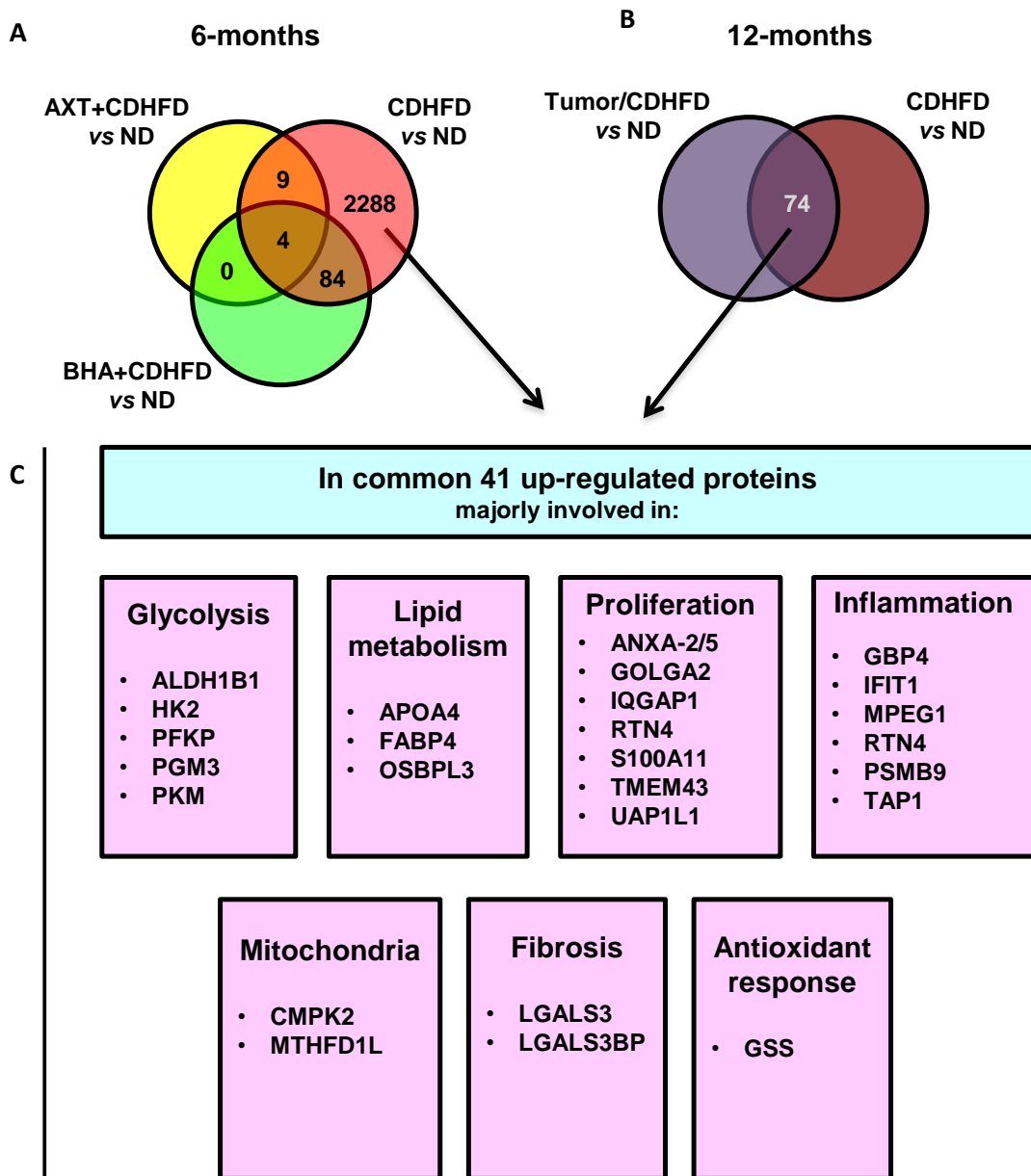
Figure 19. Proteomic analysis of protein candidates involved in tumorigenesis over-time.

A) Venn diagram of up-regulated proteins from CDHFD *vs.* ND, BHA+CDHFD *vs.* ND and AXT+CDHFD *vs.* ND comparisons of 6-months diet regiment. **B)** Venn diagram of up-regulated proteins from HCC CDHFD-induced *vs.* ND and CDHFD *vs.* ND comparisons of 12-months diet regiment. **C)** Common upregulated proteins among NASH-affected mice (6-months CDHFD vs. ND mice) and intersected proteins from the Venn diagram with CDHFD 12-months with and without tumors. Relevant proteins for metabolic pathways, inflammation and proliferation are displayed.

3.12 Therapeutic astaxanthin at early NASH stage prevents NASH exacerbation and decreases liver damage

I wanted to determine whether a therapeutic treatment at the beginning of NASH development (early NASH stage or also borderline NAFL/NASH) could potentially be more efficient with regard to cancer prevention. For this reason, I kept C57Bl/6J mice for 3-months on CDHFD, a time point in which we have observed to be sufficient to induce borderline NASH **(fig. 20H, I)**, liver damage **(fig. 20J)** and hepatic lipid accumulation **(fig. 20K)**.

Afterwards, I switched the CDHFD to AXT+CDHFD and kept mice under this feeding regimen for a period of 9-months, in which they continued to gain weight, becoming obese **(fig. 20A)**. The serum ALT systemic marker for liver damage remained high, although significantly reduced compared to the CDHFD 12-months group **(fig. 20B)**. H&E staining revealed similar degree of steatosis **(fig. 20D)** but significantly diminished NAS score **(fig. 20E)**, thus indicating that AXT-treated mice did not undergo exacerbation of NASH, contrary to the CDHFD 12-months mice. Sudan red staining showed an increase of hepatic lipid accumulation **(fig. 20F, G)**, resembling the aforementioned therapeutic treatment: this effect is probably due to the vehicle (oleoresin) of AXT itself.
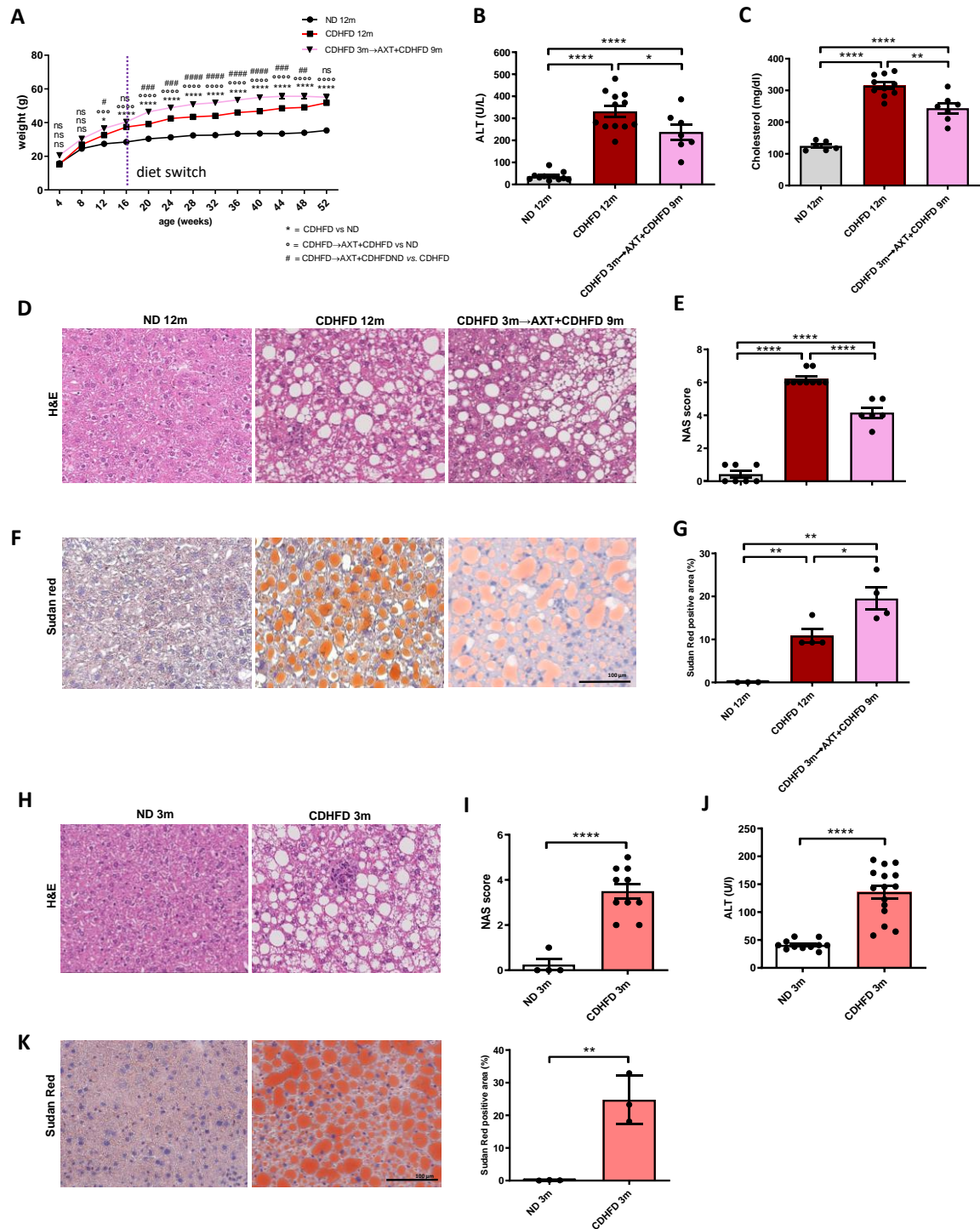
Figure 20. Therapeutic AXT at early NASH stage ameliorates NASH and decreases liver damage

A) Monthly weight measurements in male C57Bl/6 J Ola Hsd ND, CDHFD and therapeutic AXT+CDHFD mice (n ≥ 9) for early stage NASH. **B)** Quantification of serum alanine transaminase (ALT) and of free cholesterol **(C)** in male 12-month-old male mice on ND, CDHFD or therapeutic AXT+CDHFD group (n ≥ 7 each). **D)** H&E representative pictures demonstrating absence or presence of NASH of ND, CDHFD or therapeutic AXT+CDHFD livers. **E)** NAFLD Activity Score (NAS) evaluated for the three groups (n ≥ 7 each). **F)** Sudan Red staining indicating hepatic fat accumulation in ND, CDHFD or therapeutic AXT+CDHFD group. **G)** Quantification of total Sudan red positive area for the three groups

(n ≥ 3 each). **H)** H&E representative pictures demonstrating absence or presence of NASH in livers of ND, CDHFD for 3-months diet regimen. **I)** NAFLD score (NAS) evaluated for ND and CDHFD 3-months groups (n ≥ 7 each). **J)** Serological ALT measurements for ND and CDHFD 3-months groups (n ≥ 11 each). **K)** Sudan Red staining of 3-months ND and CDHFD groups, with quantification on the right side (n=3). Scale bar indicates 100 μm. All data were analyzed using two-tailed Student's t test or with one-way ANOVA with Turkey's multiple comparison test and are shown as mean ± s.e.m, with statistical significance displayed for p-values <0.05.

3.13 Therapeutic astaxanthin administered at an early stage of NASH diminished fibrosis, inflammation, hepatocyte proliferation and protects from tumor development

Sirius red staining revealed that therapeutic AXT+CDHFD at early NASH stages did not lead to hepatic fibrosis formation **(fig. 21A)**. Hepatocyte proliferation was significantly diminished compared to the CDHFD 12-month groups **(fig. 21B)** as shown by Ki67 IHC. IHC staining revealed reduction of CD3$^+$ cells **(fig. 21C)** and KCs **(fig. 21D, E)** in the AXT-treated mice. Interestingly, this therapeutic approach at early NASH stages was capable of preventing tumor development **(fig. 21F)**.
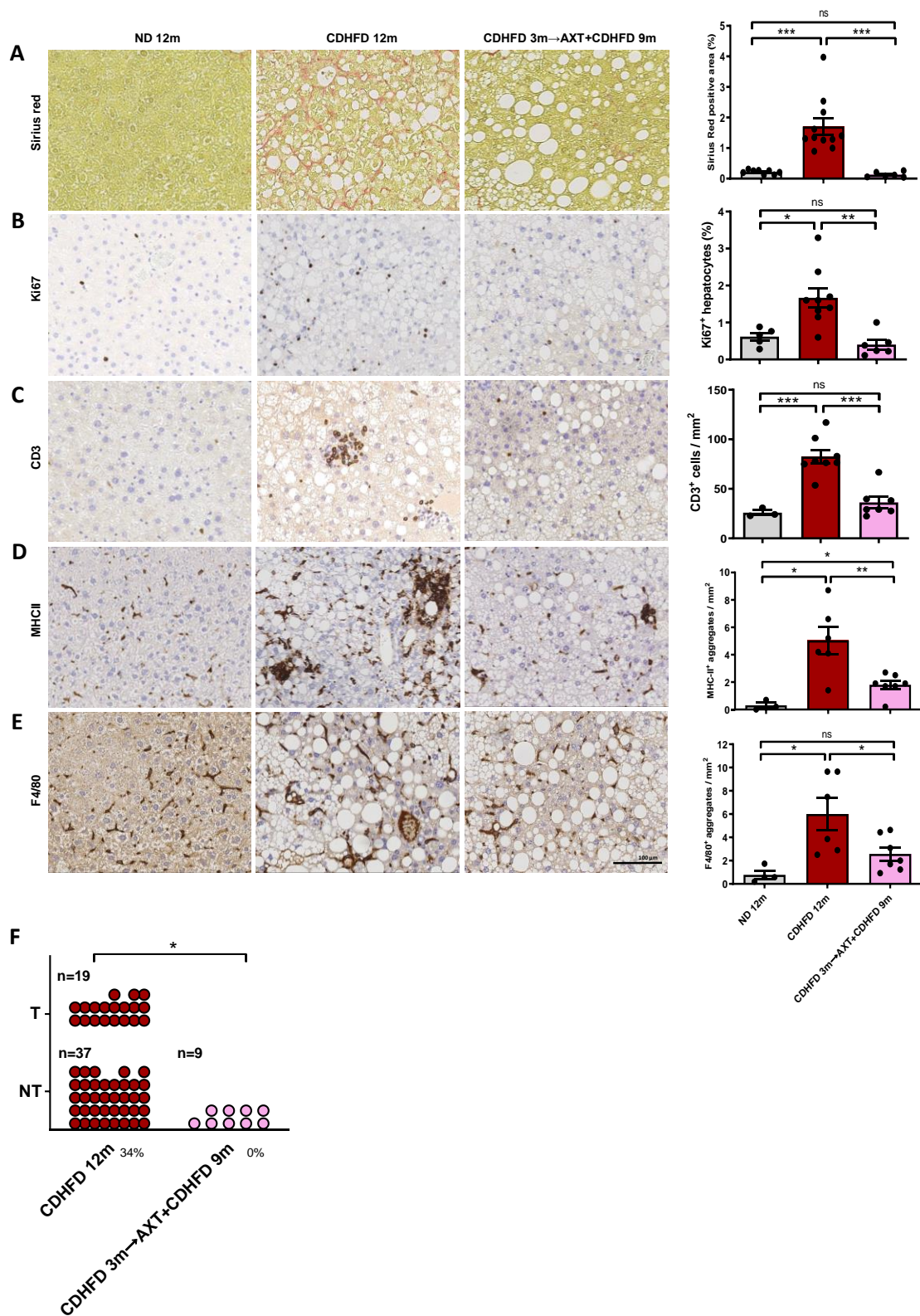
Figure 21. Therapeutic AXT at early NASH stage reduces fibrosis, infiltration of CD3+ cells, macrophages, hepatocytes proliferation and prevents liver cancer

A) Representative Sirius red staining showing perisinusoidal fibrosis, with quantifications to the right for the ND, CDHFD or therapeutic early NASH stage AXT+CDHFD group (n ≥ 7). **B)** Representative immunohistological staining for Ki67^{+} hepatocytes with respective quantification in percentages of the

right side for the three groups (n ≥ 5), **D)** Histological representative pictures for CD3$^+$ T cells (n ≥ 3), plus quantification per mm^2 on the right side, for the three groups (n ≥ 4). **D)** The myeloid compartment was evaluated by IHC staining for MHCII$^+$ and **(E)** F4/80$^+$ cells with respective quantification per mm^2 on the right side (MHCII: n ≥ 3), (F4/80: n ≥ 4). **F)** Graphical summary of individuals (in symbols) under 12-months CDHFD or under therapeutic AXT+CDHFD without tumor (NT) and with tumor (T) (n ≥ 9 each). The scale bar represents 100μm. All data were analyzed using two-tailed Student's t test and are shown as mean ± s.e.m, with statistical significance displayed for p-values <0.05. For tumor incidence comparisons was used the Exact-Fisher test, significant values showed for p-value < 0.05.

3.14 Changing CDHFD diet to normal diet at late NASH stages reverses NASH and liver damage and reduces tumor development

Next, we wanted to assess whether switching CDHFD to normal diet (ND) at 6-months would reverse NASH phenotype and prevent cancer development. The monthly weight measurements over time showed that switching to ND after 6-months of CDHFD decreased the body weight gradually **(fig. 22A)**. IPGGT showed that the diet-switch group had normal glucose regulation **(fig. 22B).** Serum analysis for ALT and cholesterol showed similar values to the control ND group **(fig. 22C, D).** From the H&E staining and NAS was evaluated that the diet-switch reverses the NASH phenotype **(fig. 22E)**. In addition, the switched-diet mice did not show any sign of hepatic fibrosis, as demonstrated by Sirius red staining, and upon ki67 IHC they displayed significantly decreased hepatocyte proliferation when compared to the CDHFD counterpart **(fig. 22F, G)**. T cells were also significantly reduced in number, reaching the same level of ND control **(fig. 22H)** as shown by CD3$^+$ IHC. The tumor incidence in the diet-switch group showed a trend towards decrease, when compared to the 12-months CDHFD fed mice **(fig. 22I)**.
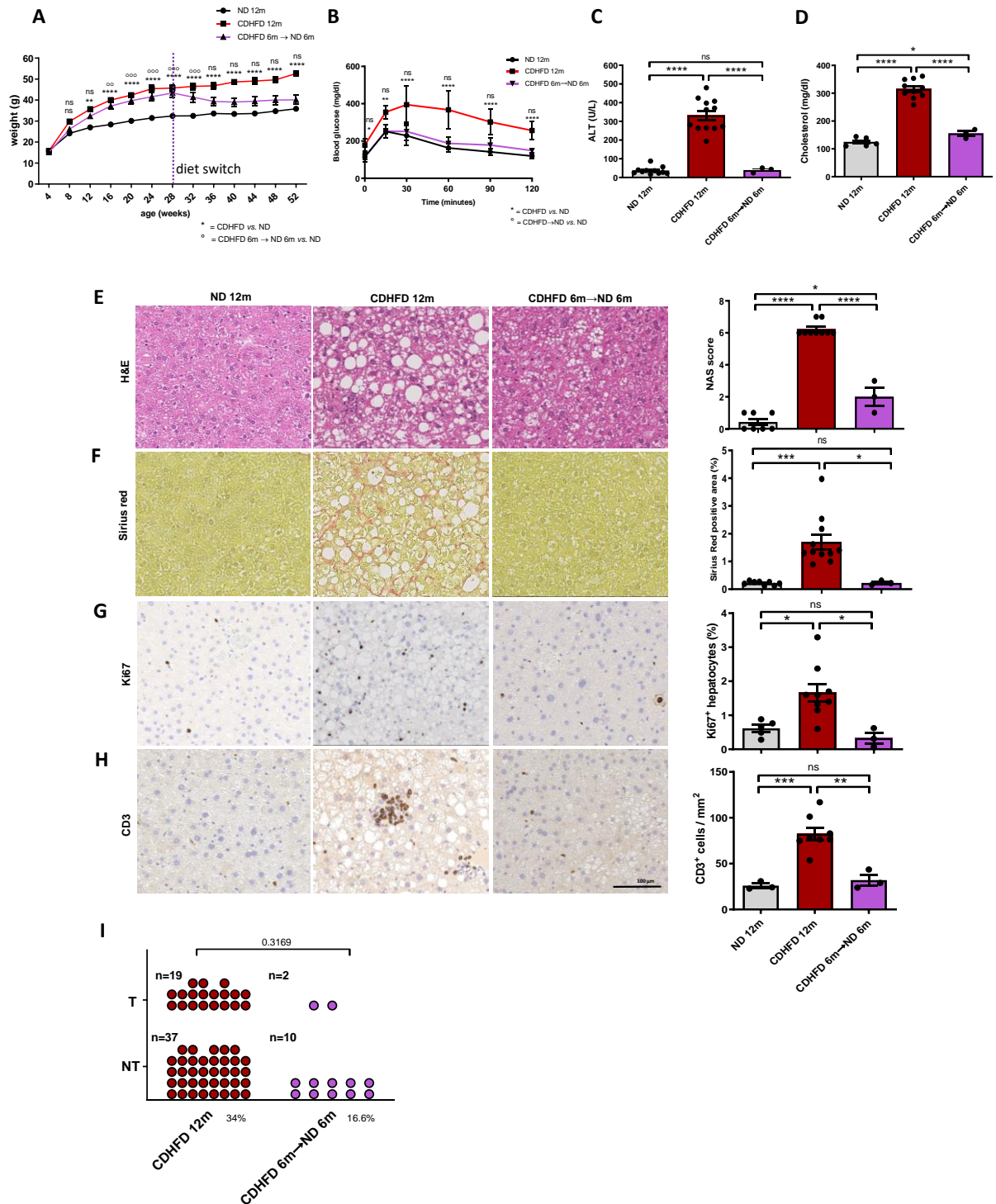
Figure 22. Switching CDHFD diet with normal diet at late NASH stage reverses NASH and reduces liver damage and tumor development

A) Monthly weight measurements in male C57Bl/6 J Ola Hsd ND, CDHFD and diet-switch ND mice (n ≥ 15) for late stage NASH (6-months diet-switch). **B)** Glucose tolerance test achieved with 12-month-old male mice on ND, CDHFD or diet-switch ND group (n ≥ 3 each). **C)** Quantification of serum alanine transaminase (ALT) and of free cholesterol **(D)** in male 12-month-old male mice on ND, CDHFD or diet-switch ND group (n ≥ 3 each). **E)** H&E representative pictures demonstrating absence or presence of NASH of ND, CDHFD or diet-switch ND livers. NAFLD Activity Score (NAS) (on right side) is evaluated for the three groups (n ≥ 3 each). **F)** Representative Sirius red staining showing perisinusoidal fibrosis,

98

with quantifications to the right for the ND, CDHFD or diet-switch ND group (n ≥ 3 each) for late NASH stage. **G)** Representative immunohistological staining for Ki67^{+} hepatocytes with respective quantification in percentages of the right side for the three groups (n ≥ 3). **H)** Histological representative pictures for CD3^{+} T cells (n ≥ 3), plus quantification per mm[2] on the right side, for the three groups (n ≥ 3). **I)** Graphical summary of individuals (in symbols) under 12-months CDHFD or under diet-switch ND without tumor (NT) and with tumor (T) (n ≥ 12 each). Scale bar indicates 100 μm. All data were analyzed using two-tailed Student's t test or with one-way ANOVA with Turkey's multiple comparison test and are shown as mean ± s.e.m, with statistical significance displayed for p-values <0.05. For tumor incidence comparisons was used the Exact-Fisher test, significant values showed for p-value < 0.05.

3.15 Changing CDHFD to normal diet at very late NASH stage reverses NASH and reduces cancer incidence, but does not significantly reduce fibrosis

The diet switch with normal diet was also performed at very late-stage NASH (9-months), to verify if that time point would be the point of no-return for reduced cancer incidence in NASH-affected mice. From the monthly weight measurements over time it was determined that switching the diet to ND after 9-months of CDHFD decreased the body weight gradually until a weight in between of CDHFD and ND fed mice **(fig. 23A)**. ALT and cholesterol serum analysis revealed very similar values to the control ND group **(fig. 23B, C)**. H&E staining and NAS evaluation demonstrated that the diet-switch reverses the NASH phenotype **(fig. 23E)**. The diet-switch group displayed reduced fibrosis with respect to CDHFD 18 months mice, although this was not significant **(fig. 23F)**. IHC for Ki67 showed a strong reduction in hepatocyte proliferation compared to 18-months CDHFD mice **(fig. 23G)**. The diet switch group showed, based on IHC for CD3, that T cells were reduced in number compared to the CDHFD group **(fig. 23H)**. Regarding the tumor incidence, the diet-switch group showed a significant decrease compared to the 18-month CDHFD fed mice **(fig. 23I)**. In terms of percentage, this tumor incidence appears to be very similar to the cancer incidence in diet-switch group 6-months CDHFD→6-months ND compared to 12-months CDHFD fed mice **(fig. 23J)**.
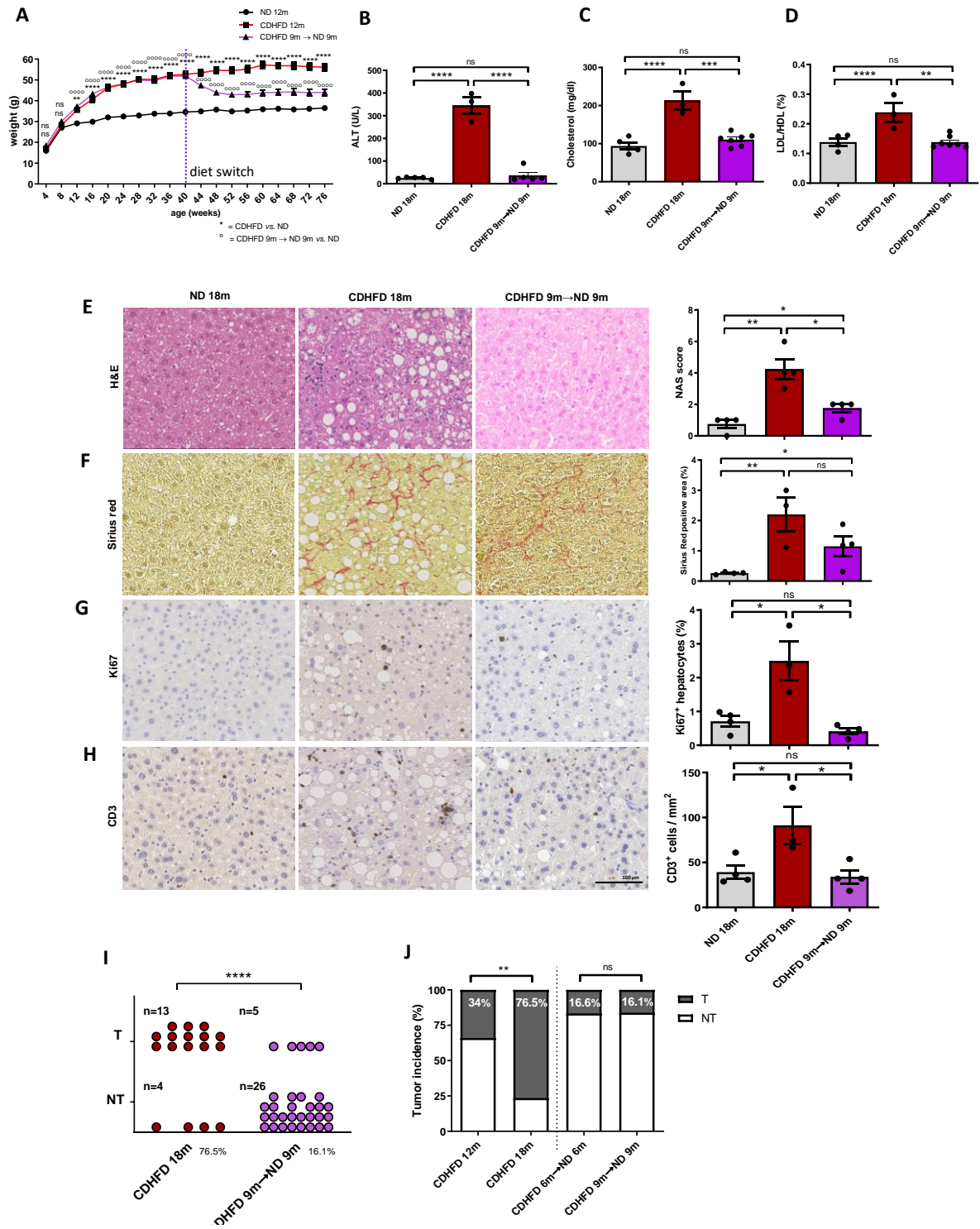
Figure 23. Switching diet with normal diet at very late NASH stage reverses NASH and liver damage and reduces cancer incidence but not fibrosis

A) Monthly weight measurements in male C57Bl/6 J Ola Hsd ND, CDHFD and diet-switch ND mice (n ≥ 15) for very late stage NASH (9-months diet-switch). **B)** Quantification of serum alanine transaminase (ALT), free cholesterol **(C)** and LDL/HDL (in percentage) ratio **(D)** in male 12-month-old male mice on ND, CDHFD or diet-switch ND group (n ≥ 3 each). **E)** H&E representative pictures demonstrating absence or presence of NASH of ND, CDHFD or diet-switch ND livers. NAFLD Activity Score (NAS) (on

right side) is evaluated for the three groups (n ≥ 3 each). **F)** Representative Sirius red staining showing perisinusoidal fibrosis, with quantifications to the right for the ND, CDHFD or diet-switch ND group (n ≥ 4 each) for late NASH stage. **G)** Representative immunohistological staining for Ki67^{+} hepatocytes with respective quantification in percentages of the right side for the three groups (n ≥ 3). **H)** Histological representative pictures for CD3^{+} T cells (n ≥ 3), plus quantification per mm[2] on the right side, for the three groups (n ≥ 3). **I)** Graphical summary of individuals (in symbols) under 12-months CDHFD or under diet-switch ND without tumor (NT) and with tumor (T) (n ≥ 12 each). **J)** Graphical summary of individuals (in symbols) under 18-months CDHFD or under diet-switch ND without tumor (NT) and with tumor (T) (n ≥ 17 each) **K)** Percentages of tumor incidences for time points of 12-months and of 18-months. Scale bar indicates 100 μm. All data were analyzed using two-tailed Student's t test or with one-way ANOVA with Turkey's multiple comparison test and are shown as mean ± s.e.m, with statistical significance displayed for p-values <0.05. For tumor incidence comparisons was used the Exact-Fisher test, significant values showed for p-value < 0.05.

3.16 **Serum proteomic analysis identifies potential serological biomarkers for early detection of NASH-induced HCC**

We performed mass spectrometry analysis on serum samples collected over time from NASH and HCC-affected mice. Prior to mass spectrometry analysis I have applied a depletion protocol for the most abundant proteins in serum, such as albumin and IgG, which could interfere with the detection of less abundant proteins. Serum was collected over time at 4-, 6-, 9- and 12-months from CDHFD and ND fed mice **(fig. 24A)**. For the analysis, CDHFD fed mice were compared with their age-matched ND group. Venn diagrams were used to identify common proteins among the CDHFD fed mice that develop tumors and those that did not **(fig. 24B)**.
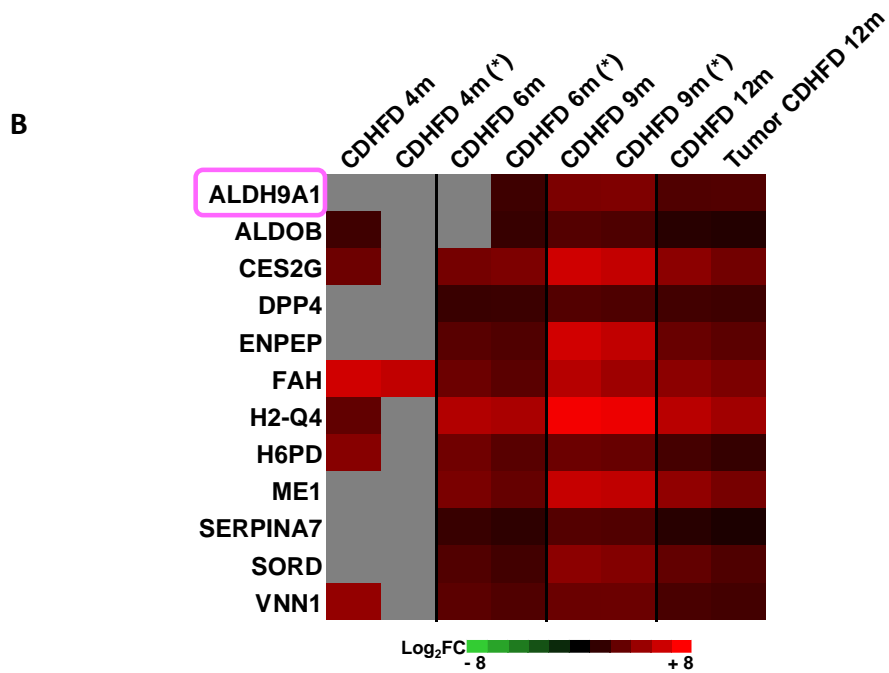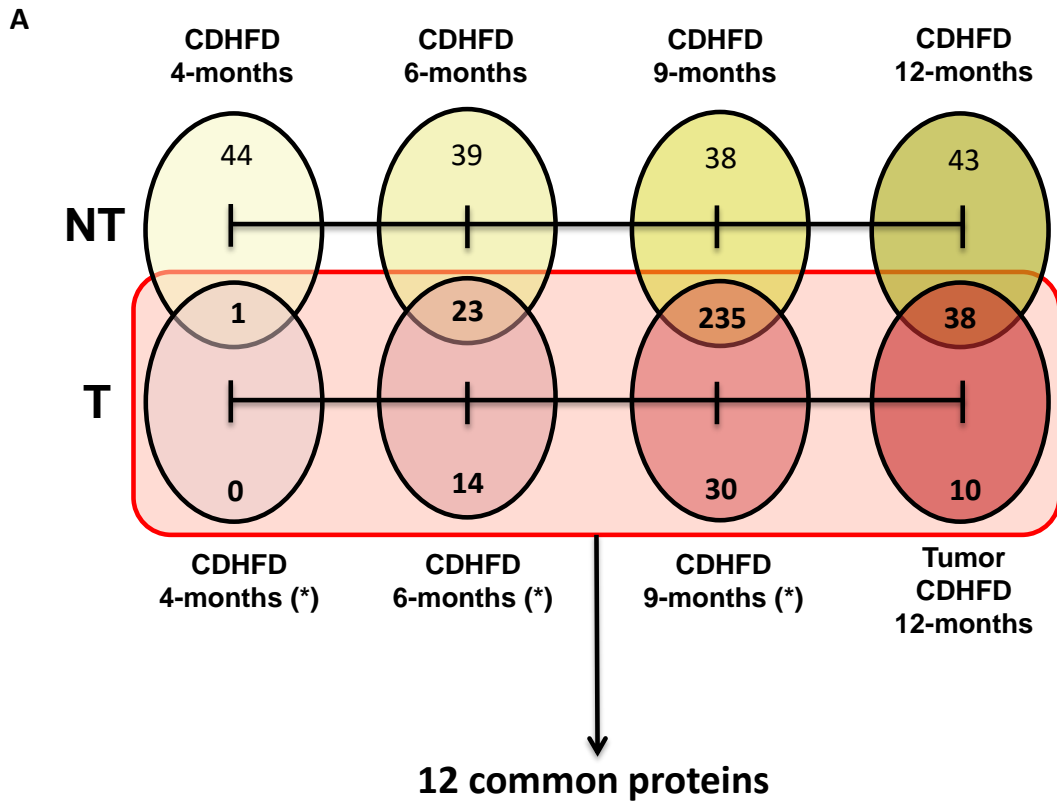
Figure 24. Serum proteomic analysis for liver cancer early biomarker identification in NASH-affected mice

A) Venn diagrams showing over-time upregulated proteins among CDHFD fed mice against their age-matched ND group. **B)** Heatmap representing 12 common upregulated proteins among tumor-developing mice (with asterisk) and NASH-affected mice without tumor, compared versus age-matched ND group. Grey color indicates not significant difference.

3.17 Suitability of human iCCA MSI-processed RNA samples for RNA sequencing

In order to characterize of inter- and intra-tumor heterogeneity in human iCCA human samples we aimed to adopt spatially resolved mass-spectrometry imaging (MALDI-MSI) metabolomics with RNA-sequencing transcriptomic analysis in combination with available clinical data **(fig. 25M, N, O, P)**. In a first step MALDI MSI was performed on FFPE tumor sections mounted on conductive ITO-slides **(fig. 25A, B)**. A consecutive H&E section was used to annotate tumor areas, defined as regions-of-interest (ROIs) **(fig. 25C)**, which were co-registered with the MALDI-MSI images for subsequent clustering of ROIs. The limitation of only using H&E histopathological evaluation is the difficulty to determine potential heterogeneity among iCCA tissues **(fig. 26A)**. The spatial clustering of MALDI MSI profiles was performed with a *k* of 5, resulting in 5 clusters. This number was chosen since has provided a meaningful tradeoff between the size of clustered regions (ROIs) and the heterogeneity between clusters **(fig. 25D, fig. 26B)**. The obtained clusters were manually dissected after laser-burning the boundaries **(fig. 25E, F)**. The dissected areas from the same clusters were pooled and subsequently subjected to RNA extraction, using a protocol optimized for low-quality RNA **(fig. 25G)**. Sufficient amounts of RNA with suitable quality for subsequent library generation for QuantSeq 3′ mRNA sequencing were obtained from all clusters from all samples. The RNA integrity determined by DV_{200} after calculation from Bioanalyzer capillary electrofluorograms, showed that every sample contained at least 20% RNA fragments with a size > 200 nucleotides **(fig.25H, I; fig.26C, D)**. The RNA integrity of all extracted RNA samples was appropriate to generate the library necessary for the subsequent sequencing.
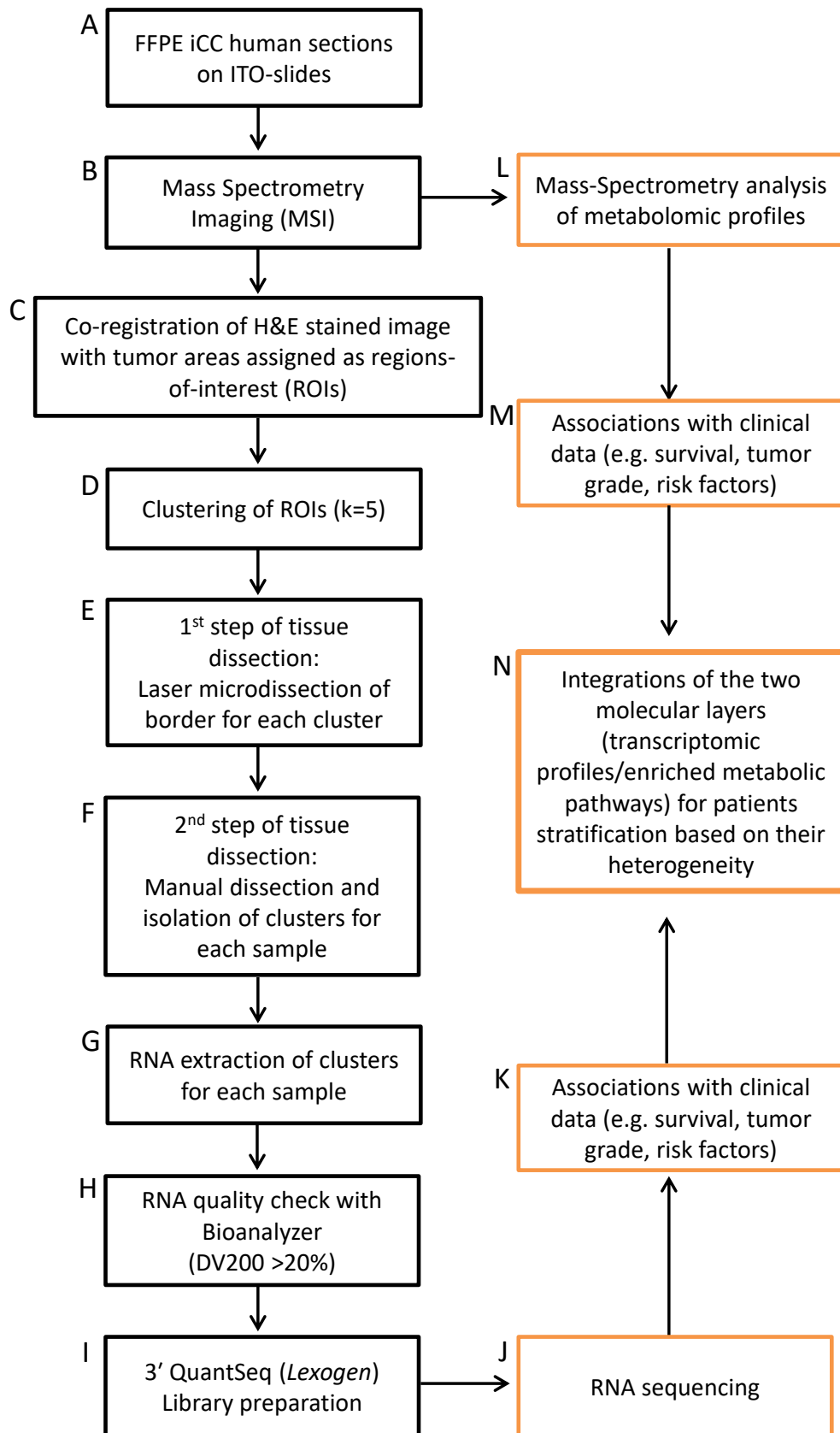
Figure 25. Workflow for RNA extraction of different metabolomics clusters based on MSI. Black framed boxes indicate performed procedures. Orange frame boxes show the next following steps for data analysis and data integration.
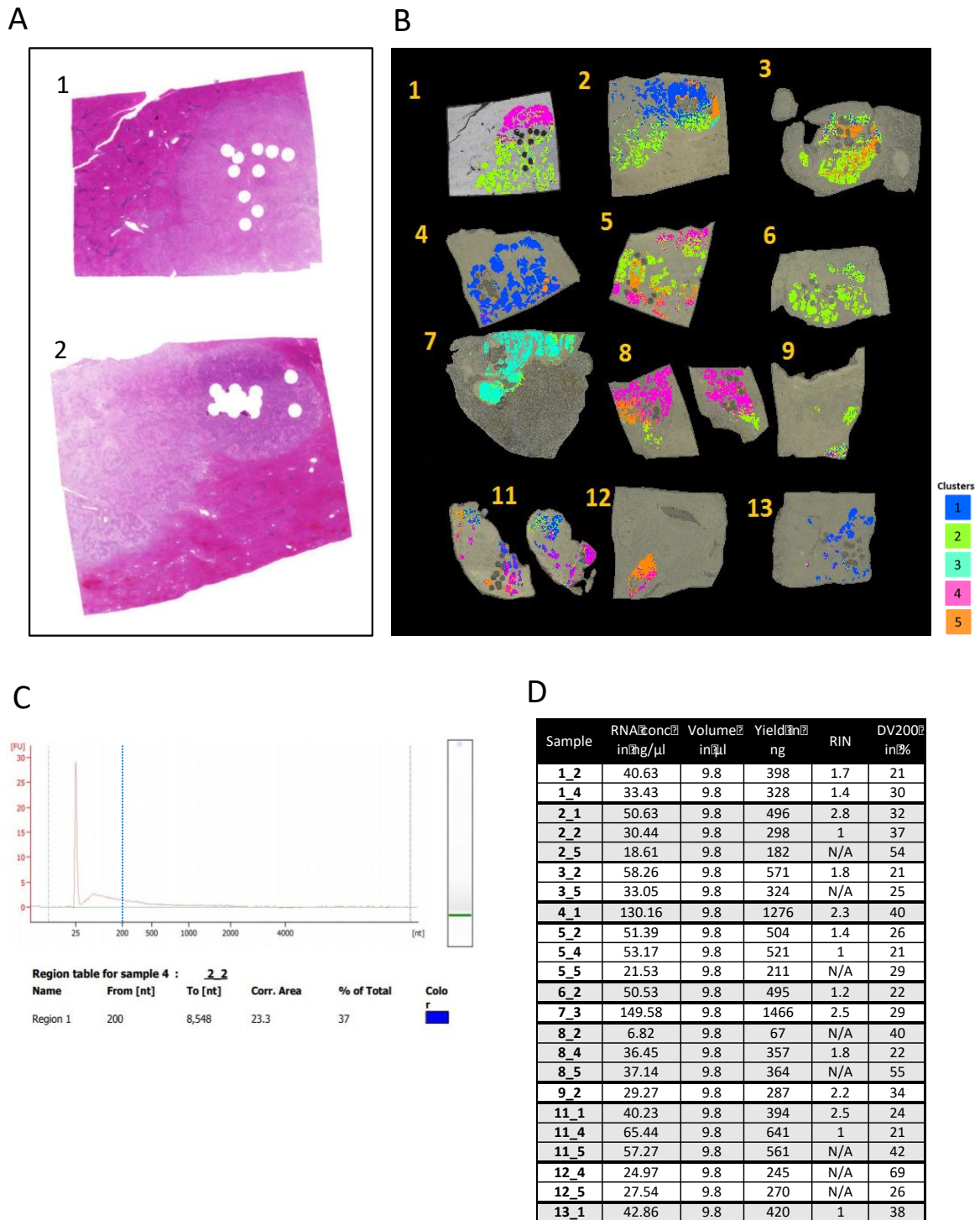
Figure 26. A) Representative H&E staining of iCCA samples with more than one identified cluster. **B)** Images of MSI-processed samples (n=12) indicating different clusters (k=5) identified with SCiLS Lab 2019b software. **C)** Bioanalyzer profile of representative extracted RNA, indicating sample integrity with DV_{200} (blue dotted line). **D)** Table with extracted RNA from different clusters from each sample, with yield, RNA concentration, and RNA quality (RIN and DV_{200} values).

Discussion

There is wide evidence linking oxidative stress with chronic inflammatory diseases and with cancer development (Reuter et al., 2010). Oxidative stress is established when the net production of radical species (ROS or RNS) and reactive metabolites exceeds the amount that the endogenous antioxidant systems are able to eliminate. Various factors can contribute to such an imbalance: viral infection, smoking, alcohol abuse, exposure to hepatotoxic agents (e.g. Aflatoxin B1) and high caloric/high lipids diets, can generate conditions that induce oxidative stress (Cichoż-Lach and Michalak, 2014). The major sources of ROS are mitochondria, ER, peroxisomes and detoxification enzymes (e.g. CYP2E1). It is well-understood that dysregulation of these organelles or enzyme functions can induce oxidative stress. In NASH, the continuous hepatic lipid overload first augments the mitochondrial β-oxidation to catabolize the lipid excess, but eventually results in ATP depletion and apoptosis. Free fatty acids induce lipotoxicity, not only affecting mitochondria but also inducing ER stress and subsequent activation of *de novo* lipogenesis, inflammation and execution of different types of cell death (Boege et al., 2017; Lebeaupin et al., 2018). Oxidative stress is also intimately related to cancer development, since ROS generate oxidized lipids: their by-products can attack proteins and generate DNA adducts. These processes favor mutations, DNA repair defects, and proliferation that eventually lead to the transformation into malignant hepatocytes (Maeda et al., 2015). In established HCC as well, levels of oxidative damage are associated with cancer recurrences and metastasis (Liu et al., 2017).

The use of antioxidants in combination with CDHFD helped to understand to what extent oxidative stress is contributing to the induction and progression of NASH and subsequent HCC.

In prophylactic treatment with BHA supplementation we observed complete prevention of steatosis, NASH **(fig. 9E, F)**, fibrosis **(fig. 10A)**, activation of CD8$^+$ T cells **(fig. 10F)**, and infiltration of KCs and macrophage infiltration **(fig. 10G, H)**. Hepatocyte proliferation instead only showed a trend towards a decrease **(fig.10B)**.

The natural antioxidant astaxanthin (AXT) added to the CDHFD was not able to prevent obesity or liver steatosis but prevented the development of NASH in 50% of the treated mice, and the other half of treated mice showed mild NASH and decreased liver damage **(fig. 11A, C, E, F, G, H)**. AXT completely prevented fibrosis **(fig. 12A)**, immune cell activation and infiltration **(fig. 12C, D, E, F, G)**, and significantly reduced hepatocyte proliferation **(fig. 12B)**.

Proteomic analysis revealed very similar profiles for the two prophylactic treatments, except for the expression of NRF2 and some of its target proteins (e.g. NQO1, CBR3), which we observed to be highly upregulated in BHA+CDHFD fed mice **(fig. 13D).**

These results in the prophylactically BHA-treated mice are in agreement with the literature (Dassarma et al., 2018), which indicates BHA as an inducer of NRF2 and of its target genes. The prevention of obesity in BHA mice might be a result of NRF2 activation, and could also be responsible the strong up-regulation of NQO1. In a study adopting NQO1$^{-/-}$ mice it was shown that the liver accumulated triglycerides and mice suffered from insulin resistance (Gaikwad et al., 2001).

Although the role of NQO1 is less known with regard to lipid metabolism, it is generally understood that NRF2 can activate target proteins involved in lipid catabolism (Hayes et al., 2014; Kay et al., 2011). In our prophylactically BHA-treated mice, we observed a down-regulation of ACC2 (*Acacb*) **(fig. 13B)**, a protein responsible for fatty acid synthesis. Similarly, treatment with an inducer of NRF2, CDDO-Imidazolide reduced expression of *Acacb* mRNA (Shin et al., 2009). In NASH-affected mice, NRF2 was down-regulated **(fig. 13D)**. NRF2 expression is progressively reduced also in the process of aging (Hayes et al., 2014), perhaps suggesting that oxidative stress detrimental effects can impair protective mechanisms over time.

In contrast to the prophylactic BHA-supplemented CDHFD treatment, mice under AXT supplementation were obese, probably due to the upregulation of the protein PNPLA8 (also called iPLA$_2$γ), similar to CDHFD fed mice (data not shown). Consistent with these findings, a mouse model with depleted

PNPLA8 showed resistance to high fat diet-induced weight gain (Mancuso et al., 2010).

During the early stage of NASH, the lipid overload induces increased activity of β-oxidation of FAs, which consumes a considerable amount of oxygen. In addition, hepatic sinusoids are constricted due to fat-laden hepatocytes and this can prevent the exchange of substrates and favor the development of hypoxia (Suzuki et al., 2014). In our CDHFD model, we observed upregulation of hypoxia protein 1 (HYOU1), but not in prophylactic antioxidant treatments **(fig. 13F)**. It is known that the high-fat diet induces dysregulation of hepatic oxygen gradients and mitochondrial function. The hypoxic state of the liver is associated with an increased number of proteins modified by oxidative stress (Mantena et al., 2009). Furthermore, hypoxia is linked to increased ROS production and to HCC aggressiveness (Liu et al., 2017).

In NASH mice under CDHFD for 6-months, we could see up-regulated (compared to normal diet mice) proteins belonging to the following pathways, which were not activated in antioxidant treatments **(fig. 13B, C, D, E, F)**: inflammation (e.g. NFKB1, STAT1/3, RELA, PIK3AP1, IL-6st, MAPKs); inflammatory cascades (enzymes producing eicosanoids); macrophage activation (e.g. CD36, MRC1, MYD88, MPEG1), proliferation (e.g. RRAS, CTNNB1, MYCBP); apoptosis (e.g. BCL2L13, TRADD, FADD, CASP8, BID, SUMO2/3, cytochrome c); DNA damage (e.g. RPA1, DDB1); ER stress (e.g. EIF2a, ERO1L, ERO1LB, TRAP1); fibrosis (e.g. desmin, lumican, galectin); lipogenesis (e.g. ChREBP, ACC1/2, FASN, ACLY), lipid peroxidation (e.g. CYP2E1, AOX, XDH) and tumor-related proteins (e.g. YAP1, HDGF, HGS, GLUL, APOB, HYOU1).

Although these results provide a strong indication of an involvement of the pathways indicated above, further analytical assays and functional tests are required.

Lipotoxicity is the initial step in driving hepatocellular damage, and I hypothesize that antioxidants can potentially prevent this process since ER stress, apoptosis and typical enzymes which produce ROS and lipid

peroxidation products were not differentially expressed at the protein level when compared to normal diet mice **(fig. 13)**.

The experiments with AXT indicate that most likely the lipids *per se* are not toxic, but become toxic in the context of oxidative stress. Oxidized LDLs can induce inflammation via CD36 scavenger receptor of macrophages, but non-oxidized LDLs are instead internalized by hepatocytes through the LDL receptor and not via CD36 (van de Sluis et al., 2017). Further proof of the pathogenic nature of oxLDL is the observation that high oxLDL levels correlate with severity of NAFLD in lean NAFL-affected patients (Ampuero et al., 2016).

Among the products of lipid peroxidation, there are oxidized forms of cholesterol which can be part of oxLDL (Levitan et al., 2010). Interestingly, in a cholesterol-based NASH-induced HCC model it was found that oxysterol pathway genes were dysregulated and that major cholesterol metabolites (27-hydroxycholesterol and 6-oxocholestan-3beta,5alpha-diol) had tumor-promoting properties (Liang et al., 2018). This suggests that counteracting oxidative stress might prevent the need to increase proteins involved in internalization (CD36) and metabolism (CYP2E1) of oxidized lipids, including oxidized forms of cholesterol.

To test this hypothesis, in future studies we might use CDHFD or western diet (containing high-fat, cholesterol and fructose) feeding regimen on mice having the ablation of CD36 in macrophages and/or in hepatocytes.

Prophylactically, antioxidant-treated mice showed a significant decrease in KCs and infiltrating macrophages in the liver compared to NASH-affected mice **(fig. 10G, H; fig. 12G, H)**. The expression of CD36 and oxysterol-binding proteins was completely abrogated in prophylactic AXT+CDHFD **(fig. 13D).** Whereas in livers of prophylactic BHA+CDHFD fed mice CD36 and the oxysterol-binding proteins (except for Osbpl3) were significantly reduced compared to CDHFD **(fig. 13D)**. Several studies, especially those that focused on atherosclerosis and NASH, support the link between oxLDL and macrophage activation. OxLDLs not only upregulate levels of CD36, but also favor IL-6 release and activate NF-kB (Nickel et al., 2009). In the context of

NASH, the deletion in monocytes of CD36 and another scavenger receptor termed MRSR1 (Macrophage Scavenger Receptor 1) ameliorates hepatic inflammation, fibrosis and augments production of natural antibodies against oxLDL (Bieghs et al., 2010). Furthermore, murine bone marrow-derived macrophages (BMDM) upregulate CD36 after treatment with oxLDLs. Human macrophages derived from CD14^{+} monocytes also upregulate CD36 following stimulation with oxLDL (McGettigan et al., 2019). Hepatic inflammation is triggered by recognition of oxLDLs by KCs, something demonstrated by Bieghs and collaborators using immunization with pneumococci (Bieghs et al., 2012). Interestingly, CD36 seems to play a role also in enhancing susceptibility to nonalcoholic fatty liver disease during aging, but in this context the hepatocytes mainly express the receptor (Sheedfar et al., 2014). In some studies on atherosclerosis, it was observed that the antioxidant vitamin E could prevent atherosclerotic lesions induced by cholesterol and avoid the upregulation of CD36 (Ozer et al., 2006; Ricciarelli et al., 2000). Another antioxidant, quercentin, reduced levels of oxLDL and of the uptake of LDL in the liver via down-regulation of CD36 and increased autophagic degradation of oxLDL in an NAFLD model fed with HFD (Liu et al., 2015). In the context of atherosclerosis, astaxanthin could prove efficacy in preventing oxidation of LDL (Gaut et al., 2001; Iwamoto et al., 2000), in addition to reduce LDL levels and decreasing toxic lipid peroxidation products, such as MDA and isoprostane (Choi et al., 2011a).

Iwamoto and collaborators have shown in 24 volunteers that astaxanthin can protect plasma LDL against oxidative attack, and LDL oxidation was induced by 2,2-azobis-4-methoxy-2,4-dimethylvaleronitrile (AMVN-CH$_3$O) *in vitro* (Iwamoto et al.,2000).

Astaxanthin treatment in overweight and obese patients lowers oxidative stress and levels of LDL, APOB and APOE (Choi 2011b). In our NASH model we observed that APOB and APOE levels were increased, in contrast to the prophylactic antioxidant treatments **(fig. 13D).**

Of note, after stimulation of macrophages by oxLDL, isoprostane and prostaglandins derived from arachidonic acid, dihomo-gamma-linoleic and

eicosapentaenoic acid, are strongly induced in atherosclerosis (Lara-Guzmán et al., 2018). In our NASH model treated with CDHFD, but not in antioxidant-supplemented CDHFD, we saw the upregulation of proteins involved in the production of prostaglandins and leukotriene LTB4 and in the production of bioactive lipid species as ceramide and arachidonic acid **(fig. 13D).** In particular, ceramide is associated with NASH mitochondrial damage (by inactivating ETC complexes II and IV, augmenting ROS production, and increasing membrane permeability), thus inducing apoptosis. Furthermore, ceramide triggers the activation of NF-κB and SREBP1/2 and the release of pro-inflammatory cytokines and the stimulation of *de novo* lipogenesis, respectively (Musso et al., 2018). Regarding proteins producing prostaglandins, we observed upregulation in CDHFD fed mice of epi-PGF2α-producing enzymes (15-hydroxyprostaglandin dehydrogenase [NAD(+)] (HPGD), Prostaglandin E synthase 2 (PTGES2)). Epi-PGF2α is secreted by macrophages and is known to be an inducer of inflammation and proliferation (Wang and Dubois, 2010).

The scavenger receptor CD36 has been shown to stimulate proliferation of ovarian carcinoma cells by oxLDL (Scoles et al., 2010), suggesting an important aspect of CD36 activation not only for inflammation but also for the typical behavior of transformed cells to proliferate.

In several studies, it has been reported that induction of hepatoxicity, for example in a CCl_4 model, is sufficient to induce oxidative stress, following lipid peroxidation and further modifications in DNA and proteins. Furthermore, CCl_4 treatment induced instability of hepatocyte membranes. The addition of a high-fat diet or Western diet to CCl_4 treatment exacerbates hepatoxicity, leading from NAFL to NASH with fibrosis firstly, and eventually to HCC (Tsuchida et al., 2018; Owada et al., 2018). Some studies have revealed that astaxanthin treatment not only prevented lipid peroxidation but also ameliorated hepatic injury and fibrosis in a CCl_4-induced NAFLD model (Islam et al., 2017; Kang et al., 2001).

In NASH models, the administration of vitamin E (Pickett-Blakely et al., 2018) or of astaxanthin could reduce MDA formation by diminishing lipid

peroxidation (Ni et al., 2015). Further evaluation with the TBARS (Thiobarbituric Acid Reactive Substances) assay, which detects the level of the lipid peroxidation product malondialdehyde, is needed to estimate whereas this is also the case in our CDHFD model.

A major contributor to lipid peroxidation during NASH pathogenesis is CYP2E1. This enzyme exerts high oxidase activity for the detoxification of PUFAs, ethanol and drugs. This process leads to high production of ROS (hydrogen peroxide, hydroxyl radical, and superoxide anion (Abdelmegeed et al., 2017). CYP2E1 is increased in the liver of patients with NASH, compared with livers from healthy subjects (Weltman et al., 1998). In our prophylactic antioxidant treatments, CYP2E1 was not up-regulated, instead it did show upregulation in NASH-affected mice **(fig. 13D)**.

Therefore, we can hypothesize that in the absence of lipotoxicity and lipid peroxidation, the activation of pro-inflammatory pathways, cell death and compensatory proliferation should not occur. In order to assess this, we should implement our data on the hepatocyte's proliferation with the evaluation of cell death markers for apoptosis and necroptosis, beyond to perform the aforementioned assay for lipid peroxidation quantification.

Notably, in the context of oxidative stress, NASH and NASH-induced HCC, mitochondrial dysfunction is crucial for the pathogenesis (Mansouri et al., 2018). We observed from the proteomic analysis that the prophylactic antioxidant treatments prevented the upregulation of the apoptotic pathway **(fig. 13C)**. The proteomic analysis not only revealed upregulated proteins in NASH-affected mice for extrinsic apoptosis but also for intrinsic apoptosis, which is indicated by upregulation of BCL2L13 and AIFM1 **(fig. 13C)**.

Several studies affirmed that mitochondrial damage is associated with the transition from NAFLD to subsequent NASH, since mitochondria are the major producers and targets of ROS, modifying mitochondrial DNA, proteins and membrane lipids (Schröder et al., 2016; Taliento et al., 2019).

An important mitochondrial protein, called NAD(P)-transhydrogenase (NNT) which catalyzes the production of NADPH necessary for the functioning of

antioxidant enzymes, was highly downregulated in our CDHFD 6-months fed mice, but not in the supplemented diet with antioxidants **(fig. 13D)**. Navarro at al. demonstrated that NNT deficiency in high fat diet-fed mice leads to redox imbalance, higher susceptibility to permeability transition pore opening, and this favors the exacerbation to NAFLD toward NASH (Navarro et al., 2017).

An impaired electron chain transport activity lowers the mitochondrial formate production, inducing an adaptive response to increase both one-carbon (1C) donors and mitochondrial 1C metabolic enzymes. In a model of mitochondrial myopathy induced by mutation of the mitochondrial DNA helicase TWINKLE, the reduced levels of formate and derivatives triggered increased expression of mitochondrial folate 1C enzymes (MTHFD2 and MTHFD1L) (Nikkanen et al., 2016).

We have seen in our NASH model that not only at 6- and 12-months' time points, but in HCC as well MTHFD1L is upregulated, compared to healthy livers from age-matched mice **(fig. 19C)**. Indeed, it was recently published that MTHFD1L confers metabolic advantages for HCC growth and proliferation (Lee et al., 2017). MTHFD1L, a pivotal enzyme of the folate cycle localized to the mitochondria, is often overexpressed in cancers and allows cancer cells to survive oxidative stress-inducing apoptosis. The knockdown or knockout of MTHFD1L or the use of a folate analog inhibits growth of cancer cells, further sensitizing them to sorafenib treatment. Overexpressed MTHFD1L is also present in half of HCC patients and is correlated with tumor aggressiveness and lower overall survival rates (Lee et al., 2017; Bidkhori et al., 2018).

Together with MTHFD1L, a protein we observed to be overexpressed among NASH and HCC samples was glutathione synthetase (GSS) **(fig. 19C)**. Under conditions of intense oxidative stress, hepatic glutathione synthesis is increased in an attempt to prevent cell death driven by oxidative damage (De Matteis et al., 2018).

In obese patients with NAFLD, a low-carbohydrate diet (for 7 days) could increase all genes involved in the folate cycle, except for MTHFD1L which is decreased, together with APOA2 (Mardinoglu et al., 2018). In our NASH and

HCC model we could observe upregulation of the protein homolog APOA4 **(fig. 13F).** APOA4 is associated with NAFLD (Cazanave et al., 2017) and cholangiocarcinoma (Padden et al., 2016).

NASH-affected mice most likely attempted to contain the levels of ROS by upregulating antioxidant enzymes **(fig. 13D)**, and this confers to the cells a sub-lethal intermediate production of ROS that favors cancer progression. In the case of increased ROS production above the sub-lethal threshold, cancer cells can upregulate antioxidant pathways, in order to protect themselves and to metastasize (Piskounova et al., 2015). Consistent with this idea, in our NASH and in NASH-HCC mice, glutathione synthetase was upregulated **(fig. 19C).**

Proliferation is a crucial factor for the development of the foci of pre-neoplastic lesions, as shown by experiments using choline-deficient diet or CCl_4 plus acetylaminofluorene (Columbano et al., 1980).

We could show that prophylactic and therapeutic AXT (switch at 3-months and switch at 6-months) significantly reduced hepatocyte proliferation **(fig. 21B** and **fig. 17B**, respectively). Even in nodules derived from therapeutic AXT+CDHFD livers 6-months switch time point, despite being of similar size to control nodules of CD-HFD 12 months fed mice, we could observe significantly reduced proliferation of hepatocytes **(fig. 18F)**.

An interesting protein indicator of proliferation, upregulated at both CDHFD 6- and 12-months only for CDHFD fed mice, was PARP10 **(fig. 13F)**, also termed ADP-ribosyltransferase. This protein interacts with the replication protein proliferating cell nuclear antigen and allows the bypass of DNA lesions by recruiting specialized, non-replicative DNA polymerases (Schleicher et al., 2018). The activity of PARP10 is linked to NAD+ depletion and mitochondrial dysfunction in NASH (Gariani et al., 2017). Interestingly, silencing PARP10 decreases mitochondrial superoxide production and, in parallel, increases the expression of antioxidant genes and fatty acid oxidation (Márton et al., 2018). The adoption of PARP inhibitors in NAFLD can reduce ROS production, ER stress, fibrosis, and hepatic injury. In addition, PARP inhibitors increase mitochondrial biogenesis and β-oxidation (Gariani et al., 2017).

Cell proliferation is a process that requires a rapid supply of nutrients. During this process, typical of tumor cells, the cell shifts its metabolism into aerobic glycolysis, also called "Warburg effect", in which the final metabolism of glucose is lactate (DeBerardinis et al., 2008). This shift happens due the impaired oxidative metabolism of mitochondria, and the glycolytic flux appears to be a compensatory mechanism. In our NASH model I could observe an increase of glycolytic genes, contrary to the antioxidant-treated mice **(fig. 13F)**.

Intriguingly, key glycolytic enzymes such as hexokinase 2 (HK2), aldolase A (ALDOA), and pyruvate kinase M2 (PKM2) may represent potential HCC markers and molecular targets for early detection and chemoprevention (Lee et al., 2018). Another study based on integrative analysis of human databases and validation in a DEN-induced HCC model demonstrated that upregulated glycolysis is linked to HCC aggressiveness (Benfeitas et al., 2019).

An inflamed hepatic microenvironment is necessary to establish pre-neoplastic lesion and then cancer. Indeed, He and collaborators demonstrated the crucial role of a pro-inflammatory microenvironment for the development of HCC starting from HCC progenitor cells (HcPCs). HcPCs lead to cancer only when introduced into a liver undergoing chronic damage and compensatory proliferation, such as a liver treated with CCl_4 or MUP-uPA mice (He et al., 2013). It was demonstrated that paracrine IL-6 production (plus other pro-inflammatory cytokines, such as TNF-α) by KCs and macrophages, in addition to cytokines produced by HcPCs, was essential for the development and progression of HCC (since also tumor cells display IL-6 expression). Furthermore, they could show that the pre-neoplastic lesions were enriched with F4/80[+] macrophages and several cells expressed YAP, STAT3, c-Jun and PCNA. In addition, it was demonstrated that CYP2E1 plays an important role in hepatocellular damage since CYP2E1 KO mice were refractory to DEN (He et al., 2013).

Our CDHFD NASH model similarly displayed upregulation at the protein level of IL-6 receptor **(fig. 13E)**, YAP **(fig. 13F)**, CYP2E1 **(fig. 13D)** and increased proliferation **(fig. 13F)** with respect to the normal diet mice.

Antioxidant treatments with BHA or with AXT in combination with CDHFD brought all the above proteins back to normal levels **(fig. 13)** and inhibited hepatocyte proliferation, particularly in the AXT treatment **(fig. 12B; fig. 17B; fig. 13F)**. Furthermore, in prophylactically treated mice we had indications of prevention of DNA damage, as shown by the absence of upregulation of proteins involved in DNA repair mechanisms **(fig. 13D)**.

In NASH-affected mice 6 months on CDHFD, we identified protein candidates linked to tumorigenesis that were absent in livers from prophylactic antioxidant supplemented diet fed mice **(fig. 13F)**. This included hepatoma-derived growth factor (HDGF) (Min et al., 2018), hepatocyte growth factor regulator (HGS) (Ogunwobi and Liu, 2011) and glutamine synthetase (GLUL) (Hale et al., 2016), APOB (Yan et al., 2019) and SQSTM1 (Umemura et al., 2016). Interestingly, in the fatty liver Shionogi (FLS) mouse model, mice spontaneously develop steatosis without obesity, and the expression of hepatoma-derived growth factor was found to be gradually increased even before hepatocarcinogenesis (Yoshida et al., 2003). HDGF was also reported to be a prognostic factor for HCC (Yoshida et al., 2006).

By applying the therapeutic treatments, I aimed to assess whether supplementing the CDHFD mice at late-stage NASH (6 months) or at early-stage NASH (3 months) with BHA or AXT we could, respectively, reverse or ameliorate NASH and therefore reduce cancer incidence. The BHA therapeutic treatment CDHFD 6m→BHA+CDHFD 6m reversed NASH and abrogated obesity, liver damage, inflammation and fibrosis **(fig. 14; fig. 15)**. BHA treatment induced a trend of decrease in hepatocyte proliferation and significantly decreased tumor incidence **(fig. 15B, I)**. The CDHFD 3m→BHA+CDHFD 9m treatment led instead to high tumor incidence (75%) (data not shown), probably due to the long-term treatment with BHA. It has been reported that high BHA dosage administration or long-term consumption can induce cancer, in particular gastric cancer (Kahl and Kappus, 1993).

Therapeutic astaxanthin CDHFD 6m→AXT+CDHFD 6m was not able to reverse NASH and liver damage but it reduced NAS score, fibrosis, proliferation and inflammation **(fig. 16; fig. 17)**. FACS data revealed that

activated CD8^{+} cells were not reduced compared to the CDHFD control **(fig. 17F)**. The cancer incidence in AXT treated mice was significantly decreased **(fig. 18D)**.

Switching the diet at early-stage NASH (3-months CDHFD) significantly reduced liver damage and NAS score **(fig. 20B, E)**, together with hepatic fibrosis, inflammation and proliferation **(fig. 21A, B, C, D, E)**. Most notably, the mice did not display any tumor **(fig. 21F)**.

From our proteomic data, we tried to identify putative candidates for tumorigenesis intersecting significantly hepatic upregulated proteins (*versus* normal diet) of NASH (6- and 12-months under CDHFD diet) together with HCC affected mice. We observed that, in addition to the glycolysis markers discussed above, other proteins held in common were oxysterol-binding protein-like 3 (Osbpl3), macrophage expressed 1 (MPEG1, also called perforin 2) and the mitochondrial MTHFD1L **(fig. 19C)**. Further tests are required to validate these candidates. Specifically, these proteins are worthy of being further investigated since they link metabolic reprogramming (aerobic glycolysis) with mitochondrial activity, oxidized cholesterol pathway and activation of macrophages for tumor development and maintenance.

In addition to the therapeutic antioxidant treatment, the diet-switch experiments with normal diet in late NASH stages (6- or 9-months) further confirmed the importance of the pro-inflammatory liver microenvironment, most likely attributable to the presence of free fatty acids in combination with oxidative stress that modifies them. Supporting the hypothesis of the crucial role of the pro-inflammatory liver microenvironment is the aforementioned study of He and collaborators (He et al., 2013). Our mice under ND-diet-switch showed reduced liver damage, inflammation and proliferation **(fig. 22C, G, H)**, and most importantly, they displayed reduced liver cancer incidence **(fig. 22I)**. Switching the diet at later NASH stages (9-months) we observed almost the same cancer incidence compared to the 6-months diet-switch **(fig. 23J)**, and from this we can assume that the crucial time point at which the preconditions for cancer development are met before 6-months, as predicted by the two AXT therapeutic treatments at early- or late-stage NASH.

In an attempt to find biomarkers for early NASH-induced HCC detection, we performed a proteomic analysis of serum taken over time from NASH and NASH-tumor-bearing mice: there were identified 12 upregulated proteins from NASH stage until established HCC **(fig. 24A, B)**. Of the identified twelve over-represented proteins, the glycolytic enzyme Aldehyde Dehydrogenase 9 Family Member A1 (ALDH9A1) is particularly interesting as a potential biomarker for early liver cancer detection, since it started to be upregulated in 6-months CDHFD fed mice that will develop tumor **(fig. 24B)**. This enzyme was also found to be upregulated, together with aldolase B (ALDOB), in livers of HCC-affected patients, associated with a strong Warburg effect, hypoxia and poor survival (Bidkhori et al., 2018). In order to significantly lower the risk for HCC development, the change of lifestyle for a chronically obese patient should occur around the age of 35 years old, being comparable to the mouse age of 6 months.

Tumor heterogeneity is one of the hardest challenges when it comes to effective cancer therapy (Dagogo-Jack and Shaw, 2017). Especially for iCCA, the complexity of the genetic landscape makes this type of tumor difficult to treat, with a very dismal prognosis for affected patients (Hyder et al., 2013). Furthermore, a more comprehensive study of the iCCA is needed in order to be able to better stratify patients and to choose the most effective personalized therapy.

For an additional project within the doctoral studies, were performed the first steps towards a comprehensive transcriptomic characterization of the inter- and intra-tumor heterogeneity of human iCCA tissue samples. For this, it was applied spatially resolved mass-spectrometry imaging of formalin-fixed iCCA tissue slides at the metabolome level in order to identify heterogeneous regions within and across tissue sections. The resulting heterogeneity clusters were successfully subjected to RNA extraction after an optimizing the protocol for the use on low RNA quality from low amounts of input material (**fig. 25; fig. 26)**. The assumed heterogeneity of iCCA tissues was confirmed by the presence of five different metabolite expression clusters distributed across the tissue slides. The identification of heterogeneity among each sample it was something not achievable with only histopathological observation. For the next

step, the already successfully generated RNA-sequencing libraries will be sequenced and the resulting transcriptomic profiles analyzed and integrated with the MSI-metabolomics data. The multi-level data set will be associated with histopathological and clinical data in order to characterize the molecular features of the heterogeneous cluster-regions and possibly to identify potential prognostic markers.

In summary, we can conclude that prophylactic and therapeutic supplementation of BHA can prevent or reverse steatosis, inflammation and fibrosis. Similarly, AXT supplementation, for both prophylactic and therapeutic treatments, ameliorates NASH and also reverses inflammation and fibrosis, with the difference that the mice were obese and yet surprisingly still displayed significantly less proliferation compared to CDHFD and BHA+CDHFD. The proteomic analysis provided us with further confirmation of the important role of prophylactic antioxidant supplementation in order to prevent lipid peroxidation, mitochondrial dysfunction and subsequent DNA damage, apoptosis and hepatocyte transformation **(fig. 27)**. Lipids play a pivotal role, and our data suggest that the quality (oxidized lipids) over the quantity might be more important in driving NASH and NASH-induced HCC. Proteomic analysis indicates a putative important role for the switch of metabolism toward glycolytic pathway in hepatocytes in the context of NASH, as well as in transformed HCC cells. Furthermore, it was demonstrated through FACS, histology and proteomic analysis that macrophages are crucial not only for the initiation of NAFLD and NASH, but also in sustaining tumor development **(fig. 10D, E, G; fig. 12D, E, G; fig. 13E; fig. 19C)**. Oxidative stress is pivotal for fatty acid modification, favoring inflammation and creating the conditions for cell transformation.

A recent and significant study supporting in a way our hypothesis, is the one performed by Yuan and collaborators, which provided direct evidence of oxidative stress and HCC development. They conducted a nested case-control study of 377 HCC cases with 691 matched controls within a prospective cohort of 18244 male subjects. The authors reported that the presence of a biomarker for oxidative stress, 8-epi-PGF2α, is a risk factor for HCC, independent of the etiology (i.e. HBV infection, smoking status, alcohol

consumption). The levels of 8-epi-PGF2α were, in fact, already elevated 10 years before the clinical manifestation of HCC (Yuan et al., 2019).

The stage of NASH is crucial for a better astaxanthin curative outcome, since the therapeutic treatment at initial stages of NASH could prevent HCC. It is reasonable to hypothesize that certain events occur at late stages of NASH (e.g. oxidative damage of DNA), which cannot be reversed in order to prevent mutations and cell transformation. This assumption has to be evaluated in the future with thorough analysis of early stages of NASH compared to late stages.

Overall, our data indicate that oxidative stress is indeed a key player in NASH and NASH-induced HCC. In addition, it was evaluated the importance of changing lifestyle with a healthy diet, and were identified novel serum protein candidates which can be validated as non-invasive biomarkers for early HCC detection. For adequate HCC prevention, these approaches could be even considered in chronically obese patients prior to NASH development and in NASH-affected young adults.
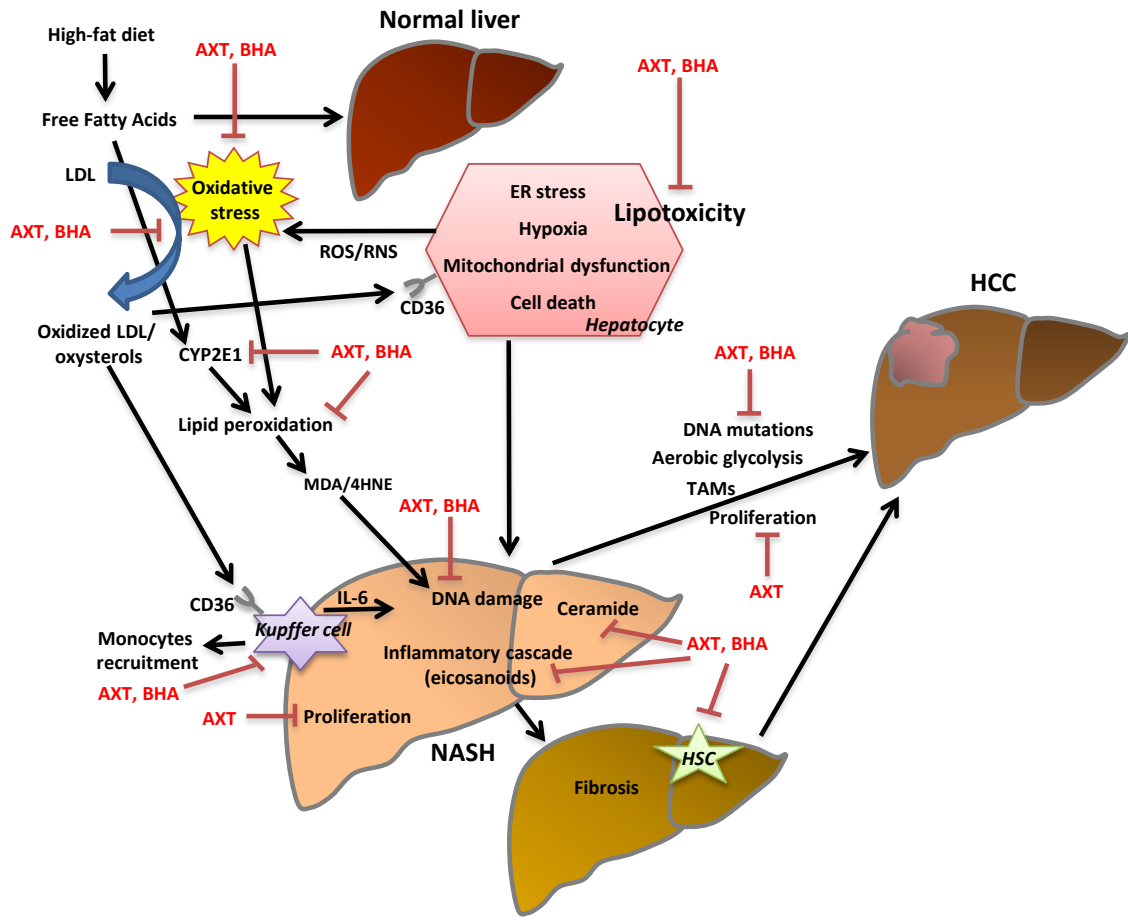
Figure 27. Effects of AXT and BHA against NASH and NASH-induced HCC

The presented data suggest possible effects of different targets of the pathogenesis of NASH and subsequent HCC. In the liver, during NASH development, mitochondria in the attempt to catabolize excessive free fatty acids augmenting β-oxidation, with consequent ROS overproduction. The persistent hepatic fat overload eventually leads to oxidative stress, mitochondrial impairment, ER stress and cell death (lipotoxicity). Hypothetically, the toxic lipids should be the oxidized ones, which activate Kupffer cells via the scavenger receptor CD36. AXT and BHA, with their antioxidant function, prevent oxidative stress and following lipid peroxidation, the latter cause of genotoxic compounds such as MDA and 4-HNE. The two antioxidants look to have an effect also in impeding the upregulation of enzymes involved in the production of eicosanoids mediators of inflammatory cascade. In addition, they prevent upregulation of enzymes producing ceramide, an important lipid known to be involved in lipotoxicity. AXT furthermore, inhibits hepatocytes proliferation also at late NASH stage which probably explains the significant reduction of cancer incidence.

121

Abbreviations

4-HNE	4-hydroxynonenal
8-oxo-dG	8-oxo-7,8-dihydro-2´-deoxyguanosine
ACACA	Acetyl-CoA carboxylase 1
ACACB	Acetyl-CoA carboxylase 2
ACLY	ATP-citrate synthase
ACOT	Acetyl-CoA thioesterase
ACOX	Acetyl-CoA oxidase
ACSS3	Acyl-CoA synthetase short-chain family member 3, mitochondrial
ADH-1/2/5	Alcohol dehydrogenase 1/2/5
ADP	Adenosine diphosphate
ADPGK	ADP-dependent glucokinase
AIFM1	Apoptosis-inducing factor 1, mitochondrial
AKR1A1	Alcohol dehydrogenase [NADP(+)]
AKT	AKT Serine/Threonine Kinase
AKT2	RAC-alpha serine/threonine-protein kinase
ALD	Alcoholic fatty liver disease
ALDH1B1	Aldehyde dehydrogenase X, mitochondrial
ALDH2	Aldehyde dehydrogenase 2, mitochondrial
ALDH3A2	Aldehyde dehydrogenase 3/Fatty aldehyde dehydrogenase
ALDH7A1	Alpha-aminoadipic semialdehyde dehydrogenase
ALDH9A1	Aldehyde dehydrogenase 9 family member A1
ALDOA	Fructose-bisphosphate aldolase A
ALDOB	Fructose-bisphosphate aldolase B
ALK	Anaplastic Lymphoma Receptor Tyrosine Kinase
ANXA-2/5	Annexin A 2/5
AOX-1/3	Aldehyde oxidase 1/3
APOA1BP	NAD(P)H-hydrate epimerase
APOA4	Apolipoprotein A-IV
APOB	Apolipoprotein B-100
APOE	Apolipoprotein E
ARAF	Serine/threonine-protein kinase A-Raf
ARID1A	AT-rich interaction domain 1A
ASH	alcoholic steatohepatitis
ASK1	Apoptosis signal-regulating kinase 1
ATP	Adenosine triphosphate
AXT	Astaxanthin
BAP1	BRCA1 associated protein 1
BAX	BCL2 associated X protein
BCL2L13	Bcl-2-like protein 13
BHA	Butylated hydroxyanisole
BHT	2,6-di-tert-butyl-4- methylphenol

BID	BH3 interacting domain death agonist
BIM	BCL2-like 11
BMI	Body mass index
BRAF	B-Raf Proto-Oncogene, Serine/Threonine Kinase
c-Src	Proto-oncogene tyrosine-protein kinase
CAPG	Macrophage-capping protein
CAPN1	Calpain-1 catalytic subunit
CAPN2	Calpain-2 catalytic subunit
CAR-T	chimeric antigen receptor (CAR) T cells
CASP-1/6/7/8	Caspase 1/6/7/8
CAT	Catalase
CBR3	Carbonyl reductase 3
CCA	Cholangiocarcinoma
CCAR-1/2	Cell division cycle and apoptosis regulator protein 1/2
CCL2	Chemokine (C-C motif) ligand 2
CCl3•	Trichloromethyl radical
CCl$_3$OO•	Trichloromethylperoxy radical
CCl$_4$	Carbon tetrachloride
CCR2	C-C chemokine receptor type 2
CD163	Scavenger receptor cysteine-rich type 1 protein M130;Soluble CD163
CD3	Cluster of differentiation 3
CD302	CD302 antigen
CD36	Cluster of differentiation 36
CD44	Cluster of differentiation 44
CD47	Leukocyte surface antigen CD47
CD8	Cluster of differentiation 8
CD81	CD81 antigen
CD82	CD82 antigen/Tetraspanin
CDHFD	Choline-deficient high fat diet
CERS2	Ceramide synthase 2
CHOP	C/EBP homologous protein
ChREBP	Carbohydrate-responsive element-binding protein
CIK	Cytokine-induced killer
CMPK2	Cytidine/Uridine Monophosphate Kinase 2
COL4A3BP	Collagen type IV alpha-3-binding protein
COX-1/2	Cyclooxygenase
CPT1	Carbohydrate responsive element binding protein
CTLA4	Cytotoxic T-Lymphocyte Associated Protein 4
CTLs	Cytotoxic T lymphocytes
CTNNB1	Catenin beta-1
CXCL1/2	Chemokine (C-X-C motif) ligand 1
CYC1	Cytochrome c1, heme protein, mitochondrial
CYCS	Cytochrome c, somatic
CYP	Cytochrome P-450

CYP2E1	Cytochrome P450 2E1
DAMPs	Damage-associated molecular pattern
DAPK2	Death-associated protein kinase 2
DCs	Dendritic cells
DDB1	DNA damage-binding protein 1
DDP-4	Dipeptidyl peptidase-4
DEN	Diethylnitrosamine
DLAT	Dihydrolipoyllysine-residue acetyltransferase component of pyruvate dehydrogenase complex, mitochondrial
DLD	Dihydrolipoyl dehydrogenase, mitochondrial
EASL	European Association for the Study of the Liver
ECSIT	Evolutionarily conserved signaling intermediate in Toll pathway, mitochondrial
EFSA	European Food Safety Authority
EIF2A	Eukaryotic translation initiation factor 2A (eIF2a)
ELOVL2/5/6	Elongation of very long chain fatty acids protein 2/5/6
ENO1	Alpha-enolase
ENPEP	Glutamyl aminopeptidase
ER	Endoplasmic reticulum
ERAD	ER-associated degradation
ERBB-2	Erb-B2 Receptor Tyrosine Kinase 2
ERK	Extracellular-regulated kinase
ERLEC1	Endoplasmic reticulum lectin 1
ERO1L	ERO1-like protein alpha
ERO1LB	ERO1-like protein beta
ETC	Electron transport chain
FABP4	Fatty acid-binding protein, adipocyte
FADD	FAS-associated death domain protein
FADH$_2$	Flavin adenine dinucleotide hydroquinone
FADS-1/2	Fatty acid desaturase 1/2
FAH	Foci of altered hepatocytes
FAH	Fumarylacetoacetate hydrolase
FasL	Fas Ligand
FASN	Fatty acid synthase
FCGR2/2B	Low affinity immunoglobulin gamma Fc region receptor II
FCGRT	IgG receptor FcRn large subunit p51
FDA	Food and Drug Administration
Fe	Iron
FFPE	Formalin-fixed paraffin embedded
g	G-force
G-CSF	Granulocyte colony-stimulating factor
G6PC	Glucose-6-phosphatase
GALM	Aldose 1-epimerase
GBP4	Guanylate binding protein 4
GCK	Glucokinase
GCLC	Glutamate-cysteine ligase catalytic subunit

GCLM	Glutamate-cysteine ligase regulatory subunit
GLP-1	Glucagon
GLUL	Glutamine synthetase
GM-CSF	Granulocyte-macrophage colony-stimulating factor
GOLGA2	Golgin subfamily A member 5
gp130	Associated receptor glycoprotein 130
GPI	Glucose-6-phosphate isomerase
GPX	Glutathione peroxidase
gr	grams
GSH	Glutathione
GSR	Glutathione reductase, mitochondrial
GSS	Glutathione synthetase
GST	Glutathione-S-transferases
GSTA	Superoxide transferase alpha
GSTA3	Glutathione S-transferase A3
GSTM1	Glutathione S-transferase mu 1
H2-Q4	Histocompatibility 2, Q region locus 4
H$_2$O$_2$	Hydrogen peroxide
H6PD	Hexose-6-hosphate dehydrogenase/glucose 1-dehydrogenase
HBV	Hepatitis B virus
HCC	Hepatocellular carcinoma
HcPCs	HCC progenitor cells
HCV	Hepatitis C virus
HDGF	Hepatoma-derived growth factor
HGS	Hepatocyte growth factor-regulated tyrosine kinase substrate
HH	Hereditary hemochromatosis
HK2	Hexokinase-2
HMGB1	High mobility group box 1
HMOX1	Heme oxygenase 1
HO$^{\bullet}$	Hydroxyl free radical
HPGD	15-hydroxyprostaglandin dehydrogenase [NAD(+)]
HSCs	Hepatic stellate cells
HSD17B12	Very-long-chain 3-oxoacyl-CoA reductase
HSPA5	78 kDa glucose-regulated protein
HYOU1	Hypoxia up-regulated protein 1
iCCA	Intrahepatic cholangiocarcinoma
IDH2	Isocitrate dehydrogenases catalyze
IFIT1	Interferon induced protein with tetratricopeptide repeats 1
IGF1R	Insulin-like growth factor-1 receptor
IKKβ	Inhibitor of kappa light polypeptide gene enhancer in B-cells, kinase beta)
IL-10	Interleukin-10
IL-1α	Interleukin 1 alpha
IL-1β	Interleukin 1 beta
IL-2	Interleukin-2

IL-6	Interleukin-6
IL-6ST	Interleukin-6 receptor subunit beta
iNOS	Nitric oxide synthase
IPGTT	Intraperitoneal glucose tolerance test
IQGAP1	Ras GTPase-activating-like protein IQGAP1
IRE-1α	Inositol-requiring enzyme 1
ITO	Electrically conductive indium tin oxide
JAK	Janus Kinase
JNK	Jun-N-terminal kinase
KCs	Kupffer cells
KDSR	3-ketodihydrosphingosine reductase
KEAP	Kelch-like ECH associated protein 1
KIT	KIT proto-oncogene, receptor tyrosine kinase
KRAS	Kirsten rat sarcoma viral oncogene homolog
L$^{\cdot}$	Lipid radical
L$_4$CL	Tetralinoleicardiolipin
LDHA	L-lactate dehydrogenase A chain
LDHB	L-lactate dehydrogenase B chain
LDL	Low-density lipoprotein
LDLR	Low density lipoprotein receptor
LGALS3	Galectin-3
LGALS3BP	Galectin-3 binding protein
LIPC	Hepatic triacylglycerol lipase
LIPH	Lipase member H
LOO$^{\cdot}$	Lipid peroxyl radical
LOOH	Lipid hydroperoxide
LOX	Lipoxygenases
LPC	Lysophosphatidylcholine
LPS	Lipopolysaccharide
LSECs	Liver sinusoidal endothelial cells
LTA4H	Leukotriene A-4 hydrolase
LXR	Liver X receptor
Ly6C^{+}	Lymphocyte antigen 6 complex, locus C1
M1	Pro-inflammatory macrophages
M2	Anti-inflammatory macrophages
MALDI	Matrix-assisted laser desorption/ionization
MAPK	Mitogen-activated protein (MAP) kinase
MAPK1/ERK2	Mitogen-activated protein kinase 1
MAPK14	p38 mitogen-activated kinase
MAPK14/p38	Mitogen-activated protein kinase 14
MAPK3/ERK1	Mitogen-activated protein kinase 3;Mitogen-activated protein kinase
MAPK9/JNK2	Mitogen-activated protein kinase 9
MAPKAPK2	MAP kinase-activated protein kinase 2
MCD	Methionine-choline deficient diet

MCL1	MCL1 Apoptosis Regulator, BCL2 Family Member
MCP-1	Monocyte chemoattractant protein-1
MDA	Malondialdehyde
MDB	Mallory-Denk bodies
MDM4	Transformed 3T3 cell double minute 4, p53 binding protein
ME3	Malic enzyme 3
MET	MET proto-oncogene, receptor tyrosine kinase/hepatocyte growth factor receptor
MHC-I/MHC-II	Major histocompatibility complex I/II
MMS19	MMS19 nucleotide excision repair protein homolog
MMT	Membrane mitochondrial potential
MnSOD	Mitochondrial manganese (Mn) SOD
MoMFs	Bone-marrow monocyte-derived macrophages
MPEG1	Macrophage-expressed gene 1 protein
MPT	Mitochondrial permeability transition
MRC1/CD206	Macrophage mannose receptor 1
MSI	Mass-spectrometry imaging
mtDNA	Mitochondrial DNA
MTHFD1L	Formyltetrahydrofolate Synthetase, mitochondrial
MTHFD2	NAD-Dependent Methylene Tetrahydrofolate Dehydrogenase, mitochondrial
mTOR	Mammalian target of rapamycin
MuPA	Urokinase plasminogen activator (uPA) from the liver-specific major urinary protein (MUP) promoter
MYCBP	C-Myc-binding protein
MYD88	Myeloid differentiation primary response protein MyD88
NADH	Nicotinamide adenine dinucleotide
NADPH	Nicotinamide adenine dinucleotide posphate
NAFLD	Non-alcoholic fatty liver disease
NAS	NAFLD activity score
NASH	Non-alcoholic steatohepatitis
NCL	Nucleolin
ND	Normal diet
NEFAs	Non-esterified fatty acids
NF-κB	Nuclear factor kappa-light-chain-enhancer of activated B cells
NFKB1	Nuclear factor NF-kappa-B p105 subunit/Nuclear factor NF-kappa-B p50 subunit
NKs	Natural killer cells
NKTs	Natural killer T cells
NLRX1	NLR family member X1
NNT	Nicotinamide nucleotide transhydrogenase, mitochondrial
NO	Nitric oxide
NOS	NADPH oxidase
NQO1	NAD(P)H:quinone oxidoreductase/ NAD(P)H dehydrogenase [quinone] 1
NRF2	Nuclear erythroid 2-related factor 2
ONOO⁻	Peroxynitrite
OSBP	Oxysterol-binding protein 1
OSBPL1A	Oxysterol-binding protein-related protein 1 alpha

OSBPL3	Oxysterol-binding protein-related protein 3
OSBPL9	Oxysterol-binding protein-related protein 9
oxLDL	Oxidized low-density lipoprotein
oxPC	Oxidized phosphatidylcholine
OxS	Oxidative stress
PAMPs	Pathogen-associated molecular pattern
PARP10	Poly(ADP-Ribose) Polymerase Family Member 10
PBRM1	Polybromo 1
PCNA	proliferating cell nuclear antigen
PCX	Pyruvate carboxylase, mitochondrial
PD-1	Programmed Cell Death 1
PD-1L	Programmed Cell Death 1 Ligand 1
PDGF	Platelet-derived growth factor
PDGFRB	Platelet-derived growth factor receptor beta
PDHA1	Pyruvate dehydrogenase E1 component subunit alpha, somatic form, mitochondrial
PERK	PKR-like ER kinase
PFKFB1	Fructose-2,6-bisphosphatase
PFKL	ATP-dependent 6-phosphofructokinase, liver type
PFKP	ATP-dependent 6-phosphofructokinase, platelet type
PGAM1	Phosphoglycerate mutase 1
PGK1	Phosphoglycerate kinase 1
PGM1	Phosphoglucomutase-1
PGM2	Phosphoglucomutase-2
PGM3	Phosphoacetylglucosamine mutase
PI3K	Phosphoinositide 3-kinase
PIK3AP1	Phosphoinositide 3-kinase adapter protein 1
PKM	Pyruvate kinase PKM
PLA2G7	Phospholipase A2
PLAA	Phospholipase A-2-activating protein
PNPLA2	Patatin-like phospholipase domain containing 2
PNPLA3	Patatin-like phospholipase domain-containing protein 3
PNPLA8	Patatin like phospholipase domain containing 8
POR	NADPH--cytochrome P450 reductase
PPARα	Peroxisome proliferator-activated receptors alpha
PPARδ	Peroxisome proliferator-activated receptors delta
PPARγ	Peroxisome proliferator-activated receptors gamma
PRDX	Peroxiredoxin
PRDX-3/6	Peroxiredoxin 3/6
PRKACA	cAMP-dependent protein kinase catalytic subunit alpha
PRKC-A/B	Protein kinase C, alpha type/beta type
PRRs	Pattern recognition receptors
PSMB9	Proteasome subunit beta 9
PSME-1	Proteasome activator complex subunit 1/2/3/4
PTEN	Phosphatidylinositol 3,4,5-trisphosphate 3-phosphatase and dual-specificity protein phosphatase PTEN

PTGES2	Prostaglandin E synthase 2
PTGES3	Prostaglandin E synthase 3
PTGR2	Prostaglandin reductase 2
PTGS1	Prostaglandin G/H synthase 1
PUFAs	Poly-unsaturated fatty acids
PXR	Pregnane X receptor
RAC-1/3	Ras-related C3 botulinum toxin substrate 1;Ras-related C3 botulinum toxin substrate 3
RAD23A	UV excision repair protein RAD23 homolog A
RAD23B	UV excision repair protein RAD23 homolog B
RAF	Raf-1 proto-oncogene, serine/threonine kinase
RAP1A	Ras-related protein Rap-1A
RCF	Relative centrifugal force
RELA	Transcription factor p65
RET	Ret proto-oncogene
RFA	Radiofrequency ablation
RHOT1	Mitochondrial Rho GTPase 1
RNS	Reactive nitrogen species
ROIs	Regions-of-interest
ROS	Radical oxygen species
ROS1	ROS proto-oncogene 1
RPA1	Replication protein A 70 kDa DNA-binding subunit
rpm	revolutions per minute
RRAS2	Ras-related protein R-Ras2
RTN4	Reticulon-4
S100A11	Protein S100-A11
SCARB1	Scavenger receptor class B member 1
SEL1L	E3 ubiquitin-protein ligase synoviolin
SERPINA7	Serpin Family A Member 7
SFAs	Saturated fatty acids
SGPP1	Sphingosine-1-phosphate phosphatase 1
SH3BP5/SAB	SH3-domain binding protein 5
SMPD2	Sphingomyelin phosphodiesterase 2
SOD	Superoxide dismutase
SOD3	Extracellular superoxide dismutase [Cu-Zn]
SORD	Sorbitol Dehydrogenase
SPAG9	C-Jun-amino-terminal kinase-interacting protein 4
SPTLC1	Serine palmitoyltransferase 1
SQSTM1	Sequestosome 1
SREBP1	Sterol regulatory element binding protein 1
STAT1	Signal transducer and activator of transcription 1
STAT3	Signal transducer and activator of transcription 3
STAT5A	Signal transducer and activator of transcription 5A
STK24	Serine/Threonine Kinase 24
STK38	Serine/Threonine Kinase 38
STK4	Serine/Threonine Kinase 4

SUMO-2/3	Small ubiquitin-related modifier 2/3
SYVN1	Protein sel-1 homolog 1
T2DM	Type 2 diabetes mellitus
TACE	transcatheter chemoembolization
TAMs	Tumor-associated macrophages
TAP1	Transporter, ATP-binding cassette, major histocompatibility complex, 1
TCTPT	T cell tyrosine phosphatase
TERT	Telomerase reverse transcriptase
TGF-β1	Transforming growth factor-β 1
TGs	Triglycerides
Th17	T helper cells 17
TLRs	Toll-like receptors
TM6SF2	Transmembrane 6 superfamily 2
TMEM43	Transmembrane Protein 43
TNF-α	Tumor necrosis factor alpha
TPI1	Triosephosphate isomerase
TRADD	Tumor necrosis factor receptor type 1-associated DEATH domain protein
TRAIL	TNF-α-related apoptosis-inducing ligand
TXN	Thioredoxin
TXN2	Thioredoxin, mitochondrial
TXNRD1	Thioredoxin reductase 1, cytoplasmic
TXNRD2	Thioredoxin reductase 2, mitochondrial
UAP1L1	UDP-N-acetylhexosamine pyrophosphorylase-like protein 1
UBA2	SUMO-activating enzyme subunit 2
UPR	Unfolded protein response
URI	Unconventional prefoldin RPB5 interactor 1
VAP-1	Vascular adhesion protein-1
VAPA	Vesicle-associated membrane protein-associated protein A
VCTE	Vibration-controlled transient elastography
VEGF	Vascular endothelial growth factor
VEGFR	Vascular endothelial growth factor receptor
VIM	Vimentin
VLDL	Very low density lipoprotein
VNN1	Vanin 1
WHO	World Health Organization
WNT	Wingless-type MMTV integration site
XBP-1	X-box binding protein 1
XDH	Xanthine dehydrogenase
XO	Xanthine oxidase
YAP1	Yes associated protein 1
γ-OHPdG	Propanodeoxyguanosine

References

Abdelmegeed, M.A., Ha, S.K., Choi, Y., Akbar, M., and Song, B.J. (2017). Role of CYP2E1 in Mitochondrial Dysfunction and Hepatic Injury by Alcohol and Non-Alcoholic Substances. Curr Mol Pharmacol *10*, 207-225.

Abu-el-Zahab, H.S., Saad, M.A., and el-Sisi, S.F. (1993). Role of dietary lipids and butylated hydroxy anisol (BHA) administration on albino rats. Part II. Liver and heart unsaturated fatty acids. Nahrung *37*, 561-570.

Afshin, A., and GBD 2015 Obesity Collaborators (2017). Health Effects of Overweight and Obesity in 195 Countries over 25 Years. New England Journal of Medicine *377*, 13-27.

Akazawa, Y., and Nakao, K. (2018). To die or not to die: death signaling in nonalcoholic fatty liver disease. J Gastroenterol *53*, 893-906.

Alkhouri, N., Carter-Kent, C., and Feldstein, A.E. (2011). Apoptosis in nonalcoholic fatty liver disease: diagnostic and therapeutic implications. Expert Rev Gastroenterol Hepatol *5*, 201-212.

Altekruse, S.F., McGlynn, K.A., Dickie, L.A., and Kleiner, D.E. (2012). Hepatocellular carcinoma confirmation, treatment, and survival in surveillance, epidemiology, and end results registries, 1992-2008. Hepatology *55*, 476-482.

Ampuero, J., Ranchal, I., Gallego-Durán, R., Pareja, M.J., Del Campo, J.A., Pastor-Ramírez, H., Rico, M.C., Picón, R., Pastor, L., García-Monzón, C.*, et al.* (2016). Oxidized low-density lipoprotein antibodies/high-density lipoprotein cholesterol ratio is linked to advanced non-alcoholic fatty liver disease lean patients. J Gastroenterol Hepatol *31*, 1611-1618.

Ansar, S., and Iqbal, M. (2016). Antioxidant and nephroprotective potential of butylated hydroxyanisole against ferric nitrilotriacetate-induced oxidative stress and early tumor events. Hum Exp Toxicol *35*, 448-453.

Anstee, Q.M., Reeves, H.L., Kotsiliti, E., Govaere, O., and Heikenwalder, M. (2019). From NASH to HCC: current concepts and future challenges. Nat Rev Gastroenterol Hepatol *16*, 411-428.

Arab, J.P., Hernández-Rocha, C., Morales, C., Vargas, J.I., Solís, N., Pizarro, M., Robles, C., Sandoval, D., Ponthus, S., Benítez, C.*, et al.* (2017). Serum cytokeratin-18 fragment levels as noninvasive marker of nonalcoholic steatohepatitis in the chilean population. Gastroenterol Hepatol *40*, 388-394.

Armstrong, M.J., Gaunt, P., Aithal, G.P., Barton, D., Hull, D., Parker, R., Hazlehurst, J.M., Guo, K., Abouda, G., Aldersley, M.A.*, et al.* (2016). Liraglutide safety and efficacy in patients with non-alcoholic steatohepatitis (LEAN): a multicentre, double-blind, randomised, placebo-controlled phase 2 study. Lancet *387*, 679-690.

Ashraf, N.U., and Sheikh, T.A. (2015). Endoplasmic reticulum stress and Oxidative stress in the pathogenesis of Non-alcoholic fatty liver disease. Free Radic Res *49*, 1405-1418.

Aubert, J., Begriche, K., Knockaert, L., Robin, M.A., and Fromenty, B. (2011). Increased expression of cytochrome P450 2E1 in nonalcoholic fatty liver disease: mechanisms and pathophysiological role. Clin Res Hepatol Gastroenterol *35*, 630-637.

Aviram, M., Kent, U.M., and Hollenberg, P.F. (1999). Microsomal cytochromes P450 catalyze the oxidation of low density lipoprotein. Atherosclerosis *143*, 253-260.

Ayala, A., Muñoz, M.F., and Argüelles, S. (2014). Lipid peroxidation: production, metabolism, and signaling mechanisms of malondialdehyde and 4-hydroxy-2-nonenal. Oxid Med Cell Longev *2014*, 360438.

Baburina, Y., Krestinin, R., Odinokova, R., Sotnikova, L., Kruglov, A., and Krestinina, O. (2019). Astaxanthin Inhibits Mitochondrial Permeability Transition Pore Opening in Rat Heart Mitochondria. Antioxidants.

Baffy, G., Brunt, E.M., and Caldwell, S.H. (2012). Hepatocellular carcinoma in non-alcoholic fatty liver disease: an emerging menace. J Hepatol *56*, 1384-1391.

Balaban, R.S., Nemoto, S., and Finkel, T. (2005). Mitochondria, oxidants, and aging. Cell *120*, 483-495.

Balkwill, F., and Mantovani, A. (2001). Inflammation and cancer: back to Virchow? Lancet *357*, 539-545.

Banales, J.M., Cardinale, V., Carpino, G., Marzioni, M., Andersen, J.B., Invernizzi, P., Lind, G.E., Folseraas, T., Forbes, S.J., Fouassier, L., et al. (2016). Expert consensus document: Cholangiocarcinoma: current knowledge and future perspectives consensus statement from the European Network for the Study of Cholangiocarcinoma (ENS-CCA). Nat Rev Gastroenterol Hepatol 13, 261-280.

Bao, X.R., Ong, S.E., Goldberger, O., Peng, J., Sharma, R., Thompson, D.A., Vafai, S.B., Cox, A.G., Marutani, E., Ichinose, F*., et al.* (2016). Mitochondrial dysfunction remodels one-carbon metabolism in human cells. Elife *5*.

Barreyro, F.J., Holod, S., Finocchietto, P.V., Camino, A.M., Aquino, J.B., Avagnina, A., Carreras, M.C., Poderoso, J.J., and Gores, G.J. (2015). The pan-caspase inhibitor Emricasan (IDN-6556) decreases liver injury and fibrosis in a murine model of non-alcoholic steatohepatitis. Liver Int *35*, 953-966.

Bartsch, H., and Nair, J. (2006). Chronic inflammation and oxidative stress in the genesis and perpetuation of cancer: role of lipid peroxidation, DNA damage, and repair. Langenbecks Arch Surg *391*, 499-510.
Basseri, S., and Austin, R.C. (2012). Endoplasmic reticulum stress and lipid metabolism: mechanisms and therapeutic potential. Biochem Res Int *2012*, 841362.

Begriche, K., Massart, J., Robin, M.A., Bonnet, F., and Fromenty, B. (2013). Mitochondrial adaptations and dysfunctions in nonalcoholic fatty liver disease. Hepatology *58*, 1497-1507.

Bellanti, F., Villani, R., Facciorusso, A., Vendemiale, G., and Serviddio, G. (2017). Lipid oxidation products in the pathogenesis of non-alcoholic steatohepatitis. Free Radic Biol Med *111*, 173-185.

Benfeitas, R., Bidkhori, G., Mukhopadhyay, B., Klevstig, M., Arif, M., Zhang, C., Lee, S., Cinar, R., Nielsen, J., Uhlen, M*., et al.* (2019). Characterization of heterogeneous redox responses in hepatocellular carcinoma patients using network analysis. EBioMedicine *40*, 471-487.

Bertuccio, P., Bosetti, C., Levi, F., Decarli, A., Negri, E., and La Vecchia, C. (2013). A comparison of trends in mortality from primary liver cancer and intrahepatic cholangiocarcinoma in Europe. Ann Oncol *24*, 1667-1674.

Bhattacharjee, J., Kirby, M., Softic, S., Miles, L., Salazar-Gonzalez, R.M., Shivakumar, P., and Kohli, R. (2017). Hepatic Natural Killer T-cell and CD8+ T-cell Signatures in Mice with Nonalcoholic Steatohepatitis. Hepatol Commun *1*, 299-310.

Bi, J., Cui, R., Li, Z., Liu, C., and Zhang, J. (2017). Astaxanthin alleviated acute lung injury by inhibiting oxidative/nitrative stress and the inflammatory response in mice. Biomed Pharmacother *95*, 974-982.

Bieghs, V., van Gorp, P.J., Walenbergh, S.M., Gijbels, M.J., Verheyen, F., Buurman, W.A., Briles, D.E., Hofker, M.H., Binder, C.J., and Shiri-Sverdlov, R. (2012). Specific immunization strategies against oxidized low-density lipoprotein: a novel way to reduce nonalcoholic steatohepatitis in mice. Hepatology *56*, 894-903.

Bieghs, V., Wouters, K., van Gorp, P.J., Gijbels, M.J., de Winther, M.P., Binder, C.J., Lütjohann, D., Febbraio, M., Moore, K.J., van Bilsen, M.*, et al.* (2010). Role of scavenger receptor A and CD36 in diet-induced nonalcoholic steatohepatitis in hyperlipidemic mice. Gastroenterology *138*, 2477-2486, 2486.e2471-2473.

Blüher, M. (2019). Obesity: global epidemiology and pathogenesis. Nat Rev Endocrinol *15*, 288-298.

Boege, Y., Malehmir, M., Healy, M.E., Bettermann, K., Lorentzen, A., Vucur, M., Ahuja, A.K., Böhm, F., Mertens, J.C., Shimizu, Y.*, et al.* (2017). A Dual Role of Caspase-8 in Triggering and Sensing Proliferation-Associated DNA Damage, a Key Determinant of Liver Cancer Development. Cancer Cell *32*, 342-359.e310.

Boll, M., Weber, L.W., Becker, E., and Stampfl, A. (2001). Mechanism of carbon tetrachloride-induced hepatotoxicity. Hepatocellular damage by reactive carbon tetrachloride metabolites. Z Naturforsch C *56*, 649-659.

Borrelli, A., Bonelli, P., Tuccillo, F.M., Goldfine, I.D., Evans, J.L., Buonaguro, F.M., and Mancini, A. (2018). Role of gut microbiota and oxidative stress in the progression of non-alcoholic fatty liver disease to hepatocarcinoma: Current and innovative therapeutic approaches. Redox Biol *15*, 467-479.

Brandi, G., Farioli, A., Astolfi, A., Biasco, G., and Tavolari, S. (2015). Genetic heterogeneity in cholangiocarcinoma: a major challenge for targeted therapies. Oncotarget *6*, 14744-14753.

Brenner, C., Galluzzi, L., Kepp, O., and Kroemer, G. (2013). Decoding cell death signals in liver inflammation. J Hepatol *59*, 583-594.

Brewer, M.S. (2011). Natural Antioxidants: Sources, Compounds, Mechanisms of Action, and Potential Applications (Comprehensive Reviews in Food Science and Food Safety).

Brito, A.F., Abrantes, A.M., Encarnação, J.C., Tralhão, J.G., and Botelho, M.F. (2015). Cholangiocarcinoma: from molecular biology to treatment. Med Oncol *32*, 245.

Bugianesi, E., Leone, N., Vanni, E., Marchesini, G., Brunello, F., Carucci, P., Musso, A., De Paolis, P., Capussotti, L., Salizzoni, M.*, et al.* (2002). Expanding the natural history of nonalcoholic steatohepatitis: from cryptogenic cirrhosis to hepatocellular carcinoma. Gastroenterology *123*, 134-140.

Buzzetti, E., Pinzani, M., and Tsochatzis, E.A. (2016). The multiple-hit pathogenesis of non-alcoholic fatty liver disease (NAFLD). Metabolism *65*, 1038-1048.

Calderaro, J., Couchy, G., Imbeaud, S., Amaddeo, G., Letouzé, E., Blanc, J.F., Laurent, C., Hajji, Y., Azoulay, D., Bioulac-Sage, P.*, et al.* (2017). Histological subtypes of hepatocellular carcinoma are related to gene mutations and molecular tumour classification. J Hepatol *67*, 727-738.

Caldwell, S., Ikura, Y., Dias, D., Isomoto, K., Yabu, A., Moskaluk, C., Pramoonjago, P., Simmons, W., Scruggs, H., Rosenbaum, N.*, et al.* (2010). Hepatocellular ballooning in NASH. J Hepatol *53*, 719-723.

Cao, J., Dai, D.L., Yao, L., Yu, H.H., Ning, B., Zhang, Q., Chen, J., Cheng, W.H., Shen, W., and Yang, Z.X. (2012). Saturated fatty acid induction of endoplasmic reticulum stress and apoptosis in human liver cells via the PERK/ATF4/CHOP signaling pathway. Mol Cell Biochem *364*, 115-129.

Capece, D., Fischietti, M., Verzella, D., Gaggiano, A., Cicciarelli, G., Tessitore, A., Zazzeroni, F., and Alesse, E. (2013). The inflammatory microenvironment in hepatocellular carcinoma: a pivotal role for tumor-associated macrophages. Biomed Res Int *2013*, 187204.

Cardin, R., Piciocchi, M., Bortolami, M., Kotsafti, A., Barzon, L., Lavezzo, E., Sinigaglia, A., Rodriguez-Castro, K.I., Rugge, M., and Farinati, F. (2014). Oxidative damage in the progression of chronic liver disease to hepatocellular carcinoma: an intricate pathway. World J Gastroenterol *20*, 3078-3086.

Cazanave, S., Podtelezhnikov, A., Jensen, K., Seneshaw, M., Kumar, D.P., Min, H.K., Santhekadur, P.K., Banini, B., Mauro, A.G., M Oseini, A.*, et al.* (2017). The Transcriptomic Signature Of Disease Development And Progression Of Nonalcoholic Fatty Liver Disease. Sci Rep *7*, 17193.

Chalasani, N., Younossi, Z., Lavine, J.E., Charlton, M., Cusi, K., Rinella, M., Harrison, S.A., Brunt, E.M., and Sanyal, A.J. (2018). The diagnosis and management of nonalcoholic fatty liver disease: Practice guidance from the American Association for the Study of Liver Diseases. Hepatology *67*, 328-357.

Chávez-Sánchez, L., Garza-Reyes, M.G., Espinosa-Luna, J.E., Chávez-Rueda, K., Legorreta-Haquet, M.V., and Blanco-Favela, F. (2014). The role of TLR2, TLR4 and CD36 in macrophage activation and foam cell formation in response to oxLDL in humans. Hum Immunol *75*, 322-329.

Che, L., Chi, W., Qiao, Y., Zhang, J., Song, X., Liu, Y., Li, L., Jia, J., Pilo, M.G., Wang, J.*, et al.* (2019). Cholesterol biosynthesis supports the growth of hepatocarcinoma lesions depleted of fatty acid synthase in mice and humans. Gut.

Chen, C., and Shaw, Y.S. (1974). Cyclic metabolic pathway of a butylated hydroxytoluene by rat liver microsomal fractions. Biochem J *144*, 497-501.

Chen, J., Gingold, J.A., and Su, X. (2019). Immunomodulatory TGF-β Signaling in Hepatocellular Carcinoma. Trends Mol Med *25*, 1010-1023.

Chen, J.T., and Kotani, K. (2016). Astaxanthin as a Potential Protector of Liver Function: A Review. J Clin Med Res *8*, 701-704.

Chettouh, H., Lequoy, M., Fartoux, L., Vigouroux, C., and Desbois-Mouthon, C. (2015). Hyperinsulinaemia and insulin signalling in the pathogenesis and the clinical course of hepatocellular carcinoma. Liver Int *35*, 2203-2217.

Choi, H.D., Kim, J.H., Chang, M.J., Kyu-Youn, Y., and Shin, W.G. (2011a). Effects of astaxanthin on oxidative stress in overweight and obese adults. Phytother Res *25*, 1813-1818.

Choi, H.D., Youn, Y.K., and Shin, W.G. (2011b). Positive effects of astaxanthin on lipid profiles and oxidative stress in overweight subjects. Plant Foods Hum Nutr *66*, 363-369.

Cichoż-Lach, H., and Michalak, A. (2014). Oxidative stress as a crucial factor in liver diseases. World J Gastroenterol *20*, 8082-8091.

Coia, H., Ma, N., He, A.R., Kallakury, B., Berry, D.L., Permaul, E., Makambi, K.H., Fu, Y., and Chung, F.L. (2018a). Detection of a lipid peroxidation-induced DNA adduct across liver disease stages. Hepatobiliary Surg Nutr *7*, 85-97.

Coia, H., Ma, N., Hou, Y., Dyba, M.D., Fu, Y., Cruz, M.I., Benitez, C., Graham, G.T., McCutcheon, J.N., Zheng, Y.L.*, et al.* (2018b). Prevention of Lipid Peroxidation-derived Cyclic DNA Adduct and Mutation in High-Fat Diet-induced Hepatocarcinogenesis by Theaphenon E. Cancer Prev Res (Phila) *11*, 665-676.

Columbano , A., Rajalakshmi, S., and Sarma, D.S.R. (1980). Requirement of cell proliferation for the induction of presumptive preneoplastic lesions in rat liver by a single dose of 1,2-dimethylhydrazine (Chemico-Biological Interactions).

Comporti, M., Arezzini, B., Signorini, C., Sgherri, C., Monaco, B., and Gardi, C. (2005). F2-isoprostanes stimulate collagen synthesis in activated hepatic stellate cells: a link with liver fibrosis? Lab Invest *85*, 1381-1391.

Corbin, K.D., and Zeisel, S.H. (2012). Choline metabolism provides novel insights into nonalcoholic fatty liver disease and its progression. Curr Opin Gastroenterol *28*, 159-165.

Cox, J., Hein, M.Y., Luber, C.A., Paron, I., Nagaraj, N., and Mann, M. (2014). Accurate proteome-wide label-free quantification by delayed normalization and maximal peptide ratio extraction, termed MaxLFQ. Mol Cell Proteomics *13*, 2513-2526.

Crispe, I.N. (2009). The liver as a lymphoid organ. Annu Rev Immunol *27*, 147-163.

Cui, J., Philo, L., Nguyen, P., Hofflich, H., Hernandez, C., Bettencourt, R., Richards, L., Salotti, J., Bhatt, A., Hooker, J.*, et al.* (2016). Sitagliptin vs. placebo for non-alcoholic fatty liver disease: A randomized controlled trial. J Hepatol *65*, 369-376.

Curtin, J.F., Donovan, M., and Cotter, T.G. (2002). Regulation and measurement of oxidative stress in apoptosis. J Immunol Methods *265*, 49-72.

Dagogo-Jack, I., and Shaw, A.T. (2018). Tumour heterogeneity and resistance to cancer therapies. Nat Rev Clin Oncol *15*, 81-94.

Dai, N., Zou, Y., Zhu, L., Wang, H.F., and Dai, M.G. (2014). Antioxidant properties of proanthocyanidins attenuate carbon tetrachloride (CCl4)-induced steatosis and liver injury in rats via CYP2E1 regulation. J Med Food *17*, 663-669.

Dassarma, B., Nandi, D.K., Gangopadhyay, S., and Samanta, S. (2018). Hepatoprotective effect of food preservatives (butylated hydroxyanisole, butylated hydroxytoluene) on carbon tetrachloride-induced hepatotoxicity in rat. Toxicol Rep *5*, 31-37.

Day, C.P., and Saksena, S. (2002). Non-alcoholic steatohepatitis: definitions and pathogenesis. J Gastroenterol Hepatol *17 Suppl 3*, S377-384.

De Berardinis, R.J., Lum, J.J., Hatzivassiliou, G., and Thompson, C.B. (2008). The biology of cancer: metabolic reprogramming fuels cell growth and proliferation. Cell Metab *7*, 11-20.

De Lorenzo, S. (2019). Role of nonalcoholic steatohepatitis as a risk factor for intrahepatic cholangiocarcinoma and its role in patients' prognosis: A case-control study, V.F. Tovoli F., Malvi D., D'Errico A., Brandi G., ed. (J Clin Oncol).

De Matteis, S., Ragusa, A., Marisi, G., De Domenico, S., Casadei Gardini, A., Bonafè, M., and Giudetti, A.M. (2018). Aberrant Metabolism in Hepatocellular Carcinoma Provides Diagnostic and Therapeutic Opportunities. Oxid Med Cell Longev *2018*, 7512159.

Denk, H., Stumptner, C., Fuchsbichler, A., Müller, T., Farr, G., Müller, W., Terracciano, L., and Zatloukal, K. (2006). Are the Mallory bodies and intracellular hyaline bodies in neoplastic and non-neoplastic hepatocytes related? J Pathol *208*, 653-661.

de Oliveira Pateis, V., Bracht, L., Dos Santos Castro, L., Bueno Franco Salla, G., Comar, J.F., Valderrama Parizotto, A., Peralta, R.M., and Bracht, A. (2018). The food additive BHA modifies energy metabolism in the perfused rat liver. Toxicol Lett *299*, 191-200.

Dewez, F., Martin-Lorenzo, M., Herfs, M., Baiwir, D., Mazzucchelli, G., De Pauw, E., Heeren, R.M.A., and Balluff, B. (2019). Precise co-registration of mass spectrometry imaging, histology, and laser microdissection-based omics. Anal Bioanal Chem *411*, 5647-5653.

Dey, S., Sidor, A., and O'Rourke, B. (2016). Compartment-specific Control of Reactive Oxygen Species Scavenging by Antioxidant Pathway Enzymes. J Biol Chem *291*, 11185-11197.

Dodson, R.M., Weiss, M.J., Cosgrove, D., Herman, J.M., Kamel, I., Anders, R., Geschwind, J.F., and Pawlik, T.M. (2013). Intrahepatic cholangiocarcinoma: management options and emerging therapies. J Am Coll Surg *217*, 736-750.e734.

Ducker, G.S., and Rabinowitz, J.D. (2017). One-Carbon Metabolism in Health and Disease. Cell Metab *25*, 27-42.

EASL-EASD-EASO Clinical Practice Guidelines for the management of non-alcoholic fatty liver disease. (2016). J Hepatol *64*, 1388-1402.

E.F.S.A. (2014). Scientific Opinion on the safety of astaxanthin-rich ingredients (AstaREAL A1010 and AstaREAL L10) as novel food ingredients (EFSA Journal).

EFSA (2018). Safety and efficacy of butylated hydroxyanisole (BHA) as a feed additive for all animal species (EFSA Journal).

El Bassat, H., Ziada, D.H., Hasby, E.A., Nagy, H., and Abo Ryia, M.H. (2014). Apoptotic and anti-apoptotic seromarkers for assessment of disease severity of non-alcoholic steatohepatitis. Arab J Gastroenterol *15*, 6-11.

Elgawish, R.A.R., Rahman, H.G.A., and Abdelrazek, H.M.A. (2015). Green tea extract attenuates CCl4-induced hepatic injury in male hamsters via inhibition of lipid peroxidation and p53-mediated apoptosis. Toxicol Rep *2*, 1149-1156.

El-Serag, H.B., and Rudolph, K.L. (2007). Hepatocellular carcinoma: epidemiology and molecular carcinogenesis. Gastroenterology *132*, 2557-2576.

Elgawish, R.A.R., Rahman, H.G.A., and Abdelrazek, H.M.A. (2015). Green tea extract attenuates CCl4-induced hepatic injury in male hamsters via inhibition of lipid peroxidation and p53-mediated apoptosis. Toxicol Rep *2*, 1149-1156.

Estes, C., Anstee, Q.M., Arias-Loste, M.T., Bantel, H., Bellentani, S., Caballeria, J., Colombo, M., Craxi, A., Crespo, J., Day, C.P.*, et al.* (2018a). Modeling NAFLD disease burden in China, France, Germany, Italy, Japan, Spain, United Kingdom, and United States for the period 2016-2030. J Hepatol *69*, 896-904.

Estes, C., Razavi, H., Loomba, R., Younossi, Z., and Sanyal, A.J. (2018b). Modeling the epidemic of nonalcoholic fatty liver disease demonstrates an exponential increase in burden of disease. Hepatology *67*, 123-133.

Fattovich, G., Stroffolini, T., Zagni, I., and Donato, F. (2004). Hepatocellular carcinoma in cirrhosis: incidence and risk factors. Gastroenterology *127*, S35-50.

Fausto, N., Campbell, J.S., and Riehle, K.J. (2006). Liver regeneration. Hepatology *43*, S45-53.

Feldstein, A.E., Wieckowska, A., Lopez, A.R., Liu, Y.C., Zein, N.N., and McCullough, A.J. (2009). Cytokeratin-18 fragment levels as noninvasive biomarkers for nonalcoholic steatohepatitis: a multicenter validation study. Hepatology *50*, 1072-1078.

Feng, H., and Stockwell, B.R. (2018). Unsolved mysteries: How does lipid peroxidation cause ferroptosis? PLoS Biol *16*, e2006203.

Fedorova, M., Bollineni, R.C., and Hoffmann, R. (2014). Protein carbonylation as a major hallmark of oxidative damage: update of analytical strategies. Mass Spectrom Rev *33*, 79-97.

Font-Burgada, J., Sun, B., and Karin, M. (2016). Obesity and Cancer: The Oil that Feeds the Flame. Cell Metab *23*, 48-62.

Franceschelli, S., Pesce, M., Ferrone, A., De Lutiis, M.A., Patruno, A., Grilli, A., Felaco, M., and Speranza, L. (2014). Astaxanthin treatment confers protection against oxidative stress in U937 cells stimulated with lipopolysaccharide reducing O2- production. PLoS One *9*, e88359.

Fransvea, E., Mazzocca, A., Santamato, A., Azzariti, A., Antonaci, S., and Giannelli, G. (2011). Kinase activation profile associated with TGF-β-dependent migration of HCC cells: a preclinical study. Cancer Chemother Pharmacol *68*, 79-86.

Fransen, M., Nordgren, M., Wang, B., and Apanasets, O. (2012). Role of peroxisomes in ROS/RNS-metabolism: implications for human disease. Biochim Biophys Acta *1822*, 1363-1373.

Friedman, S.L., Ratziu, V., Harrison, S.A., Abdelmalek, M.F., Aithal, G.P., Caballeria, J., Francque, S., Farrell, G., Kowdley, K.V., Craxi, A.*, et al.* (2018). A randomized, placebo-controlled trial of cenicriviroc for treatment of nonalcoholic steatohepatitis with fibrosis. Hepatology *67*, 1754-1767.

Fu, Y., and Chung, F.L. (2018). Oxidative stress and hepatocarcinogenesis. Hepatoma Res *4*.

Fu, Y., Silverstein, S., McCutcheon, J.N., Dyba, M., Nath, R.G., Aggarwal, M., Coia, H., Bai, A., Pan, J., Jiang, J.*, et al.* (2018). An endogenous DNA adduct as a prognostic biomarker for hepatocarcinogenesis and its prevention by Theaphenon E in mice. Hepatology *67*, 159-170.

Fukushima, S., Ogiso, T., Kurata, Y., Hirose, M., and Ito, N. (1987). Dose-dependent effects of butylated hydroxyanisole, butylated hydroxytoluene and ethoxyquin for promotion of bladder carcinogenesis in N-butyl-N-(4-hydroxybutyl) nitrosamine-initiated, unilaterally ureter-ligated rats. Cancer Lett *34*, 83-90.

Gaikwad, A., Long, D.J., Stringer, J.L., and Jaiswal, A.K. (2001). In vivo role of NAD(P)H:quinone oxidoreductase 1 (NQO1) in the regulation of intracellular redox state and accumulation of abdominal adipose tissue. J Biol Chem *276*, 22559-22564.

Gariani, K., Ryu, D., Menzies, K.J., Yi, H.S., Stein, S., Zhang, H., Perino, A., Lemos, V., Katsyuba, E., Jha, P.*, et al.* (2017). Inhibiting poly ADP-ribosylation increases fatty acid oxidation and protects against fatty liver disease. J Hepatol *66*, 132-141.

Gautheron, J., Vucur, M., and Luedde, T. (2015). Necroptosis in Nonalcoholic Steatohepatitis. Cell Mol Gastroenterol Hepatol *1*, 264-265.

Gentile, C.L., Frye, M., and Pagliassotti, M.J. (2011). Endoplasmic reticulum stress and the unfolded protein response in nonalcoholic fatty liver disease. Antioxid Redox Signal *15*, 505-521.

Gomes, A.L., Teijeiro, A., Burén, S., Tummala, K.S., Yilmaz, M., Waisman, A., Theurillat, J.P., Perna, C., and Djouder, N. (2016). Metabolic Inflammation-Associated IL-17A Causes Non-alcoholic Steatohepatitis and Hepatocellular Carcinoma. Cancer Cell *30*, 161-175.

Goto, S., Kogure, K., Abe, K., Kimata, Y., Kitahama, K., Yamashita, E., and Terada, H. (2001). Efficient radical trapping at the surface and inside the phospholipid membrane is responsible for highly potent antiperoxidative activity of the carotenoid astaxanthin. Biochim Biophys Acta *1512*, 251-258.

Grohmann, M., Wiede, F., Dodd, G.T., Gurzov, E.N., Ooi, G.J., Butt, T., Rasmiena, A.A., Kaur, S., Gulati, T., Goh, P.K.*, et al.* (2018). Obesity Drives STAT-1-Dependent NASH and STAT-3-Dependent HCC. Cell *175*, 1289-1306.e1220.

Guillot, A., and Tacke, F. (2019). Liver Macrophages: Old Dogmas and New Insights. Hepatol Commun *3*, 730-743.

Gupte, A.A., Lyon, C.J., and Hsueh, W.A. (2013). Nuclear factor (erythroid-derived 2)-like-2 factor (Nrf2), a key regulator of the antioxidant response to protect against atherosclerosis and nonalcoholic steatohepatitis. Curr Diab Rep *13*, 362-371.

Haas, J.T., Vonghia, L., Mogilenko, D.A., Verrijken, A., Molendi-Coste, O., Fleury, S., Deprince, A., Nikitin, A., Woitrain, E., Ducrocq-Geoffroy, L.*, et al.* (2019). Transcriptional network analysis implicates altered hepatic immune function in NASH development and resolution. *Nature Metabolism 1*, 604/614.

Hale, G., Liu, X., Hu, J., Xu, Z., Che, L., Solomon, D., Tsokos, C., Shafizadeh, N., Chen, X., Gill, R.*, et al.* (2016). Correlation of exon 3 β-catenin mutations with glutamine synthetase staining patterns in hepatocellular adenoma and hepatocellular carcinoma. Mod Pathol *29*, 1370-1380.

Halliwell, B., and Gutteridge, J.M. (1984). Oxygen toxicity, oxygen radicals, transition metals and disease. Biochem J *219*, 1-14.

Hansen, H.H., Feigh, M., Veidal, S.S., Rigbolt, K.T., Vrang, N., and Fosgerau, K. (2017). Mouse models of nonalcoholic steatohepatitis in preclinical drug development. Drug Discov Today *22*, 1707-1718.

Hapala, I., Marza, E., and Ferreira, T. (2011). Is fat so bad? Modulation of endoplasmic reticulum stress by lipid droplet formation. Biol Cell *103*, 271-285.

Hauck, A.K., and Bernlohr, D.A. (2016). Oxidative stress and lipotoxicity. J Lipid Res *57*, 1976-1986.

Hayes, J.D., Chanas, S.A., Henderson, C.J., McMahon, M., Sun, C., Moffat, G.J., Wolf, C.R., and Yamamoto, M. (2000). The Nrf2 transcription factor contributes both to the basal expression of glutathione S-transferases in mouse liver and to their induction by the chemopreventive synthetic antioxidants, butylated hydroxyanisole and ethoxyquin. Biochem Soc Trans *28*, 33-41.

Hayes, J.D., and Dinkova-Kostova, A.T. (2014). The Nrf2 regulatory network provides an interface between redox and intermediary metabolism. Trends Biochem Sci *39*, 199-218.

He, G., Dhar, D., Nakagawa, H., Font-Burgada, J., Ogata, H., Jiang, Y., Shalapour, S., Seki, E., Yost, S.E., Jepsen, K.*, et al.* (2013). Identification of liver cancer progenitors whose malignant progression depends on autocrine IL-6 signaling. Cell *155*, 384-396.

He, J., Lee, J.H., Febbraio, M., and Xie, W. (2011). The emerging roles of fatty acid translocase/CD36 and the aryl hydrocarbon receptor in fatty liver disease. Exp Biol Med (Maywood) *236*, 1116-1121.

He, J., and Liu, Y. (2016). Serum TGF-β1: A Potential Biomarker for Early Detection of Hepatocellular Carcinoma. EBioMedicine *12*, 4-5.

Hegade, V.S., Speight, R.A., Etherington, R.E., and Jones, D.E. (2016). Novel bile acid therapeutics for the treatment of chronic liver diseases. Therap Adv Gastroenterol *9*, 376-391.

He, L., Deng, L., Zhang, Q., Guo, J., Zhou, J., Song, W., and Yuan, F. (2017). Diagnostic Value of CK-18, FGF-21, and Related Biomarker Panel in Nonalcoholic Fatty Liver Disease: A Systematic Review and Meta-Analysis. Biomed Res Int *2017*, 9729107.

Helmy, K.Y., Katschke, K.J., Gorgani, N.N., Kljavin, N.M., Elliott, J.M., Diehl, L., Scales, S.J., Ghilardi, N., and van Lookeren Campagne, M. (2006). CRIg: a macrophage complement receptor required for phagocytosis of circulating pathogens. Cell *124*, 915-927.

Hirose, M., Takahashi, S., Ogawa, K., Futakuchi, M., Shirai, T., Shibutani, M., Uneyama, C., Toyoda, K., and Iwata, H. (1999). Chemoprevention of heterocyclic amine-induced carcinogenesis by phenolic compounds in rats. Cancer Lett *143*, 173-178.

Hirsova, P., and Gores, G.J. (2015). Death Receptor-Mediated Cell Death and Proinflammatory Signaling in Nonalcoholic Steatohepatitis. Cell Mol Gastroenterol Hepatol *1*, 17-27.

Hossain, N., Kanwar, P., and Mohanty, S.R. (2016). A Comprehensive Updated Review of Pharmaceutical and Nonpharmaceutical Treatment for NAFLD. Gastroenterol Res Pract *2016*, 7109270.

Houben, T., Brandsma, E., Walenbergh, S.M.A., Hofker, M.H., and Shiri-Sverdlov, R. (2017). Oxidized LDL at the crossroads of immunity in non-alcoholic steatohepatitis. Biochim Biophys Acta Mol Cell Biol Lipids *1862*, 416-429.

Houglum, K., Filip, M., Witztum, J.L., and Chojkier, M. (1990). Malondialdehyde and 4-hydroxynonenal protein adducts in plasma and liver of rats with iron overload. J Clin Invest *86*.

Houglum, K., Ramm, G.A., Crawford, D.H., Witztum, J.L., Powell, L.W., and Chojkier, M. (1997). Excess iron induces hepatic oxidative stress and transforming growth factor beta1 in genetic hemochromatosis. Hepatology *26*, 605-610.

Hu, W., Feng, Z., Eveleigh, J., Iyer, G., Pan, J., Amin, S., Chung, F.L., and Tang, M.S. (2002). The major lipid peroxidation product, trans-4-hydroxy-2-nonenal, preferentially forms DNA adducts at codon 249 of human p53 gene, a unique mutational hotspot in hepatocellular carcinoma. Carcinogenesis *23*, 1781-1789.

Huang, H., Kozekov, I.D., Kozekova, A., Wang, H., Lloyd, R.S., Rizzo, C.J., and Stone, M.P. (2010). DNA cross-link induced by trans-4-hydroxynonenal. Environ Mol Mutagen *51*, 625-634.

Hussain, S.P., Raja, K., Amstad, P.A., Sawyer, M., Trudel, L.J., Wogan, G.N., Hofseth, L.J., Shields, P.G., Billiar, T.R., Trautwein, C.*, et al.* (2000). Increased p53 mutation load in nontumorous human liver of wilson disease and hemochromatosis: oxyradical overload diseases. Proc Natl Acad Sci U S A *97*, 12770-12775.

Hussain, S.P., Hofseth, L.J., and Harris, C.C. (2003). Radical causes of cancer. Nat Rev Cancer *3*, 276-285.

Hyder, O., Hatzaras, I., Sotiropoulos, G.C., Paul, A., Alexandrescu, S., Marques, H., Pulitano, C., Barroso, E., Clary, B.M., Aldrighetti, L.*, et al.* (2013). Recurrence after operative management of intrahepatic cholangiocarcinoma. Surgery *153*, 811-818.

Ikeuchi, M., Koyama, T., Takahashi, J., and Yazawa, K. (2007). Effects of astaxanthin in obese mice fed a high-fat diet. Biosci Biotechnol Biochem *71*, 893-899.

Ikura, Y., Ohsawa, M., Suekane, T., Fukushima, H., Itabe, H., Jomura, H., Nishiguchi, S., Inoue, T., Naruko, T., Ehara, S.*, et al.* (2006). Localization of oxidized phosphatidylcholine in nonalcoholic fatty liver disease: impact on disease progression. Hepatology *43*, 506-514.

Islam, M.A., Al Mamun, M.A., Faruk, M., Ul Islam, M.T., Rahman, M.M., Alam, M.N., Rahman, A.F.M.T., Reza, H.M., and Alam, M.A. (2017). Astaxanthin Ameliorates Hepatic Damage and Oxidative Stress in Carbon Tetrachloride-administered Rats. Pharmacognosy Res *9*, S84-S91.

Itoh, K., Chiba, T., Takahashi, S., Ishii, T., Igarashi, K., Katoh, Y., Oyake, T., Hayashi, N., Satoh, K., Hatayama, I.*, et al.* (1997). An Nrf2/small Maf heterodimer mediates the induction of phase II detoxifying enzyme genes through antioxidant response elements. Biochem Biophys Res Commun *236*, 313-322.

Iwamoto, T., Hosoda, K., Hirano, R., Kurata, H., Matsumoto, A., Miki, W., Kamiyama, M., Itakura, H., Yamamoto, S., and Kondo, K. (2000). Inhibition of low-density lipoprotein oxidation by astaxanthin. J Atheroscler Thromb *7*, 216-222.

Jaiswal, M., LaRusso, N.F., Shapiro, R.A., Billiar, T.R., and Gores, G.J. (2001). Nitric oxide-mediated inhibition of DNA repair potentiates oxidative DNA damage in cholangiocytes. Gastroenterology *120*, 190-199.

Jenne, C.N., and Kubes, P. (2013). Immune surveillance by the liver. Nat Immunol *14*, 996-1006.

Jia, L., Vianna, C.R., Fukuda, M., Berglund, E.D., Liu, C., Tao, C., Sun, K., Liu, T., Harper, M.J., Lee, C.E.*, et al.* (2014). Hepatocyte Toll-like receptor 4 regulates obesity-induced inflammation and insulin resistance. Nat Commun *5*, 3878.

Jia, Y., Wu, C., Kim, J., Kim, B., and Lee, S.J. (2016). Astaxanthin reduces hepatic lipid accumulations in high-fat-fed C57BL/6J mice via activation of peroxisome proliferator-activated receptor (PPAR) alpha and inhibition of PPAR gamma and Akt. J Nutr Biochem *28*, 9-18.

Jiao, Y., Pawlik, T.M., Anders, R.A., Selaru, F.M., Streppel, M.M., Lucas, D.J., Niknafs, N., Guthrie, V.B., Maitra, A., Argani, P.*, et al.* (2013). Exome sequencing identifies frequent inactivating mutations in BAP1, ARID1A and PBRM1 in intrahepatic cholangiocarcinomas. Nat Genet *45*, 1470-1473.

Kahl, R., and Kappus, H. (1993). [Toxicology of the synthetic antioxidants BHA and BHT in comparison with the natural antioxidant vitamin E]. Z Lebensm Unters Forsch *196*, 329-338.

Kakazu, E., Mauer, A.S., Yin, M., and Malhi, H. (2016). Hepatocytes release ceramide-enriched pro-inflammatory extracellular vesicles in an IRE1α-dependent manner. J Lipid Res *57*, 233-245.

Kakisaka, K., Cazanave, S.C., Werneburg, N.W., Razumilava, N., Mertens, J.C., Bronk, S.F., and Gores, G.J. (2012). A hedgehog survival pathway in 'undead' lipotoxic hepatocytes. J Hepatol *57*, 844-851.

Kamata, H., Honda, S., Maeda, S., Chang, L., Hirata, H., and Karin, M. (2005). Reactive oxygen species promote TNFalpha-induced death and sustained JNK activation by inhibiting MAP kinase phosphatases. Cell *120*, 649-661.

Kanda, T., Matsuoka, S., Yamazaki, M., Shibata, T., Nirei, K., Takahashi, H., Kaneko, T., Fujisawa, M., Higuchi, T., Nakamura, H.*, et al.* (2018). Apoptosis and non-alcoholic fatty liver diseases. World J Gastroenterol *24*, 2661-2672.

Kang, J.O., Kim, S.J., and Kim, H. (2001). Effect of astaxanthin on the hepatotoxicity, lipid peroxidation and antioxidative enzymes in the liver of CCl4-treated rats. Methods Find Exp Clin Pharmacol *23*, 79-84.

Kargiotis, K., Athyros, V.G., Giouleme, O., Katsiki, N., Katsiki, E., Anagnostis, P., Boutari, C., Doumas, M., Karagiannis, A., and Mikhailidis, D.P. (2015). Resolution of non-alcoholic steatohepatitis by rosuvastatin monotherapy in patients with metabolic syndrome. World J Gastroenterol *21*, 7860-7868.

Karppi, J., Rissanen, T.H., Nyyssönen, K., Kaikkonen, J., Olsson, A.G., Voutilainen, S., and Salonen, J.T. (2007). Effects of astaxanthin supplementation on lipid peroxidation. Int J Vitam Nutr Res *77*, 3-11.

Katerji, M., Filippova, M., and Duerksen-Hughes, P. (2019). Approaches and Methods to Measure Oxidative Stress in Clinical Samples: Research Applications in the Cancer Field. Oxid Med Cell Longev *2019*, 1279250.

Kathirvel, E., Chen, P., Morgan, K., French, S.W., and Morgan, T.R. (2010). Oxidative stress and regulation of anti-oxidant enzymes in cytochrome P4502E1 transgenic mouse model of non-alcoholic fatty liver. J Gastroenterol Hepatol *25*, 1136-1143.

Kawano, Y., and Cohen, D.E. (2013). Mechanisms of hepatic triglyceride accumulation in non-alcoholic fatty liver disease. J Gastroenterol *48*, 434-441.

Kay, H.Y., Kim, W.D., Hwang, S.J., Choi, H.S., Gilroy, R.K., Wan, Y.J., and Kim, S.G. (2011). Nrf2 inhibits LXRα-dependent hepatic lipogenesis by competing with FXR for acetylase binding. Antioxid Redox Signal *15*, 2135-2146.

Kim, H.R., Lee, G.H., Cho, E.Y., Chae, S.W., Ahn, T., and Chae, H.J. (2009). Bax inhibitor 1 regulates ER-stress-induced ROS accumulation through the regulation of cytochrome P450 2E1. J Cell Sci *122*, 1126-1133.

Kim, B., Farruggia, C., Ku, C.S., Pham, T.X., Yang, Y., Bae, M., Wegner, C.J., Farrell, N.J., Harness, E., Park, Y.K.*, et al.* (2017). Astaxanthin inhibits inflammation and fibrosis in the liver and adipose tissue of mouse models of diet-induced obesity and nonalcoholic steatohepatitis. J Nutr Biochem *43*, 27-35.

Kim, S.H., and Kim, H. (2018). Inhibitory Effect of Astaxanthin on Oxidative Stress-Induced Mitochondrial Dysfunction-A Mini-Review. Nutrients *10*.

Kishimoto, T. (2010). IL-6: from its discovery to clinical applications. Int Immunol *22*, 347-352.

Klaunig, J.E., Kamendulis, L.M., and Hocevar, B.A. (2010). Oxidative stress and oxidative damage in carcinogenesis. Toxicol Pathol *38*, 96-109.

Ko, C., Siddaiah, N., Berger, J., Gish, R., Brandhagen, D., Sterling, R.K., Cotler, S.J., Fontana, R.J., McCashland, T.M., Han, S.H.*, et al.* (2007). Prevalence of hepatic iron overload and association with hepatocellular cancer in end-stage liver disease: results from the National Hemochromatosis Transplant Registry. Liver Int *27*, 1394-1401.

Konishi, M., Iwasa, M., Araki, J., Kobayashi, Y., Katsuki, A., Sumida, Y., Nakagawa, N., Kojima, Y., Watanabe, S., Adachi, Y.*, et al.* (2006). Increased lipid peroxidation in patients with non-alcoholic fatty liver disease and chronic hepatitis C as measured by the plasma level of 8-isoprostane. J Gastroenterol Hepatol *21*, 1821-1825.

Kowshik, J., Baba, A.B., Giri, H., Deepak Reddy, G., Dixit, M., and Nagini, S. (2014). Astaxanthin inhibits JAK/STAT-3 signaling to abrogate cell proliferation, invasion and angiogenesis in a hamster model of oral cancer. PLoS One *9*, e109114.

Krenkel, O., Puengel, T., Govaere, O., Abdallah, A.T., Mossanen, J.C., Kohlhepp, M., Liepelt, A., Lefebvre, E., Luedde, T., Hellerbrand, C.*, et al.* (2018). Therapeutic inhibition of inflammatory monocyte recruitment reduces steatohepatitis and liver fibrosis. Hepatology *67*, 1270-1283.

Krysko, D.V., Garg, A.D., Kaczmarek, A., Krysko, O., Agostinis, P., and Vandenabeele, P. (2012). Immunogenic cell death and DAMPs in cancer therapy. Nat Rev Cancer *12*, 860-875.

Kudo, M. (2019). Targeted and immune therapies for hepatocellular carcinoma: Predictions for 2019 and beyond. World J Gastroenterol *25*, 789-807.

Kudo, M. (2019). Targeted and immune therapies for hepatocellular carcinoma: Predictions for 2019 and beyond. World J Gastroenterol 25, 789-807.

Kutlu, O., Kaleli, H.N., and Ozer, E. (2018). Molecular Pathogenesis of Nonalcoholic Steatohepatitis- (NASH-) Related Hepatocellular Carcinoma. Can J Gastroenterol Hepatol *2018*, 8543763.

Lara-Guzmán, O.J., Gil-Izquierdo, Á., Medina, S., Osorio, E., Álvarez-Quintero, R., Zuluaga, N., Oger, C., Galano, J.M., Durand, T., and Muñoz-Durango, K. (2018). Oxidized LDL triggers

changes in oxidative stress and inflammatory biomarkers in human macrophages. Redox Biol *15*, 1-11.

Larsson, S.C., and Wolk, A. (2007). Overweight, obesity and risk of liver cancer: a meta-analysis of cohort studies. Br J Cancer *97*, 1005-1008.

Lata, J. (2010). Chronic Liver Diseases as Liver Tumor Precursors. Digestive Diseases *28*, 596-599.
Lee, G.H., Bhandary, B., Lee, E.M., Park, J.K., Jeong, K.S., Kim, I.K., Kim, H.R., and Chae, H.J. (2011a). The roles of ER stress and P450 2E1 in CCl(4)-induced steatosis. Int J Biochem Cell Biol *43*, 1469-1482.

Lebeaupin, C., Vallée, D., Hazari, Y., Hetz, C., Chevet, E., and Bailly-Maitre, B. (2018). Endoplasmic reticulum stress signalling and the pathogenesis of non-alcoholic fatty liver disease. J Hepatol *69*, 927-947.

Lee, Y., Hirose, H., Ohneda, M., Johnson, J.H., McGarry, J.D., and Unger, R.H. (1994). Beta-cell lipotoxicity in the pathogenesis of non-insulin-dependent diabetes mellitus of obese rats: impairment in adipocyte-beta-cell relationships. Proc Natl Acad Sci U S A *91*, 10878-10882.

Lee, G.H., Kim, D.S., Kim, H.T., Lee, J.W., Chung, C.H., Ahn, T., Lim, J.M., Kim, I.K., Chae, H.J., and Kim, H.R. (2011b). Enhanced lysosomal activity is involved in Bax inhibitor-1-induced regulation of the endoplasmic reticulum (ER) stress response and cell death against ER stress: involvement of vacuolar H+-ATPase (V-ATPase). J Biol Chem *286*, 24743-24753.

Lee, D., Xu, I.M., Chiu, D.K., Lai, R.K., Tse, A.P., Lan Li, L., Law, C.T., Tsang, F.H., Wei, L.L., Chan, C.Y.*, et al.* (2017). Folate cycle enzyme MTHFD1L confers metabolic advantages in hepatocellular carcinoma. J Clin Invest *127*, 1856-1872.

Lee, N.C.W., Carella, M.A., Papa, S., and Bubici, C. (2018). High Expression of Glycolytic Genes in Cirrhosis Correlates With the Risk of Developing Liver Cancer. Front Cell Dev Biol *6*, 138.

Lee, G.H., Kim, H.R., and Chae, H.J. (2012). Bax inhibitor-1 regulates the expression of P450 2E1 through enhanced lysosome activity. Int J Biochem Cell Biol *44*, 600-611.

Lei, P., Bai, T., and Sun, Y. (2019). Mechanisms of Ferroptosis and Relations With Regulated Cell Death: A Review. Front Physiol *10*, 139.

Leung, T.M., and Nieto, N. (2013). CYP2E1 and oxidant stress in alcoholic and non-alcoholic fatty liver disease. J Hepatol *58*, 395-398.

Levine, L. (1983). Inhibition of the A-23187-stimulated leukotriene and prostaglandin biosynthesis of rat basophil leukemia (RBL-1) cells by nonsteroidal anti-inflammatory drugs, antioxidants, and calcium channel blockers. Biochem Pharmacol *32*, 3023-3026.

Levitan, I., Volkov, S., and Subbaiah, P.V. (2010). Oxidized LDL: diversity, patterns of recognition, and pathophysiology. Antioxid Redox Signal *13*, 39-75.

Li, J., Romestaing, C., Han, X., Li, Y., Hao, X., Wu, Y., Sun, C., Liu, X., Jefferson, L.S., Xiong, J.*, et al.* (2010). Cardiolipin remodeling by ALCAT1 links oxidative stress and mitochondrial dysfunction to obesity. Cell Metab *12*, 154-165.

Li, S., Takahara, T., Fujino, M., Fukuhara, Y., Sugiyama, T., Li, X.K., and Takahara, S. (2017). Astaxanthin prevents ischemia-reperfusion injury of the steatotic liver in mice. PLoS One *12*, e0187810.

Li, S., Hong, M., Tan, H.Y., Wang, N., and Feng, Y. (2016). Insights into the Role and Interdependence of Oxidative Stress and Inflammation in Liver Diseases. Oxid Med Cell Longev *2016*, 4234061.

Li, W.C., Ye, S.L., Sun, R.X., Liu, Y.K., Tang, Z.Y., Kim, Y., Karras, J.G., and Zhang, H. (2006). Inhibition of growth and metastasis of human hepatocellular carcinoma by antisense oligonucleotide targeting signal transducer and activator of transcription 3. Clin Cancer Res *12*, 7140-7148.

Liang, J.Q., Teoh, N., Xu, L., Pok, S., Li, X., Chu, E.S.H., Chiu, J., Dong, L., Arfianti, E., Haigh, W.G.*, et al.* (2018). Dietary cholesterol promotes steatohepatitis related hepatocellular carcinoma through dysregulated metabolism and calcium signaling. Nat Commun *9*, 4490.

Linhart, K.B., Glassen, K., Peccerella, T., Waldherr, R., Linhart, H., Bartsch, H., and Seitz, H.K. (2015). The generation of carcinogenic etheno-DNA adducts in the liver of patients with nonalcoholic fatty liver disease. Hepatobiliary Surg Nutr *4*, 117-123.

Lipshutz, G.S., Brennan, T.V., and Warren, R.S. (2002). Thorotrast-induced liver neoplasia: a collective review. J Am Coll Surg *195*, 713-718.

Liu, W., Wang, Z., Hou, J.G., Zhou, Y.D., He, Y.F., Jiang, S., Wang, Y.P., Ren, S., and Li, W. (2018). The Liver Protection Effects of Maltol, a Flavoring Agent, on Carbon Tetrachloride-Induced Acute Liver Injury in Mice via Inhibiting Apoptosis and Inflammatory Response. Molecules *23*.

Liu, Y.L., Reeves, H.L., Burt, A.D., Tiniakos, D., McPherson, S., Leathart, J.B., Allison, M.E., Alexander, G.J., Piguet, A.C., Anty, R.*, et al.* (2014). TM6SF2 rs58542926 influences hepatic fibrosis progression in patients with non-alcoholic fatty liver disease. Nat Commun *5*, 4309.

Liu, L., Gao, C., Yao, P., and Gong, Z. (2015). Quercetin Alleviates High-Fat Diet-Induced Oxidized Low-Density Lipoprotein Accumulation in the Liver: Implication for Autophagy Regulation. Biomed Res Int *2015*, 607531.

Liu, Z., Tu, K., Wang, Y., Yao, B., Li, Q., Wang, L., Dou, C., Liu, Q., and Zheng, X. (2017). Hypoxia Accelerates Aggressiveness of Hepatocellular Carcinoma Cells Involving Oxidative Stress, Epithelial-Mesenchymal Transition and Non-Canonical Hedgehog Signaling. Cell Physiol Biochem *44*, 1856-1868.

Llovet, J.M., Zucman-Rossi, J., Pikarsky, E., Sangro, B., Schwartz, M., Sherman, M., and Gores, G. (2016). Hepatocellular carcinoma. Nat Rev Dis Primers *2*, 16018.

Lockwood, S.F., Penn, M.S., Hazen, S.L., Bikádi, Z., and Zsila, F. (2006). The effects of oral Cardax (disodium disuccinate astaxanthin) on multiple independent oxidative stress markers in a mouse peritoneal inflammation model: influence on 5-lipoxygenase in vitro and in vivo. Life Sci *79*, 162-174.

Loomba, R., Lawitz, E., Mantry, P.S., Jayakumar, S., Caldwell, S.H., Arnold, H., Diehl, A.M., Djedjos, C.S., Han, L., Myers, R.P.*, et al.* (2018). The ASK1 inhibitor selonsertib in patients with nonalcoholic steatohepatitis: A randomized, phase 2 trial. Hepatology *67*, 549-559.

Luedde, T., Kaplowitz, N., and Schwabe, R.F. (2014). Cell death and cell death responses in liver disease: mechanisms and clinical relevance. Gastroenterology *147*, 765-783.e764.

Ly, A., Buck, A., Balluff, B., Sun, N., Gorzolka, K., Feuchtinger, A., Janssen, K.P., Kuppen, P.J., van de Velde, C.J., Weirich, G.*, et al.* (2016). High-mass-resolution MALDI mass spectrometry imaging of metabolites from formalin-fixed paraffin-embedded tissue. Nat Protoc *11*, 1428-1443.

Lü, J.M., Lin, P.H., Yao, Q., and Chen, C. (2010). Chemical and molecular mechanisms of antioxidants: experimental approaches and model systems. J Cell Mol Med *14*, 840-860.

Ma, C., Kesarwala, A.H., Eggert, T., Medina-Echeverz, J., Kleiner, D.E., Jin, P., Stroncek, D.F., Terabe, M., Kapoor, V., ElGindi, M.*, et al.* (2016). NAFLD causes selective CD4(+) T lymphocyte loss and promotes hepatocarcinogenesis. Nature *531*, 253-257.

Machado, M.V., Michelotti, G.A., Pereira, T.e.A., Boursier, J., Kruger, L., Swiderska-Syn, M., Karaca, G., Xie, G., Guy, C.D., Bohinc, B.*, et al.* (2015). Reduced lipoapoptosis, hedgehog pathway activation and fibrosis in caspase-2 deficient mice with non-alcoholic steatohepatitis. Gut *64*, 1148-1157.

Machida, K., Cheng, K.T., Sung, V.M., Shimodaira, S., Lindsay, K.L., Levine, A.M., Lai, M.Y., and Lai, M.M. (2004). Hepatitis C virus induces a mutator phenotype: enhanced mutations of immunoglobulin and protooncogenes. Proc Natl Acad Sci U S A *101*, 4262-4267.

Maeda, S., Kamata, H., Luo, J.L., Leffert, H., and Karin, M. (2005). IKKbeta couples hepatocyte death to cytokine-driven compensatory proliferation that promotes chemical hepatocarcinogenesis. Cell *121*, 977-990.

Malehmir, M., Pfister, D., Gallage, S., Szydlowska, M., Inverso, D., Kotsiliti, E., Leone, V., Peiseler, M., Surewaard, B.G.J., Rath, D.*, et al.* (2019). Platelet GPIbα is a mediator and potential interventional target for NASH and subsequent liver cancer. Nat Med *25*, 641-655.

Malhi, H., Bronk, S.F., Werneburg, N.W., and Gores, G.J. (2006). Free fatty acids induce JNK-dependent hepatocyte lipoapoptosis. J Biol Chem *281*, 12093-12101.

Mancuso, D.J., Sims, H.F., Yang, K., Kiebish, M.A., Su, X., Jenkins, C.M., Guan, S., Moon, S.H., Pietka, T., Nassir, F.*, et al.* (2010). Genetic ablation of calcium-independent phospholipase A2gamma prevents obesity and insulin resistance during high fat feeding by mitochondrial uncoupling and increased adipocyte fatty acid oxidation. J Biol Chem *285*, 36495-36510.

Mano, C.M., Guaratini, T., Cardozo, K.H.M., Colepicolo, P., Bechara, E.J.H., and Barros, M.P. (2018). Astaxanthin Restrains Nitrative-Oxidative Peroxidation in Mitochondrial-Mimetic Liposomes: A Pre-Apoptosis Model. Mar Drugs *16*.

Mantena, S.K., Vaughn, D.P., Andringa, K.K., Eccleston, H.B., King, A.L., Abrams, G.A., Doeller, J.E., Kraus, D.W., Darley-Usmar, V.M., and Bailey, S.M. (2009). High fat diet induces dysregulation of hepatic oxygen gradients and mitochondrial function in vivo. Biochem J *417*, 183-193.

Mansouri, A., Gattolliat, C.H., and Asselah, T. (2018). Mitochondrial Dysfunction and Signaling in Chronic Liver Diseases. Gastroenterology *155*, 629-647.

Marchesini, G., Petta, S., and Dalle Grave, R. (2016). Diet, weight loss, and liver health in nonalcoholic fatty liver disease: Pathophysiology, evidence, and practice. Hepatology *63*, 2032-2043.

Marcus, N.Y., Blomenkamp, K., Ahmad, M., and Teckman, J.H. (2012). Oxidative stress contributes to liver damage in a murine model of alpha-1-antitrypsin deficiency. Exp Biol Med (Maywood) *237*, 1163-1172.

Mardinoglu, A., Wu, H., Bjornson, E., Zhang, C., Hakkarainen, A., Räsänen, S.M., Lee, S., Mancina, R.M., Bergentall, M., Pietiläinen, K.H.*, et al.* (2018). An Integrated Understanding of the Rapid Metabolic Benefits of a Carbohydrate-Restricted Diet on Hepatic Steatosis in Humans. Cell Metab *27*, 559-571.e555.

Marí, M., Caballero, F., Colell, A., Morales, A., Caballeria, J., Fernandez, A., Enrich, C., Fernandez-Checa, J.C., and García-Ruiz, C. (2006). Mitochondrial free cholesterol loading sensitizes to TNF- and Fas-mediated steatohepatitis. Cell Metab *4*, 185-198.

Márton, J., Fodor, T., Nagy, L., Vida, A., Kis, G., Brunyánszki, A., Antal, M., Lüscher, B., and Bai, P. (2018). PARP10 (ARTD10) modulates mitochondrial function. PLoS One *13*, e0187789.

Masarone, M., Rosato, V., Dallio, M., Gravina, A.G., Aglitti, A., Loguercio, C., Federico, A., and Persico, M. (2018). Role of Oxidative Stress in Pathophysiology of Nonalcoholic Fatty Liver Disease. Oxid Med Cell Longev *2018*, 9547613.

Mathew, R., Karp, C.M., Beaudoin, B., Vuong, N., Chen, G., Chen, H.Y., Bray, K., Reddy, A., Bhanot, G., Gelinas, C.*, et al.* (2009). Autophagy suppresses tumorigenesis through elimination of p62. Cell *137*, 1062-1075.

McGettigan, B., McMahan, R., Orlicky, D., Burchill, M., Danhorn, T., Francis, P., Cheng, L.L., Golden-Mason, L., Jakubzick, C.V., and Rosen, H.R. (2019). Dietary Lipids Differentially Shape Nonalcoholic Steatohepatitis Progression and the Transcriptome of Kupffer Cells and Infiltrating Macrophages. Hepatology *70*, 67-83.

McGlynn, K.A., and London, W.T. (2011). The global epidemiology of hepatocellular carcinoma: present and future. Clin Liver Dis *15*, 223-243, vii-x.

Milne, G.L., Yin, H., Hardy, K.D., Davies, S.S., and Roberts, L.J. (2011). Isoprostane generation and function. Chem Rev *111*, 5973-5996.

Min, X., Wen, J., Zhao, L., Wang, K., Li, Q., Huang, G., Liu, J., and Zhao, X. (2018). Role of hepatoma-derived growth factor in promoting de novo lipogenesis and tumorigenesis in hepatocellular carcinoma. Mol Oncol *12*, 1480-1497.

Miura, K., Ishioka, M., Minami, S., Horie, Y., Ohshima, S., Goto, T., and Ohnishi, H. (2016). Toll-like Receptor 4 on Macrophage Promotes the Development of Steatohepatitis-related Hepatocellular Carcinoma in Mice. J Biol Chem *291*, 11504-11517.

Miura, K., Yang, L., van Rooijen, N., Brenner, D.A., Ohnishi, H., and Seki, E. (2013). Toll-like receptor 2 and palmitic acid cooperatively contribute to the development of nonalcoholic steatohepatitis through inflammasome activation in mice. Hepatology *57*, 577-589.

Moroishi, T., Nishiyama, M., Takeda, Y., Iwai, K., and Nakayama, K.I. (2011). The FBXL5-IRP2 axis is integral to control of iron metabolism in vivo. Cell Metab *14*, 339-351.

Morrow, J.D., Frei, B., Longmire, A.W., Gaziano, J.M., Lynch, S.M., Shyr, Y., Strauss, W.E., Oates, J.A., and Roberts, L.J. (1995). Increase in circulating products of lipid peroxidation (F2-isoprostanes) in smokers. Smoking as a cause of oxidative damage. N Engl J Med *332*, 1198-1203.

Murakami, Y., Kawata, A., Katayama, T., and Fujisawa, S. (2015). Anti-inflammatory activity of the artificial antioxidants 2-tert-butyl-4-methoxyphenol (BHA), 2,6-di-tert-butyl-4-methylphenol (BHT) and 2,4,6-tri-tert-butylphenol (TBP), and their various combinations. In Vivo.

Musso, G., Gambino, R., and Cassader, M. (2010). Non-alcoholic fatty liver disease from pathogenesis to management: an update. Obes Rev *11*, 430-445.

Musso, G., Cassader, M., Paschetta, E., and Gambino, R. (2018). Bioactive Lipid Species and Metabolic Pathways in Progression and Resolution of Nonalcoholic Steatohepatitis. Gastroenterology *155*, 282-302.e288.

Muto, Y., Moroishi, T., Ichihara, K., Nishiyama, M., Shimizu, H., Eguchi, H., Moriya, K., Koike, K., Mimori, K., Mori, M.*, et al.* (2019). Disruption of FBXL5-mediated cellular iron homeostasis promotes liver carcinogenesis. J Exp Med *216*, 950-965.

Nakagawa, H., Umemura, A., Taniguchi, K., Font-Burgada, J., Dhar, D., Ogata, H., Zhong, Z., Valasek, M.A., Seki, E., Hidalgo, J.*, et al.* (2014). ER stress cooperates with hypernutrition to trigger TNF-dependent spontaneous HCC development. Cancer Cell *26*, 331-343.

Navarro, C.D.C., Figueira, T.R., Francisco, A., Dal'Bó, G.A., Ronchi, J.A., Rovani, J.C., Escanhoela, C.A.F., Oliveira, H.C.F., Castilho, R.F., and Vercesi, A.E. (2017). Redox

imbalance due to the loss of mitochondrial NAD(P)-transhydrogenase markedly aggravates high fat diet-induced fatty liver disease in mice. Free Radic Biol Med *113*, 190-202.

Neuschwander-Tetri, B.A. (2010). Hepatic lipotoxicity and the pathogenesis of nonalcoholic steatohepatitis: the central role of nontriglyceride fatty acid metabolites. Hepatology *52*, 774-788.

Nguyen, J., Jiao, J., Smoot, K., Watt, G.P., Zhao, C., Song, X., Stevenson, H.L., McCormick, J.B., Fisher-Hoch, S.P., Zhang, J.*, et al.* (2018). Toll-like receptor 4: a target for chemoprevention of hepatocellular carcinoma in obesity and steatohepatitis. Oncotarget *9*, 29495-29507.

Ni, Y., Nagashimada, M., Zhuge, F., Zhan, L., Nagata, N., Tsutsui, A., Nakanuma, Y., Kaneko, S., and Ota, T. (2015). Astaxanthin prevents and reverses diet-induced insulin resistance and steatohepatitis in mice: A comparison with vitamin E. Sci Rep *5*, 17192.

Ni, Y., Zhuge, F., Nagashimada, M., and Ota, T. (2016). Novel Action of Carotenoids on Non-Alcoholic Fatty Liver Disease: Macrophage Polarization and Liver Homeostasis. Nutrients *8*.

Nickel, A.G., von Hardenberg, A., Hohl, M., Löffler, J.R., Kohlhaas, M., Becker, J., Reil, J.C., Kazakov, A., Bonnekoh, J., Stadelmaier, M.*, et al.* (2015). Reversal of Mitochondrial Transhydrogenase Causes Oxidative Stress in Heart Failure. Cell Metab *22*, 472-484.

Nikkanen, J., Forsström, S., Euro, L., Paetau, I., Kohnz, R.A., Wang, L., Chilov, D., Viinamäki, J., Roivainen, A., Marjamäki, P.*, et al.* (2016). Mitochondrial DNA Replication Defects Disturb Cellular dNTP Pools and Remodel One-Carbon Metabolism. Cell Metab *23*, 635-648.

Nobuoka, D., Yoshikawa, T., Sawada, Y., Fujiwara, T., and Nakatsura, T. (2013). Peptide vaccines for hepatocellular carcinoma. Hum Vaccin Immunother *9*, 210-212.

Ogawa, Y., Imajo, K., Honda, Y., Kessoku, T., Tomeno, W., Kato, S., Fujita, K., Yoneda, M., Saito, S., Saigusa, Y.*, et al.* (2018). Palmitate-induced lipotoxicity is crucial for the pathogenesis of nonalcoholic fatty liver disease in cooperation with gut-derived endotoxin. Sci Rep *8*, 11365.

Ogunwobi, O.O., and Liu, C. (2011). Hepatocyte growth factor upregulation promotes carcinogenesis and epithelial-mesenchymal transition in hepatocellular carcinoma via Akt and COX-2 pathways. Clin Exp Metastasis *28*, 721-731.

Oh, C.J., Kim, J.Y., Min, A.K., Park, K.G., Harris, R.A., Kim, H.J., and Lee, I.K. (2012). Sulforaphane attenuates hepatic fibrosis via NF-E2-related factor 2-mediated inhibition of transforming growth factor-β/Smad signaling. Free Radic Biol Med *52*, 671-682.

Ohta, G., Nakanuma, Y., and Terada, T. (1984). Pathology of hepatolithiasis: cholangitis and cholangiocarcinoma. Prog Clin Biol Res *152*, 91-113.

O'Rourke, J.M., Sagar, V.M., Shah, T., and Shetty, S. (2018). Carcinogenesis on the background of liver fibrosis: Implications for the management of hepatocellular cancer. World J Gastroenterol *24*, 4436-4447.

Owada, Y., Tamura, T., Tanoi, T., Ozawa, Y., Shimizu, Y., Hisakura, K., Matsuzaka, T., Shimano, H., Nakano, N., Sakashita, S.*, et al.* (2018). Novel non-alcoholic steatohepatitis model with histopathological and insulin-resistant features. Pathol Int *68*, 12-22.

Ozer, N.K., Negis, Y., Aytan, N., Villacorta, L., Ricciarelli, R., Zingg, J.M., and Azzi, A. (2006). Vitamin E inhibits CD36 scavenger receptor expression in hypercholesterolemic rabbits. Atherosclerosis *184*, 15-20.

Padden, J., Ahrens, M., Kälsch, J., Bertram, S., Megger, D.A., Bracht, T., Eisenacher, M., Kocabayoglu, P., Meyer, H.E., Sipos, B.*, et al.* (2016). Immunohistochemical Markers Distinguishing Cholangiocellular Carcinoma (CCC) from Pancreatic Ductal Adenocarcinoma

(PDAC) Discovered by Proteomic Analysis of Microdissected Cells. Mol Cell Proteomics *15*, 1072-1082.

Palmer, W.C., and Patel, T. (2012). Are common factors involved in the pathogenesis of primary liver cancers? A meta-analysis of risk factors for intrahepatic cholangiocarcinoma. J Hepatol *57*, 69-76.

Palozza, P., Torelli, C., Boninsegna, A., Simone, R., Catalano, A., Mele, M.C., and Picci, N. (2009). Growth-inhibitory effects of the astaxanthin-rich alga Haematococcus pluvialis in human colon cancer cells. Cancer Lett *283*, 108-117.

Pan, X., Hussain, F.N., Iqbal, J., Feuerman, M.H., and Hussain, M.M. (2007). Inhibiting proteasomal degradation of microsomal triglyceride transfer protein prevents CCl4-induced steatosis. J Biol Chem *282*, 17078-17089.

Paradies, G., Paradies, V., Ruggiero, F.M., and Petrosillo, G. (2014). Oxidative stress, cardiolipin and mitochondrial dysfunction in nonalcoholic fatty liver disease. World J Gastroenterol *20*, 14205-14218.

Park, E.J., Lee, J.H., Yu, G.Y., He, G., Ali, S.R., Holzer, R.G., Osterreicher, C.H., Takahashi, H., and Karin, M. (2010). Dietary and genetic obesity promote liver inflammation and tumorigenesis by enhancing IL-6 and TNF expression. Cell *140*, 197-208.

Park, J.S., Chyun, J.H., Kim, Y.K., Line, L.L., and Chew, B.P. (2010). Astaxanthin decreased oxidative stress and inflammation and enhanced immune response in humans. Nutr Metab (Lond) *7*, 18.

Pedersen, T.C., and Aust , S.D. (1973). The role of superoxide and singlet oxygen in lipid peroxidation promoted by xanthine oxidase (Biochem Biophys Res Commun.), pp. 8;52(53):1071-1078.

Pelusi, S., Baselli, G., Pietrelli, A., Dongiovanni, P., Donati, B., McCain, M.V., Meroni, M., Fracanzani, A.L., Romagnoli, R., Petta, S.*, et al.* (2019). Rare Pathogenic Variants Predispose to Hepatocellular Carcinoma in Nonalcoholic Fatty Liver Disease. Sci Rep *9*, 3682.

Pessayre, D. (2007). Role of mitochondria in non-alcoholic fatty liver disease. J Gastroenterol Hepatol *22 Suppl 1*, S20-27.

Petrick, J.L., Campbell, P.T., Koshiol, J., Thistle, J.E., Andreotti, G., Beane-Freeman, L.E., Buring, J.E., Chan, A.T., Chong, D.Q., Doody, M.M.*, et al.* (2018a). Tobacco, alcohol use and risk of hepatocellular carcinoma and intrahepatic cholangiocarcinoma: The Liver Cancer Pooling Project. Br J Cancer *118*, 1005-1012.

Petrick, J.L., Thistle, J.E., Zeleniuch-Jacquotte, A., Zhang, X., Wactawski-Wende, J., Van Dyke, A.L., Stampfer, M.J., Sinha, R., Sesso, H.D., Schairer, C.*, et al.* (2018b). Body Mass Index, Diabetes and Intrahepatic Cholangiocarcinoma Risk: The Liver Cancer Pooling Project and Meta-analysis. Am J Gastroenterol *113*, 1494-1505.

Pickett-Blakely, O., Young, K., and Carr, R.M. (2018). Micronutrients in Nonalcoholic Fatty Liver Disease Pathogenesis. Cell Mol Gastroenterol Hepatol *6*, 451-462.

Pikarsky, E., Porat, R.M., Stein, I., Abramovitch, R., Amit, S., Kasem, S., Gutkovich-Pyest, E., Urieli-Shoval, S., Galun, E., and Ben-Neriah, Y. (2004). NF-kappaB functions as a tumour promoter in inflammation-associated cancer. Nature *431*, 461-466.

Piłacik, B., Nofer, T.W., and Wasowicz, W. (2002). F2-isoprostanes biomarkers of lipid peroxidation: their utility in evaluation of oxidative stress induced by toxic agents. Int J Occup Med Environ Health *15*, 19-27.

Piskounova, E., Agathocleous, M., Murphy, M.M., Hu, Z., Huddlestun, S.E., Zhao, Z., Leitch, A.M., Johnson, T.M., DeBerardinis, R.J., and Morrison, S.J. (2015). Oxidative stress inhibits distant metastasis by human melanoma cells. Nature *527*, 186-191.

Polednak, A.P. (2008). Estimating the number of U.S. incident cancers attributable to obesity and the impact on temporal trends in incidence rates for obesity-related cancers. Cancer Detect Prev *32*, 190-199.

Poultsides, G.A., Zhu, A.X., Choti, M.A., and Pawlik, T.M. (2010). Intrahepatic cholangiocarcinoma. Surg Clin North Am *90*, 817-837.

Povsic, M., Wong, O.Y., Perry, R., and Bottomley, J. (2019). A Structured Literature Review of the Epidemiology and Disease Burden of Non-Alcoholic Steatohepatitis (NASH). Adv Ther *36*, 1574-1594.

Prame Kumar, K., Nicholls, A.J., and Wong, C.H.Y. (2018). Partners in crime: neutrophils and monocytes/macrophages in inflammation and disease. Cell Tissue Res *371*, 551-565.

Putra, J., de Abreu, F.B., Peterson, J.D., Pipas, J.M., Mody, K., Amos, C.I., Tsongalis, G.J., and Suriawinata, A.A. (2015). Molecular profiling of intrahepatic and extrahepatic cholangiocarcinoma using next generation sequencing. Exp Mol Pathol *99*, 240-244.

Ratziu, V., Caldwell, S., and Neuschwander-Tetri, B.A. (2010). Therapeutic trials in nonalcoholic steatohepatitis: insulin sensitizers and related methodological issues. Hepatology *52*, 2206-2215.

Ratziu, V., Harrison, S.A., Francque, S., Bedossa, P., Lehert, P., Serfaty, L., Romero-Gomez, M., Boursier, J., Abdelmalek, M., Caldwell, S.*, et al.* (2016). Elafibranor, an Agonist of the Peroxisome Proliferator-Activated Receptor-α and -δ, Induces Resolution of Nonalcoholic Steatohepatitis Without Fibrosis Worsening. Gastroenterology *150*, 1147-1159.e1145.

Ratziu, V., Sheikh, M.Y., Sanyal, A.J., Lim, J.K., Conjeevaram, H., Chalasani, N., Abdelmalek, M., Bakken, A., Renou, C., Palmer, M.*, et al.* (2012). A phase 2, randomized, double-blind, placebo-controlled study of GS-9450 in subjects with nonalcoholic steatohepatitis. Hepatology *55*, 419-428.

Rau, M., Schilling, A.K., Meertens, J., Hering, I., Weiss, J., Jurowich, C., Kudlich, T., Hermanns, H.M., Bantel, H., Beyersdorf, N.*, et al.* (2016). Progression from Nonalcoholic Fatty Liver to Nonalcoholic Steatohepatitis Is Marked by a Higher Frequency of Th17 Cells in the Liver and an Increased Th17/Resting Regulatory T Cell Ratio in Peripheral Blood and in the Liver. J Immunol *196*, 97-105.

Reuter, S., Gupta, S.C., Chaturvedi, M.M., and Aggarwal, B.B. (2010). Oxidative stress, inflammation, and cancer: how are they linked? Free Radic Biol Med *49*, 1603-1616.

Ricciarelli, R., Zingg, J.M., and Azzi, A. (2000). Vitamin E reduces the uptake of oxidized LDL by inhibiting CD36 scavenger receptor expression in cultured aortic smooth muscle cells. Circulation *102*, 82-87.

Ringelhan, M., Pfister, D., O'Connor, T., Pikarsky, E., and Heikenwalder, M. (2018). The immunology of hepatocellular carcinoma. Nat Immunol 19, 222-232.

Ross, D., and Siegel, D. (2017). Functions of NQO1 in Cellular Protection and CoQ. Front Physiol *8*, 595.

Rossaint, J., Margraf, A., and Zarbock, A. (2018). Role of Platelets in Leukocyte Recruitment and Resolution of Inflammation. Front Immunol *9*, 2712.

Saha, S.K., Zhu, A.X., Fuchs, C.S., and Brooks, G.A. (2016). Forty-Year Trends in Cholangiocarcinoma Incidence in the U.S.: Intrahepatic Disease on the Rise. Oncologist *21*, 594-599.

Sanyal, A.J., Chalasani, N., Kowdley, K.V., McCullough, A., Diehl, A.M., Bass, N.M., Neuschwander-Tetri, B.A., Lavine, J.E., Tonascia, J., Unalp, A*., et al.* (2010). Pioglitazone, vitamin E, or placebo for nonalcoholic steatohepatitis. N Engl J Med *362*, 1675-1685.

Schaper, F., and Rose-John, S. (2015). Interleukin-6: Biology, signaling and strategies of blockade. Cytokine Growth Factor Rev *26*, 475-487.

Schleicher, E.M., Galvan, A.M., Imamura-Kawasawa, Y., Moldovan, G.L., and Nicolae, C.M. (2018). PARP10 promotes cellular proliferation and tumorigenesis by alleviating replication stress. Nucleic Acids Res *46*, 8908-8916.

Schildberg, F.A., Hegenbarth, S.I., Schumak, B., Scholz, K., Limmer, A., and Knolle, P.A. (2008). Liver sinusoidal endothelial cells veto CD8 T cell activation by antigen-presenting dendritic cells. Eur J Immunol *38*, 957-967.

Schröder, T., Kucharczyk, D., Bär, F., Pagel, R., Derer, S., Jendrek, S.T., Sünderhauf, A., Brethack, A.K., Hirose, M., Möller, S*., et al.* (2016). Mitochondrial gene polymorphisms alter hepatic cellular energy metabolism and aggravate diet-induced non-alcoholic steatohepatitis. Mol Metab *5*, 283-295.

Schulze, K., Imbeaud, S., Letouzé, E., Alexandrov, L.B., Calderaro, J., Rebouissou, S., Couchy, G., Meiller, C., Shinde, J., Soysouvanh, F*., et al.* (2015). Exome sequencing of hepatocellular carcinomas identifies new mutational signatures and potential therapeutic targets. Nat Genet *47*, 505-511.

Schwimmer, J.B., Lavine, J.E., Wilson, L.A., Neuschwander-Tetri, B.A., Xanthakos, S.A., Kohli, R., Barlow, S.E., Vos, M.B., Karpen, S.J., Molleston, J.P*., et al.* (2016). In Children With Nonalcoholic Fatty Liver Disease, Cysteamine Bitartrate Delayed Release Improves Liver Enzymes but Does Not Reduce Disease Activity Scores. Gastroenterology *151*, 1141-1154.e1149.

Scoles, D.R., Xu, X., Wang, H., Tran, H., Taylor-Harding, B., Li, A., and Karlan, B.Y. (2010). Liver X receptor agonist inhibits proliferation of ovarian carcinoma cells stimulated by oxidized low density lipoprotein. Gynecol Oncol *116*, 109-116.

Serviddio, G., Bellanti, F., Tamborra, R., Rollo, T., Capitanio, N., Romano, A.D., Sastre, J., Vendemiale, G., and Altomare, E. (2008). Uncoupling protein-2 (UCP2) induces mitochondrial proton leak and increases susceptibility of non-alcoholic steatohepatitis (NASH) liver to ischaemia-reperfusion injury. Gut *57*, 957-965.

Seydel, G.S., Kucukoglu, O., Altinbas, A., Demir, O.O., Yilmaz, S., Akkiz, H., Otan, E., Sowa, J.P., and Canbay, A. (2016). Economic growth leads to increase of obesity and associated hepatocellular carcinoma in developing countries. Ann Hepatol *15*, 662-672.

Shaib, Y.H., Davila, J.A., McGlynn, K., and El-Serag, H.B. (2004). Rising incidence of intrahepatic cholangiocarcinoma in the United States: a true increase? J Hepatol *40*, 472-477.

Shaib, Y.H., El-Serag, H.B., Davila, J.A., Morgan, R., and McGlynn, K.A. (2005). Risk factors of intrahepatic cholangiocarcinoma in the United States: a case-control study. Gastroenterology *128*, 620-626.

Sharma, R.S., Harrison, D.J., Kisielewski, D., Cassidy, D.M., McNeilly, A.D., Gallagher, J.R., Walsh, S.V., Honda, T., McCrimmon, R.J., Dinkova-Kostova, A.T*., et al.* (2018). Experimental Nonalcoholic Steatohepatitis and Liver Fibrosis Are Ameliorated by Pharmacologic Activation of Nrf2 (NF-E2 p45-Related Factor 2). Cell Mol Gastroenterol Hepatol *5*, 367-398.

Sheedfar, F., Sung, M.M., Aparicio-Vergara, M., Kloosterhuis, N.J., Miquilena-Colina, M.E., Vargas-Castrillón, J., Febbraio, M., Jacobs, R.L., de Bruin, A., Vinciguerra, M*., et al.* (2014). Increased hepatic CD36 expression with age is associated with enhanced susceptibility to nonalcoholic fatty liver disease. Aging (Albany NY) *6*, 281-295.

Shen, J., Tsoi, H., Liang, Q., Chu, E.S., Liu, D., Yu, A.C., Chan, T.F., Li, X., Sung, J.J., Wong, V.W.*, et al.* (2016). Oncogenic mutations and dysregulated pathways in obesity-associated hepatocellular carcinoma. Oncogene *35*, 6271-6280.

Shevchenko, A., Tomas, H., Havlis, J., Olsen, J.V., and Mann, M. (2006). In-gel digestion for mass spectrometric characterization of proteins and proteomes. Nat Protoc *1*, 2856-2860.

Shiao, M.S., Chiablaem, K., Charoensawan, V., Ngamphaiboon, N., and Jinawath, N. (2018). Emergence of Intrahepatic Cholangiocarcinoma: How High-Throughput Technologies Expedite the Solutions for a Rare Cancer Type. Front Genet *9*, 309.

Shiffman, M., Freilich, B., Vuppalanchi, R., Watt, K., Chan, J.L., Spada, A., Hagerty, D.T., and Schiff, E. (2019). Randomised clinical trial: emricasan versus placebo significantly decreases ALT and caspase 3/7 activation in subjects with non-alcoholic fatty liver disease. Aliment Pharmacol Ther *49*, 64-73.

Shimozono, R., Asaoka, Y., Yoshizawa, Y., Aoki, T., Noda, H., Yamada, M., Kaino, M., and Mochizuki, H. (2013). Nrf2 activators attenuate the progression of nonalcoholic steatohepatitis-related fibrosis in a dietary rat model. Mol Pharmacol *84*, 62-70.

Shimada, S., Mogushi, K., Akiyama, Y., Furuyama, T., Watanabe, S., Ogura, T., Ogawa, K., Ono, H., Mitsunori, Y., Ban, D.*, et al.* (2019). Comprehensive molecular and immunological characterization of hepatocellular carcinoma. EBioMedicine *40*, 457-470.

Shin, S., Wakabayashi, J., Yates, M.S., Wakabayashi, N., Dolan, P.M., Aja, S., Liby, K.T., Sporn, M.B., Yamamoto, M., and Kensler, T.W. (2009). Role of Nrf2 in prevention of high-fat diet-induced obesity by synthetic triterpenoid CDDO-imidazolide. Eur J Pharmacol *620*, 138-144.

Shindo, R., Kakehashi, H., Okumura, K., Kumagai, Y., and Nakano, H. (2013). Critical contribution of oxidative stress to TNFα-induced necroptosis downstream of RIPK1 activation. Biochem Biophys Res Commun *436*, 212-216.

Showalter, L.A., Weinman, S.A., Østerlie, M., and Lockwood, S.F. (2004). Plasma appearance and tissue accumulation of non-esterified, free astaxanthin in C57BL/6 mice after oral dosing of a disodium disuccinate diester of astaxanthin (Heptax). Comp Biochem Physiol C Toxicol Pharmacol *137*, 227-236.

Sia, D., Hoshida, Y., Villanueva, A., Roayaie, S., Ferrer, J., Tabak, B., Peix, J., Sole, M., Tovar, V., Alsinet, C.*, et al.* (2013). Integrative molecular analysis of intrahepatic cholangiocarcinoma reveals 2 classes that have different outcomes. Gastroenterology *144*, 829-840.

Siddiqui, M.S., Vuppalanchi, R., Van Natta, M.L., Hallinan, E., Kowdley, K.V., Abdelmalek, M., Neuschwander-Tetri, B.A., Loomba, R., Dasarathy, S., Brandman, D.*, et al.* (2019). Vibration-Controlled Transient Elastography to Assess Fibrosis and Steatosis in Patients With Nonalcoholic Fatty Liver Disease. Clin Gastroenterol Hepatol *17*, 156-163.e152.

Simões, I.C.M., Fontes, A., Pinton, P., Zischka, H., and Wieckowski, M.R. (2018). Mitochondria in non-alcoholic fatty liver disease. Int J Biochem Cell Biol *95*, 93-99.

Singh, R., Wang, Y., Schattenberg, J.M., Xiang, Y., and Czaja, M.J. (2009). Chronic oxidative stress sensitizes hepatocytes to death from 4-hydroxynonenal by JNK/c-Jun overactivation. Am J Physiol Gastrointest Liver Physiol *297*, G907-917.

Sircana, A., Paschetta, E., Saba, F., Molinaro, F., and Musso, G. (2019). Recent Insight into the Role of Fibrosis in Nonalcoholic Steatohepatitis-Related Hepatocellular Carcinoma. Int J Mol Sci *20*.

Song, X.D., Zhang, J.J., Wang, M.R., Liu, W.B., Gu, X.B., and Lv, C.J. (2011). Astaxanthin induces mitochondria-mediated apoptosis in rat hepatocellular carcinoma CBRH-7919 cells. Biol Pharm Bull *34*, 839-844.

Sookoian, S., and Pirola, C.J. (2011). Meta-analysis of the influence of I148M variant of patatin-like phospholipase domain containing 3 gene (PNPLA3) on the susceptibility and histological severity of nonalcoholic fatty liver disease. Hepatology *53*, 1883-1894.

Soresi, M., Giannitrapani, L., D'Antona, F., Florena, A.M., La Spada, E., Terranova, A., Cervello, M., D'Alessandro, N., and Montalto, G. (2006). Interleukin-6 and its soluble receptor in patients with liver cirrhosis and hepatocellular carcinoma. World J Gastroenterol *12*, 2563-2568.

Spiller, G.A., and Dewell, A. (2003). Safety of an astaxanthin-rich Haematococcus pluvialis algal extract: a randomized clinical trial. J Med Food *6*, 51-56.

Sripa, B., Kaewkes, S., Sithithaworn, P., Mairiang, E., Laha, T., Smout, M., Pairojkul, C., Bhudhisawasdi, V., Tesana, S., Thinkamrop, B*., et al.* (2007). Liver fluke induces cholangiocarcinoma. PLoS Med *4*, e201.

St-Pierre, J., Buckingham, J.A., Roebuck, S.J., and Brand, M.D. (2002). Topology of superoxide production from different sites in the mitochondrial electron transport chain. J Biol Chem *277*, 44784-44790.

Strazzabosco, M., Spirlí, C., and Okolicsanyi, L. (2000). Pathophysiology of the intrahepatic biliary epithelium. J Gastroenterol Hepatol *15*, 244-253.

Sumida, Y., Niki, E., Naito, Y., and Yoshikawa, T. (2013). Involvement of free radicals and oxidative stress in NAFLD/NASH. Free Radic Res *47*, 869-880.

Sumida, Y., and Yoneda, M. (2018). Current and future pharmacological therapies for NAFLD/NASH. J Gastroenterol *53*, 362-376.

Suzuki, T., Shinjo, S., Arai, T., Kanai, M., and Goda, N. (2014). Hypoxia and fatty liver. World J Gastroenterol *20*, 15087-15097.

Suzuki, Y., Imai, K., Takai, K., Hanai, T., Hayashi, H., Naiki, T., Nishigaki, Y., Tomita, E., Shimizu, M., and Moriwaki, H. (2013). Hepatocellular carcinoma patients with increased oxidative stress levels are prone to recurrence after curative treatment: a prospective case series study using the d-ROM test. J Cancer Res Clin Oncol *139*, 845-852.

Suzuki, Y.J. (2019). Oxidant-Mediated Protein Amino Acid Conversion. Antioxidants (Basel) *8*.

Syn, W.K., Choi, S.S., and Diehl, A.M. (2009). Apoptosis and cytokines in non-alcoholic steatohepatitis. Clin Liver Dis *13*, 565-580.

Tacke, F. (2017). Targeting hepatic macrophages to treat liver diseases. J Hepatol *66*, 1300-1312.

Tacke, F., and Zimmermann, H.W. (2014). Macrophage heterogeneity in liver injury and fibrosis. J Hepatol *60*, 1090-1096.

Takahashi, K., Watanabe, M., Takimoto, T., and Akiba, Y. (2004). Uptake and distribution of astaxanthin in several tissues and plasma lipoproteins in male broiler chickens fed a yeast (Phaffia rhodozyma) with a high concentration of astaxanthin. Br Poult Sci *45*, 133-138.

Takahashi, Y. and Fukusato, T. (2014). Histopathology of nonalcoholic fatty liver disease/nonalcoholic steatohepatitis. World J Gastroenterol 20, 15539-15548.

Takaki, A., Kawai, D., and Yamamoto, K. (2013). Multiple hits, including oxidative stress, as pathogenesis and treatment target in non-alcoholic steatohepatitis (NASH). Int J Mol Sci *14*, 20704-20728.

Takaki, A., and Yamamoto, K. (2015). Control of oxidative stress in hepatocellular carcinoma: Helpful or harmful? World J Hepatol *7*, 968-979.

Taliento, A.E., Dallio, M., Federico, A., Prati, D., and Valenti, L. (2019). Novel Insights into the Genetic Landscape of Nonalcoholic Fatty Liver Disease. Int J Environ Res Public Health *16*.

Tanaka, S., Hikita, H., Tatsumi, T., Sakamori, R., Nozaki, Y., Sakane, S., Shiode, Y., Nakabori, T., Saito, Y., Hiramatsu, N*., et al.* (2016). Rubicon inhibits autophagy and accelerates hepatocyte apoptosis and lipid accumulation in nonalcoholic fatty liver disease in mice. Hepatology *64*, 1994-2014.

Tanaka, S., Miyanishi, K., Kobune, M., Kawano, Y., Hoki, T., Kubo, T., Hayashi, T., Sato, T., Sato, Y., Takimoto, R*., et al.* (2013). Increased hepatic oxidative DNA damage in patients with nonalcoholic steatohepatitis who develop hepatocellular carcinoma. J Gastroenterol *48*, 1249-1258.

Theise, N.D. (1996). Cirrhosis and hepatocellular neoplasia: more like cousins than like parent and child. Gastroenterology *111*, 526-528.

Tilg, H., and Moschen, A.R. (2010). Evolution of inflammation in nonalcoholic fatty liver disease: the multiple parallel hits hypothesis. Hepatology *52*, 1836-1846.

Tirmenstein, M.A., Nicholls-Grzemski, F.A., Schmittgen, T.D., Zakrajsek, B.A., and Fariss, M.W. (2000). Characterization of nitric oxide production following isolation of rat hepatocytes. Toxicol Sci *53*, 56-62.

Tomás-Loba, A., Manieri, E., González-Terán, B., Mora, A., Leiva-Vega, L., Santamans, A.M., Romero-Becerra, R., Rodríguez, E., Pintor-Chocano, A., Feixas, F*., et al.* (2019). p38γ is essential for cell cycle progression and liver tumorigenesis. Nature *568*, 557-560.

Topic, A., Ljujic, M., and Radojkovic, D. (2012). Alpha-1-antitrypsin in pathogenesis of hepatocellular carcinoma. Hepat Mon *12*, e7042.

Tosello-Trampont, A.C., Landes, S.G., Nguyen, V., Novobrantseva, T.I., and Hahn, Y.S. (2012). Kuppfer cells trigger nonalcoholic steatohepatitis development in diet-induced mouse model through tumor necrosis factor-α production. J Biol Chem *287*, 40161-40172.

Tran, K.T., Coleman, H.G., McCain, R.S., and Cardwell, C.R. (2019). Serum Biomarkers of Iron Status and Risk of Primary Liver Cancer: A Systematic Review and Meta-Analysis. Nutr Cancer, 1-9.

Triantafyllou, E., Pop, O.T., Possamai, L.A., Wilhelm, A., Liaskou, E., Singanayagam, A., Bernsmeier, C., Khamri, W., Petts, G., Dargue, R*., et al.* (2018). MerTK expressing hepatic macrophages promote the resolution of inflammation in acute liver failure. Gut *67*, 333-347.

Trivedi, P.J., and Cullen, S. (2011). Autoimmune hepatitis, cirrhosis, and hepatocellular carcinoma (HCC). Dig Dis Sci *56*, 276-278.

Tsuchida, T., Lee, Y.A., Fujiwara, N., Ybanez, M., Allen, B., Martins, S., Fiel, M.I., Goossens, N., Chou, H.I., Hoshida, Y*., et al.* (2018). A simple diet- and chemical-induced murine NASH model with rapid progression of steatohepatitis, fibrosis and liver cancer. J Hepatol *69*, 385-395.

Tuma, D.J. (2002). Role of malondialdehyde-acetaldehyde adducts in liver injury. Free Radic Biol Med *32*, 303-308.

Tyanova, S., and Cox, J. (2018). Perseus: A Bioinformatics Platform for Integrative Analysis of Proteomics Data in Cancer Research. Methods Mol Biol *1711*, 133-148.

Tyanova, S., Temu, T., and Cox, J. (2016). The MaxQuant computational platform for mass spectrometry-based shotgun proteomics. Nat Protoc *11*, 2301-2319.

Umemura, A., He, F., Taniguchi, K., Nakagawa, H., Yamachika, S., Font-Burgada, J., Zhong, Z., Subramaniam, S., Raghunandan, S., Duran, A.*, et al.* (2016). p62, Upregulated during Preneoplasia, Induces Hepatocellular Carcinogenesis by Maintaining Survival of Stressed HCC-Initiating Cells. Cancer Cell *29*, 935-948.

Unger, R.H., and Zhou, Y.T. (2001). Lipotoxicity of beta-cells in obesity and in other causes of fatty acid spillover. Diabetes *50 Suppl 1*, S118-121.

van de Sluis, B., Wijers, M., and Herz, J. (2017). News on the molecular regulation and function of hepatic low-density lipoprotein receptor and LDLR-related protein 1. Curr Opin Lipidol *28*, 241-247.

van de Wiel, M.A., Kim, K.I., Vosse, S.J., van Wieringen, W.N., Wilting, S.M., and Ylstra, B. (2007). CGHcall: calling aberrations for array CGH tumor profiles. Bioinformatics *23*, 892-894.

van de Wiel, M.A., and Wieringen, W.N. (2007). CGHregions: dimension reduction for array CGH data with minimal information loss. Cancer Inform *3*, 55-63.

Van Herck, M.A., Vonghia, L., and Francque, S.M. (2017). Animal Models of Nonalcoholic Fatty Liver Disease-A Starter's Guide. Nutrients *9*.

Visioli, F., and Artaria, C. (2017). Astaxanthin in cardiovascular health and disease: mechanisms of action, therapeutic merits, and knowledge gaps. Food Funct *8*, 39-63.

Waisberg, D.R., Pinheiro, R.S., Nacif, L.S., Rocha-Santos, V., Martino, R.B., Arantes, R.M., Ducatti, L., Lai, Q., Andraus, W., and D'Albuquerque, L.C. (2018). Resection for intrahepatic cholangiocellular cancer: new advances. Transl Gastroenterol Hepatol *3*, 60.

Wakabayashi, N., Slocum, S.L., Skoko, J.J., Shin, S., and Kensler, T.W. (2010). When NRF2 talks, who's listening? Antioxid Redox Signal *13*, 1649-1663.

Walter, D., Döring, C., Feldhahn, M., Battke, F., Hartmann, S., Winkelmann, R., Schneider, M., Bankov, K., Schnitzbauer, A., Zeuzem, S.*, et al.* (2017). Intratumoral heterogeneity of intrahepatic cholangiocarcinoma. Oncotarget *8*, 14957-14968.

Wan, F.C., Zhang, C., Jin, Q., Wei, C., Zhao, H.B., Zhang, X.L., You, W., Liu, X.M., Liu, G.F., Liu, Y.F.*, et al.* (2019). Protective Effects of Astaxanthin on Lipopolysaccharide-Induced Inflammation in Bovine Endometrial Epithelial Cells. Biol Reprod.

Wang, D., and Dubois, R.N. (2010). Eicosanoids and cancer. Nat Rev Cancer *10*, 181-193.

Wang, X.J., Hayes, J.D., Higgins, L.G., Wolf, C.R., and Dinkova-Kostova, A.T. (2010). Activation of the NRF2 signaling pathway by copper-mediated redox cycling of para- and ortho-hydroquinones. Chem Biol *17*, 75-85.

Weltman, M.D., Farrell, G.C., Hall, P., Ingelman-Sundberg, M., and Liddle, C. (1998). Hepatic cytochrome P450 2E1 is increased in patients with nonalcoholic steatohepatitis. Hepatology *27*, 128-133.

Welzel, T.M., Graubard, B.I., El-Serag, H.B., Shaib, Y.H., Hsing, A.W., Davila, J.A., and McGlynn, K.A. (2007). Risk factors for intrahepatic and extrahepatic cholangiocarcinoma in the United States: a population-based case-control study. Clin Gastroenterol Hepatol *5*, 1221-1228.

Weston, C.J., Shepherd, E.L., Claridge, L.C., Rantakari, P., Curbishley, S.M., Tomlinson, J.W., Hubscher, S.G., Reynolds, G.M., Aalto, K., Anstee, Q.M.*, et al.* (2015). Vascular adhesion protein-1 promotes liver inflammation and drives hepatic fibrosis. J Clin Invest *125*, 501-520.

Weston, C.J., Zimmermann, H.W., and Adams, D.H. (2019). The Role of Myeloid-Derived Cells in the Progression of Liver Disease. Front Immunol *10*, 893.

wheeler@bcm.edu, C.G.A.R.N.E.a., and Network, C.G.A.R. (2017). Comprehensive and Integrative Genomic Characterization of Hepatocellular Carcinoma. Cell *169*, 1327-1341.e1323.

White, D.L., Kanwal, F., and El-Serag, H.B. (2012). Association between nonalcoholic fatty liver disease and risk for hepatocellular cancer, based on systematic review. Clin Gastroenterol Hepatol *10*, 1342-1359.e1342.

W.H.O. (2017). Obesity and overweight (https://www.who.int).

Win, S., Than, T.A., Le, B.H., García-Ruiz, C., Fernandez-Checa, J.C., and Kaplowitz, N. (2015). Sab (Sh3bp5) dependence of JNK mediated inhibition of mitochondrial respiration in palmitic acid induced hepatocyte lipotoxicity. J Hepatol *62*, 1367-1374.

Win, S., Than, T.A., Zhang, J., Oo, C., Min, R.W.M., and Kaplowitz, N. (2018). New insights into the role and mechanism of c-Jun-N-terminal kinase signaling in the pathobiology of liver diseases. Hepatology *67*, 2013-2024.

Winczura, A., Czubaty, A., Winczura, K., Masłowska, K., Nałęcz, M., Dudzińska, D.A., Saparbaev, M., Staroń, K., and Tudek, B. (2014). Lipid peroxidation product 4-hydroxy-2-nonenal modulates base excision repair in human cells. DNA Repair (Amst) *22*, 1-11.

Wires, E.S., Trychta, K.A., Bäck, S., Sulima, A., Rice, K.C., and Harvey, B.K. (2017). High fat diet disrupts endoplasmic reticulum calcium homeostasis in the rat liver. J Hepatol *67*, 1009-1017.

Wolf, A.M., Asoh, S., Hiranuma, H., Ohsawa, I., Iio, K., Satou, A., Ishikura, M., and Ohta, S. (2010). Astaxanthin protects mitochondrial redox state and functional integrity against oxidative stress. J Nutr Biochem *21*, 381-389.

Wolf, M.J., Adili, A., Piotrowitz, K., Abdullah, Z., Boege, Y., Stemmer, K., Ringelhan, M., Simonavicius, N., Egger, M., Wohlleber, D.*, et al.* (2014). Metabolic activation of intrahepatic CD8^{+} T cells and NKT cells causes nonalcoholic steatohepatitis and liver cancer via cross-talk with hepatocytes. Cancer Cell *26*, 549-564.

Xiong, J., Lu, X., Xu, W., Bai, Y., Huang, H., Bian, J., Zhang, L., Long, J., Xu, Y., Wang, Z.*, et al.* (2018a). Metabolic syndrome and the risk of cholangiocarcinoma: a hospital-based case-control study in China. Cancer Manag Res *10*, 3849-3855.

Xiong, J., Yin, Z., Xu, W., Shen, Z., Li, Y., and Lu, X. (2018b). Alcoholic liver disease and risk of cholangiocarcinoma: a systematic review and meta-analysis. Onco Targets Ther *11*, 8211-8219.

Yan, X., Yao, M., Wen, X., Zhu, Y., Zhao, E., Qian, X., Chen, X., Lu, W., Lv, Q., Zhang, L.*, et al.* (2019). Elevated apolipoprotein B predicts poor postsurgery prognosis in patients with hepatocellular carcinoma. Onco Targets Ther *12*, 1957-1964.

Yang, Y., Pham, T.X., Wegner, C.J., Kim, B., Ku, C.S., Park, Y.K., and Lee, J.Y. (2014). Astaxanthin lowers plasma TAG concentrations and increases hepatic antioxidant gene expression in diet-induced obesity mice. Br J Nutr *112*, 1797-1804.

Yang, W.S., and Stockwell, B.R. (2016). Ferroptosis: Death by Lipid Peroxidation. Trends Cell Biol *26*, 165-176.

Yang, J.D., Hainaut, P., Gores, G.J. et al. (2019). A global view of hepatocellular carcinoma: trends, risk, prevention and management. Nat Rev Gastroenterol Hepatol 16, 589–604.

Yang, J., Trépo, E., Nahon, P., Cao, Q., Moreno, C., Letouzé, E., Imbeaud, S., Gustot, T., Deviere, J., Debette, S*., et al.* (2019). PNPLA3 and TM6SF2 variants as risk factors of hepatocellular carcinoma across various etiologies and severity of underlying liver diseases. Int J Cancer *144*, 533-544.

Yasui, Y., Hosokawa, M., Mikami, N., Miyashita, K., and Tanaka, T. (2011). Dietary astaxanthin inhibits colitis and colitis-associated colon carcinogenesis in mice via modulation of the inflammatory cytokines. Chem Biol Interact *193*, 79-87.

Ye, Q., Qian, B.X., Yin, W.L., Wang, F.M., and Han, T. (2016). Association between the HFE C282Y, H63D Polymorphisms and the Risks of Non-Alcoholic Fatty Liver Disease, Liver Cirrhosis and Hepatocellular Carcinoma: An Updated Systematic Review and Meta-Analysis of 5,758 Cases and 14,741 Controls. PLoS One *11*, e0163423.

Yoboue, E.D., Sitia, R., and Simmen, T. (2018). Redox crosstalk at endoplasmic reticulum (ER) membrane contact sites (MCS) uses toxic waste to deliver messages. Cell Death Dis *9*, 331.

Yoon, J.H., Canbay, A.E., Werneburg, N.W., Lee, S.P., and Gores, G.J. (2004). Oxysterols induce cyclooxygenase-2 expression in cholangiocytes: implications for biliary tract carcinogenesis. Hepatology *39*, 732-738.

Yoshida, H., Yanai, H., Ito, K., Tomono, Y., Koikeda, T., Tsukahara, H., and Tada, N. (2010). Administration of natural astaxanthin increases serum HDL-cholesterol and adiponectin in subjects with mild hyperlipidemia. Atherosclerosis *209*, 520-523.

Yoshida, K., Nakamura, H., Okuda, Y., Enomoto, H., Kishima, Y., Uyama, H., Ito, H., Hirasawa, T., Inagaki, S., and Kawase, I. (2003). Expression of hepatoma-derived growth factor in hepatocarcinogenesis. J Gastroenterol Hepatol *18*, 1293-1301.

Yoshida, K., Tomita, Y., Okuda, Y., Yamamoto, S., Enomoto, H., Uyama, H., Ito, H., Hoshida, Y., Aozasa, K., Nagano, H*., et al.* (2006). Hepatoma-derived growth factor is a novel prognostic factor for hepatocellular carcinoma. Ann Surg Oncol *13*, 159-167.

Yoshimoto, S., Loo, T.M., Atarashi, K., Kanda, H., Sato, S., Oyadomari, S., Iwakura, Y., Oshima, K., Morita, H., Hattori, M*., et al.* (2013). Obesity-induced gut microbial metabolite promotes liver cancer through senescence secretome. Nature *499*, 97-101.

Younossi, Z., and Henry, L. (2016). Contribution of Alcoholic and Nonalcoholic Fatty Liver Disease to the Burden of Liver-Related Morbidity and Mortality. Gastroenterology 150, 1778-1785.

Younossi, Z., Anstee, Q.M., Marietti, M., Hardy, T., Henry, L., Eslam, M., George, J., and Bugianesi, E. (2018). Global burden of NAFLD and NASH: trends, predictions, risk factors and prevention. Nat Rev Gastroenterol Hepatol *15*, 11-20.

Younossi, Z., Tacke, F., Arrese, M., Chander Sharma, B., Mostafa, I., Bugianesi, E., Wai-Sun Wong, V., Yilmaz, Y., George, J., Fan, J*., et al.* (2019). Global Perspectives on Nonalcoholic Fatty Liver Disease and Nonalcoholic Steatohepatitis. Hepatology *69*, 2672-2682.

Yu, L.X., Ling, Y., and Wang, H.Y. (2018). Role of nonresolving inflammation in hepatocellular carcinoma development and progression. NPJ Precis Oncol *2*, 6.

Yuan, J.P., Peng, J., Yin, K., and Wang, J.H. (2011). Potential health-promoting effects of astaxanthin: a high-value carotenoid mostly from microalgae. Mol Nutr Food Res *55*, 150-165.

Yuan, D., Huang, S., Berger, E., Liu, L., Gross, N., Heinzmann, F., Ringelhan, M., Connor, T.O., Stadler, M., Meister, M*., et al.* (2017). Kupffer Cell-Derived Tnf Triggers

Cholangiocellular Tumorigenesis through JNK due to Chronic Mitochondrial Dysfunction and ROS. Cancer Cell *31*, 771-789.e776.

Yuan, J.M., Grouls, M., Carmella, S.G., Wang, R., Heskin, A., Jiang, Y., Tan, Y.T., Adams-Haduch, J., Gao, Y.T., and Hecht, S.S. (2019). Prediagnostic levels of urinary 8-epi-prostaglandin F2α and prostaglandin E2 metabolite, biomarkers of oxidative damage and inflammation, and risk of hepatocellular carcinoma. Carcinogenesis *40*, 989-997.

Zatloukal, K., French, S.W., Stumptner, C., Strnad, P., Harada, M., Toivola, D.M., Cadrin, M., and Omary, M.B. (2007). From Mallory to Mallory-Denk bodies: what, how and why? Exp Cell Res *313*, 2033-2049.

Zhang, W., Zhu, X.D., Sun, H.C., Xiong, Y.Q., Zhuang, P.Y., Xu, H.X., Kong, L.Q., Wang, L., Wu, W.Z., and Tang, Z.Y. (2010). Depletion of tumor-associated macrophages enhances the effect of sorafenib in metastatic liver cancer models by antimetastatic and antiangiogenic effects. Clin Cancer Res *16*, 3420-3430.

Zhang, L., and Wang, H. (2015). Multiple Mechanisms of Anti-Cancer Effects Exerted by Astaxanthin. Mar Drugs *13*, 4310-4330

Zhang, J., Wang, X., Vikash, V., Ye, Q., Wu, D., Liu, Y., and Dong, W. (2016). ROS and ROS-Mediated Cellular Signaling. Oxid Med Cell Longev *2016*, 4350965.

Zhong, H., Xiao, M., Zarkovic, K., Zhu, M., Sa, R., Lu, J., Tao, Y., Chen, Q., Xia, L., Cheng, S.*, et al.* (2017). Mitochondrial control of apoptosis through modulation of cardiolipin oxidation in hepatocellular carcinoma: A novel link between oxidative stress and cancer. Free Radic Biol Med *102*, 67-76.

Acknowledgments

This thesis represents for me the completion of one of the most exciting, challenging and revealing periods of my life, for my personal and professional growth.

I could have never imagined reaching this much-desired goal with such satisfaction, and for this I have to especially thank the incredible support of my friend and colleague Dr. Elena Kotsiliti, who has always been my guide and my best example.

I want to thank my supervisors, Prof. Dr. Mathias Heikenwälder and Dr. Kristian Unger, who believed in me, supported me and guided me wisely during these years. I am really grateful to you.

Thanks also to my great colleagues of Munich, Dr. Tracy O´Connor, Paul Vandersee and Dr. Sukumar Namineni. It has been a great journey with you all, and I will never forget the scientific and emotional support you provided me. And lot of thanks also to the amazing support of the technical assistance in Munich of Anne Jacob, Robert Baier, and Olga Seelbach.

I would like to thank also my colleagues and technical assistance team of the DKFZ in Heidelberg (F180) and of the Helmholtz Zentrum Munchen (ZYTO), for their kind and professional support.

Thanks to the other members of my thesis committee Prof. Dr. Radu Roland Rad, Prof. Dr. Horst Zitzelsberger and Prof. Dr. Dirk Haller, for their fruitful discussions, support when needed and help to reach my goal in the best way.

Special thanks to my parents and to my sister Sara, for always believing in me and supporting me, also from far away. My family gave me the strength and the motivation to follow my dreams. They are my greatest inspiration for hard work, resiliency, and to be a kind and fair person towards others.

Last but not least I want to thank my boyfriend Paolo, who has been my greatest emotional support, my lighthouse, the reason why I never give up. Thanks to you I have understood what really matters in life, and that hard challenges can lead you to gain the most, helping you realize what you are capable of.